

An investigation into the feasibility of integrating intermediate-temperature solid oxide electrolysers with power plants

Mithila Nilupulie Manage

A thesis submitted to University College London
for the degree of Doctor of Philosophy

July 2014

Department of Chemical Engineering
Torrington Place, London, WC1E 7JE



I, Mithila Nilupulie Manage, confirm that the work presented in this thesis is my own. Where information has been derived from other sources, I confirm that this has been indicated in the thesis.

Signature

Date

Acknowledgements

Firstly, I would like to thank Prof. Stef Simons and Dr. Dan Brett for giving me the opportunity to do a PhD; especially to Dan for guiding me through electrochemistry and for his support throughout. I would also like to thank my supervisor Dr. Eva Sorensen for everything she has done for me throughout my time at UCL, her encouragement and kindness will be remembered.

Thank you to Mike Gorecki and Simon Barrass for supporting me in all things technical and safety, and to Pattie, Mae and Agata in the departmental office for processing my purchasing orders, which ensured that I could get my experiments done. Thank you to Graham and Erick in the mechanical workshop for their assistance throughout the years. Thank you also to Tom and Joe from the Chemistry department for kindly allowing me to use the spot welder. A very special thank you to Daniel Marfany and Michele Farmer for giving me hope and the resources I needed to overcome the challenges I faced, their support through the trying times has meant a lot.

Thank you to Vladislav at Imperial College for the use of materials and advice on cells. To all at EIL, thank you for all the great times. To Flora, Ishanka and Amal, their friendship, support and great shared moments have meant a lot. Thank you to my friends Toby, Jay and Rhod for their help in the lab and for the many 50 p's. Thank you to Phil, Dave, Chara and Aliya for making the very early morning starts worthwhile with plenty of tea. To my friends 'upstairs', Shade, Asif and Mozhdeh for making me feel so welcome at my new desk, I settled in great because of them. Thank you to Laura for her super postdoc advice. Thank you to Ruth and Edd for their wise words of encouragement, constant understanding and reminding me that there is nothing a good cup of tea won't solve. I would also like to thank all my friends outside of work who have put up with my dodgy working hours and saw me through to the end.

Finally, I would like to thank my parents Prem and Dulcie, and my sister Shakya, for their unfailing love and support through everything I do. Their invaluable advice has kept me going over the past few years. They have always been amazing role models and have inspired me to always aim for the stars, for this and so much more – thank you.

Abstract

The detrimental effect of increasing global emissions of CO₂ on the environment has prompted action to be taken to improve the environmental impact of hydrocarbon-based processes and fuel use. Therefore, producing hydrogen as an alternative fuel for vehicles fitted with fuel cells through solid oxide electrolyser cells (SOECs) has been considered.

Coal fired power plants are major energy providers and are operational all day. Introducing SOECs into the plant to utilise hot steam and electricity during times of low energy demand may provide a step to large scale hydrogen production. Through modelling and experimentation of power plants and SOECs, this project aims to evaluate the feasibility of an integrated system based on the thermodynamic, techno-economic and SOEC performance analyses.

Results show that SOECs, which operate between 600 and 1000 °C, take advantage of the heat of the steam, which increases electrolyser efficiency. Steam from before the intermediate pressure turbine at 560 °C and 46 atm was located from a simulation of a coal fired power plant. The intermediate-temperature steam of the plant was applicable to less used Gd-doped CeO₂ (CGO) than yttria stabilised zirconia (YSZ) electrolyte that performs best at 900 °C, as shown experimentally.

Modelling showed SOEC efficiency was improved by 25.2 % through an integrated system rather than traditional methods of heating water to steam, due to reduced energy requirements. Furthermore, the thermoneutral point of 4,644 A m⁻² (1.31 V) formed a guide for the design and operation of SOECs. Analysis on the integrated system showed that 250 MW (7500 kg hr⁻¹) and 290 MW (8700 kg hr⁻¹) H₂ can be produced with SOECs sized at 43,300 and 50,100 m², respectively, for scenarios of 7 % steam extraction and a purely H₂ production plant, at a cost of 3.76 \$ kg_{H₂}⁻¹. Although an integrated system shows promise for large scale hydrogen production, further development for suitable electrolytes and hydrogen storage and infrastructure is required.

Table of Contents

| | |
|--|----|
| Acknowledgements..... | 2 |
| Abstract | 3 |
| List of Tables..... | 8 |
| List of Figures..... | 9 |
| List of Appendices | 16 |
| 1 Introduction..... | 17 |
| 1.1 Overview | 17 |
| 1.2 Fundamentals of electrolyzers | 21 |
| 1.2.1 Thermodynamics of water electrolysis | 21 |
| 1.2.2 Definitions of electrolyser modes..... | 23 |
| 1.3 Research Aims | 30 |
| 1.4 Thesis outline | 30 |
| 2 Literature review | 32 |
| 2.1 Hydrogen production | 32 |
| 2.1.1 Hydrogen production from hydrocarbons..... | 33 |
| 2.1.2 Alternative technologies for hydrogen production..... | 38 |
| 2.2 Electrolysis of water and steam..... | 40 |
| 2.2.1 Low temperature electrolysis | 40 |
| 2.2.2 High temperature electrolysis..... | 43 |
| 2.3 Products of electrolysis | 46 |
| 2.4 Conclusions | 47 |
| 3 Techno-economic analysis | 48 |
| 3.1 Supplying power and heat to electrolyzers..... | 48 |
| 3.1.1 Electrical power from renewable and nuclear sources | 48 |
| 3.2 Techno-economic comparison of hydrogen generation technologies | 54 |
| 3.2.1 Cost of electricity production..... | 55 |

| | | |
|-------|--|-----|
| 3.2.2 | The cost of producing hydrogen from hydrocarbons | 57 |
| 3.2.3 | Comparison of hydrogen generation as a function of technology type and cost | 58 |
| 3.3 | Capital costs | 60 |
| 3.4 | Conclusions | 60 |
| 4 | Experimental verification and analysis | 62 |
| 4.1 | Experimental verification in literature | 62 |
| 4.2 | Experimental setup | 66 |
| 4.2.1 | Workstation | 66 |
| 4.2.2 | Rig design..... | 68 |
| 4.3 | Solid oxide cell preparation..... | 72 |
| 4.4 | Methodology | 73 |
| 4.5 | Techniques | 75 |
| 4.5.1 | Linear sweep polarisation | 75 |
| 4.5.2 | Electrochemical impedance spectroscopy | 76 |
| 4.5.3 | Scanning electron microscopy..... | 79 |
| 4.6 | Experimental method development and results..... | 79 |
| 4.6.1 | Symmetrical cell..... | 80 |
| 4.6.2 | Electrolyser cell | 87 |
| 4.7 | Conclusions | 103 |
| 5 | Modelling and analysis of coal fired plants..... | 105 |
| 5.1 | Modelling and analysis of power plants in literature..... | 105 |
| 5.1.1 | Review of energy market | 105 |
| 5.1.2 | Review of power stations | 106 |
| 5.1.3 | Literature review of modelling of power plants | 108 |
| 5.2 | Power plant modelling and simulation | 111 |
| 5.2.1 | Model validation..... | 112 |

| | | |
|-------|--|-----|
| 5.3 | Power plant simulation and results | 113 |
| 5.4 | Conclusions | 115 |
| 6 | Modelling and analysis of solid oxide electrolyser cells..... | 117 |
| 6.1 | Modelling of solid oxide electrolysers in literature..... | 117 |
| 6.2 | Solid oxide electrolyser cell model..... | 119 |
| 6.2.1 | Conservation of mass..... | 121 |
| 6.2.2 | Cell potential | 126 |
| 6.2.3 | Energy requirement | 129 |
| 6.2.4 | Efficiency | 132 |
| 6.3 | Solid oxide electrolyser modelling results | 133 |
| 6.3.1 | Model validation..... | 133 |
| 6.4 | Solid oxide electrolyser results..... | 140 |
| 6.4.1 | Case A: Producing hot steam at 1 atm..... | 142 |
| 6.4.2 | Case B: Producing hot and pressurised steam..... | 147 |
| 6.5 | Conclusions | 148 |
| 7 | Operation of an integrated power-solid oxide electrolyser plant..... | 151 |
| 7.1 | Integrated systems in literature..... | 151 |
| 7.2 | Results of system integration | 153 |
| 7.3 | Other considerations | 163 |
| 7.3.1 | Economic | 164 |
| 7.3.2 | Infrastructure | 166 |
| 7.3.3 | Storage | 166 |
| 7.3.4 | Social | 167 |
| 7.4 | Conclusions | 168 |
| 8 | Conclusions and Future work..... | 169 |
| 8.1 | Conclusions | 169 |
| 8.2 | Future work | 172 |

| | | |
|------|-------------------------------------|-----|
| 9 | Nomenclature..... | 175 |
| 10 | References | 179 |
| 11 | Appendix | 213 |
| 12 | Publications and presentations..... | 227 |
| 12.1 | Papers..... | 227 |
| 12.2 | Book chapters..... | 227 |
| 12.3 | Presentations..... | 227 |

List of Tables

| | |
|--|-----|
| Table 1-1: The applications of primary fuels in the UK [10]..... | 20 |
| Table 1-2: Reactions and data for alkaline, PEM and solid oxide electrolyser technologies [15;19;20;24;25]..... | 24 |
| Table 3-1: Costs associated with producing H ₂ from electricity produced by wind energy, adapted from Ref. [94]..... | 50 |
| Table 3-2: Costs associated with producing H ₂ from electricity produced by solar energy, adapted from Ref. [94]..... | 51 |
| Table 3-3: Comparison of costs based on solar and nuclear power generators, adapted from References [96;99;101]..... | 53 |
| Table 3-4: Cost of producing power from various sources..... | 57 |
| Table 3-5: Costs of producing H ₂ from conventional methods, adapted from Reference [21]. | 57 |
| Table 3-6: Investment costs of electrolyzers based on electrolyser type. | 59 |
| Table 4-1: Relationship between circuit elements and impedance..... | 78 |
| Table 4-2: Conductivities of the YSZ electrolyte at a range of temperatures under steam, hydrogen and carbon dioxide environments..... | 87 |
| Table 5-1: Typical operating conditions for different types of coal fired power plants [169]..... | 107 |
| Table 5-2: Coal fired plant model validation based on literature values. | 112 |
| Table 5-3: Parameters used in modelling a coal fired power station in this study. . | 113 |
| Table 5-4: Results obtained from CHEMCAD simulations of steam extraction for cases 1 to 3 for full and 50% load..... | 114 |
| Table 6-1: Values taken from literature to validate the model..... | 137 |
| Table 6-2: List of parameters used in the SOEC model. | 150 |
| Table 7-1: A comparison of SOEC efficiency based on the general (Chapter 6) and integrated cases at current densities of 5000 A m ⁻² | 155 |
| Table 7-2: The change in SOEC and power plant efficiency, and H ₂ production with SOEC operation at and above the thermoneutral point..... | 158 |

List of Figures

| | |
|--|----|
| Figure 1-1: Percentage of carbon dioxide emissions by continent in 2011 [1]. | 18 |
| Figure 1-2: The percentage of primary fuels used in the UK in 2011 is shown on the left [10]. The application of each primary fuel is shown in figures (a) to (d) on the right. | 20 |
| Figure 1-3: Effect of temperature on thermodynamic properties of the water electrolysis process. | 22 |
| Figure 1-4: Schematic of different electrolysers and their operation. | 25 |
| Figure 1-5: Effect of temperature on thermodynamic properties of the carbon dioxide electrolysis process. | 27 |
| Figure 1-6: Electrical energy requirement for steam and carbon dioxide co-electrolysis. | 29 |
| Figure 2-1: Flowsheet of the steam methane reforming process. | 33 |
| Figure 2-2: Flowsheet of the partial oxidation process (ASU – air separation unit). | 34 |
| Figure 2-3: Flowsheet of the autothermal reforming process. | 35 |
| Figure 2-4: Schematic of a simplified plasma reforming unit [15]. | 36 |
| Figure 2-5: Biomass gasification with integrated steam electrolyser, adapted from Ref. [46]. | 37 |
| Figure 3-1 Integrating a stand-alone wind energy generator with an electrolyser, adapted from Ref. [15]. | 50 |
| Figure 3-2: Nuclear power plant with electrolysis of steam [24]. | 54 |
| Figure 3-3: The relationship between the costs of electricity, efficiency of the electrolysis process (values around periphery of graph) and the resultant cost of hydrogen production. Analysis neglects capital, maintenance and the cost of water feed. | 58 |
| Figure 4-1: Experimental workstation. | 67 |
| Figure 4-2: The cell holder design, Mark 1; creating two separate regions for the hydrogen and oxygen sides. | 68 |
| Figure 4-3: Solid oxide electrolyser rig setup: Mark 2. (a) The whole rig, (b) ceramic holder for tubes to be positioned at the inlet of steam, (c) ceramic holder for the cell | |

| | |
|--|----|
| to sit in (left side where steam enters), (d) ceramic holder for the cell to be held in place where oxygen can leave the rig, (e) ceramic holder for the tubes to be positioned for air to enter and oxygen to leave. | 69 |
| Figure 4-4: CAD of hydrogen side ceramic tube positioning, Mark 2. | 69 |
| Figure 4-5: CAD drawings of the changes to SOEC holder design, drawn in Rhinoceroses, Mark 3 (a) Cell holder secured with nichrome wires hooks, (b) area to place the cell and allow gas flow, (c) deeper holes in the bottom of the holder to support ceramic tubing, (d) a side view of the top piece showing greater thickness for support and reducing has leaks. | 70 |
| Figure 4-6: A top view of the solid oxide electrolyser rig setup, Mark 3. Changes made to the gas outlet on the hydrogen side and ceramic tubing to house all thermocouples and electrical connections. | 71 |
| Figure 4-7: Solid oxide electrolyser cell holder machined on the CNC, Mark 3; (a) holder with Pt current collector and electrical connections, (b) placement of sealed SOEC within the holder, (c) silicone bung with sealant. | 72 |
| Figure 4-8: SOEC cells after sintering; (a) Ni-CGO cathode, (b) YSZ electrolyte, (c) LSM anode. | 73 |
| Figure 4-9: Process flow diagram for symmetrical cell testing. | 74 |
| Figure 4-10: Process flow diagram for SOEC testing with steam. | 74 |
| Figure 4-11: Process flow diagram for SOEC testing with CO ₂ | 75 |
| Figure 4-12: A general voltage – current density curve. | 76 |
| Figure 4-13: An example of a Nyquist plot representing the Real (Z_{Re}) and Imaginary (Z_{Im}) terms , where L is the inductance, R_0 is the high frequency resistance, R_{ct} is the charge transfer resistance. | 77 |
| Figure 4-14: An equivalent circuit for a two electrode and electrolyte cell. | 78 |
| Figure 4-15: Impedance spectroscopy of the electrical connections at temperatures of between 500 and 800 °C. | 80 |
| Figure 4-16: Changes to electrolyte resistance over time of symmetrical Ni-CGO/YSZ/Ni-CGO cell at 650 °C, with H ₂ and N ₂ mixture at 50 %:50 % (a) resistance of the electrolyte, (b) resistance of the cathode, and 50% H ₂ : 50% N ₂ | |

| | |
|--|----|
| mixture at 40 %:50 %:10% (c) resistance of the electrolyte and (d) resistance of the cathode. | 81 |
| Figure 4-17: Impedance of the cell to variations in temperature (from 600 °C to 700 °C and then back down again to 600 °C) under 50% H ₂ : 50 % N ₂ | 82 |
| Figure 4-18: Sensitivity of electrolyte and electrodes resistance to changes in temperature. At 50 % H ₂ : 50 % N ₂ resistance of electrolyte (left) and resistance of cathode (right)..... | 82 |
| Figure 4-19: Impedance of the cell to variations in hydrogen concentration at 600 °C. | 83 |
| Figure 4-20: Sensitivity of electrolyte and electrode resistance to changes in concentration at 600 °C; resistance of electrolyte (left) and resistance of cathode (right). | 83 |
| Figure 4-21: Impedance of the cell to variations in temperature under 100 ml min ⁻¹ (50 % H ₂ : 50 % N ₂) and steam relative humidity of 75 % environment. | 84 |
| Figure 4-22: Sensitivity of electrolyte and electrode resistance to changes in temperature at 100 ml min ⁻¹ (50 % H ₂ : 50 % N ₂) and steam relative humidity of 75%. Resistance of electrolyte (left) and resistance of electrode (right). | 85 |
| Figure 4-23: Conductivity of electrolyte at varying temperatures at 100 ml min ⁻¹ (50 % H ₂ : 50 % N ₂) and steam relative humidity of 75 %..... | 85 |
| Figure 4-24: Impedance of the symmetrical cell to variations in temperature in 50 % CO ₂ : 50 % N ₂ environment. | 86 |
| Figure 4-25: SEM of the hydrogen electrode at 15 kV and ×5,000 (5 μm) (a) before sintering and using the cell, (b) After using the cell sintered at 1,300 °C and operated at 650 °C in a humidified gas with 50% H ₂ and 50% N ₂ | 88 |
| Figure 4-26: Voltage-current (V-i) density curves of SOEC (Ni-CGO / YSZ / LSM) operating at 650 °C with humidified gas at 75 % RH and 20 % H ₂ : 80 % N ₂ | 88 |
| Figure 4-27: Impedance at OCV of 0.1 V at 650 °C with humidified gas at 75 % RH and 20 % H ₂ : 80 % N ₂ , based on Figure 4-26 of SOEC (Ni-CGO / YSZ / LSM). ... | 89 |
| Figure 4-28: Impedance at OCV of 0.2 V at 650 °C after 1 hour of SOEC (Ni-CGO / YSZ / LSM)..... | 89 |

| | |
|--|----|
| Figure 4-29: Impedance of SOEC (Ni-CGO / YSZ / LSM) at OCV of 0.004 V at 700 °C with humidified gas at 75 % RH and 20 % H ₂ : 80 % N ₂ | 90 |
| Figure 4-30: Impedance of SOFC (Ni-CGO / YSZ / LSM) at OCV of 0.14 V at 700 °C with 90 % H ₂ : 10 % N ₂ | 91 |
| Figure 4-31: Voltage-current (V-i) density curves of bought (Ni-CGO / ScSZ / LSM) operating at 750 °C with SOEC at humidified gas at 75 % RH and 10 % H ₂ : 90 % N ₂ and SOFC at 90 % H ₂ : 10 % N ₂ | 92 |
| Figure 4-32: NextCell™ Electrolyte Supported Button Cell (a) Ni-CGO cathode painted onto the bought cell (insert), (b) LSM anode painted onto the bought cell (insert), (c) Ni-CGO cathode after sintering at 1250 °C and (d) LSM anode after sintering at 1250 °C. | 93 |
| Figure 4-33: Voltage-current (V-i) density curves of commercial Ni-CGO / ScSZ / LSM operating at 750 °C. SOEC conditions- humidified gas at 75 % RH. Resistance correction shown is based on impedance. | 94 |
| Figure 4-34: Impedance at SOEC (Ni-CGO / ScSZ / LSM) OCV of 0.8 V at 750 °C based on Figure 4-33. SOEC conditions- humidified gas at 75 % RH..... | 94 |
| Figure 4-35: Voltage-current (V-i) density curves of commercial Ni-CGO / ScSZ / LSM operating at 750, 800, 850 and 900 °C with humidified gas at 75 % RH and 10 % H ₂ : 90 % N ₂ . Insert shows real and IR corrected data. | 95 |
| Figure 4-36: Impedance of SOEC (Ni-CGO / ScSZ / LSM) at 0.91, 1.2 and 1.4 V at 750 °C based on Figure 4-35, with humidified gas at 75 % RH and 10 % H ₂ : 90 % N ₂ | 96 |
| Figure 4-37: Impedance of SOEC (Ni-CGO / ScSZ / LSM) at 0.86, 1.2, 1.5 and 1.8 V at 800 °C based on Figure 4-35, with humidified gas at 75 % RH and 10 % H ₂ : 90 % N ₂ | 96 |
| Figure 4-38: Impedance of SOEC (Ni-CGO / ScSZ / LSM) at 0.77, 1.2 and 1.8 V at 850 °C based on Figure 4-35, with humidified gas at 75 % RH and 10 % H ₂ : 90 % N ₂ | 97 |
| Figure 4-39: Impedance of SOEC (Ni-CGO / ScSZ / LSM) at 0.73, 1.3 and 1.8 V at 900 °C based on Figure 4-35, with humidified gas at 75 % RH and 10 % H ₂ : 90 % N ₂ | 97 |

| | |
|---|-----|
| Figure 4-40: Impedance at OCV of 0.91, 0.86, 0.77 and 0.73 V for temperatures of 750, 800, 850 and 900 °C, respectively. Based on Figure 4-35, with humidified gas at 75 % RH and 10 % H ₂ : 90 % N ₂ | 98 |
| Figure 4-41: Impedance at 1.8 V for temperatures of 800, 850 and 900 °C, respectively. Based on Figure 4-35, with humidified gas at 75 % RH and 10 % H ₂ : 90 % N ₂ | 98 |
| Figure 4-42: SEM of the hydrogen electrode (Ni-CGO) (a) before sintering and using the cell, (b) After using the cell sintered with Pt painted to secure the Pt mesh current collector and operated at 750 °C and (c) After using the cell sintered with Ni-CGO painted to secure the Pt mesh current collector and operated at 900 °C..... | 99 |
| Figure 4-43: SEM of the oxygen electrode (LSM) (a) before sintering and using the cell, (b) After using the cell sintered with Pt painted to secure the Pt mesh current collector and operated at 750 °C and (c) After using the cell sintered with LSM painted to secure the Pt mesh current collector and operated at 900 °C..... | 100 |
| Figure 4-44: SEM of the oxygen electrode (Ni-CGO) at the boundary with the electrolyte (a) before sintering and using the cell, (b) After using the cell sintered with Pt painted to secure the Pt mesh current collector and operated at 750 °C and (c) After using the cell sintered with LSM painted to secure the Pt mesh current collector and operated at 900 °C..... | 100 |
| Figure 4-45: SOEC (Ni-CGO / ScSZ / LSM) testing with 50% N ₂ : 50% CO ₂ at 850 °C. | 101 |
| Figure 4-46: Impedance of SOEC (Ni-CGO / ScSZ / LSM) at OCV of 0.63 and 0.18 V before and after leak, respectively at 800 °C with 50 % CO ₂ : 50 % N ₂ | 102 |
| Figure 4-47: Impedance of SOEC (Ni-CGO / ScSZ / LSM) at OCV of 0.5 V and 850 °C. Based on Figure 4-45, with 50 % CO ₂ : 50 % N ₂ | 102 |
| Figure 5-1: Power generation in the UK by different technologies per settlement period from 09:30 on 19.03.2012 to 09:30 on 20.03.2012, adapted from BM reports (2012) [163]..... | 106 |
| Figure 5-2: A schematic of a conventional coal fired power plant..... | 108 |
| Figure 5-3: A flowsheet to represent the coupling of streams from the power plant with the SOEC. The diagram refers to cases 1, 2 and 3 from the power plant. | 114 |

| | |
|--|-----|
| Figure 5-4: The extent of efficiency loss of the power plant with varying fractions of steam extracted for cases 1 to 4..... | 115 |
| Figure 6-1: SOEC operation and a representation of the basis of the energy model. | 120 |
| Figure 6-2: An overview of the inputs and outputs to the SOEC. The links between each section of the model in relation to physical inputs are shown..... | 121 |
| Figure 6-3: The conductivity (σ) of Ni-YSZ and the estimated values for Ni-CGO extrapolated from $60000 \Omega^{-1} \text{ m}^{-1}$ at $650 \text{ }^\circ\text{C}$ [122;215]. | 134 |
| Figure 6-4: The exchange current density of Ni-YSZ and the estimated values for Ni-CGO extrapolated from 1580 A m^{-2} [225;226]. | 135 |
| Figure 6-5: Comparison of model and experimental results at (a) $750 \text{ }^\circ\text{C}$, (b) $800 \text{ }^\circ\text{C}$, (c) $850 \text{ }^\circ\text{C}$ and (d) $900 \text{ }^\circ\text{C}$ at 90% N_2 : 10% H_2 and RH 75%..... | 136 |
| Figure 6-6: Validation of ohmic overpotential with values from Udagawa et al. 2007 [25]. | 138 |
| Figure 6-7: Validation of Activation overpotentials with values from Chan <i>et al.</i> 2002 [191]. | 138 |
| Figure 6-8: Validation of concentration overpotentials with values from Udagawa <i>et al.</i> 2007 [25] and Ni <i>et al.</i> 2006 [190]. | 139 |
| Figure 6-9: Process flow diagrams showing modelled systems: (Case A) The entering feed is heated and then used to operate the SOEC. (Case B) The entering feed is pressurised, heated and then used to operate the SOEC. | 141 |
| Figure 6-10: Energy required to heat water or steam to the SOEC operating temperature ($500, 600$ or $700 \text{ }^\circ\text{C}$) at SOEC operating pressure of 1 atm. | 142 |
| Figure 6-11: The SOEC efficiency across a range of operating temperatures and inlet feed water / steam temperatures for an SOEC operating at $5,000 \text{ A m}^{-2}$. The inserts show a cross section of the contour plot: (above) SOEC efficiency at SOEC operating temperature of $650 \text{ }^\circ\text{C}$ and (right) SOEC efficiency with feed temperature of $560 \text{ }^\circ\text{C}$ | 143 |
| Figure 6-12: The efficiency across a range of current density and inlet feed water / steam for an SOEC operating at $650 \text{ }^\circ\text{C}$ and 1 atm. The inserts show a cross section | |

| | |
|---|-----|
| of the contour plot: (above) SOEC efficiency at SOEC operating at 5000 A m ⁻² and (right) SOEC efficiency with feed temperature of 560 °C..... | 144 |
| Figure 6-13: Ohmic overpotentials at SOEC operating temperature of 500, 600 and 700 °C, and SOEC operating pressure of 1 atm. | 145 |
| Figure 6-14: Activation overpotentials at SOEC operating temperature of 500, 600 and 700 °C, and SOEC operating pressure of 1 atm..... | 146 |
| Figure 6-15: Concentration overpotentials at SOEC operating temperature of 500, 600 and 700 °C, and SOEC operating pressure of 1 atm. | 146 |
| Figure 6-16: Thermal energy required for raising steam to various operating pressures at 500, 600, 650 and 700 °C from water at 25 °C and 1 atm. | 147 |
| Figure 7-1: SOEC efficiency with changing current density at an operating temperature of 650 °C for Cases 1, 2 and 3. The insert shows the operating potential with current density for the three Cases. | 154 |
| Figure 7-2: Total additional power requirement for SOEC operating at 650 °C with steam from cases 1, 2 and 3. Insert: a close up of the peaks of the curves to show the maximum amount of additional heating power needed. | 155 |
| Figure 7-3: The loss of power plant efficiency (left axis) and associated hydrogen production (right axis) vs. current density and associated fraction of steam extracted from the plant; for an integrated system based on cases 1 to 3. | 156 |
| Figure 7-4: SOEC efficiency and power generation via hydrogen based on steam from Cases 1, 2 and 3..... | 157 |
| Figure 7-5: The maximum SOEC area and associated integrated system efficiency with varying current densities from case 2: IP at (a) with a constant steam extraction of 7% and (b) a case where the plant is producing hydrogen only i.e. zero electrical output to the grid..... | 161 |
| Figure 7-6: Minimum cost of producing hydrogen to maintain average power plant income compared with integrated system efficiencies for Case 2: IP at (a) with a constant steam extraction of 7%. (b) a case where the plant is producing hydrogen only i.e. zero electrical output to the grid..... | 165 |

List of Appendices

| | |
|--|-----|
| A1: Summary of experimental results of area specific resistance for a range of electrolyser technologies. | 213 |
| A2: Flowsheet of power plant produced in CHEMCAD 6.0 TM | 217 |
| A3: Table of data to show flowrates and conditions of the streams in of the power plant in A2. | 217 |
| A4: Table of data to show operating conditions of the units of the power plant in A2. | 220 |
| A5: A summary of the main electrochemical equations of the SOEC model..... | 221 |
| A6: Derivation of the Butler-Volmer and activation overpotential..... | 222 |

1 Introduction

In this chapter, an overview of this thesis is given. The motivation behind integrating solid oxide electrolyzers into a coal fired power plant will be outlined together with the aims and contributions of this work. Finally, an outline of the subsequent chapters is presented.

1.1 Overview

Concerns over the dependence on hydrocarbon-based fuels worldwide are growing due to the environmental concerns over high carbon dioxide emissions, where 32,600 Mt of CO₂ was emitted globally in 2011. Asia was seen to be the largest contributor to CO₂ emissions, as shown in Figure 1-1, with China emitting 27 % of the total emissions, followed by US, Russia and India emitting 17, 5.5 and 5.3 %, respectively (the UK contributed 1.5 % of CO₂ emissions) [1]. Through changes in the energy market, an increase of carbon emissions of almost 25 % was seen in Asia where as a decrease in 7 % was seen in the US based on figures from 2007 [1].

The reason for Asia contributing greatly to CO₂ emissions is due to the dramatic growth of China and India's economies and the associated number of conventional power plants that have been built; it is predicted that 31 % of both countries power will be produced by coal in 2035 [2]. Since 2002, China has been constructing conventional coal fired power plants as part of an energy restructuring plan [3]. This has enabled the country to utilise their large coal reserves, as China holds around 1.04×10^{14} kg of coal [4]. In addition, conventional power plants were built between 2005 and 2008 to supply 50 GW of power per year and this is expected to rise to a total of 563 GW in 2020 [5].

As a result of this rapid growth, approximately 70 % of the power produced in China in 2006 was produced from coal [2;4]. As the power plants were not built with carbon capture and storage (CCS) processes, the amount of carbon dioxide and greenhouse gases released into the atmosphere is increasing and will continue to do so as there are no plans to implement CCS with the conventional power plants [6]. Without CCS in place, there are also environmental implications due to emissions of SO₂, NO_x and particulate from the release of flue gas. Furthermore, it has been predicted that without CCS processes in place, CO₂ emissions will increase to 10.8×10^{12} kg by 2020, even with China meeting their emission targets [7].

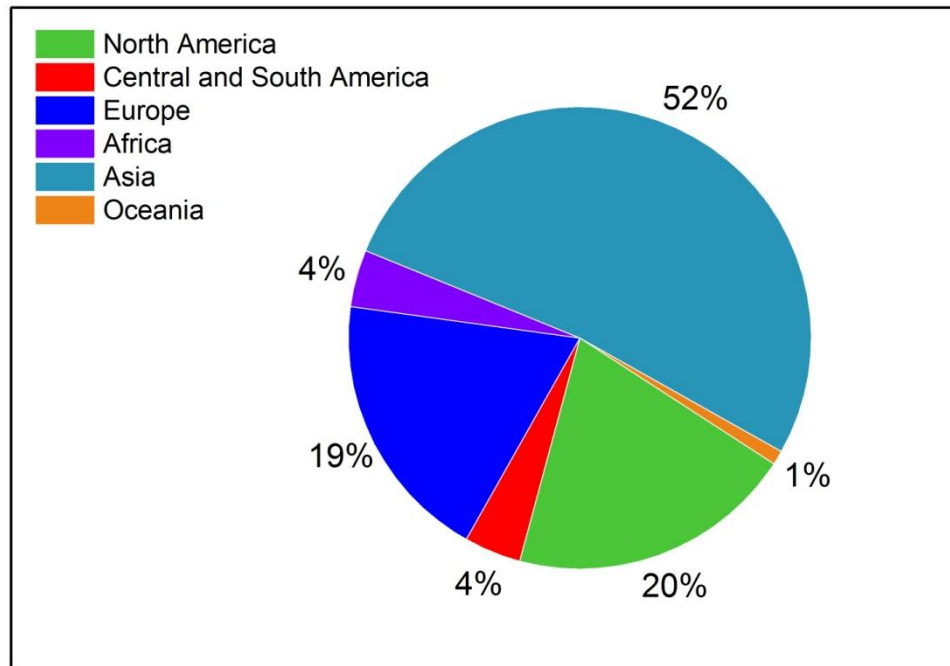


Figure 1-1: Percentage of carbon dioxide emissions by continent in 2011 [1].

The growth of development in Asia, combined with the consistent use of coal fired power plants in other parts of the world, has had a global environmental impact. The reason for the increase in CO₂ emissions lies in the increasing demand and use of fossil fuels [8;9]. In the UK, the three largest primary fuels used are hydrocarbon-based coal, petroleum (oil) and natural gas, and these fuels are used extensively for producing electricity, fuels and chemicals, as shown in Figure 1-2. The total energy consumption of primary fuels in 2011 being 138.3 Mt of oil equivalent [10].

Based on the negative effects of climate change due to both the global reliance on hydrocarbon-based primary fuels and growing carbon dioxide emissions, the United Nations Framework Convention on Climate Change was developed, which is an ongoing international treaty to reduce the impact of climate change [11]. A milestone in the reduction of carbon emissions was the Kyoto Protocol Treaty, 1997 [12]. Through discussions, the agreed treaty outlined action points for reducing the environmental impact of waste released into the atmosphere. The targets set for each country were a total of 5.2 % of greenhouse gas emissions were to be reduced by 2012 based on the levels in 1990 [11;13]. Since then, a second phase of emission reduction targets began in January 2013 for a duration of seven years based on the Cancun Agreements from 2010. The Cancun Agreements aims to keep global temperature increases to less than 2 °C above pre-industrialised levels and for

industrialised countries to develop low-carbon plans to mitigate carbon emissions and provide support through the ‘Green Climate Fund’ for developing countries. In addition, developing countries have decided to limit increasing carbon emissions and to create low-carbon plans. Though objectives for the second phase have been outlined, actual figures for targets have not yet been agreed [11].

Currently, primary fuels (coal, petroleum products, natural gas, bioenergy and waste and primary electricity) are used for a range of applications as shown in Table 1-1. The ‘other’ primary fuels include secondary fuels such as coke and blast furnace gas. It can be seen that coal is used almost in its entirety for electricity production, with natural gas and bioenergy and waste also contributing to producing electricity. Natural gas is also used for domestic purposes. The products from refining petroleum are used mainly as road and air transport fuels and chemicals production and natural gas is also used for domestic purposes. It is clear that the UK’s fuel market is heavily reliant on hydrocarbon-based fuels; however, refineries and power plants tend not to have carbon capture facilities and they therefore contribute to carbon emissions [14].

Based on the data in Figure 1-2 and Table 1-1, coal is almost solely used for electricity generation in the UK. However, through combining electrolysis with coal fired power plants coal can also be used for fuel production, thereby changing the way that primary fuel is used in order to achieve cleaner and more sustainable fuels such as hydrogen.

Hydrogen as an energy vector is considered a promising alternative to fossil fuels, particularly for transport applications when used with fuel cell technology [15]. In such a configuration, there are no CO₂ emissions at the point of use and the only waste product is water. Hydrogen as a fuel benefits from a high gravimetric energy density (140.4 MJ kg⁻¹ compared to 48.6 MJ kg⁻¹ for gasoline) [15]. Hydrogen is used extensively for the synthesis of chemicals such as ammonia and methanol; however, it is not found in its pure, uncombined form on Earth. Therefore, it is considered an energy carrier or ‘energy vector’, as it must be produced from other compounds.

1. Introduction

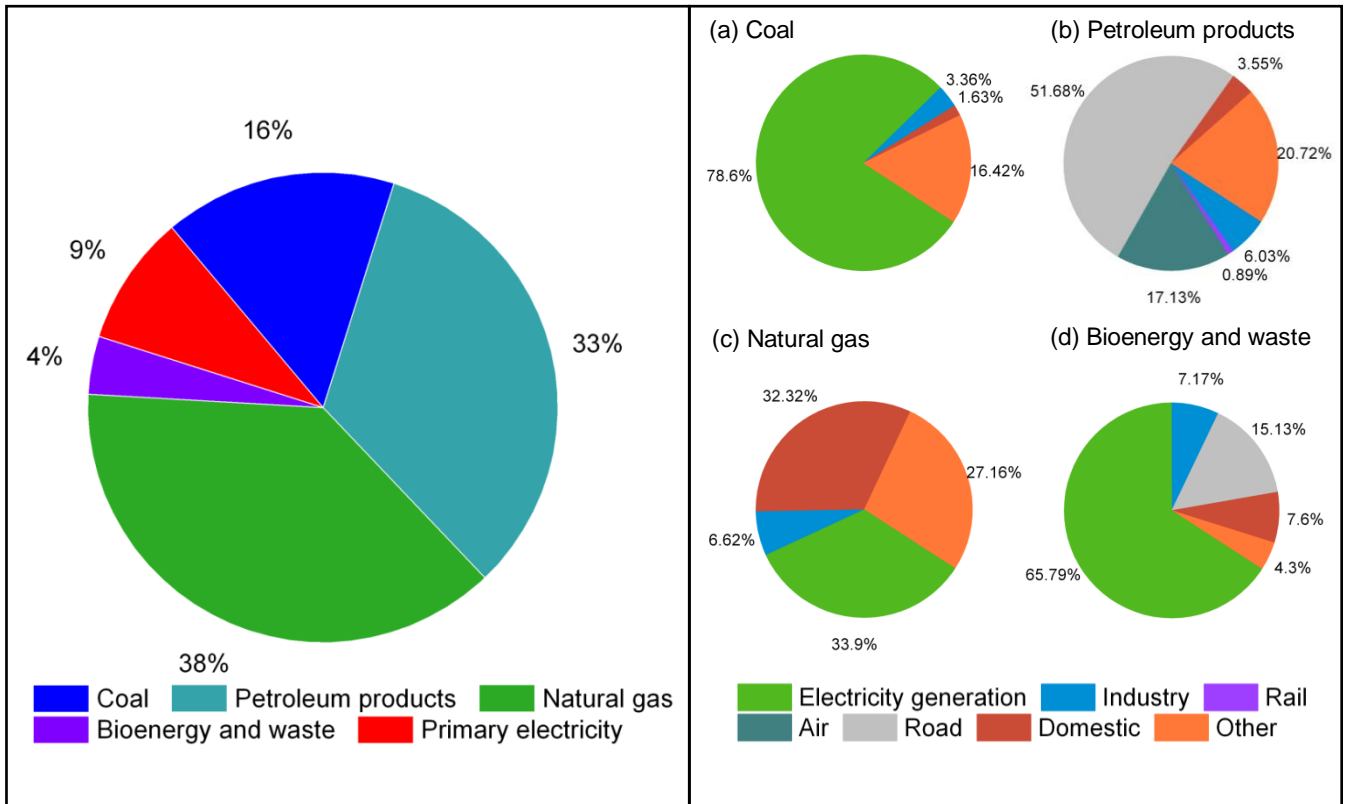


Figure 1-2: The percentage of primary fuels used in the UK in 2011 is shown on the left [10]. The application of each primary fuel is shown in figures (a) to (d) on the right.

Hydrogen, combined with fuel cell technology, is of interest as a way of reducing our reliance on hydrocarbon-based fuels. Plans have been made to reach short and long term goals towards reducing CO₂ emissions and realising a ‘*hydrogen economy*’ such as the recent UKH₂Mobility project [16]. It was suggested by the Department of Energy and Climate Change (DECC) that electrolysis would be the preferred choice for large scale hydrogen production for use in vehicles by 2050 [17].

Table 1-1: The applications of primary fuels in the UK [10].

| Primary Fuel | Application (%) | | | | | | |
|---------------------|------------------------|----------|------|------|------|----------|-------|
| | Electricity generation | Industry | Rail | Air | Road | Domestic | Other |
| Coal | 78.6 | 3.4 | | | | 1.6 | 16.4 |
| Petroleum products* | | 6.0 | 0.9 | 17.1 | 51.8 | 3.5 | 20.7 |
| Natural gas | 33.9 | 6.6 | | | | 32.3 | 27.2 |
| Bioenergy & waste | 65.8 | 7.2 | | | 15.1 | 7.6 | 4.3 |
| Primary electricity | | 100 | | | | | |
| Other | | | | | | | 100 |

*As petroleum oil is refined into various fuels, it has been shown as petroleum products.

In light of the developments in Asia of coal fired power plants and the move towards cleaner technology in the UK, this thesis focuses on the feasibility of large scale hydrogen production through integrating intermediate-temperature solid oxide electrolyser cells (SOECs) with conventional coal fired power plants as an alternative to petrol and diesel fuels for vehicles. Coal fired power plants have been chosen as both the steam and electricity needed for SOEC operation can be obtained from the plants. The study aims to establish any possible improvements in plant efficiency through an integrated system, as well as the feasibility of large scale hydrogen production from SOECs.

1.2 Fundamentals of electrolysers

Electrolysers in this work are electrochemical systems that use water or steam with electricity to separate hydrogen and oxygen molecules. In this thesis, the focus is to produce hydrogen to be used as fuel.

1.2.1 Thermodynamics of water electrolysis

Understanding the thermodynamics of the electrolysis reaction enables the correct choice of electrolyte to be used for the relevant application. The overall reaction which takes place in a water electrolyser is:



The enthalpy (ΔH) of a reaction represents the minimum amount of energy required for a reaction to occur. In this case, the enthalpy is the total amount of energy required for the steam to dissociate. In electrolysis the energy is supplied by heat (Q) and electrical power (W_{elec}) where the heat is brought in by the steam [18]:

$$\Delta H = W_{elec} + Q = \Delta G + T\Delta S \quad (2)$$

The Gibbs energy (ΔG) represents the amount of energy available within the system at constant temperature and pressure, which governs whether or not the reaction will take place. Therefore, at a certain temperature and pressure, the amount of heat energy (Q), in the steam will be constant as there is no change in conditions to drive the reaction. The difference in the heat energy available at a certain condition and the enthalpy (minimum energy requirement) then identifies the amount of electrical energy required to ensure that the minimum energy needed for the reaction is available.

For a steam electrolyser operating with one mole of steam per unit time, two electrons are required and the associated charge (q) transfer between the electrodes is shown in Equation (3) [18]:

$$q = 2N_A(-e) = 2F \quad (3)$$

where N_A is Avogadro's number, F is Faraday's constant and $-e$ is the charge on an electron.

For an electrolyser where there is a potential difference, E , between two electrodes and charge transfer through the circuit, electrical work (W_{elec}) is being done on the system [18]:

$$W_{elec} = qE = nFE = \Delta G \quad (4)$$

where n relates to the number of electrons per mole.

Therefore, ΔG corresponds to W_{elec} and the $T\Delta S$ term corresponds to Q :

$$\Delta G = -nFE \quad (5)$$

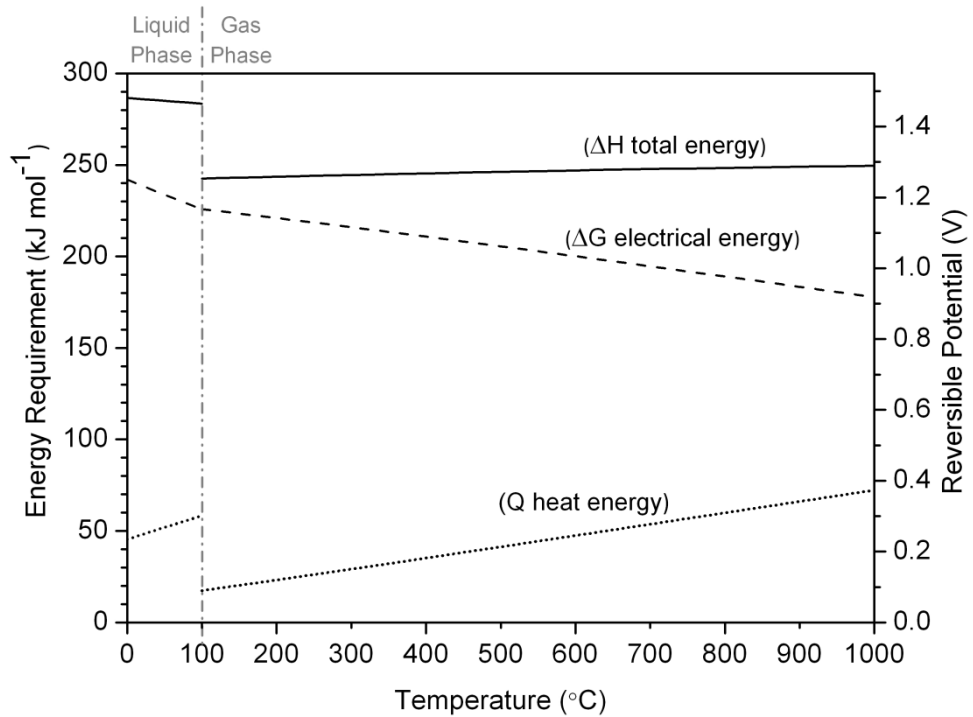


Figure 1-3: Effect of temperature on thermodynamic properties of the water electrolysis process.

By considering the variation of state functions ($\Delta H, \Delta G, T\Delta S$) with temperature, the overall change in Gibbs energy, and thus the electrochemical potential of the reaction, can be determined. Figure 1-3 shows the change of each of these parameters with temperature. It can be seen that the total energy requirement is relatively insensitive to temperature variation. However, due to the positive change in entropy associated with the reaction, the heat required increases with temperature. Consequently, the Gibbs energy (electrical energy required) decreases with increasing temperature.

1.2.2 Definitions of electrolyser modes

There are three main types of electrolysers: alkaline, proton exchange membrane and solid oxide. Table 1-2 summarises the main characteristics of each electrolyser type. In this study, the electrolyser efficiency is described as:

$$\text{Efficiency} = \frac{2F(E_{op} - E_{overpot})\dot{N}_{H_2}}{iE_{op}} \times 100 \quad (6)$$

Where E_{op} and $E_{overpot}$ are the operating voltage and overpotentials, respectively, \dot{N}_{H_2} is the molar flowrate of hydrogen produced and i is the current density.

1.2.2.1 Low temperature electrolysis

Low temperature electrolysers refers to those which operate at below 100 °C; alkaline and proton exchange membrane cells (PEM). In alkaline electrolysis, the water enters at the cathode side and decomposes to H_2 and OH^- . The operation is shown in Figure 1-4(a). The OH^- ions migrate through the $KOH_{(aq)}$ electrolyte, which is typically 25 to 30 wt. % KOH [19;20]. Increasing the concentration up to 47 wt. % enables a higher conductivity; however, the components of the cell corrode much faster at higher concentrations [20]. At the anode, the OH^- ions gain electrons and produces H_2O and O_2 . The hydrogen needs to be separated from the water at the cathode side which can be done through dehumidification [20].

Alkaline electrolysers have been in operation for decades and are considered to be a mature technology. They produce H_2 with efficiencies between 64 and 70 % [21] and are mainly used in industry for small on-site applications where the need for high purity H_2 is important. There are a range of electrolyser sizes available with the capability of producing from 10 to 100 $m^3 h^{-1}$ of hydrogen [22].

Table 1-2: Reactions and data for alkaline, PEM and solid oxide electrolyser technologies [15;19;20;23;24].

| | Alkaline Electrolyser | PEM Electrolyser | Solid Oxide Electrolyser |
|--------------------------------------|--|--|---|
| Operating Temperature (°C) | 70 – 90 | 25 – 100 | 500 – 1000 |
| Electrolyte ion and material | OH ⁻ KOH(aq), NaOH(aq) | H ⁺ Sulfonated polymers e.g. Nafion TM | O ²⁻ Yttria, Yttria stabilised zirconia (YSZ), Scandia-stabilized zirconia |
| Cathode reaction and material | 2H ₂ O + 2e ⁻ → H ₂ + 2OH ⁻ Nickel with platinum catalytic coating | 2H ⁺ + 2e ⁻ → H ₂ Platinum black, iridium oxide (IrO ₂), ruthenium oxide (RuO ₂) | H ₂ O + 2e ⁻ → H ₂ + O ²⁻ Nickel-YSZ cermet |
| Anode reaction and material | 2OH ⁻ → ½O ₂ + H ₂ O + 2e ⁻ Nickel or Copper coated with metal oxides | H ₂ O → ½O ₂ + 2H ⁺ + 2e ⁻ Platinum black, iridium oxide (IrO ₂), ruthenium oxide (RuO ₂) | O ²⁻ → ½O ₂ + 2e ⁻ Perovskite oxides (e.g. lanthanum manganate) |

Although generally small in size, the alkaline electrolysers are used in a wide range of production processes, including the food industry for increasing saturation in oils and fats, their melting points and resistance to oxidation. In addition, the nuclear industry requires H₂ for removing O₂ as it can cause stress corrosion cracking and power stations use H₂ as a coolant for its generators due to its high thermal conductivity. Hydrogen is sometimes used in the pharmaceutical and plasma industries as well [15]. Oxygen, normally considered a by-product of electrolysis, can be used in many chemical processes.

In PEM electrolysers, the electrolyte is made of a proton conducting material that enables the H⁺ ions to travel through the electrolyte to the cathode (Figure 1-4b). The water enters at the anode side of the cell and decomposes to H⁺ and O₂. The advantage of this type of electrolyser is that pure hydrogen can be obtained without the need for a further separation process. At low temperatures there may be some water molecules present in the hydrogen as water is required for conduction to occur. Proton exchange membrane electrolysers have the advantage that only hydrogen is produced at the cathode due to the proton conducting electrolyte. In PEM electrolysers, water is required for conduction and therefore there may be some water molecules in the hydrogen output. However, at higher temperatures the hydrogen is drier [20;25]. Furthermore, the ionic resistance has been seen to be lower in PEM electrolysers, which increases efficiency compared with alkaline

electrolysers. The PEM electrolyser has been shown to have efficiencies between 55 and 70 % [19].

1.2.2.2 High temperature electrolysis

1.2.2.2.1 Steam electrolysis

High temperature electrolysis in solid oxide electrolyser cells (SOECs) operates by steam entering at the cathode side where it dissociates into protons (H^+) and oxide ions (O^{2-}). The solid oxide electrolyte is an oxide ion conductor and so the O^{2-} ions are then transported through the electrolyte where they lose electrons and oxygen is formed at the anode. This can be seen in Figure 1-4(c). The hydrogen can be separated from the steam in another stage after leaving the SOEC.

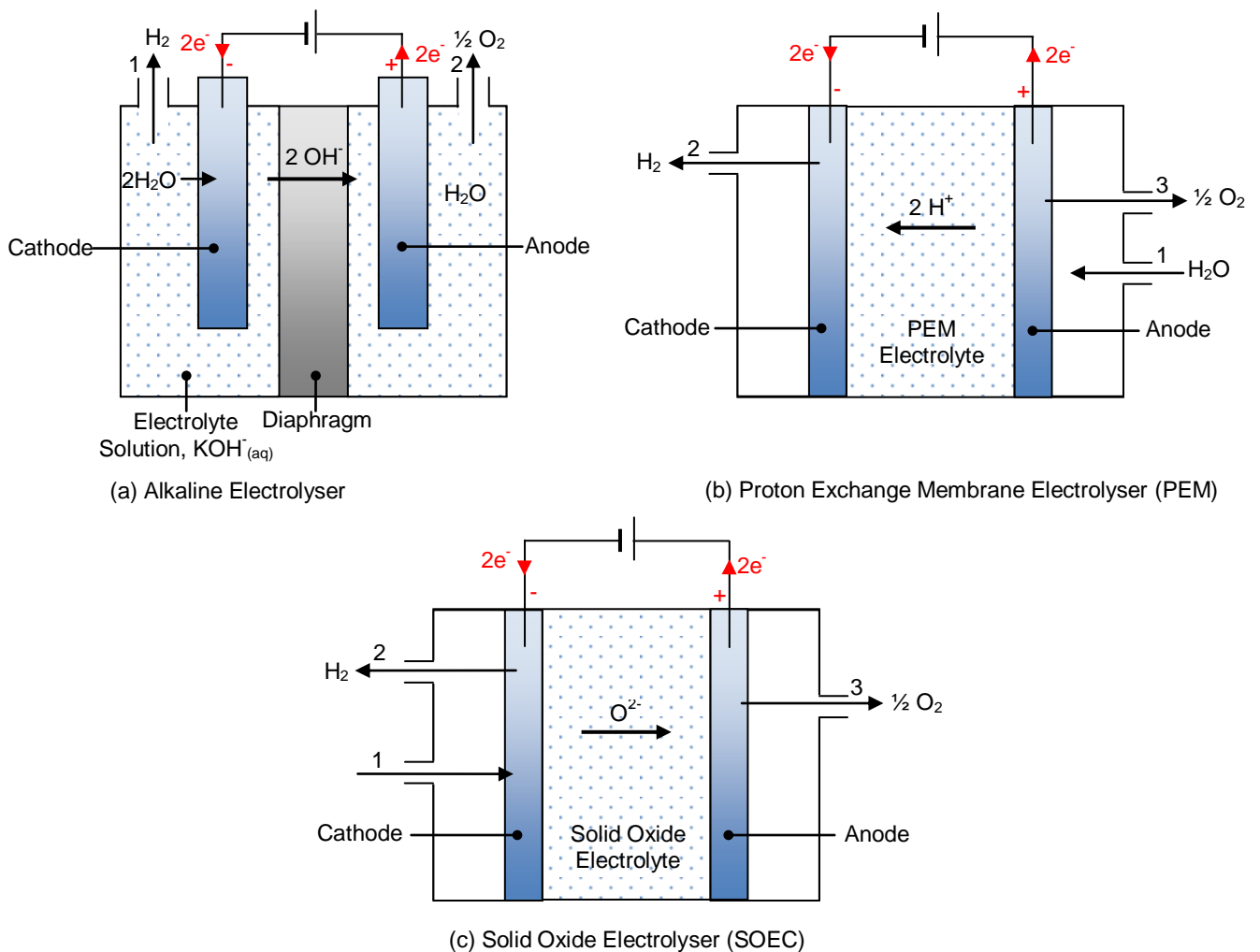


Figure 1-4: Schematic of different electrolysers and their operation.

SOEC technology provides advantages compared with low temperature cells due to the elevated operating conditions. As described previously, high temperature operation imparts higher electrical efficiency to the water or steam electrolysis process based on thermodynamic considerations. Furthermore, high temperatures also favour the kinetics of the electrode reactions.

It has also been shown based on a life cycle assessment for manufacturing SOFC (and by extension SOEC) materials, that the environmental impact is fairly small; the emissions from manufacturing SOFCs contribute to 1 % of lifetime CO₂ emissions for both planar and tubular geometries [26].

One of the advantages of a solid electrolyte is that they can be manufactured to any shape, the two most common is planar or tubular designs; the preferred choice is usually the former. Tubular cells were designed as a way of reducing sealing problems commonly seen in planar cells, large active area and have shown quick start up [27]. However, planar designs are now being used to allow a high packing density and lower volume in the system and are also cheaper to manufacture [24].

Extensive research is being performed to identify the best materials for use in SOECs, as the conventional materials used in solid oxide fuel cells (SOFCs) are not optimised for these reactions. However, SOFC analogues are being used as the starting point, with typical materials for the cathode, electrolyte and anode being Ni-YSZ (nickel-yttria stabilised zirconia) which is a ceramic metal mixture, YSZ and perovskite oxides (e.g. lanthanum manganate), respectively [22;25]. Laboratory-scale SOEC operation has demonstrated hydrogen production efficiencies of between 70 and 90 % [28]. As the electrolyte dictates the operation, electrode choice and performance of the cell, a number of studies of various electrolyte materials have been published, such as strontium and manganate doped lanthanum gallate (LSGM) and samarium doped ceria (SDC)-carbonate composite, which showed good performance [29]. Research is also being carried out into the strength, toughness and durability of LSGM. However, results have shown that it is stable with a current density of 700 mA cm⁻² for 350 hours [20]. At the moment, this is not a commercial option as research continues in order to find a material suitable for the electrodes as well.

SOECs are versatile as they have been shown to be a viable method of reducing steam, carbon dioxide and a steam-carbon dioxide mix to hydrogen, carbon

monoxide and syngas, respectively [30;31]. It has been noted that power plants operate with steam at elevated temperatures. The ability of the SOEC to operate at elevated temperatures and the improvement seen in electrolyser efficiency of such conditions makes SOECs the most suitable option for integrating with power plants. Therefore, this thesis will focus on SOEC electrolysis for hydrogen production.

1.2.2.2 Carbon dioxide electrolysis

Early research of carbon dioxide electrolysis was in the area of oxygen production for undersea uses, space travel and exploration to Mars [32-34]. However, more recent research is being done on using carbon dioxide from industrial sources for the production of syngas [32].

As with steam electrolysis, the thermodynamic characteristics are shown in Figure 1-5, where it can be seen that increasing temperatures results in a significant reduction of electrical energy requirement. Therefore, high temperature electrolysis is the preferred option for CO₂ electrolysis.

There have only been two types of electrolytes that have shown to manage the electrolysis of carbon dioxide, which are solid oxide and molten carbonate electrolytes at high temperatures [34].

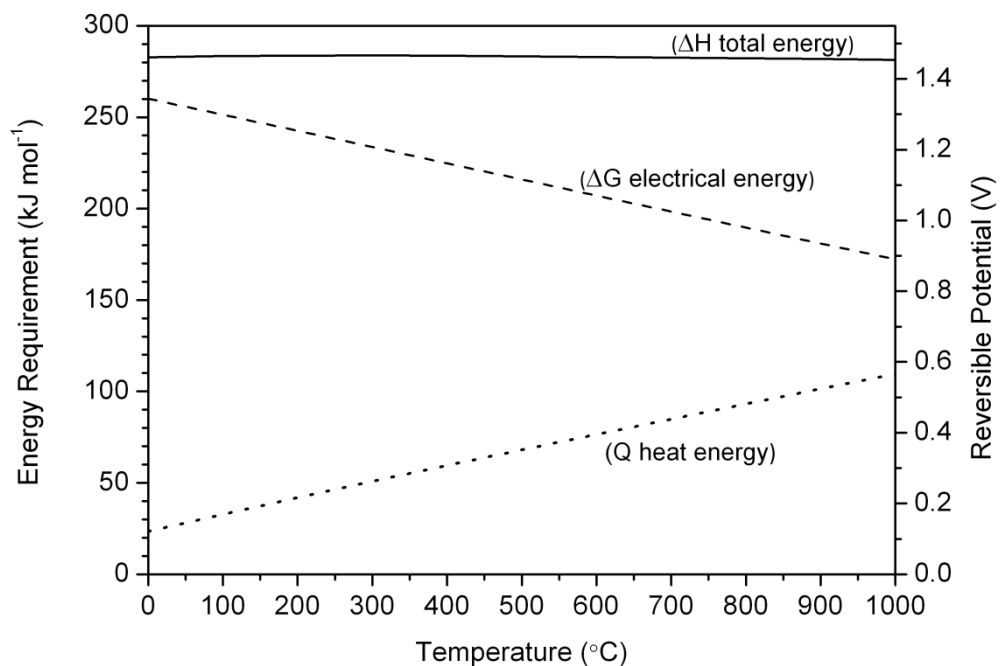
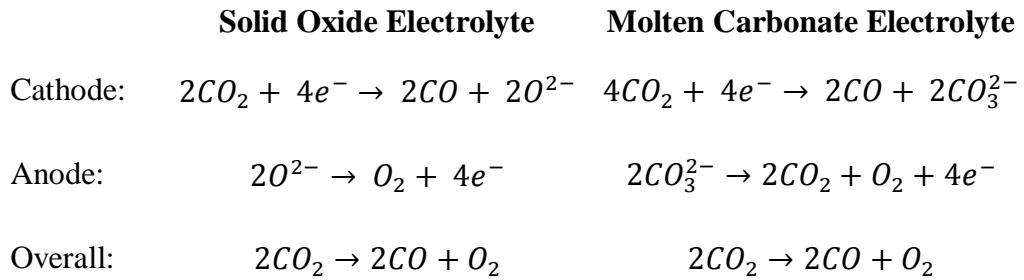


Figure 1-5: Effect of temperature on thermodynamic properties of the carbon dioxide electrolysis process.

The reactions that occur in these electrolytes are shown in the following Equations [34]:



Molten carbonates work best at temperatures of 550 °C and have proven to produce oxygen efficiently over long periods of time. Combining molten carbonates with platinum electrodes have produced results which correlate closely with theory based on Faraday’s Law. Due to good performance, porous ceramic wafers saturated with carbonate electrolytes were being developed for space explorations. Solid oxide electrolytes of YSZ combined with platinum electrodes have also shown high efficiencies with a transference number of 1. The transference number represents the ratio of actual oxygen produced to the oxygen that would have been produced if the total current was ionic. Furthermore, the cell endurance was seen to be high after tests were carried out for over 3600 hours and results showed very little deterioration [33;34].

This shows that both the electrolytes are suitable for carbon dioxide electrolysis at high temperatures as they produce good results. However, there are still problems with overpotentials in the solid oxide electrolyte, which may reduce the efficiency of the cell [33].

1.2.2.2.3 Co-electrolysis

Research into co-electrolysis of carbon dioxide and steam was prompted by large carbon emissions from industrial processes such as power plants, which included high steam and carbon contents such as flue gas [35].

The water-gas shift reaction occurs under co-electrolysis of CO₂ and steam electrolysis [36;37], which requires control to obtain the ratio of syngas required. It is further complicated by side reactions whereby methane is produced occasionally at intermediate temperatures and high potentials [38]. Comparing the thermodynamics of co-electrolysis from Figure 1-6, it can be seen that at lower

temperatures, the steam reaction is favoured as less electrical energy is required for the process. As with both steam and carbon dioxide electrolysis, at higher temperatures the carbon dioxide electrolysis is favoured to producing syngas.

Patents have also been released based on the use of flue gas in electrolysis. One such patent considered the use of co-electrolysis for methanol production using alkaline electrolyzers, which enables the electrolyser to be used for more than just hydrogen production [39]. Co-electrolysis using the heat generated from gasification plants has also been patented whereby a solid oxide electrolyser can be used to produce syngas. This shows that there is potential in the market for such processes to be implemented [40].

Therefore, the operating temperature and energy input has a direct effect on the products to be produced. Controlling these variables will enable suitable hydrogen to carbon monoxide ratios to be achieved in order for the products to be used in processes such as Fischer Tropsch.

It has been noted that power plants operate with steam at elevated temperatures. The ability of the SOEC to operate at elevated temperatures and the improvement seen in electrolyser efficiency of such conditions makes SOECs the most suitable option for integrating with power plants. Therefore, this thesis will focus on SOEC electrolysis of steam for hydrogen production.

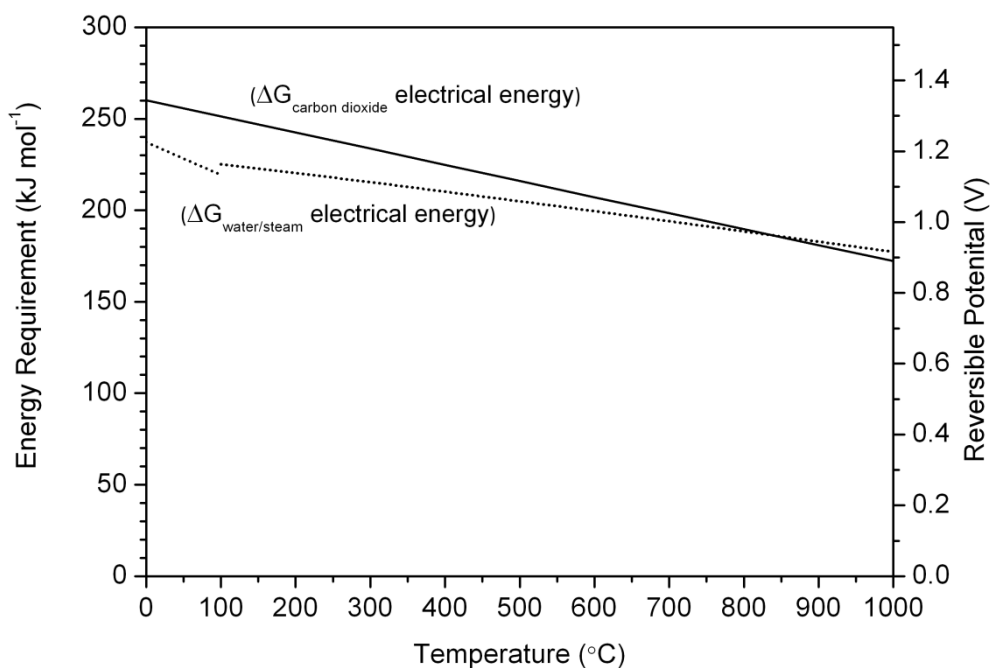


Figure 1-6: Electrical energy requirement for steam and carbon dioxide co-electrolysis.

1.3 Research Aims

The overall aim of this thesis is to assess the feasibility of integrating solid oxide electrolyser cells (SOECs) into a conventional coal fired power plant by considering thermodynamic principles, economic viability, and SOEC and power plant efficiency variations. This study aims to offer an engineering perspective on the operation of SOECs as well as propose steps toward SOEC commercialisation. Furthermore, the study seeks to examine the current situation of the fuel and energy sectors and to create a pathway toward producing hydrogen as an alternative fuel by utilising existing technologies.

The aims are further described as follows:

- To carry out a thermodynamic and techno-economic analysis to assess the viability of solid oxide electrolysers for commercial hydrogen production.
- To identify the key characteristics of high temperature operation through experimentation of conventional SOECs.
- To assess the performance of an integrated system compared with independent operation of SOECs and power plant with varying operating conditions through modelling.
- To evaluate other factors that may facilitate or limit the success of an integrated system.

1.4 Thesis outline

The outline of the thesis is as follows:

Chapter 2 considers the current technologies available for hydrogen production and outlines the research that has been published on such technologies including steam methane reforming (SMR) as well as low and high temperature electrolysers.

Chapter 3 identifies and assesses the current state of conventional and new technologies for hydrogen production and provides a techno-economic analysis of solid oxide electrolysers. The chapter also shows the major economic limitations of commercialising solid oxide electrolysers (SOECs).

Chapter 4 is focused on the design of an experimental facility for SOEC testing. Through testing on both symmetrical cells and SOECs, the behaviour of SOECs based on traditional materials is discussed.

In Chapter 5, a conventional coal fired power plant simulation is presented. The analysis identifies possible areas of the plant where high temperature steam can be extracted with the intention of being used in SOECs. The chapter also provides a description of the role of coal fired power plant in the energy market.

Chapter 6 presents a model of SOECs with the aim of evaluating the extent to which efficiency is affected by the overall energy requirements of electrolysis. Two general cases A and B are considered for a system consisting of a heater and SOECs. Case A examines the effect on SOEC efficiency with water/steam being fed to the system at varying temperatures between 25 °C and 700 °C at 1 atm. Case B considers the energy consumption of producing hot and pressurised steam from water sourced at 25 °C and 1 atm.

In Chapter 7 an integrated system of SOECs with a coal fired power plant is analysed. The changes in system efficiency when using steam from before the high pressure (Case 1), intermediate pressure (Case 2) and low pressure (Case 3) turbines is shown. The analysis in this chapter also considers the factors affecting SOEC size and economics of hydrogen production. Consideration is given to storage, infrastructure and social factors.

Finally, Chapter 8 concludes the thesis and discusses the results obtained in this study. Possible steps for future work to further this project for implementing an integrated system are also outlined.

2 Literature review

An overview of the literature representing current methods of hydrogen production and electrolyser technology is discussed in this chapter. The literature has shown a range of technologies, both commercially available, such as steam methane reforming and those still in research development such as biological methods. The review outlines hydrogen producing technologies and shows the current trends in research.

2.1 Hydrogen production

Hydrogen is currently produced predominantly from hydrocarbons. Approximately 48 % of the world's hydrogen is produced from methane, 30 % from crude oil, 18 % from coal and only 4 % from electrolysis. Electrolysis of water is currently the main way of producing hydrogen in a sustainable way [15]. The following section describes industrial and researched methods of hydrogen production, which are alternatives to electrolysers. As SOECs are not yet commercial they must be able to meet current standards in order to be competitive in the market. Therefore, industrial processes used at the moment, such as steam methane reforming (SMR), partial oxidation (POX), autothermal reforming and gasification are discussed.

Syngas, a valuable gaseous mixture of hydrogen and carbon monoxide, is widely used for synthetic fuel production through the Fischer-Tropsch process. It is a product that can be generated from a variety of sources such as coal, biomass, waste materials and sewage sludge [41]. Current technologies which use hydrocarbon-fuel produce syngas first, which is then further processed to generate hydrogen. Therefore, SMR, POX, autothermal reforming and gasification are all methods of syngas production. Though hydrogen is considered as an alternative fuel, syngas can be useful for synthetic fuel production. Furthermore, pyrolysis can be used, where the fuel is heated until it decomposes to syngas [41]. Pyrolysis of sewage sludge has shown to give high efficiencies where 95 % of the gases produced were syngas when using multi-chambered microwave ovens. The multi-chambered oven enables both conventional and microwave heating [41].

The most efficient and versatile method of syngas production is seen to be gasification as the process is able to cope with a variety of carbon based materials rapidly. The most significant waste produced is slag, with negligible amounts of fly ash, at high temperatures and pressures. This reduces the amount of cleaning

required and is more cost efficient. In addition to hydrocarbon based hydrogen production, the following section also includes research of alternative hydrogen production technologies via plasma reforming, photolysis, anaerobic digestion, fermentation and electrolysis.

2.1.1 Hydrogen production from hydrocarbons

2.1.1.1 Steam methane reforming

The majority of the world's H₂ is produced using steam methane reforming (SMR) as illustrated in Figure 2-1 [15]. Depending on the purpose of the SMR plant (i.e. whether it is primarily for the production of either H₂ or syngas, where syngas is a mixture of CO and H₂); hydrogen will be produced at varying purities and compositional amounts.

In SMR, methane first undergoes a two-stage desulphurisation process to remove sulphur to acceptable levels compatible with the downstream catalytic processes, which are liable to be poisoned by sulphur containing compounds. Typically, a Co – Mo catalyst is used to produce H₂S. For sulphur removal the H₂S gas is then reacted with a bed of ZnO in a scrubbing process [21]. The treated methane is then reacted in the reformer with steam to produce H₂ and CO using Ni as the catalyst, as shown in Equation (7).

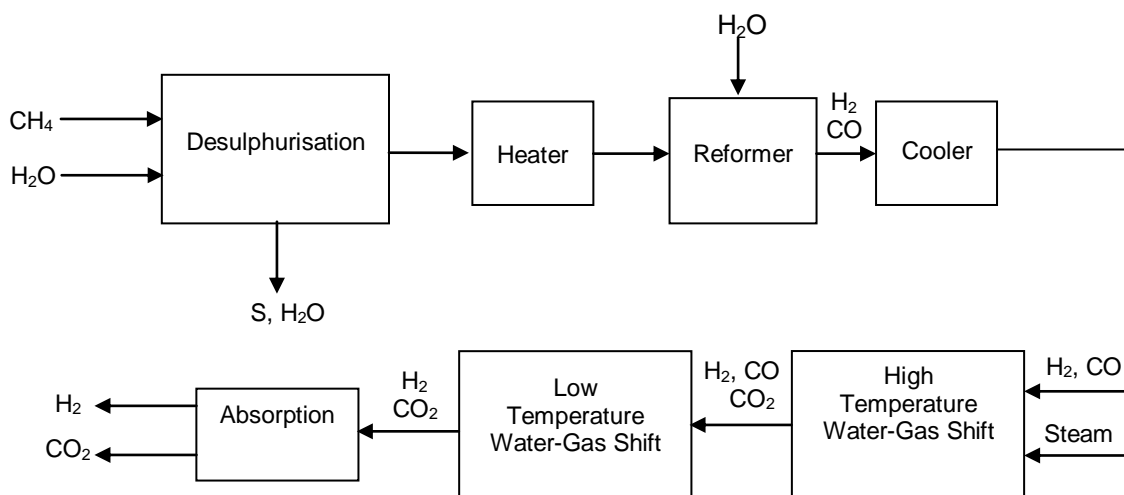
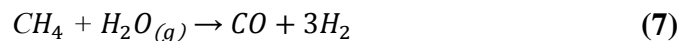
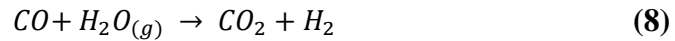


Figure 2-1: Flowsheet of the steam methane reforming process.

The syngas can be used as a feedstock for other processes, such as the Fischer-Tropsch reaction, or can be passed through water-gas shift reactors to produce more hydrogen:



The process has a high thermal efficiency (Equation (9)) of around 85 % and has the best ratio for hydrogen production of 3:1 (hydrogen: carbon monoxide); however, it is a very large producer and emitter of carbon dioxide [19].

$$Efficiency_{Thermal} = \frac{\dot{W}}{\dot{Q}_H} \quad (9)$$

where \dot{W} , is the net work output and \dot{Q}_H , is the energy supplied to the system.

2.1.1.2 Partial oxidation

The partial oxidation (POX) process combusts larger hydrocarbons such as oils in a controlled environment to produce syngas (Figure 2-2). The syngas then undergoes the shift reaction (Equation (8)) and the H_2 is separated from the CO_2 in an absorption process. The process requires high operating temperatures, between 1250 °C and 1500 °C, and pressures of between 29 and 118 atm, which means that a catalyst is not required. Due to the exothermic nature of the process, additional heat is not required as the heat produced is sufficient to maintain the operating conditions within the reactor. However, unlike SMR the process produces soot, which means that an additional cleaning process is necessary to remove solid particulates from the gas [15;19]. The process is illustrated in Figure 2-2.

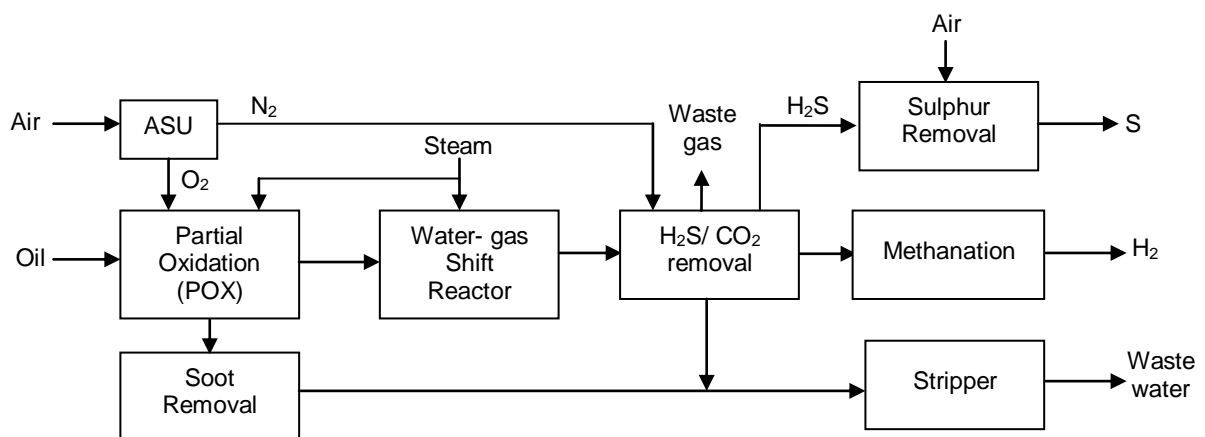


Figure 2-2: Flowsheet of the partial oxidation process (ASU – air separation unit).

Although POX can be more versatile as larger hydrocarbons can be used, it produces hydrogen at a higher cost and SMR is therefore usually favoured for large-scale production of hydrogen [42]. Furthermore, a hydrogen-to-carbon monoxide ratio of 3:1 is produced using SMR in comparison to only 1:1 or 2:1 from POX [19].

2.1.1.3 Autothermal reforming

Autothermal reforming (Equation (10)) can be separated into two main reactions. The first, partial oxidation; where heat is produced due to the exothermic nature of the reaction, creating a thermal zone. The second is the endothermic steam reforming reaction, which occurs using the heat produced from partial oxidation in the catalytic zone. The catalyst used in the bed is normally alumina-supported Ni [15;19].

The process requires pure oxygen though less than that used by partial oxidation only. This makes the process more economically viable as less O₂ per unit of H₂ produced is required. However, to ensure the efficiency does not decrease, tight control is required on the oxygen to fuel ratio, as well as the steam to carbon ratio, for the reactions. Due to the control on the steam-to-carbon ratio, the syngas produced can be used directly in the Fischer-Tropsch process without further processing.

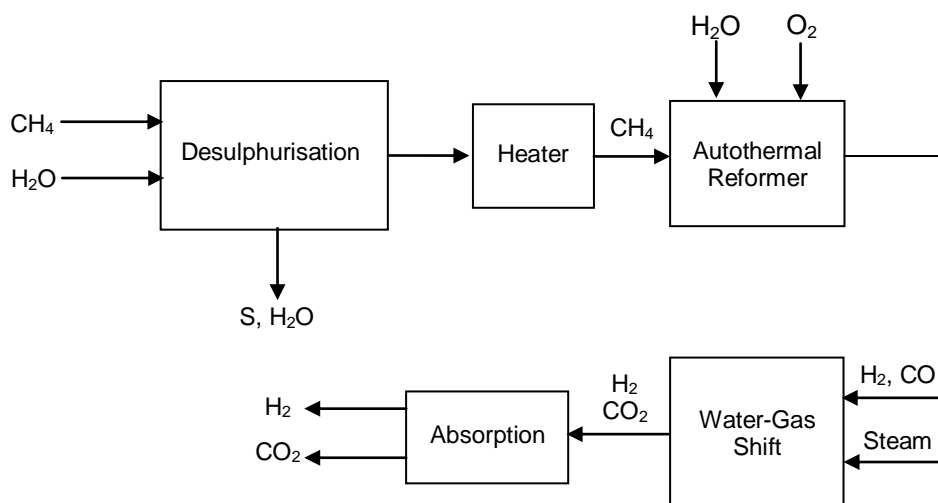
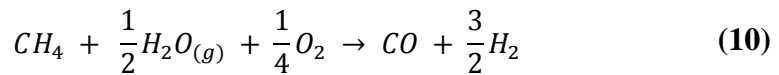


Figure 2-3: Flowsheet of the autothermal reforming process.

2.1.1.4 Plasma reforming

Plasma, the ionised gas generated by electricity or heat, provides the energy needed to reform hydrocarbons, which undergo the reaction in Equation (7). The plasma created from steam consists of H, OH and O radicals and electrons [19]. Plasma reforming can be either thermal or non-thermal, where the difference lies in the operating temperature of the process [43]. The process is claimed to overcome the disadvantages of the conventional reforming process in terms of cost, the short life of the catalyst and size and weight requirements [15].

Thermal plasma reforming requires a large amount of electric discharge; greater than 1 kW [44]. The power is required to increase the temperatures of electrons and neutral species to temperatures of around 5,000 °C. Power is also required to ensure that the electrodes do not deteriorate at the high temperatures [15;19]. Figure 2-4(a) shows a thermal plasma reformer, where free radicals of H, OH and O are formed as well as electrons which act as catalysts for the reaction. The schematic of non-thermal plasma reforming can be seen in Figure 2-4(b). In this type of plasma reforming the temperature of the electrons alone is increased to above 5,000 °C. The temperatures of the ions, radicals and neutral species are generally at room temperature [45]. The power is used to heat up the electrons only and not the bulk species [15;19]. As the bulk of the plasma is at room temperature, the power requirement is significantly lower than for thermal plasma reforming as only a few hundred watts of power is needed. A reduced amount of power is also required to cool the electrodes compared with thermal reforming, which saves space and enables the reactor to be smaller. The electric discharge produces electrons, ions and radicals.

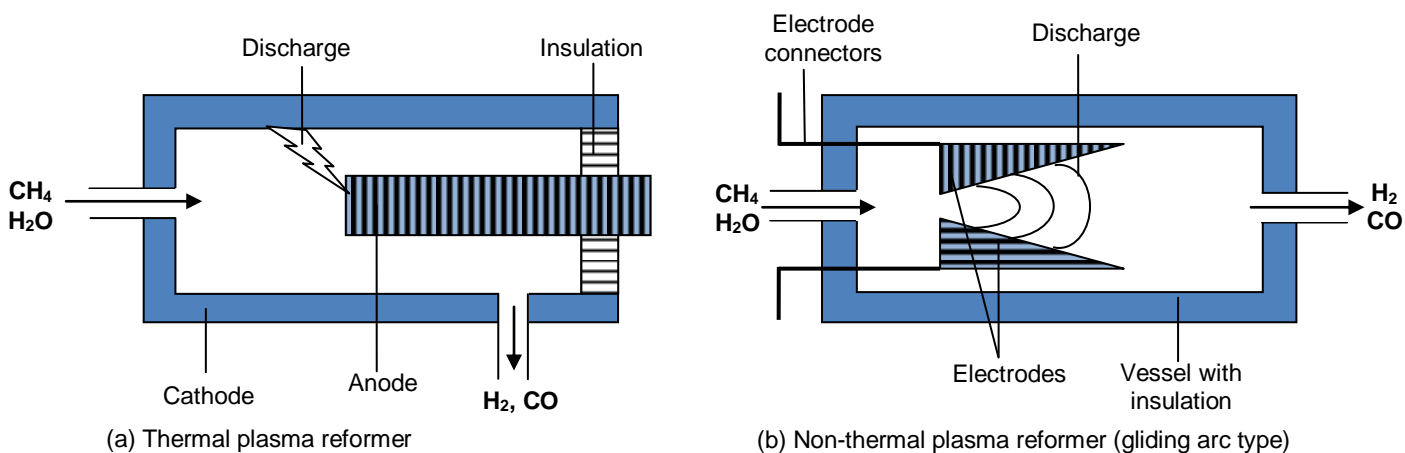


Figure 2-4: Schematic of a simplified plasma reforming unit [15].

2.1.1.5 Gasification

The gasification process operates by combusting either coal or biomass at high temperatures and pressures to produce syngas (Equations (11) to (15)). There are three main types of gasification reactors; fixed bed, fluidised bed and entrained flow reactors. Gasifiers operate at different conditions and have different efficiencies, and biomass gasifiers are usually smaller in size than coal gasifiers [15;46].

Fixed bed reactors were favoured when the technology was first introduced; however, fluidised bed and entrained flow reactors are more commonly used in industry today [47]. A fluidised bed reactor operates at temperatures of 800 – 950 °C and pressures of around 25 atm. This process involves the introduction of either oxygen or air into the reactor with the coal/biomass particles until the particles act like a fluid. The entrained flow gasifier operates at temperatures between 1,200 and 1,500 °C and pressures between 30 and 40 atm. The feed is milled to small particles of ~100 µm diameter and dried before entering the reactor, where they react with the oxygen and steam that is also fed to the reactor.

The syngas produced can undergo the water-gas shift reaction to further improve the hydrogen yield, as shown in Equation (13) [15]. Gasification is a much faster reaction than both POX and SMR; however, the capital costs are greater as there are more pre-treatment processes required for coal than for methane, and the syngas needs more cleaning to remove particulates [19;21].

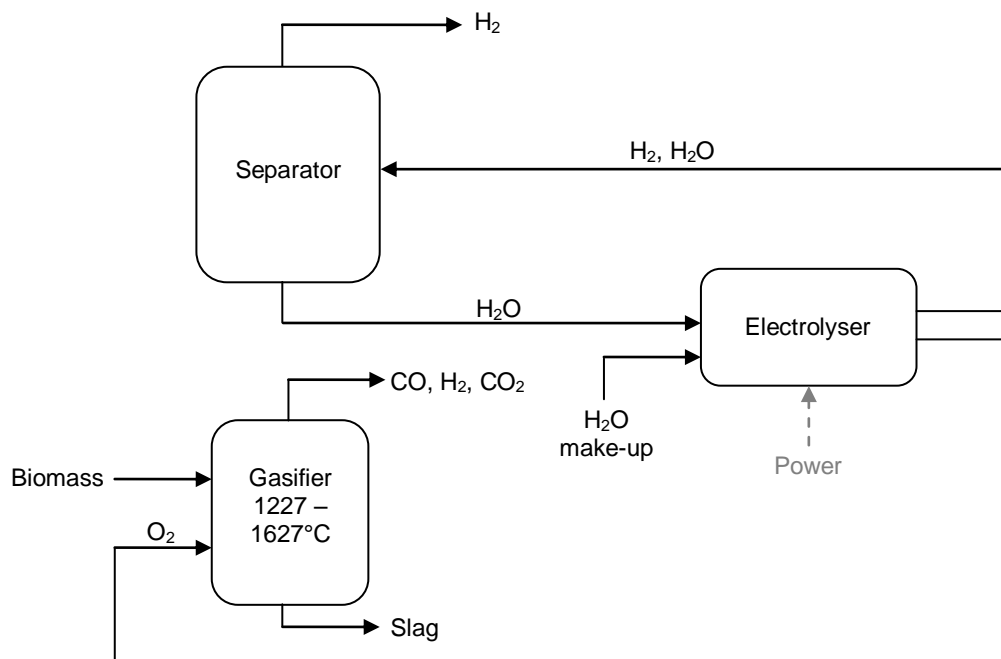


Figure 2-5: Biomass gasification with integrated steam electrolyser, adapted from Ref. [46].



In addition, SMR has been shown to be 65 and 80 % thermally efficient, based on small and large plants, respectively [21]. In contrast, gasification of coal and biomass are only 53 and 60 % efficient, respectively [18]. Biomass gasification is not as simple as coal gasification and therefore, to improve biomass gasification the use of electrolysers to produce O₂ for combustion rather than air has been studied, represented in Figure 2-5. Due to the complexity of biomass gasification, SMR provides more H₂ for the same energy input and is less costly than other hydrocarbon processes.

2.1.2 Alternative technologies for hydrogen production

Other options for hydrogen production, which do not require hydrocarbon combustion, have also been studied. The studies have focused on techniques using biomass and catalysts for hydrogen production. These processes are currently in the research and development stage and are not yet ready for commercialisation on a large scale.

2.1.2.1 Photolysis

Photolysis is a process which uses solar energy and microbes such as green algae and cyanobacteria and takes advantage of photosynthesis. The photosynthesis process uses solar radiation and separates water, where H₂ is a by-product. The process takes place in the thylakoid membrane in the chloroplast of the algae, where light energy is converted to chemical energy. The electrons produced in the membrane when water is split are transferred to a soluble protein called ferredoxin. Under normal situations, enzymes (ferredoxin-NADP⁺ oxidoreductase) accept the electrons which are used to form NADPH₂, which is an enzyme used to enable the CO₂ to convert to glucose and starch. However, at times when the conditions are anaerobic or when too much light

has been absorbed, the light energy can be released by converting the hydride ions in the ferredoxin to H₂ gas [15;19;48].

Photolysis requires large surface areas and also a way for the microorganisms to produce hydrogen, and not only undergo photosynthesis. So far, results have not shown this to be a commercially viable process and significant research is still needed to reduce the amount of oxygen produced and to find a suitable organism to work with [19].

2.1.2.2 Anaerobic digestion

A process which uses microorganisms (bacteria) to break down biodegradable materials has also been studied and is known as anaerobic digestion, where the anaerobic digestion takes place in an oxygen free environment. Biofuel (a mixture of methane and CO₂) can be produced from a two-stage process. In the first reactor H₂ is produced from acidogenic bacteria breaking down biomass into H₂, acetic acid and CO₂. The second reactor uses methanogenic bacteria to convert two acetic acid molecules or H₂ and CO₂ to methane [49;50]. The process can be used to optimise hydrogen production over that of methane. However, the process requires specific bacteria depending on the type of material used, as well as very good control to ensure that the optimum conditions are maintained within each reactor [51]. There are currently over 200 anaerobic digestion plants operating in the UK and are combined with combined heat and power plants to produce over 170 MW of electricity [52]. Therefore, changes to plants are necessary to obtain hydrogen only.

2.1.2.3 Dark fermentation

A similar technology to anaerobic digestion is dark fermentation which uses anaerobic bacteria on carbohydrate rich substrates grown in the dark. The carbohydrates are produced from biomass such as cellulose agricultural waste, waste sludge from wastewater treatment plants, starch agricultural and food industry waste, which are hydrolysed by the microorganisms [53]. The biomass requires pre-treatment to remove unwanted materials and to biodegrade some of the material. This is then added to the fermentative bacteria which use the sugar such as glucose to produce hydrogen. Other products such as CO, CO₂ and H₂S are also produced depending on the feed. To obtain pure H₂, a cleaning step is required which adds costs to the process. This process is a fairly new one and more research needs to be

carried out to reduce the amount of by-products as well as to improve the efficiency [19].

2.1.2.4 Photocatalysis

Solar energy has also been considered for splitting water using photocatalysts for hydrogen production. The light is used to provide energy to the catalyst, which forms electron-hole pairs. The electrons are transferred through a band gap to the conduction band where the electrons can be used for splitting water. Many potential catalysts have been studied such as TiO₂, RuO₂/zeolite Y, RuO₂/PbWO₄, cadmium sulphide and zeolite-based catalyst from TiO₂, heteropolyacid and cobalt [54]. It has however, been shown that cadmium sulphide based photocatalysts have been oxidised and corroded due to photogenerated holes [55]. Although the studies into this area have been increasing, the current technology is not efficient for large scale H₂ production.

It has been shown that there are a number of technologies at different stages of research and development and those which are commercially available that have the potential to produce hydrogen. The most advanced technologies such as SMR and gasification use hydrocarbon-based fuels to extract hydrogen, however produce CO₂, which has detrimental consequences to the environment. Alternative technologies that use bacteria or algae require more research and control in order to limit by-products, improve efficiency and scale up for large scale hydrogen production. Therefore, this study focuses on using electrolysis as a sustainable option for producing hydrogen.

2.2 Electrolysis of water and steam

2.2.1 Low temperature electrolysis

Research into alkaline electrolyzers includes developing new electrode materials, testing variables of temperature and pressure and creating pilot plants in order to reduce costs and improve performance. Electrode materials have been tested based on Ni, such as Ti-Ni, Ni-Co-LaNi₅ and Ni-Fe to reduce the costs of expensive traditional electrode materials such as Nickel and C-Pt [56]. To reduce costs alternative electrodes such as Nickel-Molybdenum-Resorcinol-Formaldehyde (Ni-Mo RF) carbon catalyst have been tested. The results showed a promising reduction in cell losses from 310.7 Ω cm⁻² with C-Pt to 206.1 Ω cm⁻² for Ni-Mo RF [57]. Ni-Mo alloys developed for electrodes have shown significant cost improvements of up

to 20 % [58]. Further testing of Ni electrodes by means of mechanical polishing and electrochemical deposition was conducted in a 0.5 M KOH solution at 30 °C. Results show a reduction in overpotential by polishing the Ni electrode with sandpaper P400, thereby achieving overpotentials of 422 mV at 750 A m⁻² [59].

The main variables of electrolysis operation are temperature and pressure. The performance of alkaline cells with increasing pressure from 5 to 25 atm reduces efficiency from 82.4 % to 80.5 %, respectively, due to the energy consumption increasing. However, increasing temperature with constant pressure shows increasing efficiencies. The temperature and pressure results show that increasing temperatures provides better electrolyser performance, and agrees with theory [60].

Alkaline electrolysers have also been used for a number of pilot projects globally for continuous hydrogen production. The pilot projects consist of alkaline electrolysers in combination with PEM fuel cells and a renewable energy source such as solar PV-cells and wind technologies [61]. Although temperature improves the electrolyser performance, it was seen that for an integrated system ambient temperatures were favourable as the demand on auxiliary equipment was lower and the efficiency of hydrogen production improved by 12 % from 80 °C to 23 °C [61]. Combining alkaline electrolysers with solar PV cells shows that the system is limited to times of the day with high solar irradiance and has the ability to produce 20.5 l in a 9 hr period [62]. Further research is required in the area to further these preliminary results.

The use of alkaline electrolysers to enhance hydrogen production from a coal gasification power plant with carbon capture technology has been studied by Herdem *et al* [63]. By introducing alkaline electrolysers to the power plant and using electricity directly from the power plant, a system energy efficiency of around 58 % was achieved and a 4 % increase in hydrogen production [63]. The study does not consider the use of water from the plant, only the use of electricity. Combining alkaline electrolysers to create a hybrid wind-photovoltaic (PV) system has also been considered as a way of producing hydrogen from renewable sources of power. The study indicates that the production rate of hydrogen is dependent on the power produced by the renewable energy sources. For a hybrid wind-PV system combined with a 10 kW alkaline electrolyser, 10,462 mol of hydrogen can be achieved per week by combining nominal power of 10 and 6.1 kW from the wind turbines and solar photovoltaic cells, respectively [64].

Alternative low temperature electrolyzers to commercially available alkaline cells are proton exchange membrane (PEM) electrolyzers. The electrolyte is based on a polymer, which conducts protons and therefore produces hydrogen at one electrode and has water and oxygen at the other, as discussed in chapter 1 [65]. As with alkaline cells, temperature is a key factor to improving PEM performance [66]. The operating pressure of between 30 and 45 atm for PEM electrolyser has shown to reduce costs as the need for hydrogen compression for storage is not necessary. Furthermore increasing temperature and pressure has shown improved performance of the electrolyser [67;68]. However, increasing pressure above 100 atm may result in cross-permeation, which limits the use of PEM cells [65].

Recent research conducted intermediate-temperature tests of Solid Oxide-PEM cells, operating at a range of between 500 and 800 °C. The electrolytes, which were made of doped barium cerates, $\text{BaCe}_{0.9}\text{Y}_{0.1}\text{O}_{3-\delta}$ (BCY10) and doped barium zirconates, $\text{BaZr}_{0.9}\text{Y}_{0.1}\text{O}_{3-\delta}$ (BZY10) showed promising preliminary results. BYC10 was noted to perform well as a reversible electrolyser [25]. However, intermediate-temperature PEM cells are far from commercialisation as further research into improving the hydration of the cell for more efficient proton conduction is needed. Furthermore, platinum was used as the electrode material which is suitable but costly and therefore, further work is being done to find a suitable material for the electrodes [20;25].

Due to the expensive precious metals used in the electrodes an electrocatalyst support has been implemented to increase the number of crystallisation sites to create a uniform distribution of electrocatalyst particles as well as to increase the surface area [69]. Furthermore, the support enhances electrocatalytic activity and size of the electrocatalyst particles. Usually the support is formed of carbon; however, carbon tends to corrode quickly. Solutions to the carbon support have been SnO_2 , which can improve performance, however, also increases ohmic overpotentials [70;71]. Using materials such as IrO_2 supported on TaC, which are conductive, reduces the ohmic overpotentials and allow for enhanced PEM electrolyser performance [69]. It was shown that 70 wt. % IrO_2 on TaC can improve PEM electrolyser performance by 36 % compared with unsupported IrO_2 , through optimising the precious metal load [69]. Using bi-metallic ($\text{Ru}_{0.9}\text{Ir}_{0.1}\text{O}_2$) rather than tri-metallic ($\text{Ru}_{0.85}\text{Ir}_{0.05}\text{Ti}_{0.1}\text{O}_2$) oxides for electrodes has shown improved PEM electrolyser performance. At 25 °C and 5,000 A m^{-2} , voltages of 1.8 and 2.2 were seen with bi-metallic and tri-metallic oxides,

respectively [72]. Through further electrode development, PEM electrolyzers may become more cost effective.

Combining PEM electrolyzers with renewable electricity producers has been researched and results showed successful output of 2 kW of power from a stack of 14,100 cm² area [73]. The results show the possibility of utilising renewable energy sources for hydrogen production and take into account the balance-of-plant, which focus on not only the source of electricity but the ancillary units needed for electrolysis as well. For a 1 kW, 10-cell stack PEM electrolyser, it was seen that system efficiencies of 60 and 65 % can be achieved at 75 and 40 °C, respectively. However, the stack efficiency decreased from 88 to 86 % at electrolyser temperatures of 75 and 40 °C, respectively. The improvement in system efficiency with decreasing temperature is due to a reduced energy requirement of heating the system [74]. Therefore, using low temperature electrolyzers for hydrogen production is feasible, more study is necessary to improve the cost of materials and system efficiency.

2.2.2 High temperature electrolysis

High temperature electrolysis refers to solid oxide electrolyzers (SOECs), which operate at temperatures of between 500 and 1,000 °C, as discussed in Chapter 1. The advantages of reduced electrical energy, due to the elevated operating temperatures, and therefore improved efficiency compared with low temperature electrolyzers has created further options for producing hydrogen at a cost competitive with steam methane reforming.

Many studies have considered SOECs for hydrogen production through steam electrolysis [75-77]. Studies have shown that a SOEC with a 10 mm dense YSZ film on porous NiO-YSZ support operating at 850 °C produces an open circuit voltage (OCV) of 1.069 V. Furthermore, current densities of 6810 A m⁻² can be achieved at 1.5 V [78]. However, such results are dependent on variables such as sintering temperature of the YSZ electrolyte, which affects the density of the electrolyte. At low sintering temperatures of 1300 °C, the electrolyte cannot be densified and at high temperatures of 1500 °C the pores of the electrodes are minimised [78]. The preparation of the cell, including electrode thickness, sintering temperature and porosity can impact the performance of the cell.

The elevated temperatures of SOECs require specialised ceramic-metal composites suitable for the operating temperature. Studies have developed suitable electrolytes such as yttria stabilised zirconia (YSZ), the most common as well as ceramics based on ceria and scandia. $\text{La}_{0.6}\text{Sr}_{0.4}\text{Co}_{0.2}\text{Fe}_{0.8}\text{O}_{3-\delta}$ (LSCF) anode with $\text{Gd}_{0.2}\text{Ce}_{0.8}\text{O}_{2-\delta}$ (GDC) as an interlayer, combined with YSZ electrolyte was studied to understand the stability of the materials [79]. Operating the SOEC at 800 °C for 100 hrs at 8,000 A m^{-2} showed that delamination generally seen with electrode-electrolyte interface can be reduced by introducing an interlayer and sintering at appropriate temperatures of 1,400 °C [79]. Introducing a GDC interlayer can also provide more stability for long term SOEC use [80]. For an SOEC consisting of Ni-YSZ (cathode) / YSZ / GDC (electrolyte) / LSCF (anode) and operating at 776 °C and 10,000 A m^{-2} , a degradation rate during the first 7,600 hrs (of 9,000 hrs) was 3.0 % hr^{-1} [80]. Degradation occurring in SOECs need to be investigated further to enhance the life of the cells in order to become a commercially viable option to meet future hydrogen production targets.

Although high temperature SOECs can produce good performance, heating steam to elevated temperatures and producing materials to meet the conditions can be costly. Therefore, intermediate temperature operation using NiO-ScSZ (cathode) / ScSZ (electrolyte) / LSCF-CGO (anode) SOEC can provide an alternative to high temperature SOEC operation. The SOEC system consisting of the electrolyser, pumps, heat exchangers and H_2 blower gave an overall efficiency of 83 % [81]. Such efficiencies show that intermediate-temperature SOECs may be able to produce hydrogen in a cost effective manner.

Stacks, which are many electrolyser cells connected together in a modular arrangement, have been developed and tested to produce large amounts of hydrogen. A 30-cell SOEC stack operating at 800 °C and at a current density of 1,500 A m^{-2} , based on traditional Ni-YSZ (cathode) / YSZ (electrolyte) / LSM-YSZ (anode) has shown to achieve an efficiency of 87.4 % from a study by Zheng *et al.* [82]. Based on an active area of 0.189 m^2 , the SOEC was able to produce 103.6 l h^{-1} of hydrogen. However, degradation occurred due to delamination while carrying out durability testing, which resulted in poor performance. Improvements in the durability of the SOECs may provide a suitable option for large scale hydrogen production. Stack testing carried out by Zhang *et al.*, on a Ni-ceria (cathode) / scandia-stabilized zirconia (electrolyte) / LaCoFe oxide based perovskite (anode) has shown an

improvement in stack operation to over 1,000 hrs through improving SOEC materials, interconnect coating and electrolyte-electrode interface microstructures. Degradation of 5.66 % hr^{-1} was seen at low current density of 2,500 A m^{-2} and 4.62 % hr^{-1} at 3170 A m^{-2} [83].

More recent studies have focused on using SOECs to electrolyse CO_2 or a combination of steam and CO_2 known as co-electrolysis have also been studied for producing CO and syngas, respectively. One study used $\text{Cu-Ce}_{0.9}\text{Gd}_{0.1}\text{O}_{2-\delta}$ (cathode) / $\text{Ce}_{0.8}\text{Gd}_{0.2}\text{O}_{2-\delta}$ (electrolyte) / $\text{Ba}_{0.5}\text{Sr}_{0.5}\text{Co}_{0.8}\text{Fe}_{0.2}\text{O}_{3-\delta}-\text{Ce}_{0.8}\text{Gd}_{0.2}\text{O}_{2-\delta}$ (anode) at intermediate-temperatures (600 – 700 °C) and showed that CO can be produced without deactivating the catalyst. At 700 °C and 780 A m^{-2} , an SOEC efficiency of 32 % was seen. Though the study has developed a pathway toward syngas production from electrolysis at intermediate temperatures, the amount of syngas produced and efficiency were low. Improvements in the system and operation at intermediate temperatures are needed to increase syngas yield [84].

The use of CO_2 electrolysis was initially investigated for use in space and expeditions to Mars; it is now being investigated for the producing syngas for synthetic fuel production. Based on standard SOEC materials such as Ni-YSZ / YSZ / GDC / LSCF operating conditions of greater than 700 °C resulted in improved performance and eliminated the problem of coking seen at 650 °C; furthermore, concentration of over 50 % CO_2 is required to enhance performance [85]. However, concerns over pressure build-up, which can lead to delamination of electrodes may hinder progress of commercialising SOEC technology.

Using flue gas or CO_2 from industrial plants with steam for co-electrolysis has been studied. An SOEC comprised of LSV-YSZ (cathode) / YSZ (electrolyte) / LSF-YSZ (anode) was tested at 800 °C under steam, CO_2 and co-electrolysis (CO/CO_2 (30 % H_2O)) conditions. It was seen that the best performance of the SOEC was produced under co-electrolysis conditions and steam electrolysis. Therefore, using SOECs for dry CO_2 electrolysis requires further research to enhance performance [86;87]. The steam electrolysis reaction was also seen to give a better performance with conventional materials (Ni-YSZ (cathode) /YSZ (electrolyte) /LSM (anode)) over CO_2 electrolysis; with OCV of 962 mV for steam and 959 mV for CO_2 electrolysis [31].

Studies have focused on developing the materials for solid oxide electrolyzers as well as optimising operating conditions and cell preparation. In addition, the trend toward utilising captured CO₂ has been studied. The focus of research to date has been optimising the SOEC itself rather than the overall system. This study aims to source hot water and steam from industrial sources to provide a way of alleviating SOEC energy requirements and thereby reducing costs. It further seeks to combine SOECs with coal fired power plants to utilise the steam and electricity needed for SOEC operation from one source. The focus of this study is to assess the feasibility of an integrated system for hydrogen production. However, it should be noted that the technology can also be used to support syngas production.

2.3 Products of electrolysis

Electrolysis of steam, shown in the above sections produce valuable products of hydrogen, CO and syngas from steam, carbon dioxide and co-electrolysis, respectively; with oxygen as a useful by-product [38;88].

Hydrogen is used in a variety of applications other than as an alternative fuel, such as the food industry for increased saturation in oils and fats which increases their melting points and resistance to oxidation. The nuclear industry uses H₂ for O₂ removal as O₂ can cause stress corrosion cracking and power stations use it as a coolant for its generators due to its high thermal conductivity. H₂ is also used in the pharmaceutical and plasma industries. Therefore, pure hydrogen is a valuable resource [15].

Syngas produced from co-electrolysis of CO₂ and steam can be used to produce ethanol and methanol or in the Fischer Tropsch process for the production of synthetic hydrocarbons [15;89]. The process is very well known and has been used to produce synthetic fuels in South Africa for over 50 years [90]. The Fischer Tropsch reaction requires a feed of H₂ to CO with a ratio of 2:1 which can be achieved from electrolysis with controls in place. The process can be used to produce synthetic diesel, which can be used in place of diesel itself. The fuels produced are cleaner than fossil fuels as it has been seen that the nitrogen dioxide, carbon monoxide and particulate matter emissions are less than diesel. Using fuels produced by the Fischer Tropsch process would mean that the use of fossil fuels can be extended and therefore may see a reduction in emissions. Furthermore, the current

infrastructure can be used without the need for change [90]. Therefore, providing syngas for this purpose would be beneficial.

2.4 Conclusions

In conclusion, literature has shown that there is a trend away from optimising low temperature electrolyser materials and towards high temperature SOECs to take advantage of the thermodynamic characteristics. For SOECs to become competitive with SMR and hydrocarbon-based fuels, an improvement in SOEC efficiency is needed. Furthermore, the use of fuels such as coal for electricity generation could be furthered by introducing SOEC technology to industrial processes to create a way for hydrogen to be produced and used as an alternative fuel to petroleum products. In order to understand the commercial viability of electrolyzers the economics associated with the process must be analysed; especially to indicate whether hydrogen can be produced competitively.

The more recent research has focused on hybrid electrolyser systems using the more established alkaline and PEM electrolyzers and combining with renewable energy sources. However, to take advantage of thermodynamic properties of the process, alkaline and PEM electrolyzers are not suitable to be used in chemical plants due to their low operating conditions of 80 °C. SOECs show promise; however, the literature has focused very much on the materials development at high temperatures. Therefore, this study aims to use already developed materials favoured in literature and assess the viability of using SOECs as part of an industrial application. The study aims to understand the positive aspects and limitations of the materials as well as to seek areas for development in order to facilitate hydrogen production on a large scale.

3 Techno-economic analysis

Understanding the economics of available fuel production processes is essential in order to provide a profitable and competitive contender in hydrogen for alternative fuels. Solid oxide electrolyzers combined with renewable technologies have been studied as a way to produce 'clean' fuels. The costs associated with such combinations compared with available hydrogen production technologies will be considered in this chapter. The techno-economic analysis aims to identify suitable heat and electricity generators as options for integration with solid oxide electrolyzers and considers the costs associated with the technologies in order to assess the economic situation of the current market.

3.1 Supplying power and heat to electrolyzers

In addition to steam, electrolyzers rely on electrical power for their operation; running costs are therefore directly related to the electrical efficiency and the cost of power. The source of the power will dictate the operating costs as well as the environmental impact, depending on the carbon intensity of the technology. The source of power is therefore important if electrolyser technology is to compete with steam methane reforming (SMR), which has been used as the baseline; where, hydrogen is produced at 2.50 \$ kg⁻¹. The following describes the possibility of integrating electrolyzers with power generation sources.

3.1.1 Electrical power from renewable and nuclear sources

Integrating electrolyzers with power generators has been considered by a number of researchers. The most frequently discussed has been the use of electrolyzers with nuclear, wind and solar power. Many renewable sources of power generation rely on unpredictable sources, such as wind and solar, which pose problems as the amount of energy that can be produced varies with season, location and time of day.

3.1.1.1 Wind

Power produced from wind turbines is currently the fastest growing renewable energy industry with 283 GW of wind total installed capacity globally in 2012, which is expected to rise to 540 GW by 2017 [91]. In parts of Europe such as Denmark, almost 25 % of energy is produced from wind turbines.

The technology harnesses wind to do mechanical work by rotating blades on a turbine, which rotates a generator for power [15]. Although growth has been

significant, problems such as loading, intermittency and integration with the grid, still remain. Research has been carried out into the use of combining electrolysis with wind power generators. There are two main scenarios for using electrolyzers; one is to produce H₂ in times of high power generation and low electricity demand, and the other is to continuously use the energy for H₂ production [15;92]. This provides a solution to the problems being experienced. In addition to improving efficiency, flexibility and dispatchability, surplus H₂ can be sold as fuel or as a process component. However, the costs associated with H₂ production have been shown to be prohibitive compared to mature H₂ generation technologies such as SMR [92].

The combination of electrolyser with wind generators works by controlling the energy produced in the wind turbine to ensure the requirements for electrolysis are met and excess power can be supplied to the grid. The H₂ can be stored using metal hydrides as it does not have an effect on the load consumption and can be used in fuel cells to meet grid requirements or can be sold. The auxiliary power supply, which can be a hydrogen internal combustion engine or a fuel cell, is necessary to ensure that the electrolyser is supplied with the correct amount of energy at all times. The stored hydrogen can be used to generate power for the electrolyser during times when the wind turbine is not producing sufficient energy. This is shown in Figure 3-1. The dotted lines represent connections that are possible but not necessary [15].

The continual and predicted growth of the wind technology market shows that there is promise for wind plants to be a viable option long-term for combining with electrolyzers for hydrogen production [93]. Furthermore, wind generator efficiency, flexibility and dispatchability can be improved in such combinations.

The costs associated with the technology have been assessed by a number of sources. Jorgensen and Ropenus [92] showed that the cost of producing H₂ to be a minimum cost of 6 – 6.6 \$ kg⁻¹, based on buying electricity from wind at an average cost of 5.1 US¢ kWh⁻¹ and taking into account the capital, variable and operating and maintenance (O&M) costs of 234 × 10³ \$ MW⁻¹. These costs are based on using low temperature electrolysis with demineralised water as the feed.

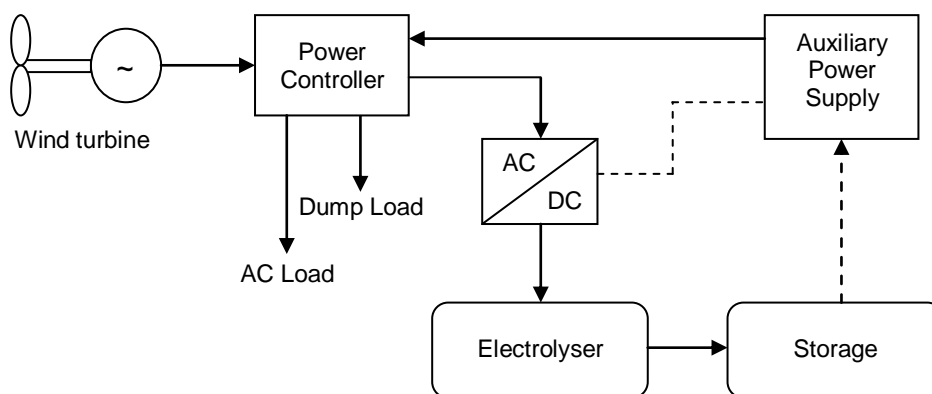


Figure 3-1 Integrating a stand-alone wind energy generator with an electrolyser, adapted from Ref. [15].

Further studies have been carried out on the variation in cost of producing electricity depending on the wind speed. The cost of electricity in this case is 4.5 and 1.89 US¢ kWh⁻¹ at average wind speeds of 6.7 and 8.9 m s⁻¹, respectively [94]. The cost of producing H₂ based on the operating costs of the electrolyser is shown in Table 3-1. It can be seen that the higher the wind speed, the lower the cost of electricity which is beneficial for a process such as electrolysis where costs are directly dependent on the cost of electricity. However, the wind speeds cannot be predicted accurately, which poses a problem when costing power for the use in electrolysis.

As wind energy production grows it will be possible for electrolysers to be integrated with the wind plant as a flexible way of producing hydrogen and storing energy. It has been predicted that in places such as Scandinavia, wind energy will become the predominant source of power once nuclear and conventional power stations have been decommissioned [95].

Table 3-1: Costs associated with producing H₂ from electricity produced by wind energy, adapted from Ref. [94].

| SOEC Temperature (°C) | Voltage at 0.1 A cm ⁻² (V) | Cost of producing H ₂ (\$ kg ⁻¹) |
|-----------------------|---------------------------------------|---|
| 25 ^a | 1.60 | 3.17 |
| 25 ^b | 1.60 | 1.89 |
| 1000 ^a | 1.00 | 2.84 |
| 1500 ^a | 0.63 | 2.11 |

^a Wind speed of 15 mph, ^b Wind speed of 20 mph

3.1.1.2 Solar

The use of solar power has been investigated as a renewable power generation source for providing electricity for both alkaline and solid oxide electrolyzers. Concentrated solar energy using a central receiver system made of honeycomb structured ceramics has been proposed. The ceramic enables solar radiation to be absorbed as well as being a reactor for energy generation [96].

Although solar photo-voltaic (PV) cells have been investigated as an energy provider, they are currently not able to compete with other technologies due to the low efficiencies and high costs; therefore, the use of solar towers with large fields of heliostats is the preferred choice of utilising solar energy in combination with electrolyzers [97].

The analysis given in Table 3-2 shows the costs of producing H₂ based on operating costs obtained from Ref. [94]. It shows that as the efficiency of solar technology increases, the costs will decrease and the cost of producing H₂ will, therefore, become more competitive. Once again it can be seen that at higher temperatures the cost for H₂ production decreases, due to the thermodynamics of the electrolysis reaction. Therefore, the use of high temperature SOEC would be a suitable option in economic terms for integrating electrolyzers with power sources for more competitive H₂ production.

Further research has shown that hydrogen can be produced at a cost of 9.15 \$ kg⁻¹ in the current market by using an alkaline electrolyser with solar energy at the scale of 50 MWe. This cost takes into account the investment and operating costs of the electrolyser as shown in Table 3-3 [96]. This is a significant improvement from earlier studies which have concluded that the cost of hydrogen would be around 14 – 15 \$ kg⁻¹ using solar PV panels due to the very low efficiencies of 6 % [98].

Table 3-2: Costs associated with producing H₂ from electricity produced by solar energy, adapted from Ref. [94].

| SOEC Temperature (°C) | Voltage at 0.1 A cm ⁻² (V) | Cost of producing H ₂ (\$ kg ⁻¹) | |
|-----------------------|---------------------------------------|---|-----------------|
| | | 15 % efficiency | 20 % efficiency |
| 25 | 1.60 | 8.01 | 6.19 |
| 1000 | 1.00 | 6.40 | 5.04 |
| 1500 | 0.63 | 5.31 | 4.22 |

One of the main reasons for the high cost of producing hydrogen with solar power is due to the additional equipment required for processes such as solar PV panels, where AC converters are required to connect to the grid as well as power lines for providing energy to the electrolyzers. Removing AC converters and operating the PV panels at the same voltage as the electrolyser has shown to improve the efficiency of stand-alone PV-electrolysers, thereby making renewable energy sources much more competitive and thus reducing the cost of hydrogen production [98]. Furthermore, it has been shown that increasing the temperature of a PEM electrolyser and combining it directly with PV solar panels would increase the efficiency of the overall process [98]. However, this only resulted in hydrogen production efficiencies of 12.4 %. This is a marked improvement in efficiency but not enough to become competitive in the current market.

3.1.1.3 Heat and power from nuclear fission

Nuclear power stations have been proposed as a source of both power and heat to raise steam for high temperature electrolyzers, as shown in Figure 3-2. High temperature gas-cooled reactors (HTGR) are considered to be the most appropriate type of nuclear reactor for this purpose due to their high temperature of operation as the HTGR can produce steam required for electrolysis at temperatures of 600 – 800 °C [15;23].

HTGR using helium operates by heating helium in the reactor to 900 °C, from where it then goes on to the turbines and does work. Some of the heat from the helium can be used to raise steam to service a high temperature electrolyser, with the high temperatures available increasing the efficiency of the process. In addition, the water used in the nuclear plant would be demineralised and therefore pure hydrogen can be produced without impurities [23;99]. However, such reactors are not currently available although plans are still being made for pilot plants in the USA. Commercially available HTGRs using either water or carbon dioxide can achieve temperatures of around 500 °C, which can enable intermediate temperature electrolysis [100].

Table 3-3: Comparison of costs based on solar and nuclear power generators, adapted from References [96;99;101].

| | Investment (M\$) | Operating and Maintenance (M\$ year ⁻¹) | Electricity (M\$ year ⁻¹) | Water (M\$ year ⁻¹) | H ₂ Production (\$ kg ⁻¹) |
|-------------------------------------|---------------------|--|--|------------------------------------|---|
| Solar PV^a [96] | 13.00 | 38.68 | 22.55 | 0.05 | 9.15 |
| Nuclear^b [99;101] | 5.82 | 2.09 | 0.12 | 0.03 | 3.23 |

^a Values are based on alkaline electrolyser producing 2,464,000 kg of hydrogen per year in 2008

^b Values are based on SOEC electrolyser and have been amended for comparison for producing 2464000 kg of hydrogen per year in 2009

O'Brien *et al.* (2010), suggested that if a 600 MWth helium-cooled HTGR is used in combination with an SOEC, hydrogen generation can be achieved at 3.23 \$ kg⁻¹; at this cost, the process starts to become competitive with H₂ produced from SMR at around 2.50 \$ kg⁻¹ which is significantly less than that for low temperature electrolysis where H₂ is priced at around 4.15 \$ kg⁻¹. The majority of the costs are associated with the capital investment (2.36 \$ kg⁻¹); the costs of fuel and maintenance were shown to be 0.57 \$ kg⁻¹ and 0.28 \$ kg⁻¹, respectively, based on fixed and variable costs [99]. The electrolyser unit itself has been priced at 200,000 \$ MW⁻¹ for a unit with around 4,000,000 cells with each cell having an active surface area of 225 cm² [101].

When comparing the economics of an alkaline electrolyser combined with solar energy, and a SOEC with nuclear, it can be seen that using nuclear energy is much more economical as power generation is cheaper. Table 3-3 shows the costs based on producing 2,464,000 kg of H₂ per year. It does not take into account the size of the electrolysers. However, these values show that SOECs require less electrical energy to produce the same amount of H₂ per year than alkaline electrolysers. Furthermore, the overall operating costs of a SOEC are lower in comparison to alkaline cells, mainly due to the reduced costs of power generation from nuclear plants. Therefore, the SOEC is shown to be potentially more economical than alkaline electrolysers when combined with nuclear power.

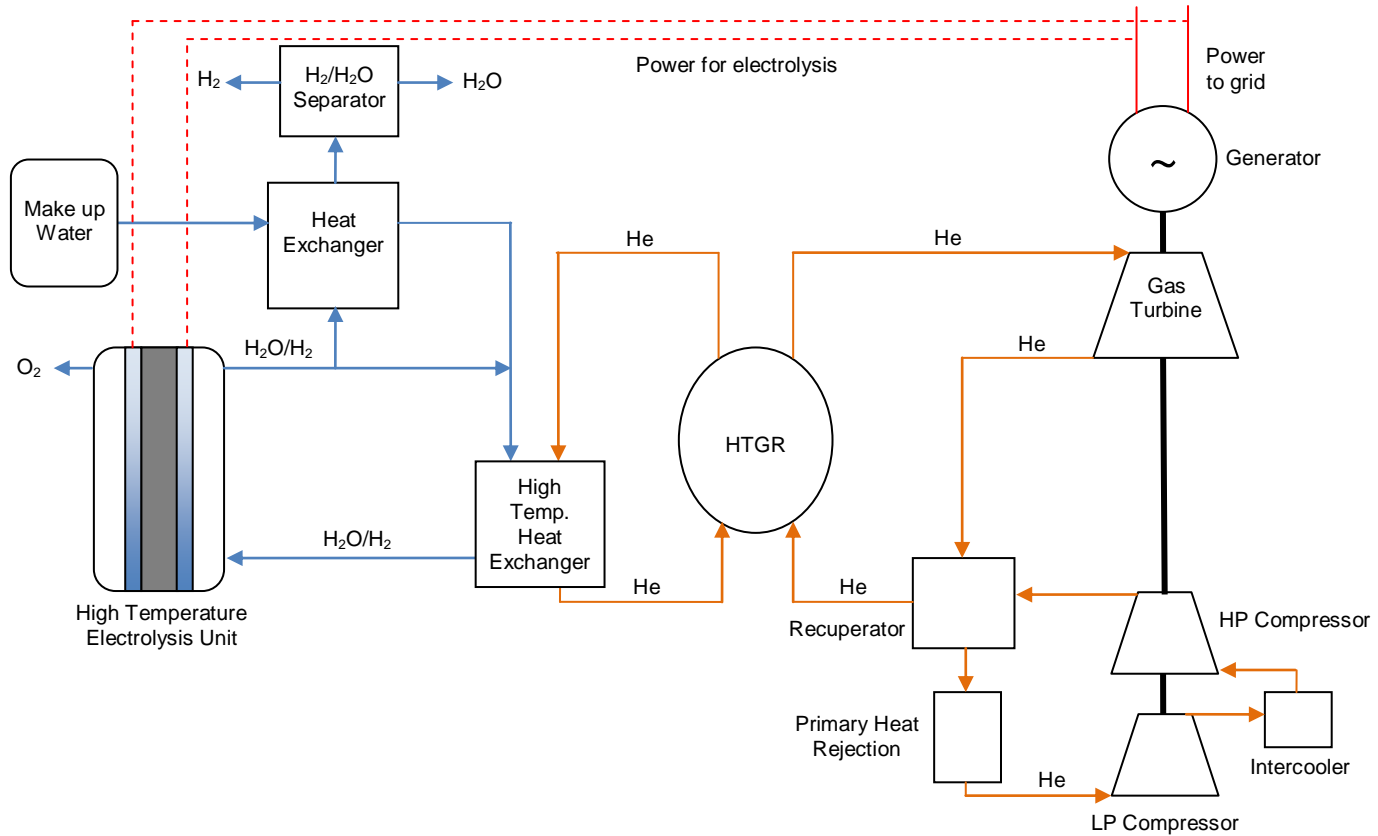


Figure 3-2: Nuclear power plant with electrolysis of steam [23].

The possibility of the integration of electrolyzers with nuclear power stations is a step towards the so-called hydrogen economy [102]. It is advantageous as the costs predicted for the future have shown that electricity from nuclear power plants will become far less expensive than other technologies. Furthermore, plans for building new nuclear power stations are being made across the world enabling electrolyzers to be included in future designs.

3.2 Techno-economic comparison of hydrogen generation technologies

The cost of hydrogen production directly from hydrocarbons is governed by the price of the feedstock. The main cost associated with electrolyzers is the cost of electrical power, which varies significantly depending on the source of the electricity. Currently, carbon-based power production from coal or gas fired plants are cheaper than renewable energy sources. The increasing costs of hydrocarbon fuel, implementation of carbon taxes, and the volume of manufacture of renewable technologies will act to narrow this margin. The relative cost of low-carbon hydrogen produced by electrolysis of water powered by renewable electricity will therefore decline.

3.2.1 Cost of electricity production

There are many power generation technologies that can contribute to the energy mix of a country and these are essentially divided into those which use fossil fuels and those which are renewable technologies. The fossil fuel based technologies include coal fired power generators such as pulverised fuel (PF), circulating fluidised bed (CFB) and integrated gasification combined cycle (IGCC) power plants. Gas fired generation include open cycle gas turbine (OCGT) and combined cycle gas turbine (CCGT) power plants.

Renewable sources of power include nuclear, wind (onshore and offshore), biomass, wave, marine and solar energies [103]. The cost of producing power is based on a large number of factors such as capital, finance and operating costs. Due to the nature of some power generation plants, such as those burning fossil fuels, these costs are also affected by carbon taxes [104].

Table 3-4 shows the cost of generating electricity from different sources, as described by various reports. The study carried out by the Royal Academy of Engineering in the UK in 2004, shows the cost of generating power at the site and does not take transmission and distribution costs into account. The data provided by the Energy Information Administration (EIA) represents predictions of the future costs of various technologies in 2016, and shows that costs will increase in the future in the USA [104]. The data takes into account financial incentives given by the US government such as tax credits to relevant power plants as well as around 0.015 \$ kg⁻¹ carbon taxes. These data also include transmission costs; however, they do not take into account the costs for stand-by and storage units for intermittent resources such as solar and wind energy. The cost of power generation as stated by the National Research Council (NRC) takes into account financing, capital, fuel and operating costs. The data shows a range of costs where the low level costs indicate plants which benefit from the Department of Energy's loan guarantee program [104]. The data is based on predictions and therefore, the uncertainty in the value of carbon taxes, changes in cost of raw materials and the effect of changes to the energy market may have an effect on the predictions.

The higher end values of the range represent the costs associated with carbon taxes estimated at \$54 per tonne of CO₂ for the coal and gas fired processes [103]. The taxes increase the cost of power generation on these technologies so much that

renewable energies become competitive. Therefore, the investment in carbon capture and storage processes would be an aid to relieving the taxes.

It can be seen from Table 3-4 that wind power is close to being competitive with mature technologies as it is one of the fastest growing energy generators in the UK. However, the problem of intermittency has meant that stand-by power generators are necessary to ensure that wind energy can be integrated with the grid.

The prices of wind power vary significantly once stand-by generators are considered. The integration of electrolyzers and fuel cells will enable the power generated to be stored as hydrogen, which can be converted back to electrical power when required. Therefore, a stand-by power generator is not required. Furthermore, costs will be reduced as the impact on the environment is reduced [103].

Using power for electrolysis from coal fired or gas fired power plants is one of the most cost effective options as both the feed (i.e. steam) and power can come from the same source. As seen in Table 3-4, the costs in terms of power would only be economical by using nuclear in the future; however, the source of the feed will need to be found for electrolysis. Currently, producing hydrogen from renewable energy sources is not economically viable; a study has shown that the production costs of H₂ using electricity generated by nuclear, wind, hydropower, geothermal, solar PV and solar thermal are 3.68, 8.14, 7.63, 9.33, 76.30 and 13.56 \$ kg⁻¹, respectively [21]. This data shows that solar PV cells are not currently competitive; however, sourcing electricity from wind and nuclear energy may be economically viable. Moreover, if waste streams from chemical plants were to be used as the feed to the electrolyser, then industrial prices for electricity will need to be paid to the grid. Currently, the average cost of electricity for large, medium and small industrial companies is 11.9, 12.2 and 15.6 US¢ kWh⁻¹, respectively in the UK [105].

As the economic viability of electrolysis is dependent on the cost of electricity, it has been shown that the most suitable form of electricity is from hydrocarbon-based or nuclear plants. Until electrolyser technology improves or the costs of renewable energy decreases, combining electrolyzers with renewable energy is not cost effective.

Table 3-4: Cost of producing power from various sources.

| Power Plant | Royal Academy of Engineering [103] | EIA [104] | National Research Council [104] |
|---------------------|------------------------------------|-----------------------|---------------------------------|
| | US¢ kWh ⁻¹ | US¢ kWh ⁻¹ | US¢ kWh ⁻¹ |
| PF | 4.5 – 9 | 9.5* | 5 – 9 |
| IGCC | 5.8 – 9.4 | 12.3* | 9 – 15 |
| OCGT | 5.6 – 8.7 | 8.4* | 10 – 16 |
| CCGT | 4 – 6.2 | 11.6* | 14 – 21 |
| Nuclear | 4.2 | 10.7 | 6 – 13 |
| Biomass | 12.3 | 10.7 | 8 – 10 |
| Wind – onshore | 6.7 – 9.8 | 14.2 | 4 – 10 |
| Wind – offshore | 10 – 13 | 23.0 | 5 – 18 |
| Solar Photo Voltaic | N/A | 39.6 | 14 – 30 |

* Costs include carbon taxes estimated at \$54 per tonne of CO₂.

3.2.2 The cost of producing hydrogen from hydrocarbons

The cost of producing hydrogen based on steam methane reforming varies depending on the size of the plant, price of methane as well as whether the plant has carbon capture and storage options. The costs associated with hydrogen production from SMR and conventional hydrocarbon gasification is predicted to rise as shown in Table 3-5. This is predominantly due to the carbon taxes imposed on such industries in order to meet carbon emission targets [42]. Including CCS would add to costs as more stages are required than conventional SMR; however, implementing CCS has shown a reduction in costs over time as the tax burden is reduced [42].

Other than the increasing costs, concerns over energy security have risen over the use of natural gas. This means that having a mix of technologies limits the dependency on the supply of natural gas. Thus, the addition of electrolysis for hydrogen into the energy industry will contribute power generation without the need for relying on the supply of raw materials from other countries.

Table 3-5: Costs of producing H₂ from conventional methods, adapted from Reference [21].

| | Cost of H ₂ Production (\$ kg ⁻¹) | | | | |
|-------------|--|--------------------------------|-----------------------------|---------------------------------|---------------------------------------|
| | Conventional SMR (medium scale) | Conventional SMR (large scale) | Conventional SMR (with CCS) | Coal Gasification (large scale) | Advanced Coal Gasification (with CCS) |
| 2007 | 3.68 | 1.46 | 1.70 | 1.46 | 1.78 |
| 2020 | 3.90 | 1.71 | 1.88 | 1.42 | 1.47 |

3.2.3 Comparison of hydrogen generation as a function of technology type and cost

From the analysis above, it can be seen that the costs of operating an electrolyser is directly related to the price of electricity. The efficiency of the water electrolysis process can be implied from the ASR of a cell. The overpotential of a process is determined by the resistance of the electrodes and electrolyte and the resistance between the electrode and electrolyte. To account for the resistances, a larger amount of voltage above the open cell voltage is required for the process to occur, which therefore dictates the efficiency.

A summary of the results from studies of electrolysis based on different technologies and variables such as the type of electrolyte, temperature, pressure, materials, voltage and current is given in Appendix A1. It can be seen that operating an SOEC at high temperatures generally gives the lowest overall area specific resistance (ASR) and, therefore is likely to be more electrically efficient than PEM and alkaline electrolysers when realised at a practical technological scale.

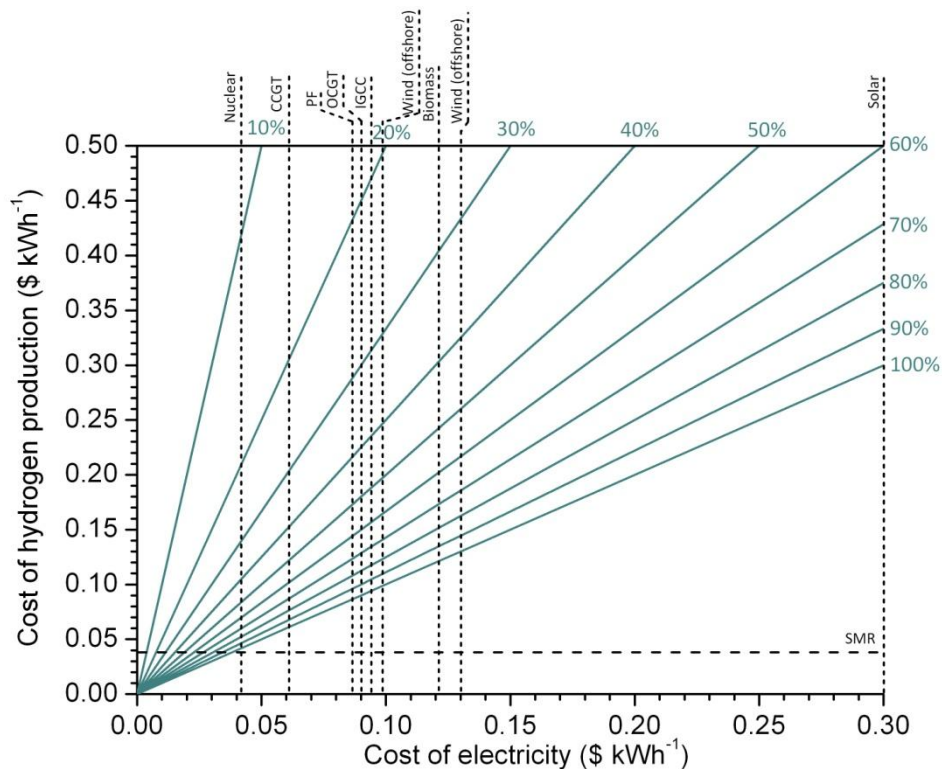


Figure 3-3: The relationship between the costs of electricity, efficiency of the electrolysis process (values around periphery of graph) and the resultant cost of hydrogen production.

Analysis neglects capital, maintenance and the cost of water feed.

Currently SOECs are not commercially available; however, plans for integration with nuclear power are driving market penetration [102]. This is due to the higher electrical efficiencies that can be attained in comparison to the current alkaline cells with efficiencies of up to 70 % [21]. Electrical efficiencies of up to 90 % have been published for SOECs [24], but this, of course, relies on a ‘free’ source of heat.

The relationship between electrolyser efficiency, cost of electricity from different generation technologies and the resultant cost of hydrogen production is summarised in Figure 3-3. The cost of electricity from different technologies is based on the values in Table 3-3 [103]. As shown in previous sections, the largest contributor to O&M costs is the electrical power. In comparison, the cost of maintenance and feed (i.e. water) is significantly smaller. Therefore, water feed and capital costs are not taken into account in this analysis.

It can be seen from Figure 3-3 that the standard representative cost of producing hydrogen is 0.04 \$ kWh⁻¹ for SMR. Therefore, for an electrolyser to be competitive the most suitable options are currently SOEC with high efficiencies (up to 90 %) using power sources such as CCGT and nuclear, where the cost of producing H₂ would be 0.07 and 0.05 \$ kWh⁻¹, respectively.

However, the high cost of most renewable technologies means that in the absence of a tax/incentive mechanism to reward low-carbon generation/hydrogen production cannot be cost competitive regardless of the efficiency obtainable from the electrolyser.

Table 3-6: Investment costs of electrolysers based on electrolyser type.

| Reference | Electrolyser Type | Capital Investment (\$ MW ⁻¹) | Electricity Source |
|---------------------|-------------------|---|--------------------|
| Meuller-Langer [21] | Alkaline | 4,663,000* | General |
| Sorensen [106] | Alkaline | 334,000 | Renewable |
| | PEM | 752,000 | |
| Jorgensen [92] | Low Temperature | 234,000 | Wind |
| Karlsson [95] | Alkaline | 147,000 | Wind |
| | PEM | 587,000 | |
| | SOEC | 734,000 | |
| Jensen [107] | SOEC | 350,000 – 550,000 | General |

*Costs include ancillary units and system inputs.

3.3 Capital costs

It has been seen that the main cost associated with electrolyser operation is that of the electrical power. However, the capital costs associated with electrolysers contribute towards costs and thus need to be taken into account when assessing the overall cost efficiency of an electrolysis process. The investment costs based on the electrolyser alone have been analysed by a number of researchers and a summary is shown in Table 3-6. The capital cost of electrolysers varies with scale and type.

Alkaline electrolysers are the most commercially mature of the technologies and their costs are therefore likely to be more accurate. SOEC costs are based on targets and estimates. From 2020, SOEC electrolysers are forecast to have an investment cost of 235,000 \$ MW⁻¹ [94].

3.4 Conclusions

The economic viability of electrolysis is crucial to implementing electrolysers for large scale production of hydrogen. It has been seen that the main costs associated with the production of hydrogen at the moment are the costs of natural gas and electrical power for steam methane reforming and electrolysis, respectively. Although the most economical and widely used technology is steam methane reforming, producing hydrogen at around 2.50 \$ kg⁻¹, the negative social and environmental impact from the process is significant. The greatest concern is the vast amounts of CO₂ emissions from plants without carbon capture and storage.

Furthermore, without retrofitting carbon capture and storage processes to the existing steam methane reforming plants, the amount of CO₂ emissions in the atmosphere will continue to grow. In the near future, these plants may be able to produce hydrogen competitively. However, as carbon taxes are implemented and the pressure increases by both the government and the public for more environmentally friendly methods of power production; steam methane reforming is likely to become more expensive.

Research into high temperature electrolysers has shown that solid oxide electrolyser cells have the possibility to produce hydrogen with electrical efficiencies of up to 90 % [28]. The most costly aspect of the process is buying the power, where combined cycle gas turbine plants have the lowest cost at 4 US¢ kWh⁻¹, and solar PV power the most expensive, costing around 30 US¢ kWh⁻¹. It has been shown that SOEC have an advantage over alkaline electrolysers as the power requirement is lower due to the

high electrical efficiencies afforded by high temperature operation. In order to produce hydrogen cost effectively, it is vital to source the electricity needed for electrolysis at a competitive rate. The improvements of renewable technology will allow cost effective hydrogen to be produced without detrimental implications on the environment. At the moment, combining electrolyzers with coal fired plants makes the most economic sense as electricity can be bought at a cost of 9 US¢ kWh⁻¹ and the steam can also be sourced from the plant itself. Therefore, this study focuses on the integration of coal fired plants with electrolyzers.

4 Experimental verification and analysis

As well as being economically viable, the electrolyser must also be suitable for an integrated system. It has been shown that there is significant research on materials development; therefore one of the aims of this study is to assess the feasibility of current material combinations for large scale hydrogen production. Experimental verification and analysis is an important technique, which allows the physical solid oxide electrolysis reaction to be characterised in real-time, and shows characteristics that may not be possible to assess through computational modelling. This chapter seeks to understand the extent of variation in performance to changes in SOEC operating conditions as well as to show the suitability of the materials for an integrated system. Furthermore, the data gathered will be used to validate the SOEC model. This chapter shows the design and setup of the experimental work station as well as the results of electrolysing steam through polarisation and electrochemical impedance spectroscopy techniques.

4.1 Experimental verification in literature

Solid oxide electrolyser cells (SOECs) can be seen to be the opposite of fuel cell technology and therefore, experimentation is based on reversible fuel cells [108]. Research focus has been on studying effects of steam / hydrogen ratios, temperature, pressure and electrode and electrolyte thickness on SOEC performance; however, unlike modelling, experimentation has also focused on the composition of electrodes and electrolytes in order for enhanced SOEC performance and understanding.

YSZ based electrolytes and Ni-YSZ cathodes have traditionally been used for SOEC experimentation [109]. Research has not only focused on using YSZ for electrolysis, but also optimising preparation methods such as sintering temperature and combining YSZ with other materials for enhanced performance [36;75;78;110]. It was seen that the sintering temperature of YSZ was paramount to producing cells which have suitable density and porosity for good SOEC performance, as at low temperatures YSZ would not be strong and too high a temperature would reduce the porosity of the material; 1,400 °C provided conditions for complete sintering giving OCV (open circuit voltage) of 1.069 V at operating temperature of 850 °C [78]. Therefore, the preparation method is an important factor to SOEC performance.

It has also been seen that composite cathodes and alternative cermet materials may offer better SOEC performance. Nickel has been the favoured metal for combining

with ceramic for cathode fabrication due to Ni being both chemically stable at general SOEC operating temperatures as well as economical [111;112], though copper has also been considered as an alternative to improving oxidation resistances and has shown improved conductivities with high metal / ceramic ratios [112]. Composites for anodes have also been studied as an extension of the electrolyte through combining LSM and YSZ, which has shown improvements in SOEC performance, with OCV close to theoretical values [113].

Optimising the electrodes and electrolyte materials and finding suitable, more cost effective and efficient alternatives to YSZ and Ni have been suggested by a number of researchers [114]. Lay *et al.*, investigated the use of CeLSCM ($\text{Ce}_x\text{La}_{0.75-x}\text{Sr}_{0.25}\text{Cr}_{0.5}\text{Mn}_{0.5}\text{O}_3$) both as an improvement to LSCM and a more stable alternative to the microstructural changes seen in Ni-YSZ [115]. It was shown that introducing cerium to LSCM improves the stability of the material compared with pure LSCM, though CeLSCM can only be used as a hydrogen electrode rather than oxygen electrode. Furthermore, CeLSCM showed improved electrical conductivity to 35 S cm^{-1} from 26 S cm^{-1} with LSCM at $900 \text{ }^\circ\text{C}$ [115].

Though YSZ is a good oxide ion conductor with high mechanical strength it cannot be used above $1,100 \text{ }^\circ\text{C}$ due to phase changes from monoclinic to tetrahedral, which can cause cracking of the cell; therefore it can be doped with materials such as Y_2O_3 and Sc_2O_3 [28]. High temperature SOEC operation poses problems with sourcing suitable materials for other parts of the electrolyser such as interconnects. Therefore, intermediate temperature (between 500 and $700 \text{ }^\circ\text{C}$) has been studied.

Intermediate temperature operation, rather than high temperature operation, offers advantages such as shorter start-up times and durability as well as allowing a range of more cost-effective materials to be used [116;117]. Therefore, it has been studied more recently in the literature, with the most common materials being ceria combined with gadolinium or samarium [118].

$\text{La}_{0.9}\text{Sr}_{0.1}\text{Ga}_{0.8}\text{Mg}_{0.2}\text{O}_3$ (LSGM), an electrolyte at intermediate temperatures show improved ionic conductivity of 0.17 S cm^{-1} compared with YSZ at 0.026 S cm^{-1} ; therefore showing an improved performance at lower temperatures. However, unlike YSZ, LSGM reacts with Ni of the electrode and must be further researched to find a solution. Studies have noted gadolinium doped ceria, Gd-doped CeO_2 (CGO) and Sm-doped CeO_2 (SDC) as more appropriate due to the lack of interactions with the

electrodes and high ionic conductivity [28;119;120]. Another solution to preventing reactions occurring between YSZ and electrodes such as BSCF (Barium-Strontium-Cobalt-Ferro) is to introduce a barrier layer between the electrode and electrolyte such as SDC ($\text{Sm}_{0.2}\text{Ce}_{0.8}\text{O}_{1.9}$). Employing SDC as a barrier layer has shown good chemical stabilities and hydrogen production three times that of a traditional LSM / YSZ / Ni-YSZ SOEC configuration [121].

Electrode materials such as Ni-1Ce10ScSZ have been developed showing promise as a hydrogen electrode with minimal resistance of around $0.79 \Omega \text{ cm}^2$, slow degradation and robust microstructure [120]. Literature has shown Ni-CGO to be stable with large ceramic grain size as well as suitably conductive for use in electrochemical devices [122] with small changes seen in conductivity based on the contact electrode [123]. Furthermore, materials such as Ni-LSCM-CGO shows promise as a way to improve overall cell performance through improved electro-catalytic performance [114].

It is well known that cell fabrication and grain sizes are important factors to cell performance; however, thermal management has been shown to also be a factor for system performance. Wang *et al.* reported system efficiencies of 98 % for an intermediate temperature SOEC operating at $5,000 \text{ A m}^{-2}$ and 1.52 V when thermal energy recovery was used [81].

Symmetrical cells, where the same material is used for the anode and cathode are now being considered as a more cost effective way of producing SOFCs and SOECs. The challenge that is faced is optimising current cermets such as ceramics with lanthanum, strontium and manganese to work under both oxidising and reducing conditions. Results have shown that symmetrical cells are promising, especially with the introduction of CGO layer or composite to the electrode mixture, though resistances may increase under large oxidising conditions [124-127].

In addition to material optimisation, testing SOECs at varying temperatures, steam concentrations, purities and for durability have been carried out. It was seen for a conventional SOEC of Ni-YSZ / YSZ / LSM stack that the cell started to degrade in steam environment after 150 hrs and passivation levelled off after 500 hrs of operation; showing promise for commercialisation though steps are still required for increasing performance [128]. Doping zirconia with scandia and ceria for enhanced electrolyte performance has shown promising results of current densities of 450 mA

cm^{-2} and 1.5 V at 900 °C [29]. Experimental studies have also shown that the concentration of gases to the SOEC has a significant effect on the OCV and performance of the cell; a drop in the OCV is seen with decreasing H_2 . Providing steam under 10 vol. % showed an increase in overpotentials and charge transfer resistances of around $1.69 \Omega \text{ cm}^2$ compared with $1.12 \Omega \text{ cm}^2$ at 40 % steam at 750 °C [129]. Kim-Lohsoontorn *et al.*, noted similar trends, with increasing resistance with decreasing steam content, thereby showing that steam content is an important factor to good output from the SOEC [36]. It has also been shown that ASR can drop from 0.34 to $0.30 \Omega \text{ cm}^2$ for a Ni-YSZ / YSZ / YDC (yttria-doped ceria) cell at 0.25 A cm^{-2} by changing the concentration of steam from 65 to 80 %, which indicates an optimum concentration before rapid oxidation of Ni to NiO [130].

The range of temperatures over which SOEC can operate, whether intermediate or high temperatures, is dictated by the electrolyte material. Too high temperature can cause phase changes and reduce stability of the material and too low would reduce ion conductivity [28]; therefore, the effect of temperature on SOEC performance has been focused on through material development as well as experiments in literature. Due to the temperature dependency of the materials, it has been shown that performance varies significantly with temperature variations. For a Ni-YSZ / YSZ / LSM-YSZ cell operating at 0.2 A cm^{-2} requires potentials of 1.5 V and 1.08 V at 700 and 850 °C, respectively. For the same materials and conditions with a cathode of BSCF, at a potential of 0.98 V and 1.39 V at 700 and 850 °C are seen, respectively [36]. A symmetrical cell of SFM / LSGM / SFM ($\text{Sr}_2\text{Fe}_{1.5}\text{Mo}_{0.5}\text{O}_{6-\delta}$) at absolute humidity of 40 vol. % has shown that increasing temperature from 800 to 900 °C at 1.3 V can improve the current density from 0.48 to 0.59 A cm^{-2} , respectively; and by using a higher steam concentration of 60 vol. % absolute humidity the improvement is furthered to 0.88 A cm^{-2} at 900 °C [131]. Based on the above studies it can be seen that not only is the material important, but also the correct operating conditions for improving performance.

Many of the studies have focused on conventional YSZ and Ni-YSZ as well as the improvement of materials to enhance the three phase boundaries and create better electro-catalytic performance. Though the understanding of the fundamental materials is important, it can be concluded that small changes in composition of metals, grain size of ceramics, sintering temperatures and preheating can make a large difference to SOEC performance. This study does not aim to create new

materials or optimise those that exist; it aims to find the most suitable material available in research at the moment for large scale commercialisation and production of hydrogen.

Therefore, the experimentation in this section uses ‘standard’ and consistent procedures to understand the effect of temperature on the performance of SOECs for model validation purposes and understanding of the materials available for this project.

4.2 Experimental setup

4.2.1 Workstation

A workstation was designed and built at UCL to run experiments and is shown in Figure 4-1. It comprises of EL-FLOW® mass flow controllers (Bronkhorst UK Ltd., UK) mounted on a board, to maintain gas flow to the required set point up to 100 ml min⁻¹ of nitrogen and hydrogen gases (BOC, UK) in zero grade purities of 99.998 % and 99.995 %, respectively.

The SOEC operating condition is maintained with a THH11/90/457-2408CP horizontal tube furnace (Elite Thermal Systems Ltd., UK) controlled by 2408 temperature controller (Eurotherm UK, UK). The power required for the SOEC system is supplied by a potentiostat (PGSTAT302N/FRA, Metrohm Autolab B.V., The Netherlands) running NOVA 1.10 software. The unit has a potential range of ±10 V and current range of 1 A to 10 nA.

The humidification system, designed at UCL, consists of silicone insulated heater (Chromalox UK Ltd.) wrapped around a stainless steel bottle. A diffuser connected to the end of ¼” stainless steel pipe bent to form a coil is positioned inside the stainless steel bottle to provide good flow and dispersion of nitrogen and hydrogen gas to be saturated with water.

A K-type thermocouple (Omega Engineering Inc., UK) placed at the top of the bottle measures the temperature of the humidified gas and the CB 7523 PID controller (Omega Engineering Inc., UK) is used to control the silicone insulated heater accordingly. The gases leaving the humidifier enters a heated line to heat the vapour to steam prior to entering the rig; which is constructed of ¼” smoothflex-S hose flexible piping (FTI Ltd., UK) with FGR080 Omegalux® rope heaters (Omega

4. Experimental verification and analysis

Engineering Inc., UK) surrounding the pipe and ceramic wool insulation. Both the humidifier and heated lines are insulated by flexible insulation.

The thermocouples are connected to a TC-08 Thermocouple Data Logger (Pico Technology, UK), which is connected to the computer. The electrical connections are 0.25 mm diameter Pt wire (Peak Sensors Ltd., UK), which was spot welded onto a 20 mm × 20 mm and nominal aperture of 0.25 mm, Pt mesh (Goodfellow Cambridge Ltd., UK) current collector.



- | | | | |
|----|--|-----|--------------------|
| 1. | Mass flow controllers mounted on a board | 7. | Potentiostat |
| 2. | Humidifier | 8. | PID Controller box |
| 3. | Heated line | 9. | Computer |
| 4. | SOEC Rig | 10. | Monitor |
| 5. | Furnace | 11. | Extraction |
| 6. | Schott water bottles | | |

Figure 4-1: Experimental workstation.

4.2.2 Rig design

The rig, designed and drawn in Rhinoceros® version 4, and built at UCL holds the SOEC. The rig itself is formed of a 70 mm (outer diameter) quartz glass tube (Cambridge Glassblowing Ltd., UK), chosen for its ability to withstand high temperatures and houses the ceramic tubes, ceramic holder, electrical connections and electrolyser cell as shown in Figure 4-3.

The cell holder was designed to form two separate sections to ensure no mixing of the gases from the cathode and anode side of the cell, enable good electrical connection and to be reusable for all experiments (Figure 4-2). In order for the holder to handle the cycling of temperatures for SOEC operation, 60 mm diameter Pyrophyllite (aluminium silicate) (Ceramic Substrates & Components Ltd., UK) was cut using a computer numerical control (CNC) machine to the desired form from diagrams drawn in Rhinoceros.

Four pieces were produced; two end plates to hold the ceramic tubing in place and to protect the silicone bungs from the heat spreading from the heated zone, and two as the holder in the centre of the rig (Figure 4-3). The ceramic discs once cut, were fired in a furnace at 1,200 °C for 2 hours at a ramp rate of 1 °C min⁻¹.

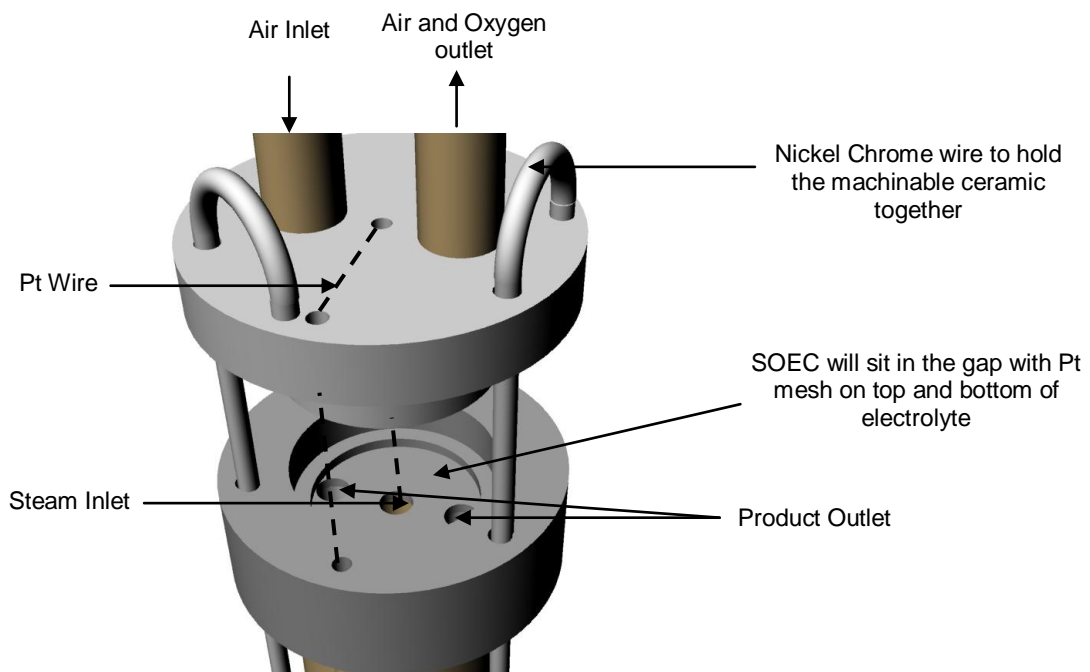


Figure 4-2: The cell holder design, Mark 1; creating two separate regions for the hydrogen and oxygen sides.

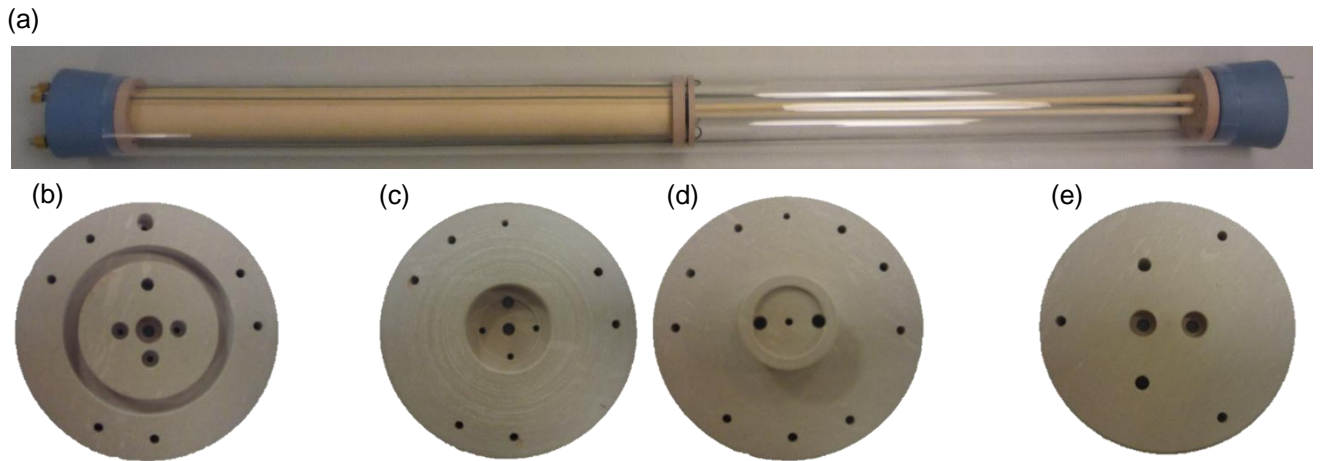


Figure 4-3: Solid oxide electrolyser rig setup: Mark 2.

(a) The whole rig, (b) ceramic holder for tubes to be positioned at the inlet of steam, (c) ceramic holder for the cell to sit in (left side where steam enters), (d) ceramic holder for the cell to be held in place where oxygen can leave the rig, (e) ceramic holder for the tubes to be positioned for air to enter and oxygen to leave.

The gases to the cell flows through 99.7 % alumina (ceramic) tubes (Multi-lab, UK), which are able to tolerate temperatures of up to 1700 °C and as such are more than suitable for use with SOEC operating temperatures created in the furnace. The ceramic tubes are used as inlet (6 mm OD) and outlet channels (40 mm OD) for gases as well as for providing casing for the Pt electrical connections (4 mm OD) and K-type thermocouples (Omega Engineering Ltd., UK), as shown in Figure 4-4.

In Mark 2, all but one ceramic tube are placed inside the large ceramic tube used for gas outlet on the hydrogen side. However, on the oxygen side, two 6 mm OD tubes were placed as sweep gas inlet and oxygen outlet. Mark 2 of the rig and holder adds ceramic tubes to house thermocouples and all Pt wires to eliminate any chance of a short circuit.

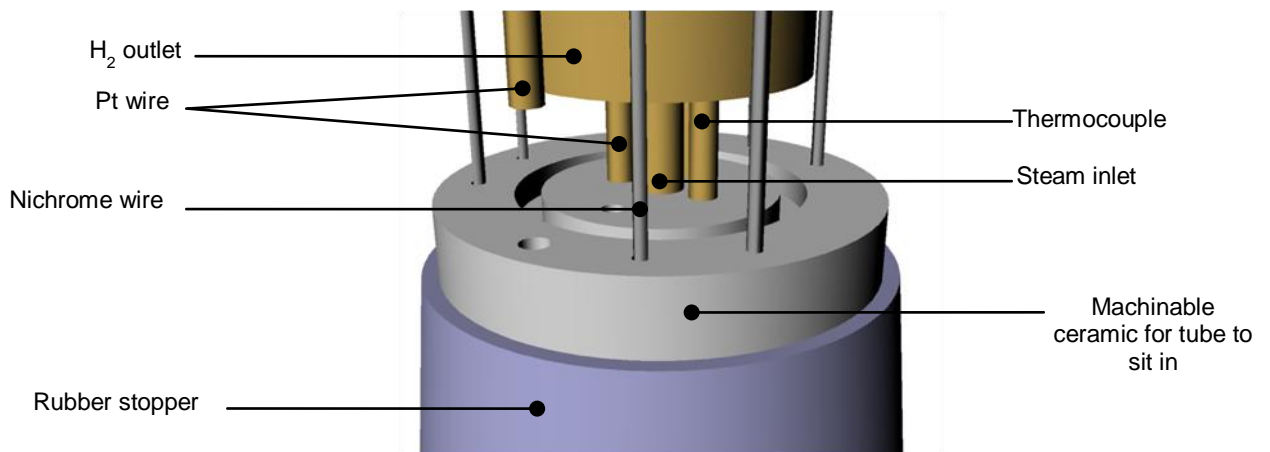


Figure 4-4: CAD of hydrogen side ceramic tube positioning, Mark 2.

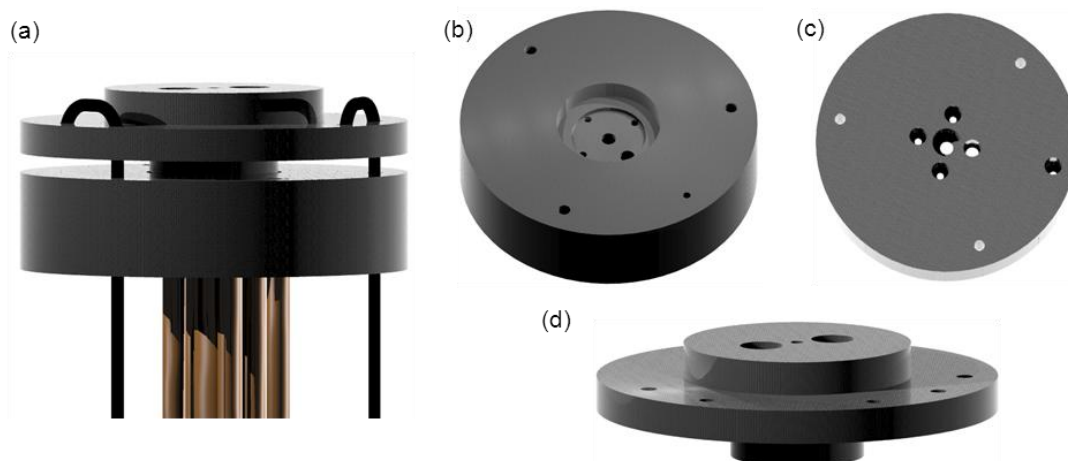


Figure 4-5: CAD drawings of the changes to SOEC holder design, drawn in Rhinoceros, Mark 3 (a) Cell holder secured with nichrome wires hooks, (b) area to place the cell and allow gas flow, (c) deeper holes in the bottom of the holder to support ceramic tubing, (d) a side view of the top piece showing greater thickness for support and reducing gas leaks.

The electrolyte is placed in the middle of the holder and connected to the platinum mesh and wires through the holes made in the ceramic, similar to that seen in Figure 4-7. The whole rig is held together with nichrome wires and a screw and spring system. The glass tube is sealed at the ends with natural solid rubber bungs (VWR International Ltd., UK).

Through preliminary testing, issues arose with sealing and ease of assembling the rig. Therefore, changes to the rig design were implemented and shown in Figure 4-5 and Figure 4-6, where for the most part the same materials were used. Preliminary testing presented a lot of noise in the symmetrical cell experiments, which were only seen at furnace temperatures at or above 700 °C, and was found to be due to the rubber bungs melting after prolonged use of the workstation. Therefore, silicon bungs (VWR International Ltd., UK) replaced the natural rubber bungs at the end of the glass tube. The temperature discrepancies of around 50 °C between that measured from the furnace controller and of the Pico logger were seen. Introducing two thermocouples to the rig, one to read the temperature at the cell and one to control the furnace temperature improved the system, where differences of 5 °C were measured.

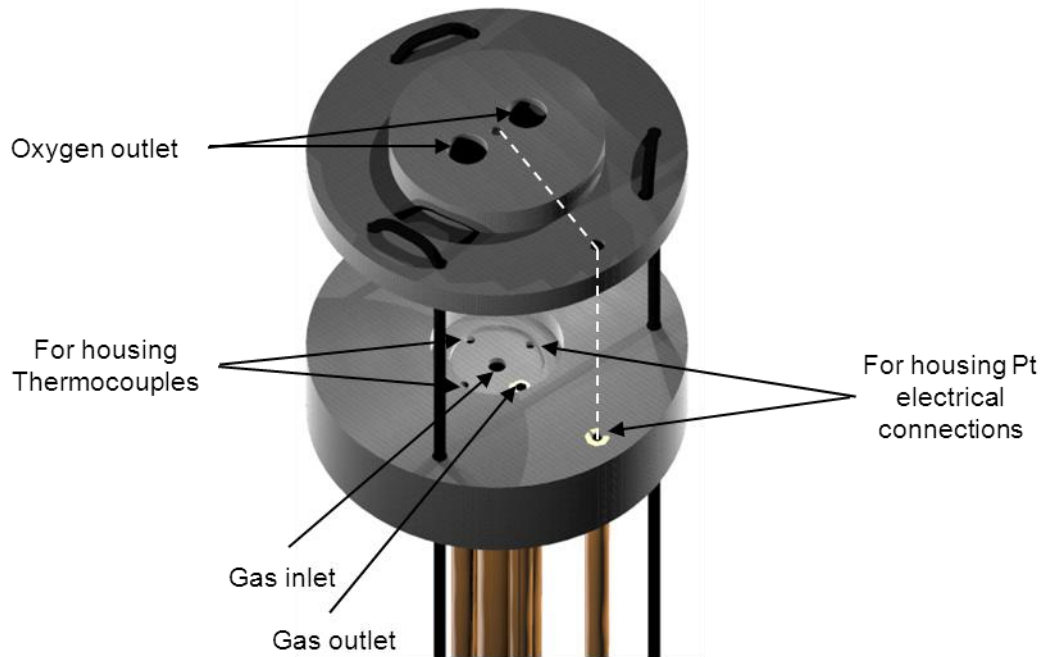


Figure 4-6: A top view of the solid oxide electrolyser rig setup, Mark 3. Changes made to the gas outlet on the hydrogen side and ceramic tubing to house all thermocouples and electrical connections.

It was also found that the spring loaded seal was effective to some extent for keeping the holder together, however, did not create a seal enough to stop air entering system via the silicone bungs and therefore, the ceramic tubing was extended to start outside the silicone bungs, which removed the sealing problems experienced on the inside of the rig and allowed easy access to the rig. Silcoset 152 (ACC Silicones Ltd., UK), a high temperature silicon sealant, was used on the exterior of the rig to prevent gas leaking.

In addition, the assembling of the rig became far easier as the tubes were tightly fitted in the silicone bungs as well as held in position by the modified ceramic plates. Furthermore, the grooves made in the cell holder to position the ceramic tubes were made deeper to provide more support, as seen in Figure 4-5. It was decided to remove the tubes on the oxygen side and have an open anode for electrolysis.

It was also noted that for electrolyser testing, the spring loaded setup was not sufficient to create two environments without cracking the cell prior to use. Therefore, to seal the SOEC inside the holder Omegabond[®] 300 (Omega Engineering Ltd., UK), a high temperature cement was used (Figure 4-7(b)).

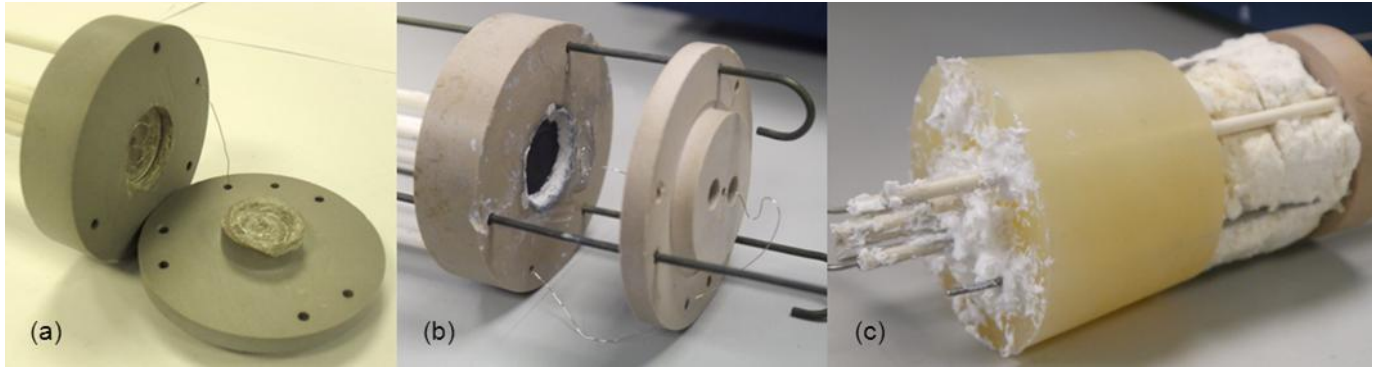


Figure 4-7: Solid oxide electrolyser cell holder machined on the CNC, Mark 3; (a) holder with Pt current collector and electrical connections, (b) placement of sealed SOEC within the holder, (c) silicone bung with sealant.

4.3 Solid oxide cell preparation

The solid oxide cell is composed of YSZ electrolyte, Ni-CGO cathode and lanthanum strontium manganate, $\text{La}_{0.8}\text{Sr}_{0.2}\text{MnO}_3$ (LSM) anode. These materials have been chosen as they have been seen to be the most commonly used materials for intermediate to high temperature operation.

YSZ-8 (8 mol. % yttria) electrolyte (fuelcellmaterials.com, NexTech Materials Ltd., USA) with a diameter of 20 mm and thickness of around 0.30 mm was chosen due to the ability of the electrolyte to operate at high temperatures as well as showing good mechanical strength and oxygen ion conductivity of 0.13 S cm^{-1} [28]. SOECs have the ability to produce hydrogen, carbon monoxide and syngas; each reaction produces O^{2-} ions, which makes YSZ electrolyte a suitable material. This is because one set of materials can be used with a number of reactions and therefore can be implemented within industrial plants while allowing flexibility.

The electrodes require properties such as high porosity and good electrical conductivity so as to form high density TPBs. In order to achieve TPBs, porous electrodes are needed for the gas to reach the active site for electrolysis to take place. In addition, the electrodes need to be able to handle the oxidative and reductive environments that the materials will be subjected to [132].



Figure 4-8: SOEC cells after sintering; (a) Ni-CGO cathode, (b) YSZ electrolyte, (c) LSM anode.

Commonly used materials for the cathode are Ni-YSZ have shown to perform well with steam at high temperatures. However, Ni-CGO was shown to allow a better reduction of CO_2 when used as a cathode at intermediate temperatures [133;134]. The nickel provides an electrical connection as it conducts electrons whereas the CGO provides an ion conducting surface, which provides more possibilities for active sites.

The most commonly used materials for anodes are oxides with perovskite structures, which provide better electron conductivity over pure oxides such as LSM [135]. LSM has been shown to be a suitable material as the cathode of SOFCs and therefore was chosen as an electrolyser anode for this investigation [28;136]. LSM paste (fuelcellmaterials.com, NexTech Materials, Ltd., USA) with a composition of $(\text{La}_{0.80}\text{Sr}_{0.20})\text{MnO}_{3-x}$ and surface area of $4 - 8 \text{ m}^2 \text{ g}^{-1}$ used in the experiments, have a conductivity greater than 200 S cm^{-1} , which is suitable for the electrolysis process.

The Ni-CGO produced in collaboration with Imperial College London, UK, was painted onto the YSZ electrolyte in a thin layer, dried at room temperature and sintered at $1,300 \text{ }^\circ\text{C}$ in a furnace for 1 hour at a ramp rate of $5 \text{ }^\circ\text{C min}^{-1}$. LSM was the painted on the other side of the YSZ electrolyte and sintered at $1,150 \text{ }^\circ\text{C}$ for 1 hour also at a ramp rate of $5 \text{ }^\circ\text{C min}^{-1}$. The cells are shown in Figure 4-8; the inconsistencies seen in the cells are due to the painting process and possible impurities in the furnace when sintering.

4.4 Methodology

The experiments were carried out on both symmetrical and full electrolyser cells. Prior to all testing and once the cell operating temperature was steady, the NiO-CGO was reduced in a hydrogen environment to Ni-CGO to ensure that the flow of gas to the active sites was not restricted by the large sized NiO. To reduce the cell, hydrogen was introduced stepwise at percentages of 4.9 % for 30 mins, 9.8 % for 15

4. Experimental verification and analysis

mins, 14.7 % for 15 mins and 24.5 % for 30 mins in a total flowrate of 100 ml min^{-1} with the remaining percentage of the flow being nitrogen [137].

For symmetrical cell testing, the cell consisted of YSZ electrolyte and Ni-CGO cathode painted on both sides. The workstation and rig was set up as shown in Figure 4-9. Once the cell had been reduced, hydrogen was introduced at the desired testing concentrations to assess the effect on such changes on the electrolyte and electrodes. Furthermore, the tests carried out on varying temperatures and concentrations were used to validate the methods used to prepare the cells and the design of the rig, through comparison to previous work carried out in the lab on the same cells.

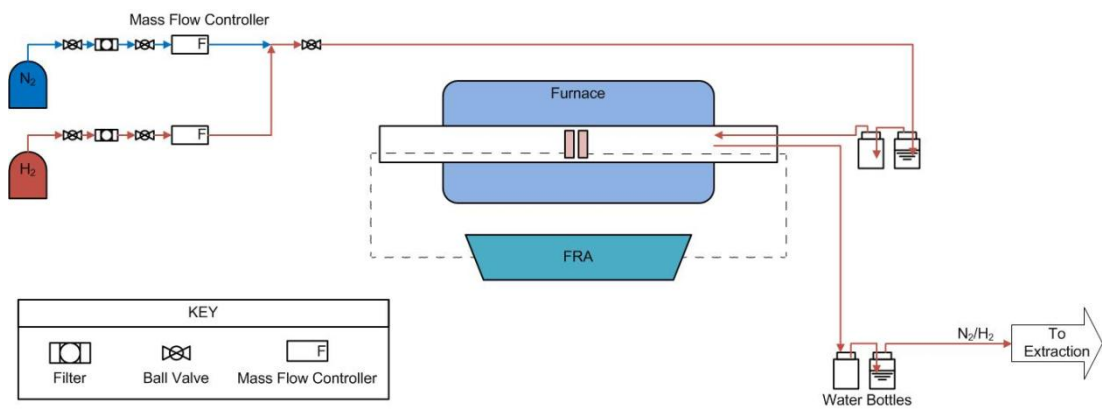


Figure 4-9: Process flow diagram for symmetrical cell testing.

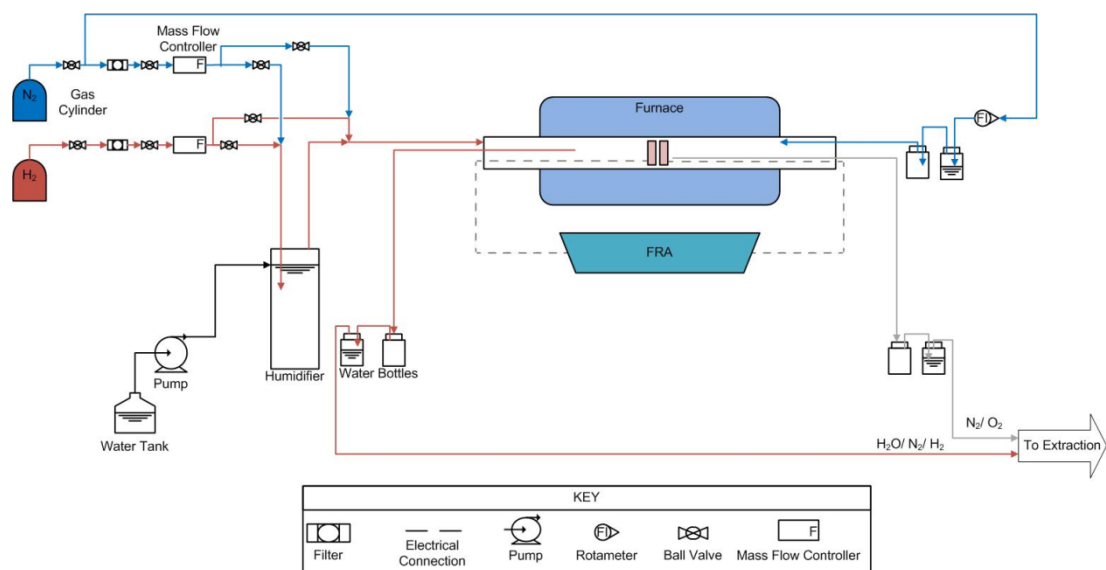


Figure 4-10: Process flow diagram for SOEC testing with steam.

4. Experimental verification and analysis

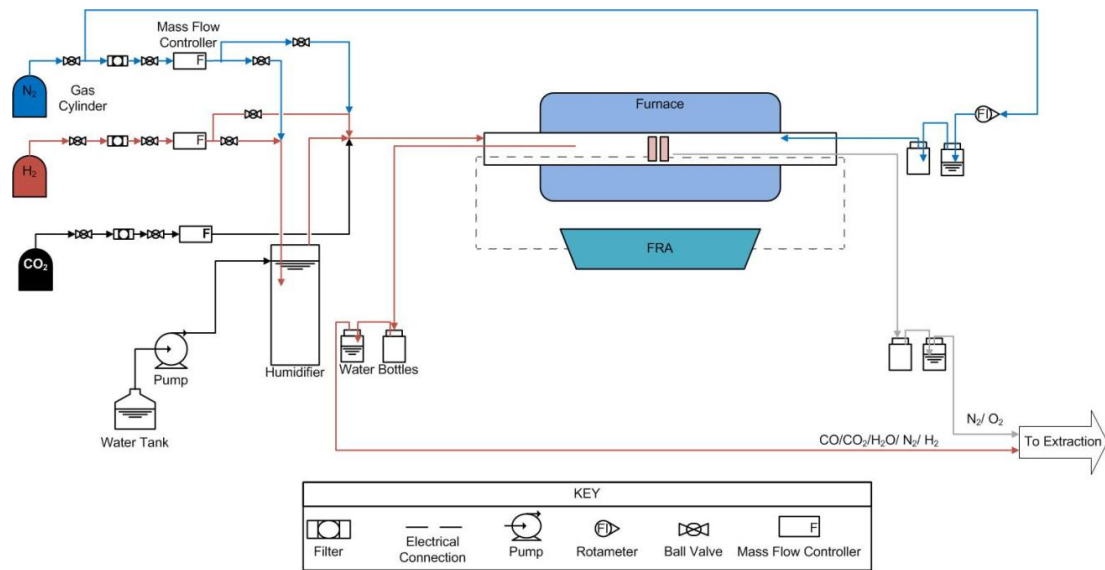


Figure 4-11: Process flow diagram for SOEC testing with CO₂.

Figure 4-10 and Figure 4-11 show the experimental setup for the SOEC testing for Ni-CGO / YSZ / LSM electrolyser shown in Figure 4-8, and can also be employed for SOFC testing. The cell was sealed with Omegabond[®] 300 and left to dry in air for 24 hours and then heat treated at 82 °C and 105 °C for 4 hours at each temperature. Once the cells were reduced, steam was introduced slowly to the system by passing a mixture of nitrogen and hydrogen through the humidifier and was allowed to reach steady state before steam electrolysis testing. For carbon dioxide electrolysis, a mixture of CO₂ and N₂ was introduced after the reduction of the cathode side and after flushing with nitrogen.

4.5 Techniques

There are two main techniques employed in the experimental analysis; linear sweep polarisation and impedance spectroscopy. Through polarising the SOEC voltage-current (V-i) curves can be obtained which show the extent of overpotentials. To further analyse the overpotentials at different points along the V-i curve, electrochemical impedance spectroscopy is used.

4.5.1 Linear sweep polarisation

Linear sweep polarisation is a technique by which a flow of current is passed through a cell and creates a shift in the potential away from the open circuit voltage; voltage – current density (V-i) curves are produced as a result, an example shown in Figure 4-12. By analysing the extent of the shift from the equilibrium potential and the

shape of the curve, the result can show the types of overpotentials occurring. The overpotentials are described in detail in Section 6.

Figure 4-12 shows a general situation, where at higher current densities concentration overpotentials are dominant whereas at lower current densities activation overpotential dominates. The black line is a general shape, usually expected in low temperature alkaline and PEM cells. At high temperatures, concentration overpotentials are minimal and are insignificant compared with activation and ohmic losses and therefore the shape of the curve changes [113;138;139]. The V-i curves will be used to assess the performance of the electrolyser.

4.5.2 Electrochemical impedance spectroscopy

Electrochemical impedance spectroscopy (EIS) is a technique used to describe an electrical circuit and further assess the factors that restrict the flow of electrons produced by electrolysis at various points along the polarisation or V-i curve. EIS can provide information on the interface, structure and reactions taking place.

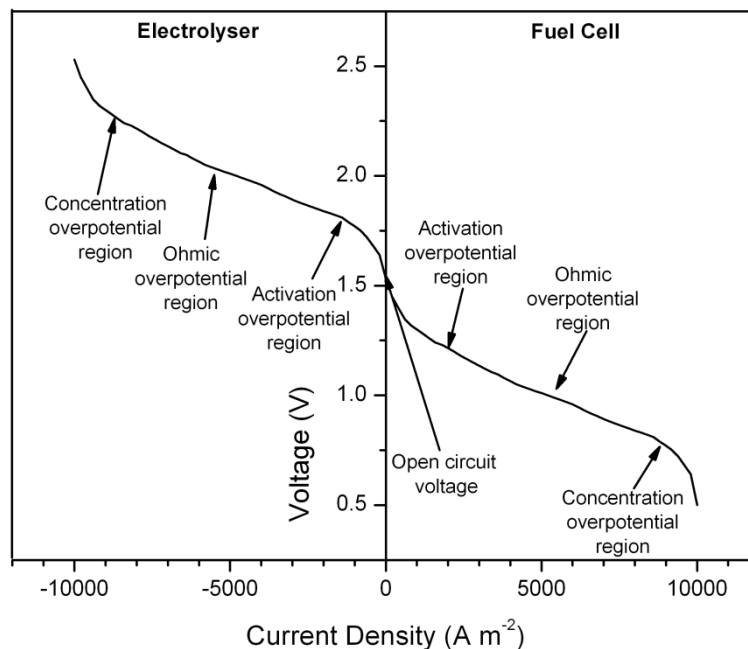


Figure 4-12: A general voltage – current density curve.

4. Experimental verification and analysis

EIS imposes an AC potential over the DC signal to the electrolyser and measures the response and changes in the AC current at a range of frequencies. The AC potential is a sinusoidal voltage of known amplitude and frequency described as [140]:

$$E(t) = E_m \sin(\omega t + \theta) \quad (16)$$

Where, $E(t)$ is the applied AC voltage, E_m is the maximum amplitude of the wave, ω is the angular frequency ($\omega = 2\pi f$), θ is the phase angle, t is time and f is the frequency. Similarly, the AC current can be written as [140]:

$$I(t) = I_m \sin(\omega t + \theta) \quad (17)$$

Where, $I(t)$ is the AC current and I_m is the maximum value of the sinusoidal current wave.

There are three main components of an electrical / electrochemical system: resistors, capacitors and inductors, each of which can be described mathematically and respond to the AC perturbation imposed on the cell in different ways. Resistors are defined by Ohm's Law (Table 4-1), and therefore by combining Equations (16) and (17), the resulting equation ($I_m = I_m R$) is frequency independent. Therefore, purely resistive materials such as electrolytes are considered resistors.

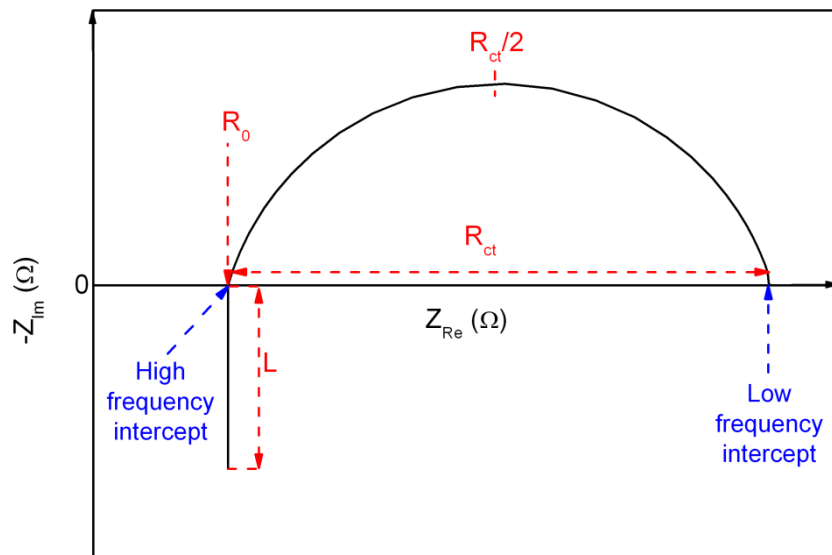

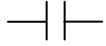



Figure 4-13: An example of a Nyquist plot representing the Real (Z_{Re}) and Imaginary (Z_{Im}) terms, where L is the inductance, R_0 is the high frequency resistance, R_{ct} is the charge transfer resistance.

Table 4-1: Relationship between circuit elements and impedance.

| Element | Equation | AC Impedance equation | Equivalent circuit symbol |
|-----------|-----------------------|-----------------------------|---|
| Resistor | $E = IR$ | $Z_R = R$ |  |
| Capacitor | $I = C \frac{dE}{dt}$ | $Z_C = \frac{1}{j\omega C}$ |  |
| Inductor | $E = L \frac{dI}{dt}$ | $Z_L = j\omega L$ |  |

Materials can also have capacitive properties (C), which represent the capability of storing energy through opposing changes in voltage. Passing an AC voltage through a pure capacitor produces an effect on the current; as capacitance is based on the change in voltage, when the voltage is at its maximum the change in voltage is zero, therefore the current is zero. As a result of passing a sinusoidal wave through a capacitor, the voltage lags current by a phase angle of 90° . Inductance (L) in a system behaves the opposite of capacitance. With an AC voltage on a purely inductive system, the current lags the voltage by a phase angle of 90° . In a system like electrolysis with a combination of elements, impedance can typically produce Nyquist plots, an example is shown in Figure 4-13.

The impedance measured is a complex value as the system is not purely resistive and therefore the current produced is out of phase with the applied voltage [141]. EIS (Z) can be denoted as the real part (Z') and imaginary part (jZ''), (where, j is the imaginary operator) as follows:

$$Z = Z' + jZ'' \quad \text{where,} \quad j = \sqrt{-1} \quad (18)$$

The electrolyser can be written in terms of an equivalent circuit, which represents different parts of the process as shown in Figure 4-14. R_0 represents the ohmic resistance of the system, R_{ct} is the charge transfer resistance and CPE is the constant phase element, which acts like a capacitor however, takes into account inconsistencies in the system [140].

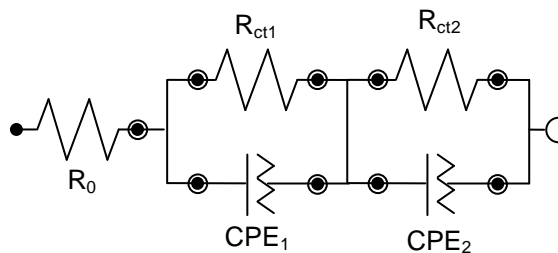


Figure 4-14: An equivalent circuit for a two electrode and electrolyte cell.

4.5.3 Scanning electron microscopy

Scanning Electron Microscopy (SEM) is used to create a 3-dimensional appearance of a sample using a focused beam of electrons which scans the incident beam horizontally over the sample to produce various signals at the surface of the sample. The electron beam is usually created using a tungsten filament [142]. The secondary electron and back-scattered electron signals released from the scan are of greatest interest as they are the most sensitive to variations in the topology of the sample, with x-rays providing elemental information [143;144].

Back-scattered electron (BSE) signals are produced through elastic interactions of the electron beam with the sample, which changes the trajectory of the electrons. It has been suggested that the back-scattering increases with increasing atomic number as the larger atoms tend to have a larger surface area. Therefore, the larger atoms produce more signals and so heavier atoms show up in a lighter colour on an image [143]. BSE is useful to show different atoms based on their mean atomic number [144].

In the context of an electrolyser, using a combination of all SEM, Energy-dispersive X-ray spectroscopy (EDS) and BSE allows the changes in morphology with reaction to be assessed and to show the difference in material porosity as well as elemental composition of various samples.

4.6 Experimental method development and results

The experimental tests that were carried out aimed to examine the workstation and rig in addition to the electrolyser. Preliminary tests were carried out on the electrical connections to ensure that the rig, while sealed provided adequate electrical connection. Impedance carried out on the Pt wires and mesh is shown in Figure 4-15 for SOEC operating temperature range of between 500 and 800 °C. The electrical connections are shown in purely the imaginary axis, which represent inductance [145].

Inductance is expected in conducting materials such as electrical connections. The impedance can be seen to increase as the temperature increases due to the temperature dependency of the resistance in the wires. During tests of the symmetrical and electrolyser cells, the resistance of the wires can be discounted from the overall result.

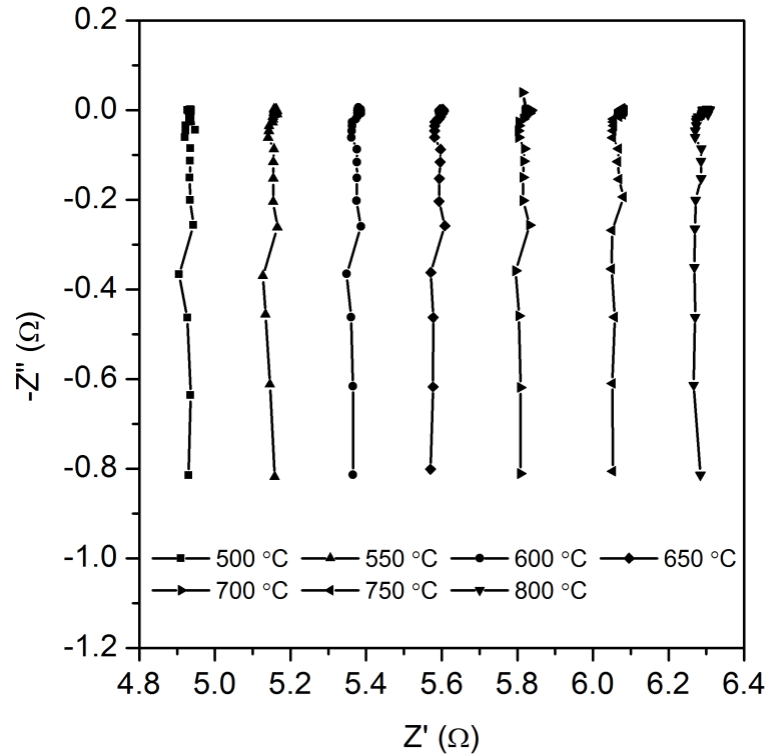


Figure 4-15: Impedance spectroscopy of the electrical connections at temperatures of between 500 and 800 °C.

4.6.1 Symmetrical cell

The symmetrical cell, as discussed in Section 4.3, is comprised of Ni-CGO cathodes painted on to an YSZ electrolyte and is described by the equivalent circuit in Figure 4-14. The tests carried out on the symmetrical cells initially aimed to validate the workstation, rig and process as well as to assess the changes in conductivity of the electrolyte and charge transfer resistance to temperature and concentration variations.

In order to differentiate between degradation of the cell and changes of resistance to operating conditions, a standard test was carried out in both hydrogen and steam environments and is shown in Figure 4-16. The degradation of the electrolyte and electrodes are consistent over time and follow the same trend.

Under steam conditions the cell degraded slightly more than in a hydrogen environment, as the system had been running for a much longer period of time to allow for the reduction of NiO-CGO before steam was introduced to the system. In addition, introducing steam creates an oxidising environment, which reverses the reduction process, this leads to the formation of NiO and can cause the cell to crack

4. Experimental verification and analysis

if steam is introduced too quickly [146]. In more complex experiments, where there are a number of variables, the trend can be useful to provide a thorough analysis of the cell behaviour. The peak seen in Figure 4-16(b) and Figure 4-16(d) at around 90 mins of being in a steam environment is due to possible changes in the system such as inconsistencies in steam concentration due to water build up.

Impedance analysis was carried out on the symmetrical cell at varying temperatures and concentrations to assess the impact of such variables on the electrode and electrolyte. The impedance spectroscopy of a symmetrical cell in a hydrogen environment shows that there is a significant impact on the operation of the cell by changing temperature, as shown in Figure 4-17; a sample of the data collected is shown in the figure to represent the characteristics of the cell.

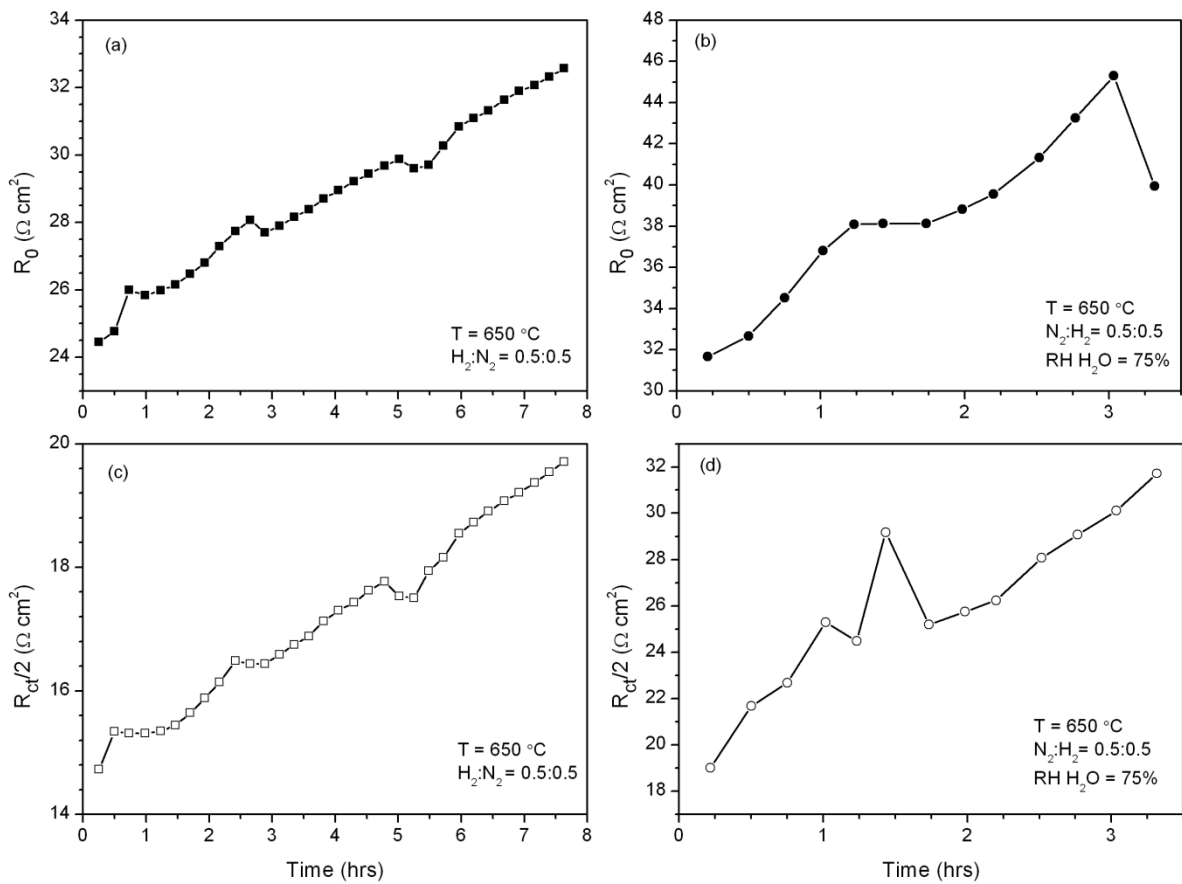


Figure 4-16: Changes to electrolyte resistance over time of symmetrical Ni-CGO/YSZ/Ni-CGO cell at 650 °C, with H₂ and N₂ mixture at 50 %:50 % (a) resistance of the electrolyte, (b) resistance of the cathode, and 50% H₂ : 50% N₂ mixture at 40 %:50 %:10% (c) resistance of the electrolyte and (d) resistance of the cathode.

4. Experimental verification and analysis

Assessing the impedance in Figure 4-17 further, the results show the effect on the electrodes and electrolyte individually. It can be seen from Figure 4-18 that temperature has a significant impact on the operation of the electrode and electrolyte. Though the difference in ohmic resistance is small with temperature, it can be seen from Figure 4-18 that the behaviour is as expected and the reason for the small changes can be attributed to the large resistances generally seen in the electrical connections. The increase in resistance at around 5 hours into testing is due to the degradation of the cell. Similar characteristics are seen for the Ni-CGO electrodes.

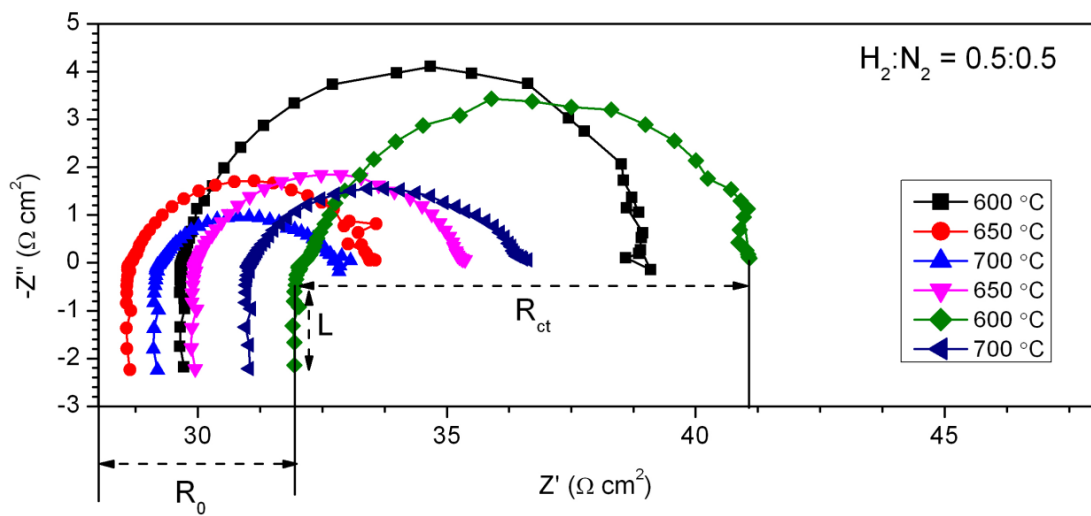


Figure 4-17: Impedance of the cell to variations in temperature (from 600 °C to 700 °C and then back down again to 600 °C) under 50% H₂: 50 % N₂.

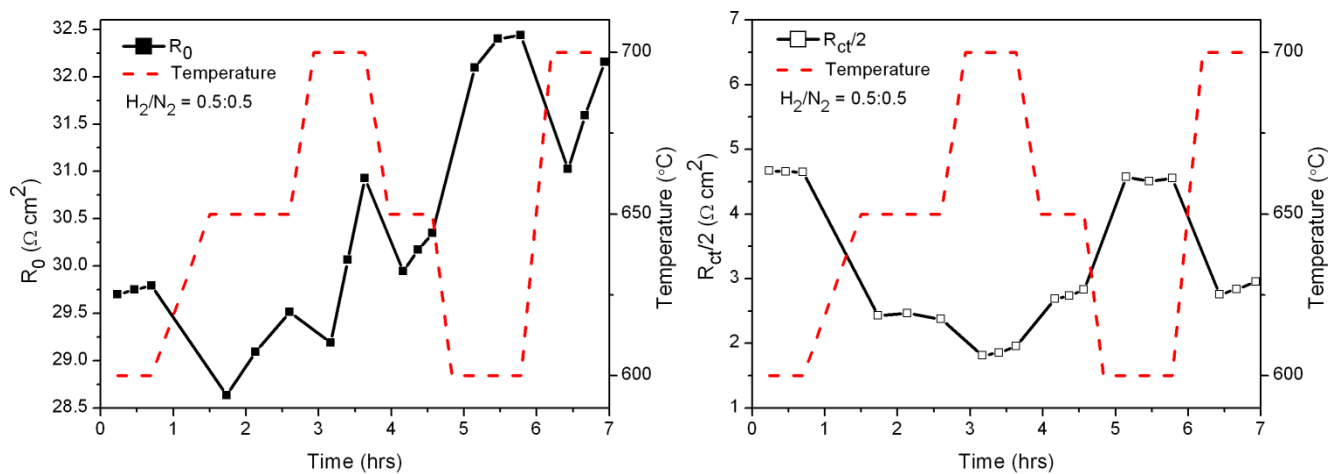


Figure 4-18: Sensitivity of electrolyte and electrodes resistance to changes in temperature. At 50 % H₂: 50 % N₂ resistance of electrolyte (left) and resistance of cathode (right).

4. Experimental verification and analysis

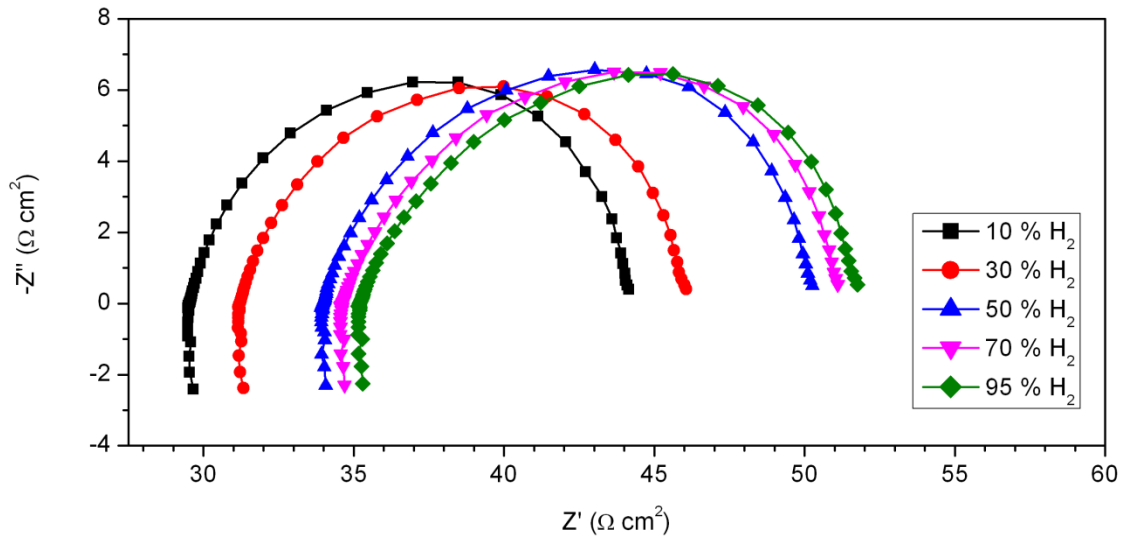


Figure 4-19: Impedance of the cell to variations in hydrogen concentration at 600 °C.

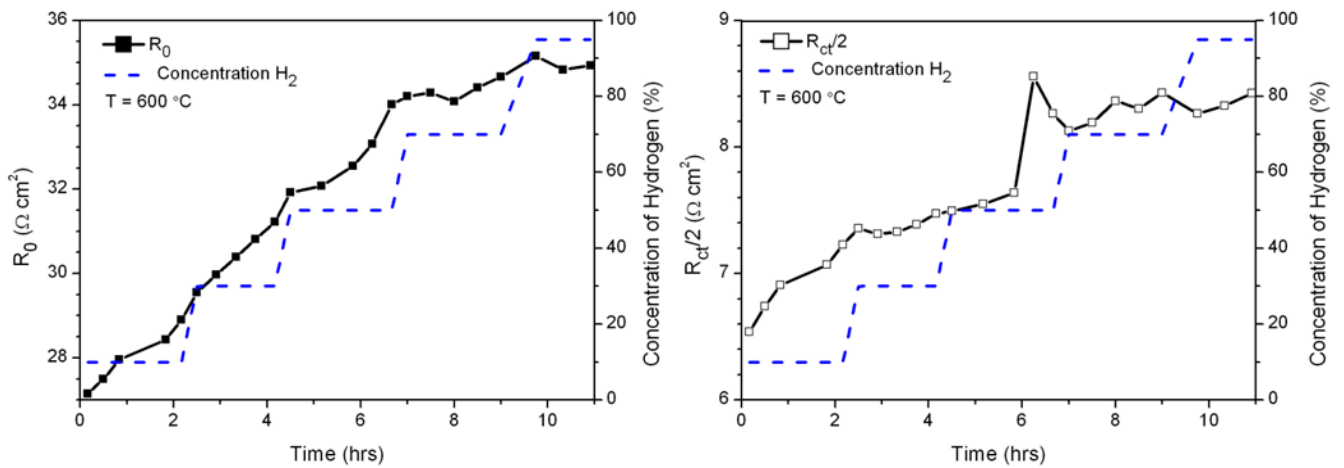


Figure 4-20: Sensitivity of electrolyte and electrode resistance to changes in concentration at 600 °C; resistance of electrolyte (left) and resistance of cathode (right).

The effect of concentration of hydrogen on the cell is shown in Figure 4-19 and Figure 4-20. It can be seen that the electrolyte is generally unaffected by concentration and the trend seen follows closely with degradation. The impedance results in Figure 4-19 show small changes in the high frequency arc and larger variations in the low frequency arc; the variation represents the relationship between the concentration and mass transport [129;147]. It was expected that a more prominent change would be seen with concentration changes; however, the curves shown in Figure 4-19 show unexpected changes in the real axis, which indicates cell degradation. Trends in literature have shown significant changes in the low frequency arcs with little change in the high frequency arc due to concentration affecting only the charge transfer of the cell. The results in the hydrogen

4. Experimental verification and analysis

environment confirmed that the design of the rig and cell making were suitable for the proposed testing as the results correlate with trends in the literature and with previous work carried out in the group [29;147].

The symmetrical cell was used to study Ni-CGO as a SOEC cathode and the effects of the cell with varying temperature in a steam environment. Temperature was the focus of the experiments in a steam environment as greater variations due to temperature rather than concentration were seen on the performance of the cell in the hydrogen environment.

Figure 4-21 shows the impedance of a symmetrical cell at varying temperatures in a steam environment. It can be seen from both Figure 4-21 and Figure 4-22 that the materials are temperature dependent, though the temperature dependency of the electrolyte does not follow the trend that would be expected, where in this case the ohmic resistance increases as the temperature increases, which could be due to the oxidising environment of steam at the cell, creating faster degradation. It can be seen however, that the overall resistance does decrease with temperature. The cathode material, Ni-CGO, did however follow the expected trend and so it can be assumed that there were irregularities with that particular YSZ electrolyte used in this case. In addition, the resistances seen in the steam environment are larger than in the hydrogen environment, which could be due to longer operation of the cell as well as a more oxidising environment.

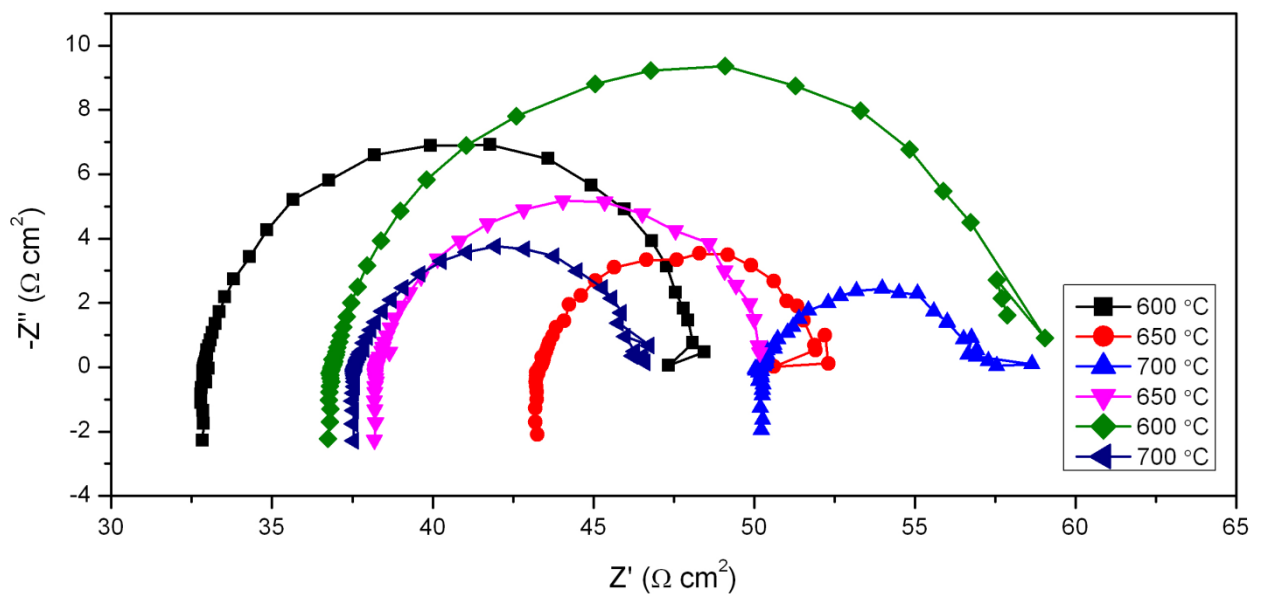


Figure 4-21: Impedance of the cell to variations in temperature under 100 ml min^{-1} (50 % H_2 : 50 % N_2) and steam relative humidity of 75 % environment.

4. Experimental verification and analysis

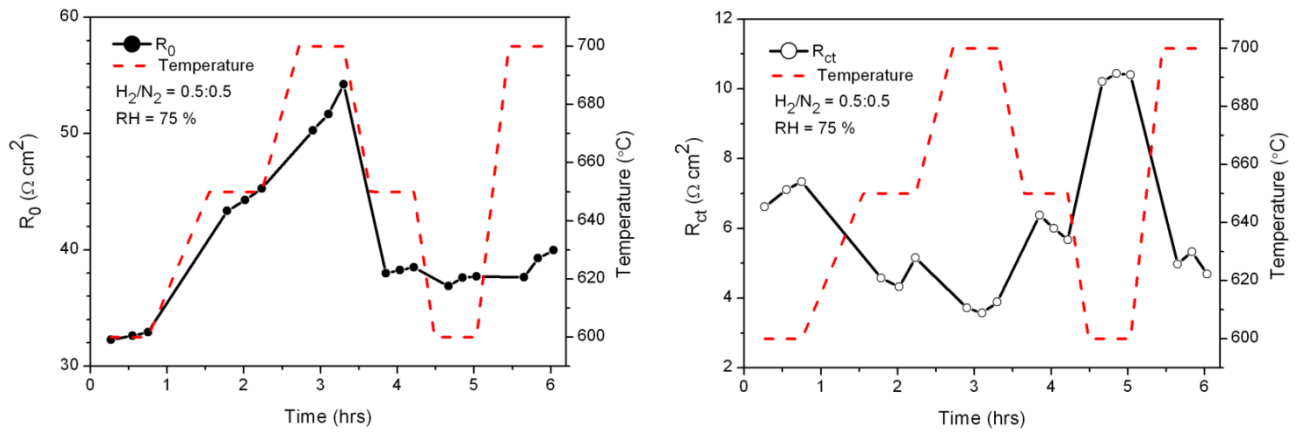


Figure 4-22: Sensitivity of electrolyte and electrode resistance to changes in temperature at 100 ml min^{-1} (50 % H_2 : 50 % N_2) and steam relative humidity of 75%. Resistance of electrolyte (left) and resistance of electrode (right).

The conductivity of a material is important to the overall performance of the cell as it represents the extent of charge transfer through the material; the greater the conductivity, the more likely the cell will perform efficiently [148]. The conductivity of the symmetrical cell in a hydrogen environment was seen to be 50 % smaller than those in literature; this could be due to the differences in operating conditions and electrolyte preparation [149;150].

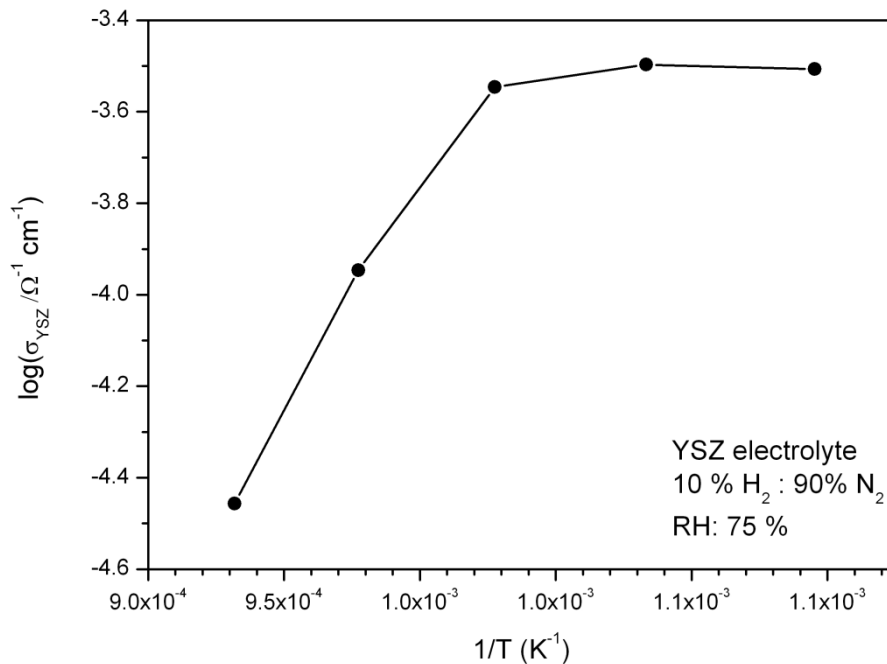


Figure 4-23: Conductivity of electrolyte at varying temperatures at 100 ml min^{-1} (50 % H_2 : 50 % N_2) and steam relative humidity of 75 %.

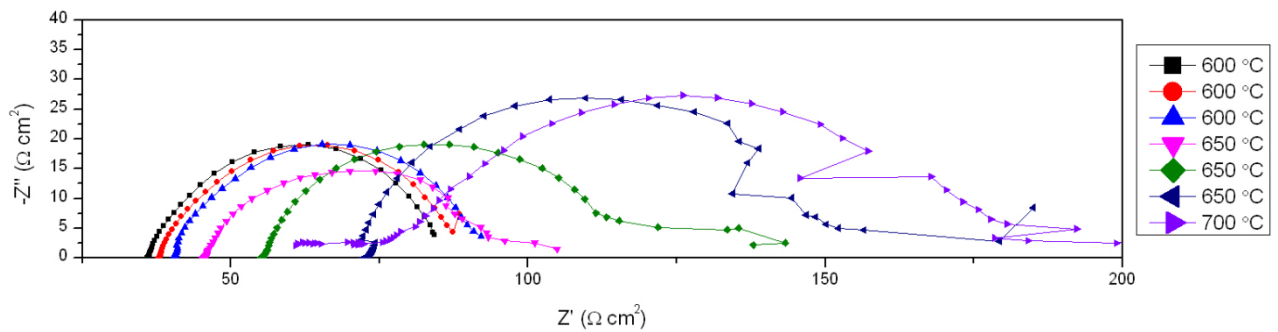


Figure 4-24: Impedance of the symmetrical cell to variations in temperature in 50 % CO₂: 50 % N₂ environment.

The conductivity of the YSZ in a steam environment is shown in Figure 4-23 and shows the dependency of temperature on the operation of the cell. YSZ is known for high temperature operation and therefore, an improvement in ionic conductivity is seen at temperatures at and above 700 °C. It has been suggested that due to the manufacturing process, the conductivity of the YSZ is dependent on the inherent resistance of the grain, the grain boundary resistance and the effective interface bonding ratio [151].

Therefore, the non-linearity of the ionic conductivity of Figure 4-23 corresponds to possible changes from the resistivity of the grain boundary to the grain dominating at increasing temperatures [150]. The change in conductivity dependence occurs after 700 °C, which is the lower limit for YSZ operation. The full range of conductivities is shown in Table 4-2. It can be seen that in general, the conductivities do not vary significantly at different operating environments and are smaller than those in literature [119;152].

As the project aims to use streams from power plants, a carbon dioxide environment was also considered. The impedance in Figure 4-24 shows that the trends were similar to that of the steam environment where the high frequency arc increases with increasing temperature. After the 650 °C curve was taken, the system developed a leak and therefore created a more oxidising environment, which is shown by the larger curves at 650 and 700 °C.

The symmetrical cells have shown that the cathode and electrolyte are dependent on temperature and dictate the resistances exhibited by the cell. Concentration changes have small effects on the performance. Furthermore, the conductivity of the YSZ in

steam is less conductive than in hydrogen, which may be due to the greater oxidising environment, which degrades the cell at a faster rate.

In order to further understand the reasons for the poor performance of the cells compared with literature, SEM was carried out. Figure 4-25 shows the difference between the cell before and after being exposed to a steam environment. It can be seen that the electrodes have small pores throughout the surface; however, as the cell is both reduced and oxidised there is little difference. The changes to the electrodes may cause structural weaknesses in the cell, however further study is required to fully assess the structure.

4.6.2 Electrolyser cell

The SOEC (Ni-CGO / YSZ / LSM) was tested to investigate the variations in electrolyser performance with changing temperature and to assess the typical operating conditions required for the cell.

A number of experiments were carried out in potentiostatic mode, which outlined critical issues with the setup and methodology. One of the greatest problems was seen with sealing the cell, which is a common problem and research is on-going to find a suitable material [153]. Other problems that arose were due to poor electrical contact with the Pt mesh and electrodes and delamination of the cell.

The sealant initially used was Omegabond[®] 300; with uneven distribution of the sealant, cracking of the cell was seen as the sealant dried, resulting in very low current densities as shown in Figure 4-26. It can be seen that the ohmic resistance dominates as the electrolysis is unable to occur in such a system. The impedance (Figure 4-27) measured at the OCV of 0.1 V shows very high resistances of the cell with large amounts of noise, which is attributed to poor electrical connections and cracking of the cell.

Table 4-2: Conductivities of the YSZ electrolyte at a range of temperatures under steam, hydrogen and carbon dioxide environments.

| Temperature (°C) | Conductivity in H ₂ environment (50% H ₂ : 50 %N ₂) (Ω ⁻¹ cm ⁻¹) | Conductivity in H ₂ O environment (10% H ₂ : 90 %N ₂ , RH: 75%) (Ω ⁻¹ cm ⁻¹) | Conductivity in H ₂ O environment (50% CO ₂ : 50 %N ₂) (Ω ⁻¹ cm ⁻¹) |
|------------------|---|--|--|
| 600 | 1.01 × 10 ⁻³ | 3.11 × 10 ⁻⁴ | 7.91 × 10 ⁻⁴ |
| 650 | 1.03 × 10 ⁻³ | 3.18 × 10 ⁻⁴ | 5.40 × 10 ⁻⁴ |
| 700 | 9.99 × 10 ⁻⁴ | 2.85 × 10 ⁻⁴ | |
| 750 | | 1.15 × 10 ⁻⁴ | |
| 800 | | 3.50 × 10 ⁻⁵ | |

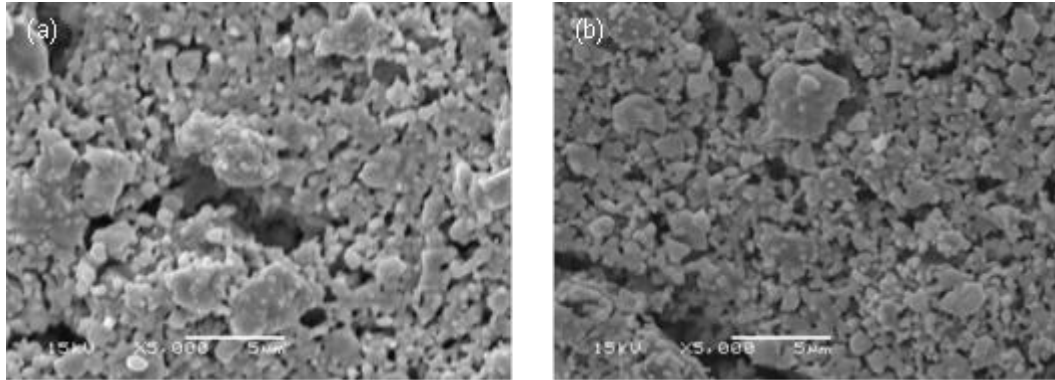


Figure 4-25: SEM of the hydrogen electrode at 15 kV and $\times 5,000$ (5 μm) (a) before sintering and using the cell, (b) After using the cell sintered at 1,300 $^{\circ}\text{C}$ and operated at 650 $^{\circ}\text{C}$ in a humidified gas with 50% H_2 and 50% N_2 .

To improve the sealing issues, 3500N Insulating Glaze (DuPont (U.K.) Ltd., UK), which is a dielectric paste was used as it dries as a glassy substance and should allow for the expansion of the cell when heating up. To set the sealant, it is suggested that the sealant be allowed to dry for 15 minutes (or until dry to the touch) at 150 $^{\circ}\text{C}$ and then fired for 10 mins at 850 $^{\circ}\text{C}$ at a ramp rate of 100 $^{\circ}\text{C min}^{-1}$ and cooled at the same rate. However, the maximum recommended ramp rate for heating the cell without cracks forming is 5 $^{\circ}\text{C min}^{-1}$ and so the dielectric paste was allowed to dry over a longer period of time.

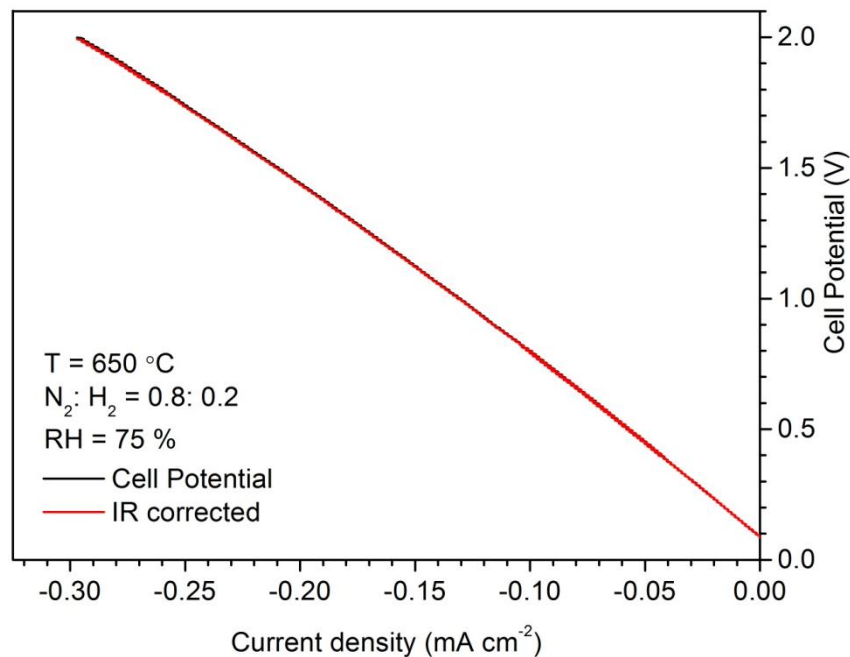


Figure 4-26: Voltage-current (V-i) density curves of SOEC (Ni-CGO / YSZ / LSM) operating at 650 $^{\circ}\text{C}$ with humidified gas at 75 % RH and 20 % H_2 : 80 % N_2 .

4. Experimental verification and analysis

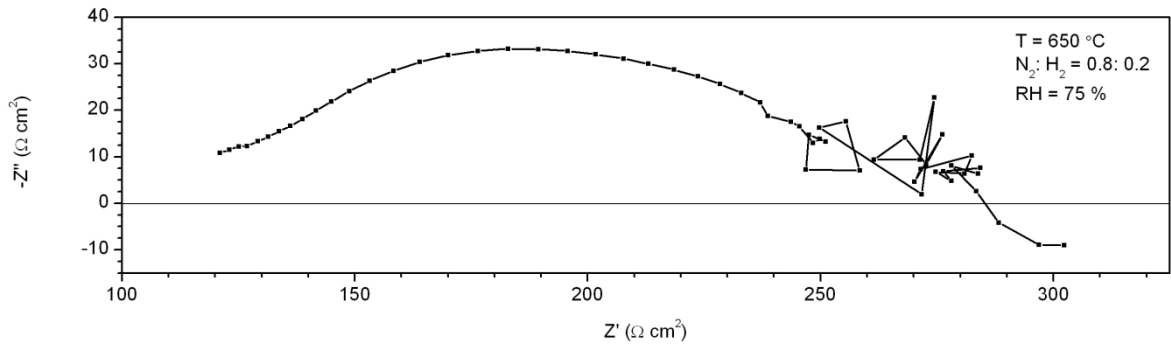


Figure 4-27: Impedance at OCV of 0.1 V at 650 °C with humidified gas at 75 % RH and 20 % H₂: 80 % N₂, based on Figure 4-26 of SOEC (Ni-CGO / YSZ / LSM).

However, it was found that sealing at a lower rate was not a suitable option based on the result shown in Figure 4-28, where low current densities continued to be produced. Furthermore, it was seen that the sealant had not sintered thoroughly enough creating ‘half seals’ of glassy and un-sintered paste, thereby allowing oxygen to enter the cathode side, which reduces the performance of the cell as well as encourages NiO to form. The impedance spectroscopy in Figure 4-28 shows large overpotentials, which is consistent with the small current densities and is a direct result of leaks in the system. The large defect seen at around a cell potential of 1 to 1.3 V is due to instability of the cell while scanning.

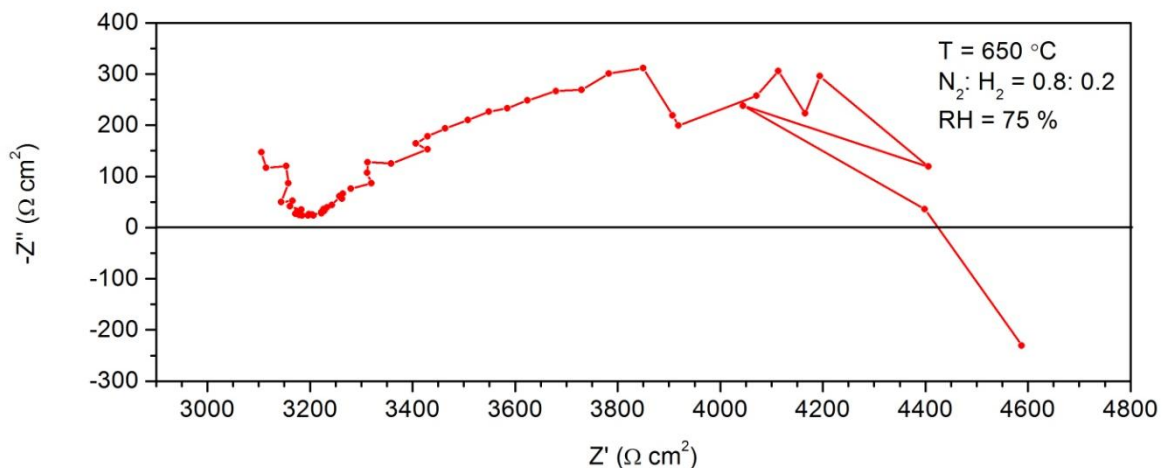


Figure 4-28: Impedance at OCV of 0.2 V at 650 °C after 1 hour of SOEC (Ni-CGO / YSZ / LSM).

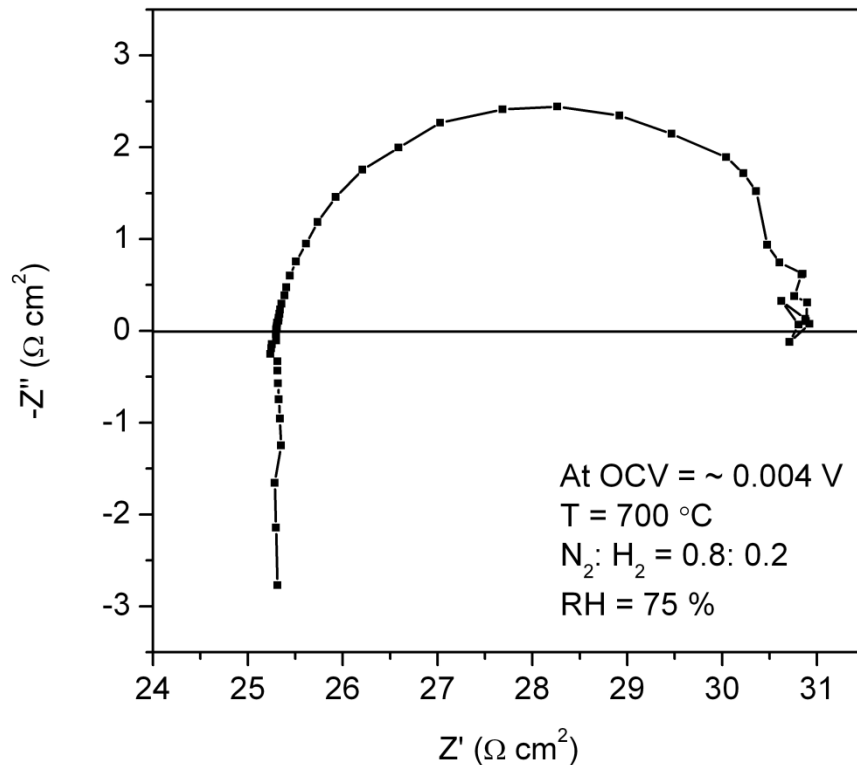


Figure 4-29: Impedance of SOEC (Ni-CGO / YSZ / LSM) at OCV of 0.004 V at 700 °C with humidified gas at 75 % RH and 20 % H₂: 80 % N₂.

A slower scan rate was used in later experiments to allow the system to adjust to the changing potentials. Based on the impedance results of a similar system in Figure 4-29, a difference between poor electrical connection and a crack and leak in the seal can be seen. Poor electrical connections give low current densities, with large resistances in the impedance; however, a crack or seal break gives noisy curves, which represent an unsteady system such as changes in concentration.

Based on the results obtained above, it was clear that a suitable option for providing good electrical connections was needed, especially at the anode. Therefore, the Pt mesh used as a current collector was secured on to the anode of a prepared cell using the same LSM paint as the anode and sintered at 1200 °C for 1 hour at a ramp rate of 1 °C min⁻¹, after being held at 100 °C for 1 hour to ensure that the binder had evaporated. It was found that though a good electrical connection was made, the LSM had delaminated off the YSZ electrolyte, resulting in poor electrolysis. Delamination occurred possibly due to high oxygen pressure build-up at the anode-electrolyte interface [83;154].

4. Experimental verification and analysis

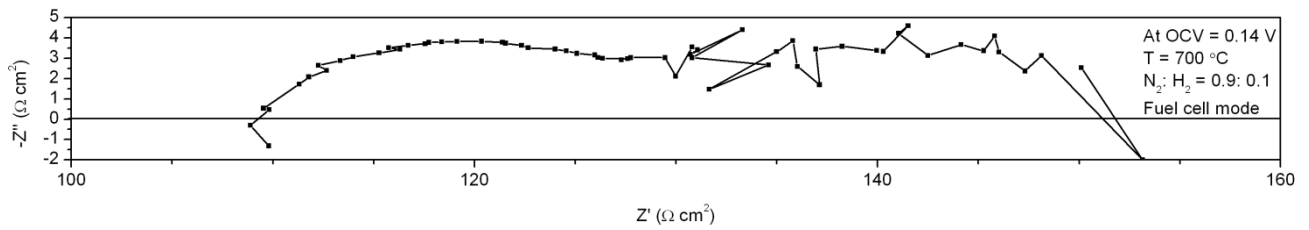


Figure 4-30: Impedance of SOFC (Ni-CGO / YSZ / LSM) at OCV of 0.14 V at 700 °C with 90 % H₂: 10 % N₂.

Operating in fuel cell mode showed large polarisation results, which reflect large resistances in the cell and correlates well with the impedance results of Figure 4-30. It can be seen from Figure 4-30 that there is mass transport limitations in the cell, with instability and poor flow of oxygen to the anode of the cell. As fuel cells rely on good flow of hydrogen and oxygen to the cell, the mass transport limitations seen suggest that a change in the rig is required to achieve improved cell performance.

In order to discount problems with the LSM paste, studies were carried out on NextCell™ Electrolyte Supported Button Cell, manufactured cells. The cells consisted of scandia-stabilised zirconia (ScSZ) electrolyte, Ni-CGO cathode and LSM anode (fuelcellmaterials.com, NexTech Materials Ltd., USA). Sc₂O₃, is a doping material used in combination with zirconia to stabilise the structure in the same way that Y₂O₃ is used [28]. Therefore, the behaviour of a ScSZ electrolyte is similar to that of YSZ but with larger conductivity; at 1,000 °C the conductivity of ScSZ and YSZ is 0.18 Ω⁻¹ cm⁻¹ and 0.13 Ω⁻¹ cm⁻¹, respectively [28]. ScSZ is a popular material as it can be used at both intermediate and high temperatures; however, ScSZ use has been limited due to the large costs associated with the availability of scandia [155;156].

The cell was tested in both electrolyser and fuel cell mode and the result is shown in Figure 4-31. There is a distinct difference in the performance of the cell as a fuel cell with dry and wet H₂ input. The wet H₂ is produced through passing the H₂ gas through a water bottle at room temperature. Though the wet hydrogen showed a decrease in cell performance due to the oxidation of Ni, it provided a less harsh operating condition within the cell, which enabled the cell to operate for a longer time, rather than the dry H₂ flow.

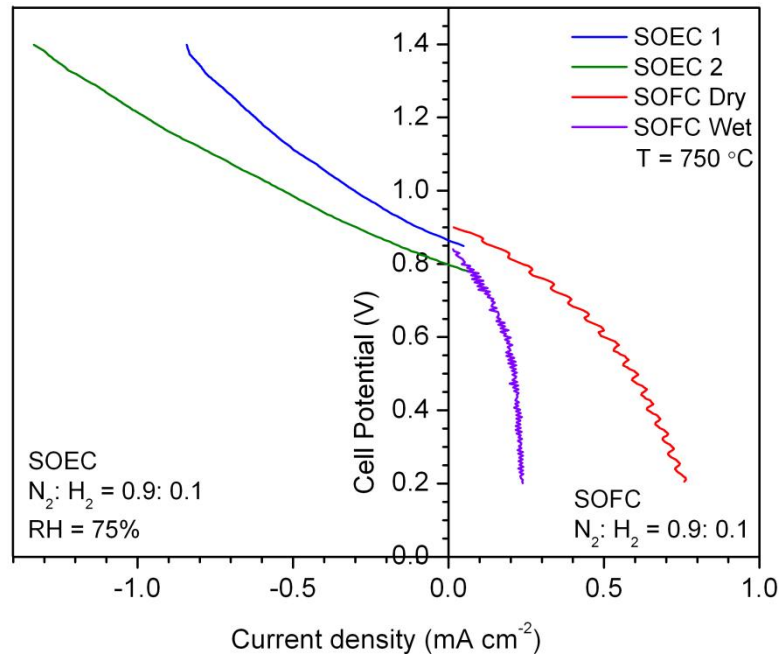


Figure 4-31: Voltage-current (V-i) density curves of bought (Ni-CGO / ScSZ / LSM) operating at 750 °C with SOEC at humidified gas at 75 % RH and 10 % H₂: 90 % N₂ and SOFC at 90 % H₂: 10 % N₂.

Operating in SOEC mode showed improved performance of the cell compared with operating in fuel cell mode. One reason is that unlike the fuel cell, which requires good mass flow of both reactants, the electrolyser only requires one reactant to the working electrode. The anode acts as a way of removing oxide ions. Poor ion conductivity and removal of oxygen can limit the performance of the electrolyser. In the case shown in Figure 4-31, poor electrical connection has caused small current densities.

In order to improve electrical connections, the Pt meshes were sintered onto the cell using Ni-CGO and LSM pastes at 1,250 °C for 1 hour and can be seen in Figure 4-32. To discount problems with LSM, Pt paste was also used on some tests and was sintered for 1 hour at 1,000 °C at a ramp rate of 1 °C min⁻¹.

Figure 4-33 shows the polarisation of an SOEC at 750 °C. Due to the size of the rig, the resistance from the electrical connections were large and therefore, resistance was corrected for using impedance results. It has been assumed that the high frequency intercept represents the resistance along the polarisation curve.

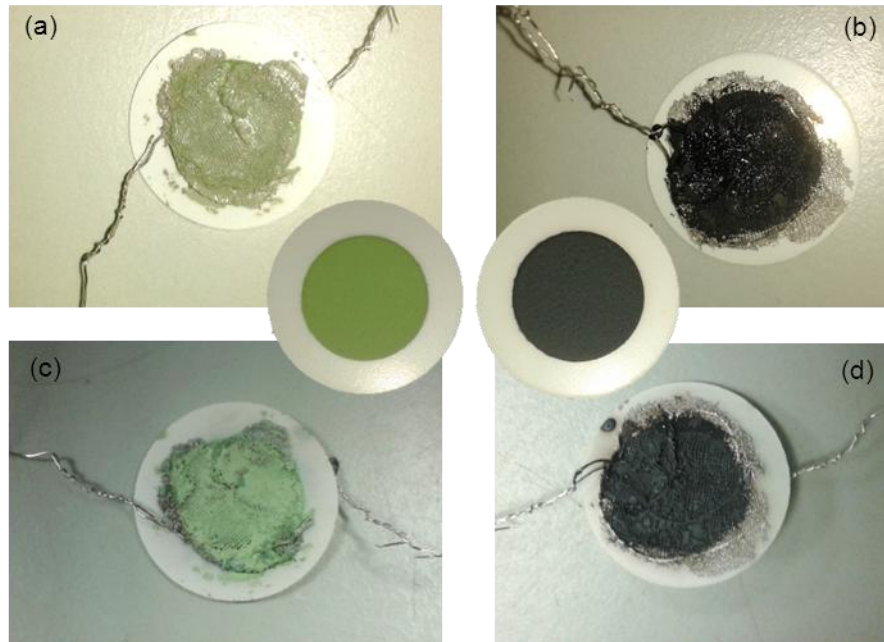


Figure 4-32: NextCell™ Electrolyte Supported Button Cell
(a) Ni-CGO cathode painted onto the bought cell (insert), (b) LSM anode painted onto the bought cell (insert), (c) Ni-CGO cathode after sintering at 1250 °C and (d) LSM anode after sintering at 1250 °C.

The gap seen in Figure 4-33 is due to the sealant cracking due to prolonged exposure at high temperature and therefore created a leak in the system. The impedance results of Figure 4-34 were taken at the OCV of 0.8 V for SOEC. It can be seen that the resistance increases with SOEC operation due to an increased oxidising environment. Furthermore, less defined curves are produced, which suggest an unstable system due to changing concentrations because of the cracked seal.

The seal was improved by using Ceramabond 552 (Aremco Products, Inc., USA) a ceramic based paste. The seal was fixed by leaving to dry in air at room temperature for 2 hours and then heating at 93 °C and 260 °C for 2 hours at each temperature.

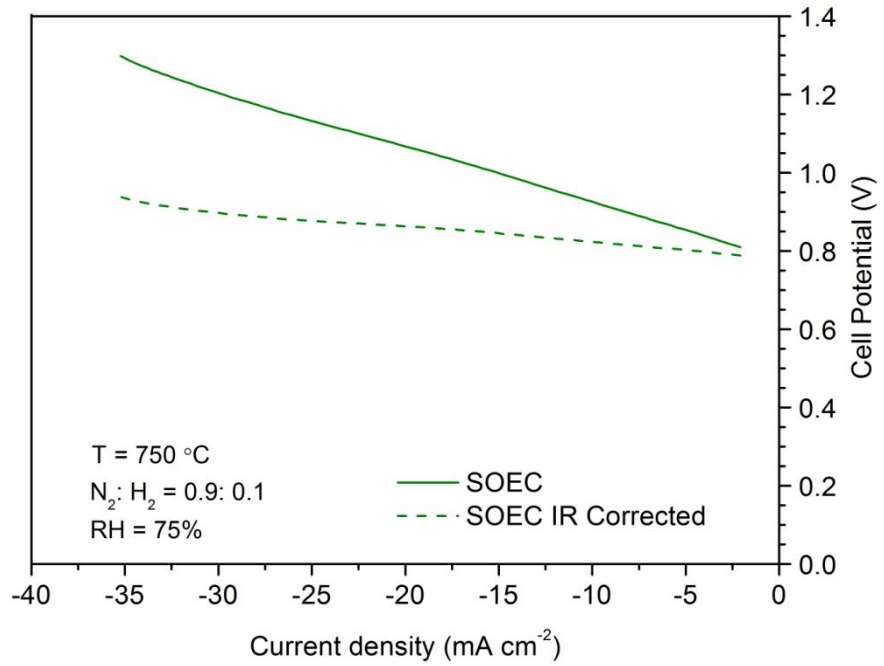


Figure 4-33: Voltage-current (V-i) density curves of commercial Ni-CGO / ScSZ / LSM operating at 750 °C. SOEC conditions- humidified gas at 75 % RH. Resistance correction shown is based on impedance.

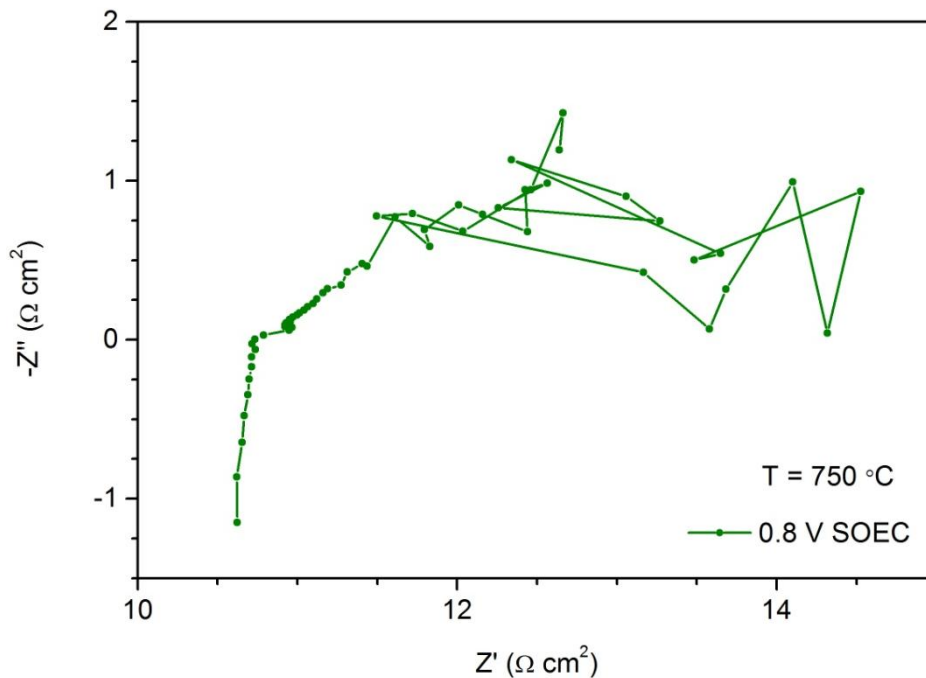


Figure 4-34: Impedance at SOEC (Ni-CGO / ScSZ / LSM) OCV of 0.8 V at 750 °C based on Figure 4-33. SOEC conditions- humidified gas at 75 % RH.

4. Experimental verification and analysis

The cells were operated at various temperatures and with N₂: H₂ ratio of 90 %: 10 % and relative humidity of 75%. The results with varying temperature can be seen in Figure 4-35. As the temperature increases the performance of the cell improves due to improved conductivity of the cell. According to the shape of the curve it can be noted that the concentration overpotentials are small and that ohmic and activation potentials dominate.

Impedance spectroscopies carried out at various potentials along the polarisation curve (Figure 4-35) are shown in Figure 4-36 to Figure 4-40. As with the symmetrical cell, the operating temperature is a significant variable to the performance of the SOEC. At temperatures of 750 and 800 °C, it can be seen from Figure 4-36 and Figure 4-37 that at low potentials charge transfer dominates, where high frequencies show the charge transfer of oxide ions and low frequency resistance is due to the diffusion of ions through the electrolyte [157]. The variations from a common Nyquist plot in the impedance curves may be due to oxygen surface exchange and transport [154].

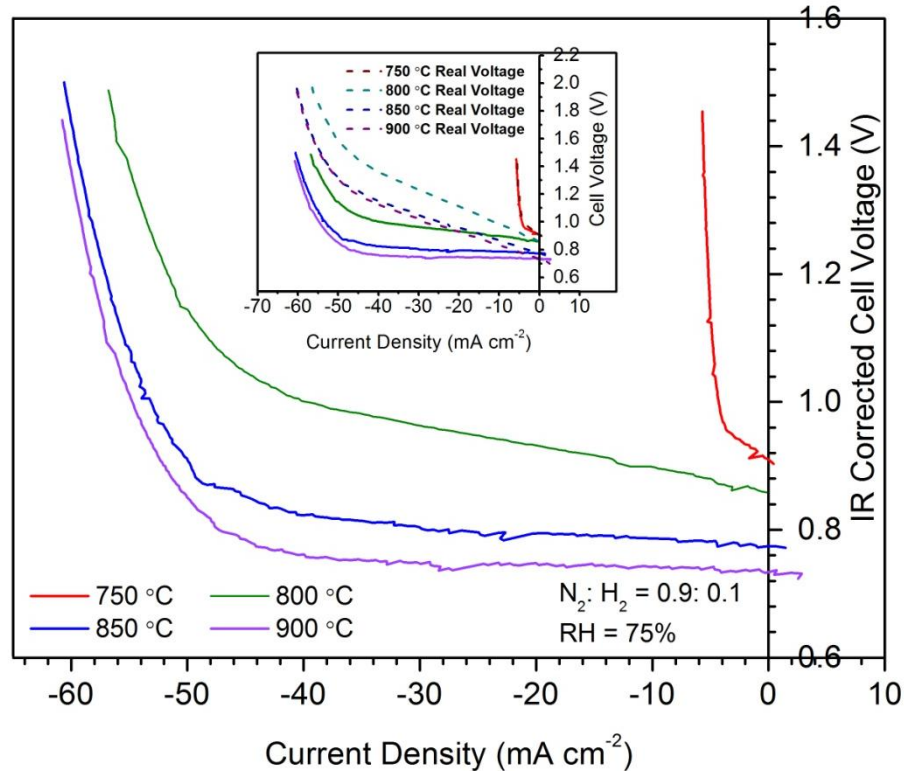


Figure 4-35: Voltage-current (V-i) density curves of commercial Ni-CGO / ScSZ / LSM operating at 750, 800, 850 and 900 °C with humidified gas at 75 % RH and 10 % H₂: 90 % N₂. Insert shows real and IR corrected data.

4. Experimental verification and analysis

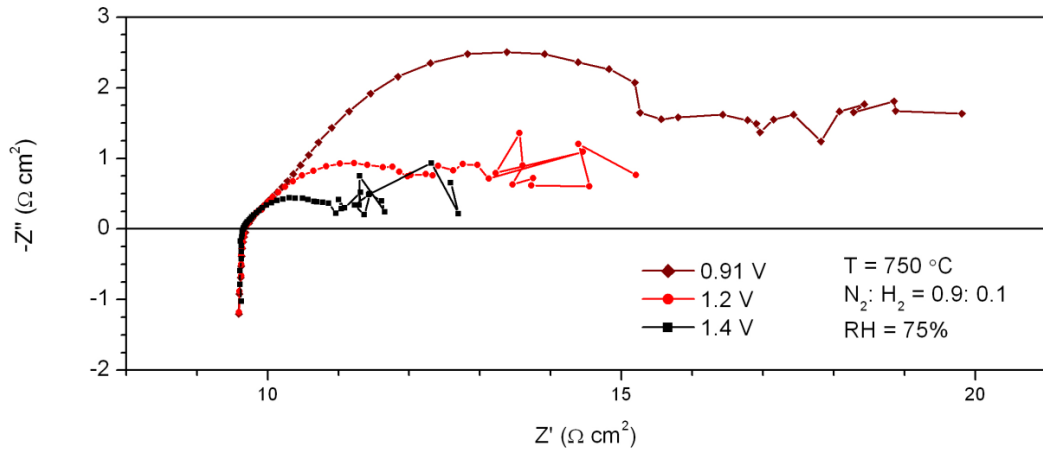


Figure 4-36: Impedance of SOEC (Ni-CGO / ScSZ / LSM) at 0.91, 1.2 and 1.4 V at 750 °C based on Figure 4-35, with humidified gas at 75 % RH and 10 % H₂: 90 % N₂.

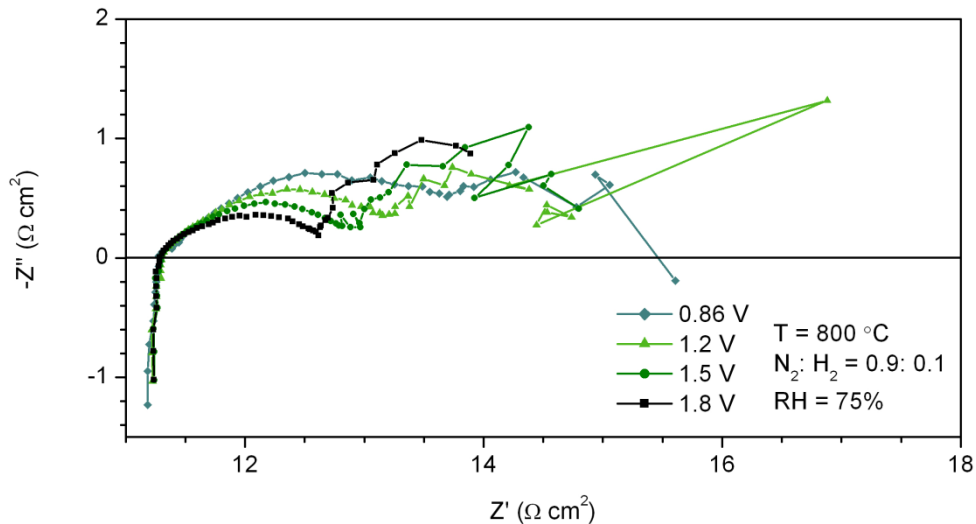


Figure 4-37: Impedance of SOEC (Ni-CGO / ScSZ / LSM) at 0.86, 1.2, 1.5 and 1.8 V at 800 °C based on Figure 4-35, with humidified gas at 75 % RH and 10 % H₂: 90 % N₂.

The decrease in the polarisation resistance at high potentials may be due to reduction of the cathode occurring at low potentials and at high potentials electrolysis dominates and the reduction process is minimal [158]. The two distinct curves with increasing potential in Figure 4-36 and Figure 4-37 suggest that reduction may still be occurring at high potentials, however with electrolysis dominating.

Increased temperatures of 850 °C and 900 °C show significant improvements in the charge transfer resistance (shown in Figure 4-38 and Figure 4-39) as the activation and diffusion terms are reduced and electrolysis rather than reduction of the cathode occurs [159].

4. Experimental verification and analysis

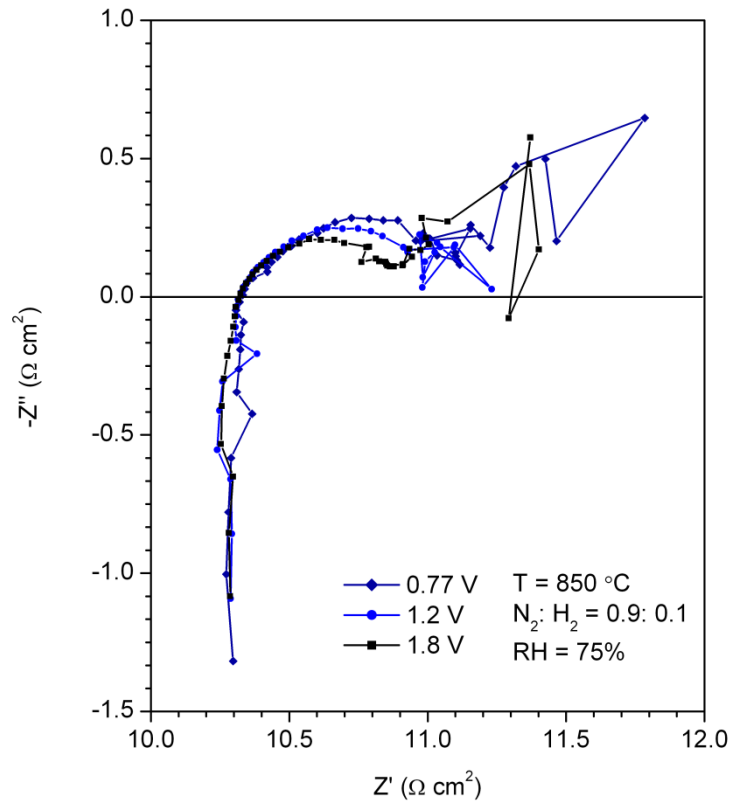


Figure 4-38: Impedance of SOEC (Ni-CGO / ScSZ / LSM) at 0.77, 1.2 and 1.8 V at 850 °C based on Figure 4-35, with humidified gas at 75 % RH and 10 % H₂: 90 % N₂.

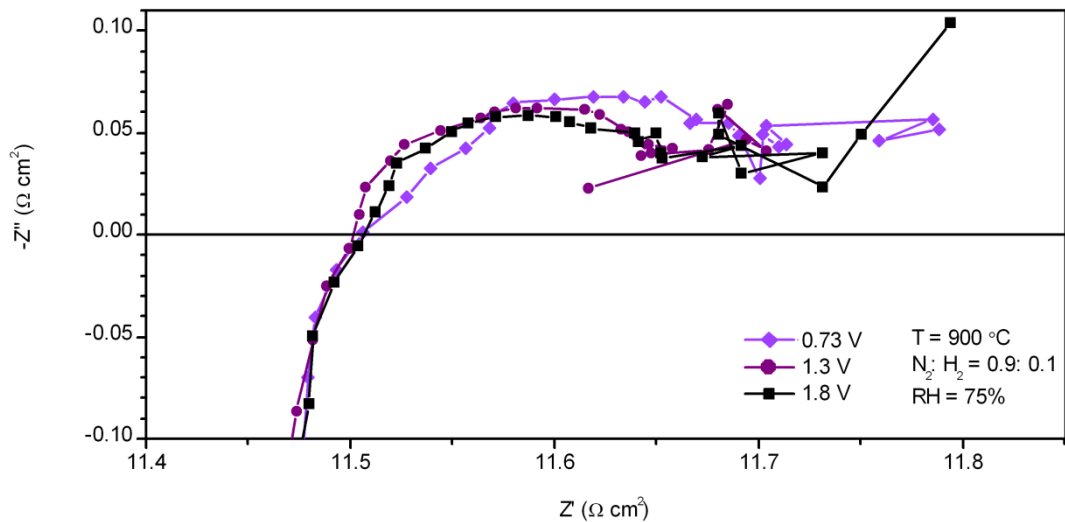


Figure 4-39: Impedance of SOEC (Ni-CGO / ScSZ / LSM) at 0.73, 1.3 and 1.8 V at 900 °C based on Figure 4-35, with humidified gas at 75 % RH and 10 % H₂: 90 % N₂.

4. Experimental verification and analysis

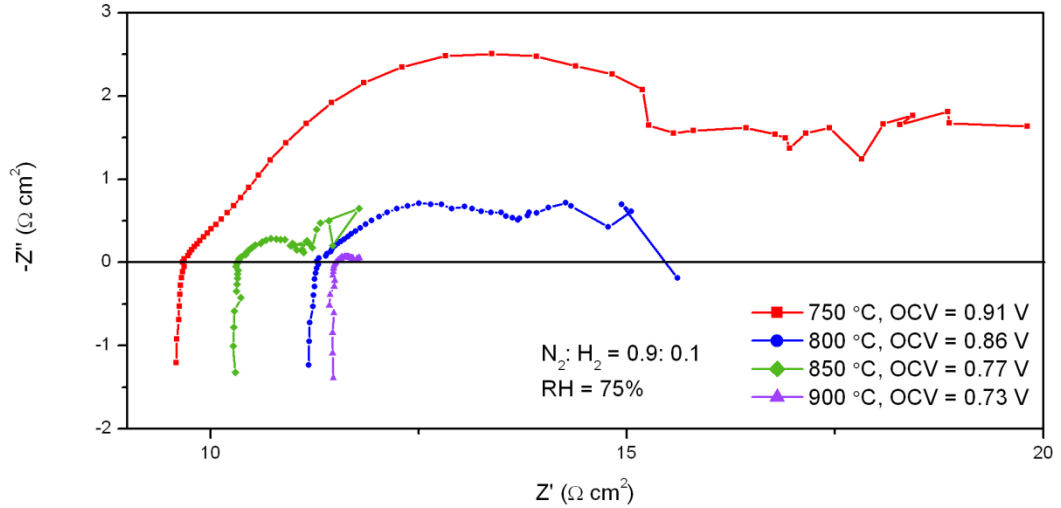


Figure 4-40: Impedance at OCV of 0.91, 0.86, 0.77 and 0.73 V for temperatures of 750, 800, 850 and 900 °C, respectively. Based on Figure 4-35, with humidified gas at 75 % RH and 10 % H₂: 90 % N₂.

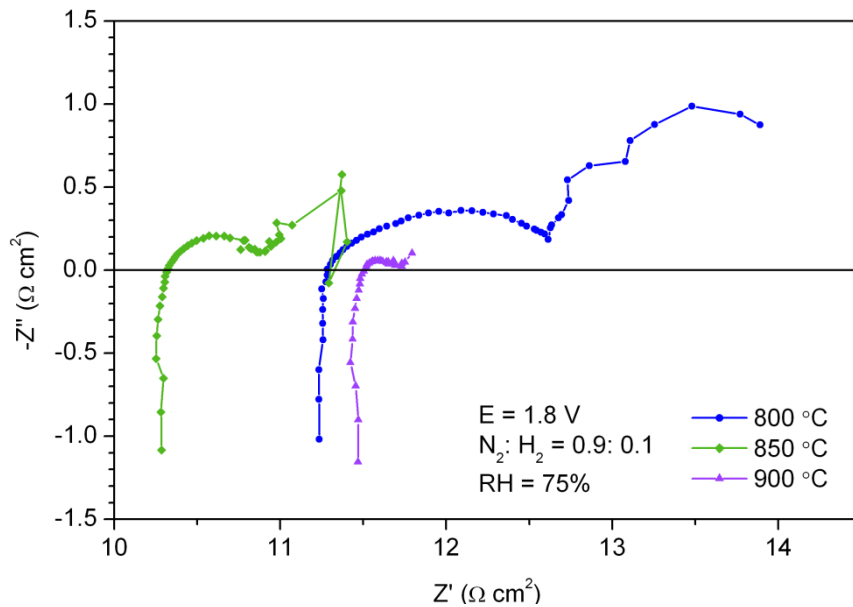


Figure 4-41: Impedance at 1.8 V for temperatures of 800, 850 and 900 °C, respectively. Based on Figure 4-35, with humidified gas at 75 % RH and 10 % H₂: 90 % N₂.

It can be seen for all the impedance curves that the ohmic resistance (high frequency resistance) remains constant and the changes that occur are dominated by changes to the electrolysis reaction. The improvement in resistance can be clearly seen in Figure 4-40 and Figure 4-41, which shows the impedance at OCV of the SOEC operating at a temperature range of between 750 and 900 °C. The shift in the OCV follows

similar trends to that shown in Figure 4-15 and suggests that there the electrical connections are influencing the results of the ohmic resistance.

The polarisation resistance has improved from $10.21 \Omega \text{ cm}^2$ to $0.31 \Omega \text{ cm}^2$ at $750 \text{ }^\circ\text{C}$ and $900 \text{ }^\circ\text{C}$, respectively. The ohmic resistance has changed due to the differences seen in cells, electrical connections and degradation of the cell due to the length of SOEC operation before the scans were taken.

To further assess the limited performance of the cell SEM was carried out before and after the experiment. The SEM of the cathode shows differences in the porosity and grain size of the commercial cells (Figure 4-42(b)) and the ones that were made in-house (Figure 4-42(c)). The cells that were made show finer particles with smaller pores compared with Figure 4-42(b). It was also seen that the Pt paste used to secure the Pt mesh to the cell was far more porous than the Ni-CGO paste and therefore is a suitable option for further experiments.

The cathode (Figure 4-42(a)) was seen to be layered on to the ScSZ electrolyte with Ni-CGO composite and Ni layer on the top. This contrasts with the cell made in the lab (Figure 4-42(c)), which shows a large amount of ceramic to Ni and is uniform throughout.

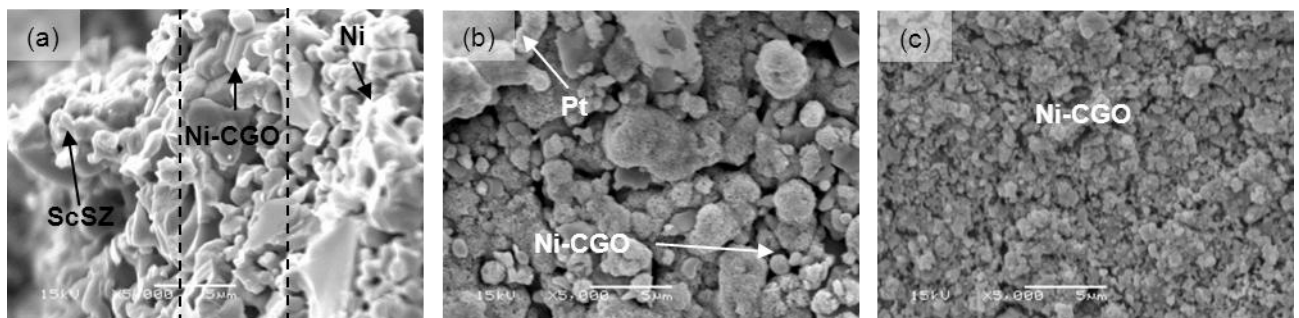


Figure 4-42: SEM of the hydrogen electrode (Ni-CGO) (a) before sintering and using the cell, (b) After using the cell sintered with Pt painted to secure the Pt mesh current collector and operated at $750 \text{ }^\circ\text{C}$ and (c) After using the cell sintered with Ni-CGO painted to secure the Pt mesh current collector and operated at $900 \text{ }^\circ\text{C}$.

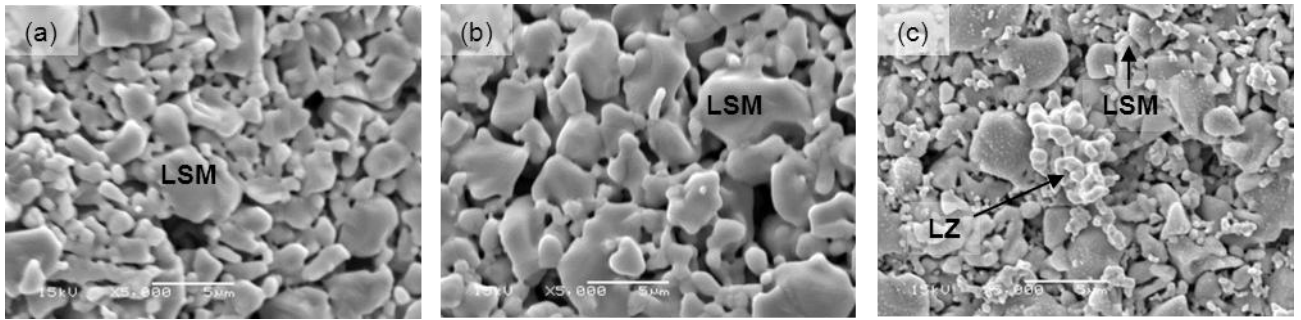


Figure 4-43: SEM of the oxygen electrode (LSM) (a) before sintering and using the cell, (b) After using the cell sintered with Pt painted to secure the Pt mesh current collector and operated at 750 °C and (c) After using the cell sintered with LSM painted to secure the Pt mesh current collector and operated at 900 °C

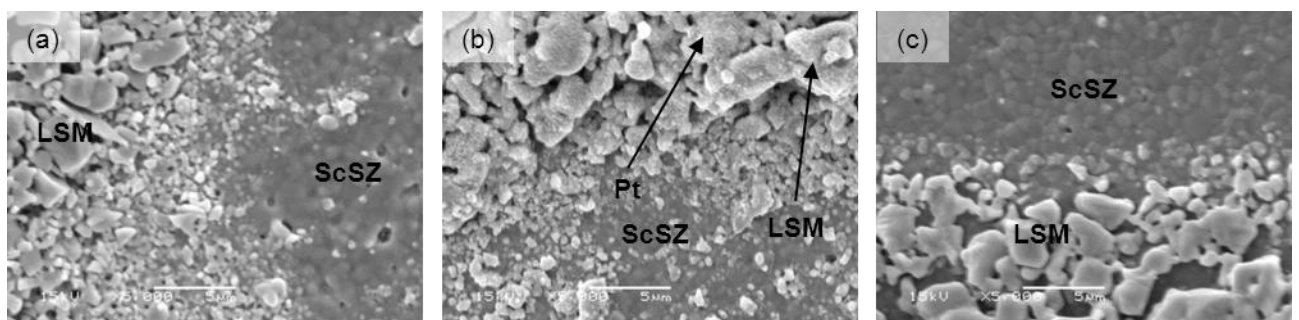


Figure 4-44: SEM of the oxygen electrode (Ni-CGO) at the boundary with the electrolyte (a) before sintering and using the cell, (b) After using the cell sintered with Pt painted to secure the Pt mesh current collector and operated at 750 °C and (c) After using the cell sintered with LSM painted to secure the Pt mesh current collector and operated at 900 °C.

The LSM anode showed instability throughout the experimentation, which was seen in the noisy second arcs of the impedance curves. The first arc follows the same trend as those of the symmetrical cell and therefore, it can be assumed that the second arc characterises the electrolyser anode. The instability resulted in poor electrolyser performance. Figure 4-43(a) shows the SEM of the LSM anode as received and before being used. It can be seen that there is an even surface and EDS showed that there was a uniform consistency of LSM throughout. After re-sintering at 1,250 °C, the particles become less defined as seen in Figure 4-43(b).

Problems with delamination of the LSM electrode were experienced throughout the investigation. It was found that the anode had turned to a powder on the electrolyte and was coming away from the cell after SOEC testing. Delamination can be caused as a result of a build-up of oxygen at the electrode-electrolyte interface [83].

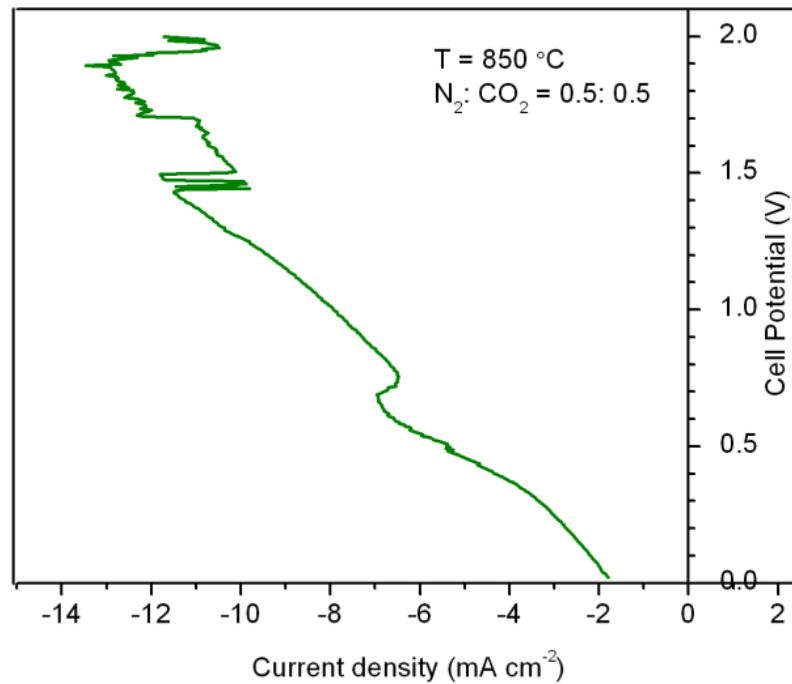


Figure 4-45: SOEC (Ni-CGO / ScSZ / LSM) testing with 50% N₂: 50% CO₂ at 850 °C.

As seen with the impedance curves, oxygen surface exchange and oxygen transport may be seen through the slant of the curve. The slant was not seen with symmetrical cell testing of the cathode and therefore, it is assumed to be a result of the anode. Delamination may also be caused by an uneven anode-electrolyte interface, which is possible as the electrode is painted on to the cell. Polarising the SOEC forms oxygen at the anode-electrolyte interface and can react with the zirconate to form lanthanum zirconate (LZ) [154]. Small amounts of LZ were seen using SEM and EDS. The SEM and EDS results suggest that the large resistances seen in the investigation is partly caused by delamination and accounts for some of the degradation in the cell after polarising [154]. Figure 4-44 shows the surface between the LSM anode and ScSZ electrolyte. It can be seen that there is a distinct difference in the dense electrolyte and the porous electrode.

With a use needed for the large amounts of CO₂ emissions and syngas being a focus for future energy solutions, electrolysis of carbon dioxide has been studied in literature [128]. The electrolysis of carbon dioxide was also carried out with the setup described above and the results shown in Figure 4-45 to Figure 4-47.

4. Experimental verification and analysis

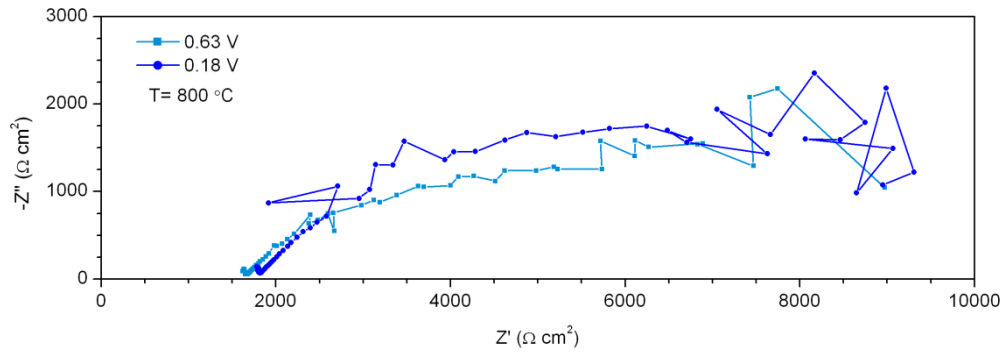


Figure 4-46: Impedance of SOEC (Ni-CGO / ScSZ / LSM) at OCV of 0.63 and 0.18 V before and after leak, respectively at 800 °C with 50 % CO₂: 50 % N₂.

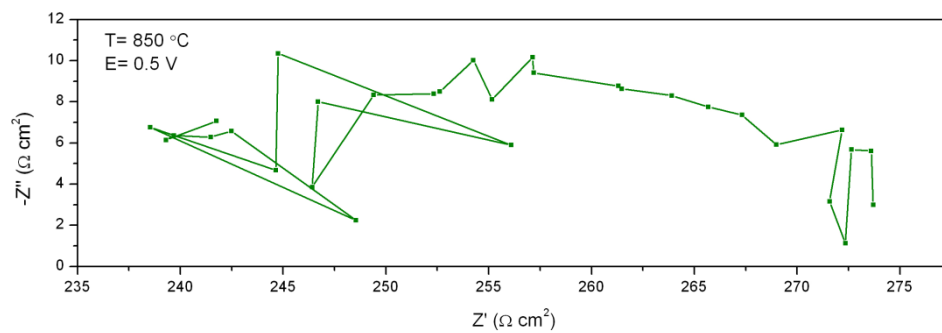


Figure 4-47: Impedance of SOEC (Ni-CGO / ScSZ / LSM) at OCV of 0.5 V and 850 °C. Based on Figure 4-45, with 50 % CO₂: 50 % N₂.

It can be seen that the electrolysis of CO₂ is more complex to operate as the system struggled with maintaining a constant OCV. This can be due to instabilities in the system such as cell degradation [160]. After the test, large cracks in the sealant were seen suggesting that the performance could be improved with a more suitable setup.

Through the particular test shown in Figure 4-46, a drop in the OCV was seen due to crossover of gases; however, the resistances and operation of the cell remained the same at OCV of 0.63 and 0.18 V. At a temperature of 850 °C the performance of the SOEC and resistance was reduced compared with operation at 800 °C (Figure 4-47). However, quick degradation of the cell was seen, which led to an unstable system. Introducing CO to the CO₂ inlet would prevent such rapid degradation and enable the system time to stabilise before testing. It is noted that the performance of the SOEC is greater with steam rather than CO₂, which agrees with literature [31;37].

Electrolysis of CO₂ though promising to produce syngas from waste CO₂ requires more research and development of materials and systems in order to enhance SOEC

performance. The rig and sealant in this investigation requires attention in order to achieve improved outputs from the electrolyzers.

4.7 Conclusions

SOEC experimentation in literature has focused on developing materials suitable for high temperature electrolysis as well as the effect of variables on performance. This investigation designed a complete workstation and rig to assess the performance of an SOEC in the range of between 700 and 900 °C with standard materials of Ni-CGO, YSZ, ScSZ and LSM.

It was seen that the temperature was a significant factor in the performance of the cell, with conductivity of the YSZ ranging from $3.11 \times 10^{-4} \Omega^{-1} \text{cm}^{-1}$ and $3.50 \times 10^{-5} \Omega^{-1} \text{cm}^{-1}$ at 600 °C and 800 °C, respectively. It was also seen that the polarisation resistance at OCV significantly decreased with increasing temperature, from $10.21 \Omega \text{cm}^2$ to $0.31 \Omega \text{cm}^2$ at 750 °C and 900 °C, respectively. This correlated with improved SOEC performance seen when polarising the SOEC. Therefore, using YSZ or ScSZ electrolytes requires high temperatures in excess of 850 °C to generate low resistance, high performance results. Similarly, electrolysis of CO₂ improved with increasing temperature, however, showed reduced performance compared with steam electrolysis.

In order to further improve performance a redesign of the rig is necessary to reduce delamination effects, such as including a sweep gas of air to ensure oxygen is removed from the anode, as well as conditioning the cell prior to testing. Improvements made to the system and the cell can enable electrolysis for hydrogen production to become feasible in the long term.

Using alternative sealant that is thermally and electrically insulating or a high temperature gasket can prevent sealing problems in the future [161]. Issues with oxygen build-up and known problems of delamination of LSM anode can be rectified through a change in the experimental rig to allow a steady flow of air to the anode, which will create a partial oxygen environment to enable diffusion as well as a ‘sweep gas’ to remove oxygen that is produced. An alternative option is to use Pt as an electrode as delamination has not been seen during testing [154].

It has also been shown in literature that the method used to produce cells affects the SOEC performance. Therefore, carrying out tests for identifying the conductivities and exchange current densities at the conditions used in this investigation would

allow for a more accurate model. Testing pellets of each electrode with Pt current collectors and connections using a four point DC technique would enable the conductivities to be gathered experimentally [122;162]. Further testing of the pellets to acquire the exchange current density of each electrode would also allow a more accurate model to be developed. A re-design of the experimental rig is required for additional testing to obtain variables for the model.

5 Modelling and analysis of coal fired plants

Coal fired power plants are relied on throughout the world to meet growing electricity demands. Most plants do not have carbon capture facilities and therefore are large emitters of carbon dioxide. The plants are operated in a cyclical manner where they are turned down at night when energy demand is low and turned up when demand is high. During the night, there is therefore a possibility of extracting steam from the plant for an electrolyser.

This chapter aims to understand whether steam extraction is possible from a general coal fired power plant and the extent of efficiency loss which would result from extraction. It further assesses the role of coal fired power plants in the UK's energy mix.

5.1 Modelling and analysis of power plants in literature

5.1.1 Review of energy market

As with many nations, the UK's energy mix includes power production through gas, coal and nuclear sources, with increasing amounts of renewable power [163;164]. Although there is a move toward a low carbon economy by 2050 in the UK [165], which is stimulated by the Climate Change Act 2008 [165], the reliance on hydrocarbon-based fuels such as coal, which currently contributes to 29 % of annual energy production, has been predicted to increase globally [166]. It is therefore very likely that conventional technologies such as coal fired power plants will still be operational in the near to medium future across the world. Projections from 2008 to 2035 indicate that the use of coal in the US and UK will remain generally constant; however, a marked rise in coal use is predicted internationally, especially in countries such as China and India [166].

In the UK, coal, combined cycle gas turbine (CCGT), nuclear, wind, hydro, pumped storage together with French, Irish and Dutch interconnects (electrical energy exchange between countries), are regularly used for producing electricity. Though there are a number of new technologies being used in the current configuration, it can be seen from Figure 5-1 that the largest power output in a 24 hour period is from coal fired plants [163].

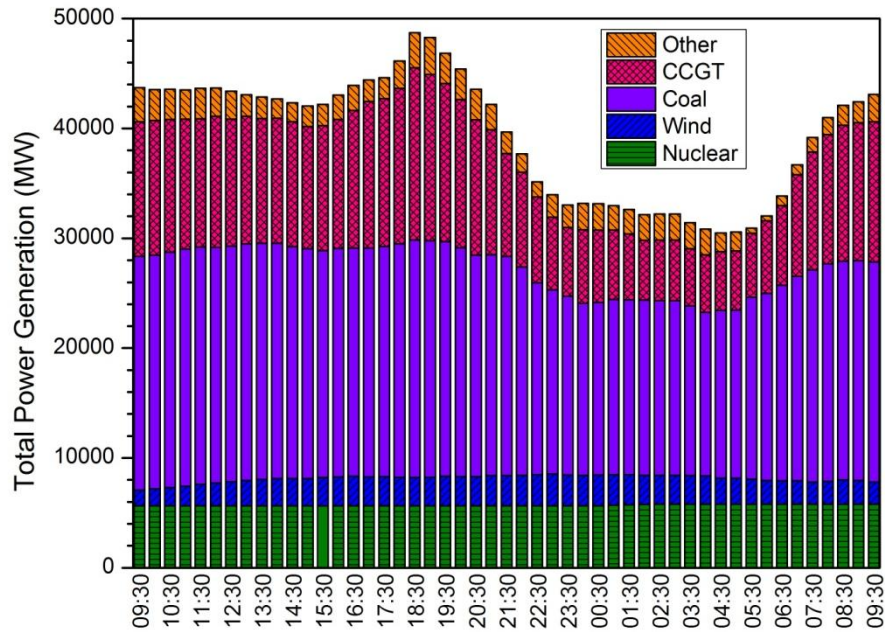


Figure 5-1: Power generation in the UK by different technologies per settlement period from 09:30 on 19.03.2012 to 09:30 on 20.03.2012, adapted from BM reports (2012) [163].

Figure 5-1 also shows that technologies such as nuclear, which are not dispatchable, produce power constantly throughout the day. However, others such as coal, which are more dispatchable, are called on in times of higher power demand. During times of low demand, the power station is operated at its minimum base load, normally from 22:00 until 06:00 the next day.

Hydrocarbon-based fuels, especially coal, will continue to be used in the near to medium future. Furthermore, the cost of coal has been seen to be more attractive than gas or oil, which has resulted in plans for the construction of coal fired plants around the world with a significant growth of construction in China [4;167].

5.1.2 Review of power stations

There are currently over 2,300 coal fired power plants operating globally [168]; around 75 % of these operational coal fired power plant are subcritical [169]. However, between 2000 and 2011, 50 % of the new build power plants have been the state-of-the-art high efficiency and low emission supercritical power stations [169]. Supercritical power plants operate with steam above the supercritical temperature and pressure, 374.15 °C and 220.87 atm, most of which are used in Europe due to increased efficiencies compared with subcritical plants. In general,

efficiencies vary between 36.7–38.6 % and 39.2–41.3 % for subcritical and supercritical plants, respectively [170;171].

As illustrated in Figure 5-2 a conventional coal-fired power plant operates by combusting coal with preheated air, which heats water into superheated steam. The superheated steam drives the steam cycle, also known as the Rankine cycle, where the high pressure turbine (HP), intermediate pressure turbine (IP) and low pressure turbine (LP) are driven, which in turn rotates the shaft for power generation [172;173]. The steam once leaving the LP turbine is condensed into water and pumped back to the boiler where it is reheated into superheated steam once more. The general operating conditions for the main coal fired power plants are shown in Table 5-1.

As power plants are operated cyclically, i.e. turndown (but not shut down) in the night, and turn-up during times of peak energy demand, they are a possible option for integrating with solid oxide electrolyser cells (SOECs), as both electricity and steam can be sourced from the plant. Unlike renewable sources of power such as nuclear, wind and solar energy where the infrastructure is not in place and therefore water needs to be purchased, demineralised and heated prior to use in SOECs; the infrastructure is already in place from the power plant and produces steam at suitable conditions. Therefore, combining SOECs with power plants rather than renewable technologies at the moment means that electrical energy requirement needed to condition the water should be lower. In order to assess the conditions of each stream of the plant and whether they are suitable for integration with SOECs, a power station model has been developed.

Table 5-1: Typical operating conditions for different types of coal fired power plants [169].

| Type of coal fired power plant | Main steam Temperature (°C) | Main steam Pressure (atm) | Typical maximum efficiency (%) |
|---------------------------------------|------------------------------------|----------------------------------|---------------------------------------|
| Subcritical | 538 | 167 | 39 |
| Supercritical | 540 – 566 | 250 | 42 |
| Ultra-supercritical | 580 – 620 | 270 – 290 | 47 |

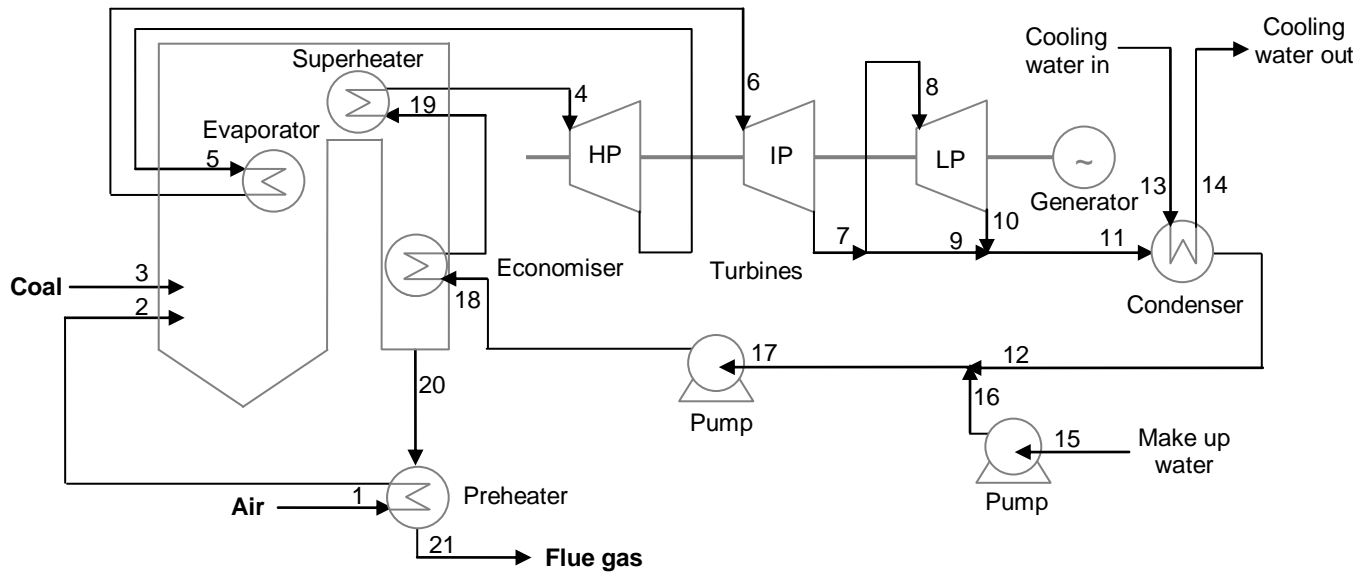


Figure 5-2: A schematic of a conventional coal fired power plant.

The power plant model that has been developed is a simulation, which is based on thermodynamic principles. Generally, power plants are turned down by reducing the amount of coal put into the boiler and reducing the flowrate of the steam cycle. If the plant is to be coupled with SOECs, the power plant must still be fully operational in order to extract both the steam and electricity needed for SOEC operation. Therefore, turndown of the plant in this study refers to steam extraction from the plant rather than a reduction in coal input. It is important to assess the extent of the reduction in power plant efficiency of steam extraction to fully understand whether an integrated system (power plant-SOEC system) is a viable option for meeting future hydrogen fuel needs. Therefore, the model is being used to assess the outcome of turndown through steam extraction on the overall efficiency of the plant.

5.1.3 Literature review of modelling of power plants

Based on future projections of an increase in coal use across the world, together with climate change objectives of reducing CO₂ emissions from industrial plants, a variety of recent research has been conducted, which model coal fired plants and carbon capture, storage and utilisation options.

Although most coal fired plants currently operational operate at subcritical conditions, the most efficient coal fired power plants are supercritical, ultra-supercritical and gasification power plants. Ultra-supercritical power plants aim to operate at 700 °C and 350 atm, which can provide power plant efficiencies of around

50 %. These plants operate at above supercritical conditions and have driven the progress in materials engineering [174]. As a result of improved efficiencies in boiler and power plant technology, many studies have investigated supercritical plant models.

Modelling of a supercritical pulverised coal fired power plant based on mass and energy balances and thermodynamics using Monte Carlo simulation showed the extent of waste produced and optimised power plant operating conditions [175;176]. The results show the optimum plant conditions were a main steam temperature and pressure of 600 °C and 250 atm, with reheat conditions of 600 °C at 32.5 atm. The exit pressure at the low pressure turbine (LP) was 0.089 atm at 180 °C. These optimised conditions for a 425 MW supercritical plant produced a net efficiency of 43 % [175]. These correlate with typical power plant information in literature [176].

Recent concerns over reducing CO₂ emissions have motivated the development of carbon capture, storage and oxy-fuel technologies. Therefore, the focus of recent work has been to assess the effect of including these technologies on plant efficiencies. It is generally accepted that carbon capture and storage (CCS) requires steam to be extracted from the plant for regenerating the solvent from the stripper, and some electrical energy to operate the compressors [167;176-178]. These studies have focused on suitable points of extraction from the steam cycle so as to ensure maximum net plant efficiency. In general, the consensus has been to use steam from the LP turbine, which provides suitable temperatures for solvent regeneration as well as having a limited impact on the plant. Sanpasertparnich *et al.* (2010), modelled an 800 MW_e coal plant with CCS through an amine-based process with 250 atm and 600 °C main steam and reheat at 54 atm and 620 °C in ProMax®. Several streams from the plant were identified to be used for the reboiler of the CCS process to separate the CO₂ from the solvent. These were shown to be the crossover pipe between IP and LP turbines, at a pressure of 9 atm, and two LP ports giving pressures 4.5 and 3 atm, respectively. As a result of steam extraction, it was seen that the smallest impact on the plant was extraction from the LP port at 3 atm, which provided 90 % CO₂ capture efficiency with a plant efficiency loss of around 12 % [167]. The efficiency in this case is describes as:

$$Efficiency_{Thermal} = \frac{W}{Q_H} \quad (9)$$

Extracting steam from the IP/LP crossover pipe for CCS technology has also been investigated by Stepczyńska-Drygas *et al.*, and showed that the post combustion chemical absorption process to capture CO₂ requires large amounts of heat to regenerate the solvent and compress the CO₂; these processes ultimately reduces the efficiency of the plant. Furthermore, the pressure of the steam in the crossover pipe was seen to be a significant factor in overall plant efficiency; a drop of the crossover pipe pressure from 5 to 3.3 atm gives an efficiency improvement of 0.75 % for a plant with single reheat [174]. Therefore, maintaining the conditions of the steam at each stage is necessary to achieve the highest possible efficiency while still capturing CO₂. Furthermore, the energy requirements of additional equipment on the plant need to be as low as possible to ensure the greatest overall energy efficiency.

Other studies have focused on improving the efficiency of the plant through combining oxy-fuel and air to the combustion process. The modelling results for an 800 MW_e supercritical pulverised coal fired plant operating with main steam condition of 290 atm and 600 °C and a reheat of 60 atm and 622 °C, showed that introducing air to the combustion process reduces efficiency from 36 to 34 %, with further losses to 30 % with CO₂ capture [179]. The reduction in efficiency may be considered necessary in order to meet carbon emission targets.

Many of the studies have concentrated on implementing CCS and oxy-fuel as a method of reducing carbon emissions and improving power plant efficiency, respectively. Alternatively, methods of hydrogen production from gasification have been simulated. One method was a high purity oxy-fuel coal gasification process with an aim of producing hydrogen at high pressures. The plant operated a three turbine system with HP, IP and LP steam at 103, 38 and 3.9 atm, respectively. It was shown that recycling the CO₂ from the syngas and using it as the coal carrier gas to the dry feed gasifier, as well as increasing the O₂ purity from the ASU, produced H₂ with purity of 96 % vol. at 63 atm. The overall plant efficiency was improved from 53 to 58 % [180].

A parametric study of coal gasification for hydrogen production by Huang *et al.* (2014) assessed the steam-to-carbon ratio to provide the maximum amount of hydrogen. As gasification has shown higher plant efficiencies than conventional coal fired plants, gasification allows for a greater yield of syngas and hydrogen [181]. It has been shown that for a gasifier operating at 1,350 °C through combusting coal in oxygen, with a steam-to-carbon ratio of 0.9, gives the maximum hydrogen yield.

Therefore, around 2,196 kg hr⁻¹ of hydrogen can be produced with 0.855 MW of power from the nitrogen turbine, thereby giving 53.8 % plant energy efficiency [181]. Furthermore, studies have shown that using NiO supported on modified dolomite catalyst rather than Ni catalyst during gasification would increase yield of hydrogen by 10 % as well as eliminating the tar produced [182].

To enable further efficiency improvements in power and hydrogen generation, as well as reducing CO₂ emissions, a coal and supercritical steam gasification process has been studied. Unlike conventional gasification, using supercritical water enables faster and more complex reactions and therefore enables the steam reforming and water gas shift reaction to occur in one reactor. Furthermore, impurities in the coal which normally created NO_x and SO_x are deposited as N and S inorganic salts. As CO₂ has a different solubility to H₂ with supercritical water it is much easier to separate without the need for expensive recovery processes. The process itself produces coal-electricity efficiencies of over 60 % [183].

Through CCS and oxy-fuel technologies, coal power plants can be made more efficient; however, utilising the plant's high temperature steam and electricity for hydrogen production through SOEC operation may provide greater energy efficiency for the plant. In order to assess the suitability of combining a power plant with electrolysis technology, a coal fired power plant has been modelled in CHEMCAD 6.0 to assess the conditions of the streams available across the plant. This type of plant was chosen as a case study as both the electricity and steam needed for SOEC operation can be sourced from the plant. The model is described next.

5.2 Power plant modelling and simulation

A steady-state simulation of a coal fired power plant based on the Rankine cycle with reheat was developed for this study in CHEMCAD 6.0, and the flowsheet is shown in Appendix, A2, with stream and unit details in A3 and A4, respectively [184]. The model simulated the combustion process of coal with air and the steam cycle, which is superheated by the heat released from the exothermic combustion reaction. The steam is then used to drive the high pressure, intermediate pressure and low pressure turbines (represented in Figure 5-2). In this model, a secondary reheat of the steam is simulated in order to achieve a greater efficiency of the power plant.

5.2.1 Model validation

The model was validated against data compiled by the US Department of Energy, based on a supercritical pulverised coal (PC) plant producing 400 MW of power and commercial data provided by International Power on a 800 MW plant [185;186]. The aim of the model validation was to assess that the simulations in this study delivered the same efficiency as the published studies. Simulations were carried out using the information in Table 5-2 and the results given in the same table for comparison.

The data of equipment settings as well as steam and coal conditions and flowrates from the publications were used as the inputs to the model developed in this study (shown in Table 5-2). Due to unavailable data from the literature such as the turbine efficiency, temperature of the preheated air and air ratio, these parameters have been assumed; the HP turbine has been assumed to operate at 79 % and the IP and LP turbines at 90 % [172]. The results show a good correlation between that of the literature and the model in this study, with errors in overall plant efficiency of 2.2 and 4.7 % in the overall efficiency. Due to the low error in plant efficiency, the power plant model is considered to be validated.

Table 5-2: Coal fired plant model validation based on literature values.

| | DOE, 1999 [185] | DOE, 1999 (this study) | International Power plc., 2003 [186] | International Power plc., 2003 (this study) |
|---|----------------------------|-----------------------------------|---|--|
| Coal type | Illinois #6 | Illinois #6 | - | Indonesian coal |
| Coal flowrate (kg hr ⁻¹) | 147,550 | 147,550 | - | 446,973 |
| Air flowrate (kg hr ⁻¹) | 1,234,884 | 1,234,884 | - | 2,298,717 |
| Main steam flowrate (kg hr ⁻¹) | 1,350,000 | 1,220,000 | 2,590,224 | 2,723,483 |
| Main steam temperature (°C) | 566.0 | 566.0 | 537.8 | 537.8 |
| Reheat steam temperature (°C) | 566.0 | 566.0 | 566.0 | 566.0 |
| Main steam pressure (atm) | 242.3 | 242.3 | 166.5 | 166.5 |
| Reheat steam pressure (atm) | 42.8 | 42.8 | 38.3 | 38.3 |
| Low pressure steam pressure out (atm) | 0.26 | 0.26 | 0.30 | 0.30 |
| HP turbine efficiency (%) [172] | - | 79.0 | - | 79.0 |
| IP turbine efficiency (%) [172] | - | 90.0 | - | 90.0 |
| LP turbine efficiency (%) [172] | - | 90.0 | - | 90.0 |
| Net Power (MW) | 427.1 | 436.7 | 855.0 | 895.4 |
| Coal fuel power (MW) | 1135.1 | 1135.1 | 2234.8 | 2234.8 |
| Plant efficiency (%) | 39.9 | 38.5 | 38.3 | 40.0 |
| Percentage error in plant efficiency (%) | 2.2 | | 4.7 | |

5.3 Power plant simulation and results

In this study, a steady-state simulation of a simplified conventional 350 MW_e supercritical coal fired power plant was developed in CHEMCAD 6.0 [184] using data in Table 5-3 (further details are shown in Appendices A2 to A4) . The conditions for the superheater are 250 atm at 560 °C and reheat conditions of 46 atm at 560 °C with LP operation at 12.9 atm. The exit temperature of the flue gas under standard operation is 340 °C [185;186]. The simulations were run with the power plant operating at full capacity, i.e., the coal and make up water input remained constant. The coal type used in this study is imported Indonesian steam coal, with the higher heating value of 30.68 MJ kg⁻¹ and the breakdown of the composition of the coal is shown in Table 5-3.

The results from the simulations aim to show the operating conditions of the plant and the extent of the reduction in efficiency as the plant is turned down through steam extraction. A schematic of the plant is shown in Figure 5-3 and represents three main areas that have been identified as possible points for steam extraction for use in solid oxide electrolyser cells. One of the aims of this work was to gain an understanding of the options available for extracting steam and the conditions of said streams, as well as to further examine the extent of turndown via steam removal on the plant's operation, rather than reducing the coal input.

Table 5-3: Parameters used in modelling a coal fired power station in this study.

| | This study | Indonesian coal data | |
|--|-------------------|--|---------------|
| Coal type | Indonesian coal | Proximate Analysis (wt %) | |
| Coal flowrate (kg hr ⁻¹) | 175,000 | Volatile material 30 min. (dry basis) | |
| Air flowrate (kg hr ⁻¹) | 900,000 | Total moisture 10 max. | |
| Main steam flowrate (kg hr ⁻¹) | 1,160,000 | Specific Energy 18 MJ kg ⁻¹ min. | |
| Main steam temperature (°C) | 560.0 | Ultimate Analysis of Indonesian coal (wt %) | |
| Reheat steam temperature (°C) | 560.0 | | |
| Main steam pressure (atm) | 250.0 | | Carbon 73.93 |
| Reheat steam pressure (atm) | 46.0 | | Hydrogen 4.65 |
| Low pressure steam pressure out (atm) | 0.05 | | Nitrogen 1.50 |
| HP turbine efficiency (%) [172] | 70.0 | | Sulphur 1.08 |
| IP turbine efficiency (%) [172] | 70.0 | | Oxygen 5.85 |
| LP turbine efficiency (%) [172] | 70.0 | Ash 13.01 | |
| Net Power (MW) | 350 | Higher Heating Value (HHV) 30.68 MJ kg ⁻¹ | |
| Coal fuel power (MW) | 875 | | |
| Plant efficiency (%) | 40.0 | | |

5. Modelling and analysis of coal fired plants

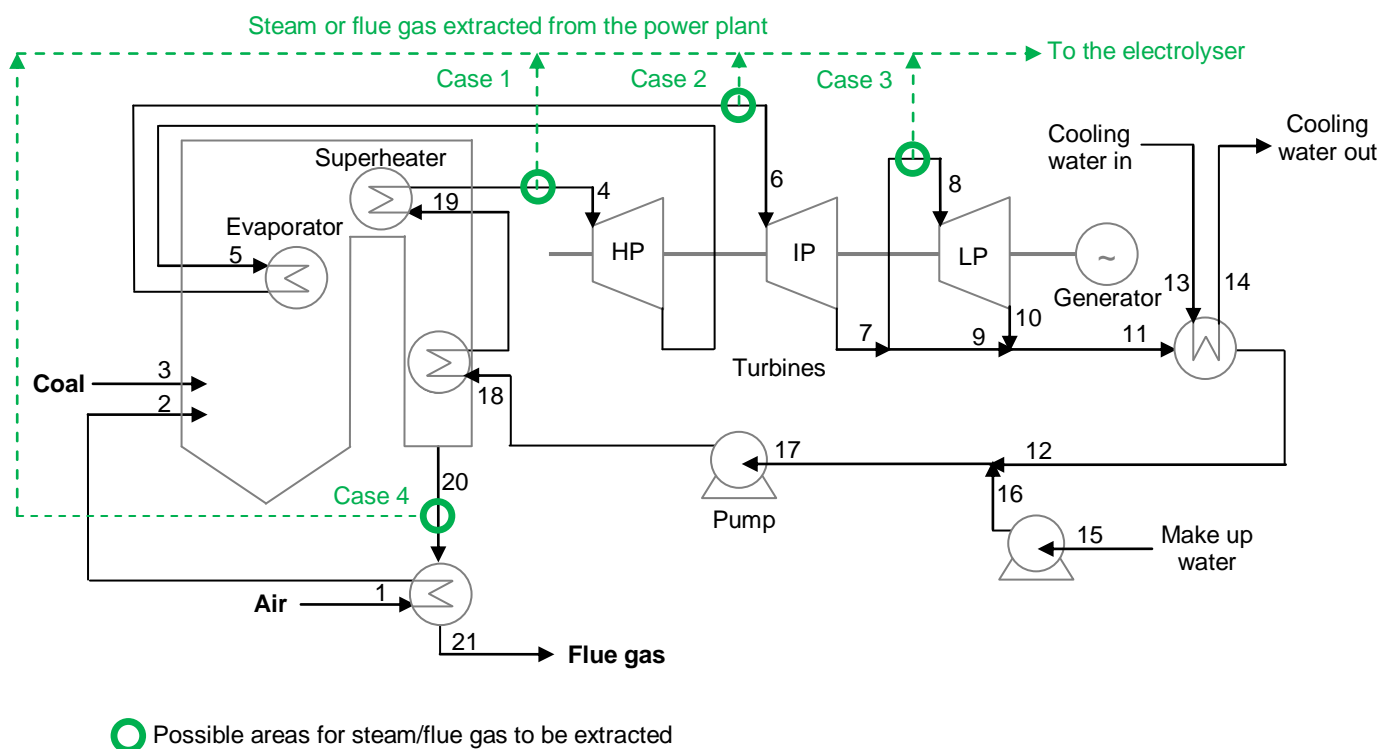


Figure 5-3: A flowsheet to represent the coupling of streams from the power plant with the SOEC. The diagram refers to cases 1, 2 and 3 from the power plant.

Table 5-4: Results obtained from CHEMCAD simulations of steam extraction for cases 1 to 3 for full and 50% load.

| | 0% turndown | | | 50% turndown | | |
|---|-------------|-----------|---------|--------------|---------|---------|
| | Case 1 | Case 2 | Case 3 | Case 1 | Case 2 | Case 3 |
| Power plant efficiency (%) | 40 | | | 20 | | |
| Steam extraction (%) [Figure 5-4] | 0 | | | 27 | 35 | 40 |
| Temperature (°C) | 560 | 560 | 409 | 560 | 560 | 409 |
| Pressure (atm) | 250 | 46 | 12.9 | 250 | 46 | 12.9 |
| Flue gas exit temperature (°C) | 276 | 276 | 276 | 785 | 660 | 681 |
| Steam flowrate extracted (kg hr ⁻¹) | 0 | 0 | 0 | 229,000 | 270,000 | 228,000 |
| Steam flowrate before extraction (kg hr ⁻¹) | 1,160,000 | 1,160,000 | 928,000 | 834,000 | 777,000 | 571,000 |

Possible streams from the plant which can provide high temperature and pressurised steam were seen to be before the HP, IP and LP turbines, which have been assigned as Cases 1, 2 and 3, respectively. Utilising flue gas is also an option (Case 4). It should be noted that extraction from the turbines itself is possible; however, it is not considered in this study for simulation simplification [167;176]. However, extracting steam directly from the turbine would mean that a reduced pressure and temperature was available, which may allow for a greater range of SOEC electrolytes to be used. However, directly taking steam from the turbine may create greater efficiency losses. The available steam extraction points are shown in the dashed lines in Figure 5-3.

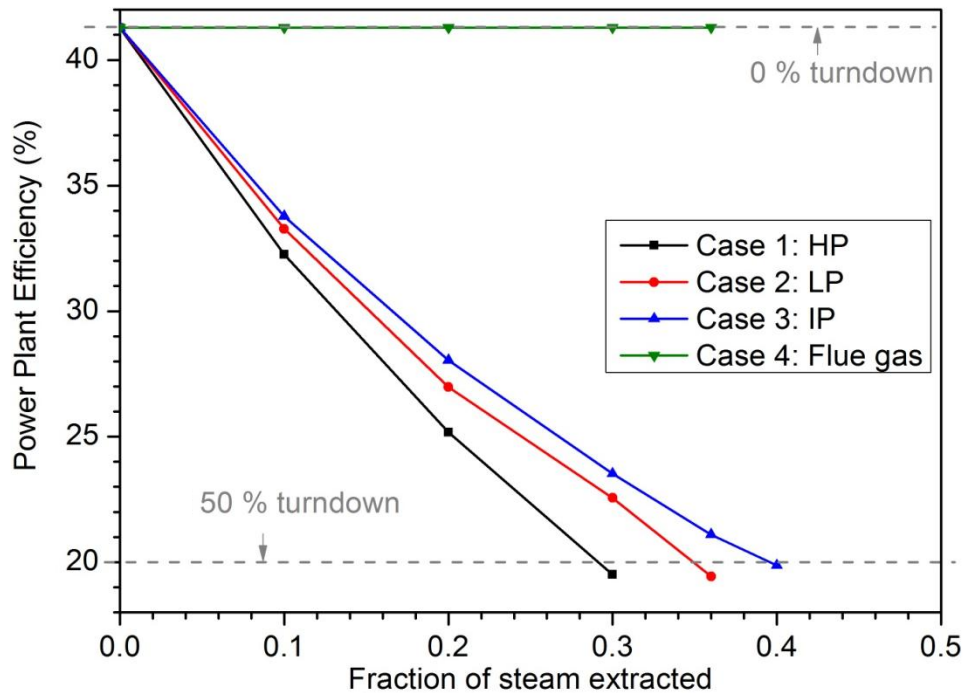


Figure 5-4: The extent of efficiency loss of the power plant with varying fractions of steam extracted for cases 1 to 4.

Based on the results from the extraction of steam, it is shown that high temperatures and pressures can be obtained. A temperature range of 409 to 560 °C can be obtained from the plant at pressures of up to 250 atm. The extraction of steam at each point had an effect on the plant's efficiency (based on Equation (9)) as shown in Figure 5-4. It can be seen that the largest impact on the plant is Case 1, as the main steam, which has the capacity to do the most work, is removed. When the extracted steam or flue gas is used as reactants in SOECs, hydrogen and syngas can be produced, respectively. The gas extracted from the flue gas will require cleaning to remove SO_x and particulates, which further reduce the temperature of the gas to around 80 °C and therefore will not be considered in this study [172].

5.4 Conclusions

The goal of 'cleaner technologies' requires changes in conventional energy production such as coal fired power plants. The suitability of using a power plant to provide steam and electricity to solid oxide electrolyser cells was investigated through modelling. It was seen that power plants operate the steam cycle at a range of temperatures of between 560 and 409 °C and pressures of between 250 and 12.9 atm.

Due to the cyclical nature of the operation, where turndown occurs at night, an option of extracting up to 50 % of steam for hydrogen production at night was identified. The results of the simulations show that 27, 35 and 40 % of steam can be extracted from the steam cycle before the HP, IP and LP turbines, respectively. However, the steam extraction results in a drop in the overall plant efficiency, with the extent of efficiency loss being the greatest for case 1 (before the HP turbine) as the steam with the greatest enthalpy is extracted. Studies have shown that steam extraction from the steam cycle for carbon capture and storage technologies is possible from between the IP and LP connecting pipe. Therefore, steam extraction in this study from various connecting pipes is possible. Furthermore, the extraction of the steam showed a similar drop in efficiency as this study.

The steady-state simulation was limited by obtaining results after the system was steady. Further testing of a more complex coal fired power plant dynamically would allow the change over time to be determined for a more thorough understanding of efficiency loss. A more complex system would provide alternative options to steam extraction points, which may be suitable. These studies can be carried out in the future.

In order to limit the efficiency loss of the power plant by extracting energy while enabling hydrogen production, it is essential to understand the operation of the electrolysers and possible ways of providing the most efficient configuration for an integrated system. Therefore, the next chapter considers the operation of solid oxide electrolyser cells.

6 Modelling and analysis of solid oxide electrolyser cells

Solid oxide electrolyser cells (SOECs) are a promising alternative to low temperature electrolyser cells. In order to assess whether SOECs are feasible for use in a large scale industrial application, the effects of key variables are investigated. Furthermore, this chapter focuses on the effects of inlet steam variations on the efficiency of the electrolyser and possible ways of improving efficiency.

The model has been developed to assess the behaviour of SOECs with variations in the inlet conditions for large scale hydrogen production. The effects of differences in temperature and pressure of the entering steam on the performance of the cell will be characterised through modelling the resistances and resulting heat which evolve from the steam reduction reaction. Combining the results from the electrochemical and thermal analysis gives the performance of the cell, which can be seen graphically in polarisation curves as well as in efficiency data.

In the following, the SOEC modelled is based on a reversible planar solid oxide fuel cell. A planar configuration was chosen over a tubular design due to ease of manufacture and greater performance [28].

6.1 Modelling of solid oxide electrolyzers in literature

With the growing interest in SOECs, several models have been developed and shown in the literature [24;99;187;188]. As SOECs are currently only available at lab scale, modelling of cells, stacks (a number of cells “stacked” together to form one unit) and more recently systems (several stacks combined with current technologies e.g. wind turbines), has been carried out in order to estimate the behaviour of the cells under varying conditions. SOECs operate as the reverse of solid oxide fuel cells (SOFCs); therefore, modelling of an electrolyser cell effectively follows the same principles [159;189;190]. Many studies have shown that variables such as temperature, steam ratio and thickness of the components have a significant impact on performance, with pressure having a relatively minor effect [24;76;187;190-193].

Results presented in the literature have highlighted factors such as the need for thin electrodes and electrolytes, in the range of 50 μm , which enables overpotentials to be kept to a minimum [190]. The overpotentials refer to ohmic, activation and concentration resistances formed from electronic and ionic conduction, electro-kinetics and reactant and product flow limitations. Furthermore, reducing overpotentials enables greater SOEC efficiencies and reduces the temperature

gradients that are generated through operation [193]. The focus in the literature has mainly been on the understanding of the electrolysis process and the components within it. Variables such as steam temperature and composition have so far been controlled variables, both experimentally [129;194] and computationally [190;193]; however, there is very limited studies on the energy required in order to produce steam for SOECs. Ni *et al.* (2007) [195] studied the energy requirements of a SOEC hydrogen plant and results have shown that the system is dependent on the operating conditions of temperature and current density. At a low SOEC temperature of 600 °C, heat from the overpotentials was shown to be produced at current densities above 500 A m⁻²; however, at 1,000 °C this was increased to 17,000 A m⁻². In order to meet SOEC energy requirements, additional electrical energy is required. It was shown that the most energy losses occurred in the SOEC and the heat exchangers, therefore to improve the overall system efficiency SOEC overpotentials need to be reduced [188;195]. A similar assessment was studied by Stempien *et al.* (2012), which assessed a possible CO₂ mitigation device. The study showed that an SOEC system with flue gas as the inlet can produce CO₂ with system efficiencies of 50 %. The most energy intensive process was shown to be the electrolysis process itself [196]. This study aims to assess the sensitivity of SOEC efficiency to variations in the temperature and pressure of the steam inlet. The integration of SOECs with a power station is then considered in the next chapter with a view to identifying the options and potential for efficiency optimisation.

Limited research has also been presented in the literature examining systems-level operation and integration. Combining SOECs with nuclear technologies has been of great interest due to the high quality heat available from gas cooled reactors as steam at 800 °C and 4 atm can be produced. Hydrogen production efficiencies of 53 % were reported with such a combination by Fujiwara *et al.* [197], where the efficiency is related to the electrical requirements of the system. Thermal-to-hydrogen efficiency (heating value of hydrogen / total thermal input) of around 50 %, with current density and temperature being influential variables, were shown by O'Brien *et al.* [99].

Studies have also been reported that examine the combination of wind and solar technologies with low temperature electrolysers. The modelling has focused on assessing the controls required on providing power to the electrolyser with variations in power load from wind turbines as well as the control of the power output to the

grid from the electrolyser / wind turbine hybrid system [198]. Solar photovoltaic cells were shown to produce hydrogen from electrolysers at thermal efficiencies of 10.9 % [199] and around 8 % [200].

6.2 Solid oxide electrolyser cell model

The simplistic model of a planar solid oxide electrolyser cell is described and the SOEC is represented in Figure 6-1. Although there are more complex models available in the literature that consider 2D and 3D electrolysers, this study has considered a simplistic model as a basis for an integrated system analysis. Therefore, this model has used appropriate models available in literature as a basis to develop a suitable model to meet the objectives of this investigation. This model has focused on the work by Ni *et al.*, which is based on the mass balance of the electrolyser. Furthermore, the work by Udagawa *et al.* has been used to represent the cell potentials; although this study has not taken into account variations across the thickness of the cell. The aim of the SOEC model is to assess the main variables that have an impact on overall cell efficiency as well as the energy requirements of the electrolyser. The SOEC model applied here assumes:

1. The electrolyser operates under steady-state conditions [190;201], with most of the steam reduction reaction occurring at a 2D interface between the electrode and electrolyte, rather than at distributed three phase boundaries (TPBs) within a 3D porous electrode [190;191].
2. The system is assumed to be well mixed.
3. The model considers the movement of material across the 1D x-plane only.
4. The temperature gradients across the electrodes have been neglected as it has been assumed that the operating temperature of the cell is constant. A sufficient pressure gradient is produced at the anode side for the O₂ produced to permeate through the anode [190].
5. Ideal gas behaviour has been assumed for the gas streams [24].
6. This model considers the resistances from the electrical connections and contacts to be negligible.

The equations governing the performance of the SOEC model is composed of mass balances, energy requirements and cell potential, as shown in Figure 6-2. The thermodynamic equations calculate the enthalpy (ΔH), and Gibbs free energy (ΔG), to determine the minimum amount of total energy and electrical energy, respectively,

needed for the reaction (Equation (1)). Enthalpy sets the theoretical energy requirement which is used to calculate the SOEC efficiency. Gibbs free energy is used to calculate both the Nernst (the voltage when current is zero) and the reversible (E_{rev}) potentials.



The reversible potential (E_{rev}), which is based on (ΔG), together with ohmic (E_{ohm}), activation ($E_{act,tot}$) and concentration ($E_{conc,tot}$) overpotentials account for the operating potential (E_{op}). The operating potential is used to find the heat energy produced by electrolysis (Joule heating and overpotentials).

The analysis considers the power necessary for raising steam to the the desired SOEC operating conditions and the power required for the electrolysis process. The resistances occurring during electrolysis, which are affected by temperature and pressure, generate thermal power ($\dot{Q}_{electrolysis}$). In addition, heat is introduced to the system by the entering steam (\dot{Q}_{steam}). The total thermal power (\dot{Q}_{total}), as part of the thermal analysis shows the total thermal power needed to meet SOEC operating conditions, which varying based on the condition of the entering steam.

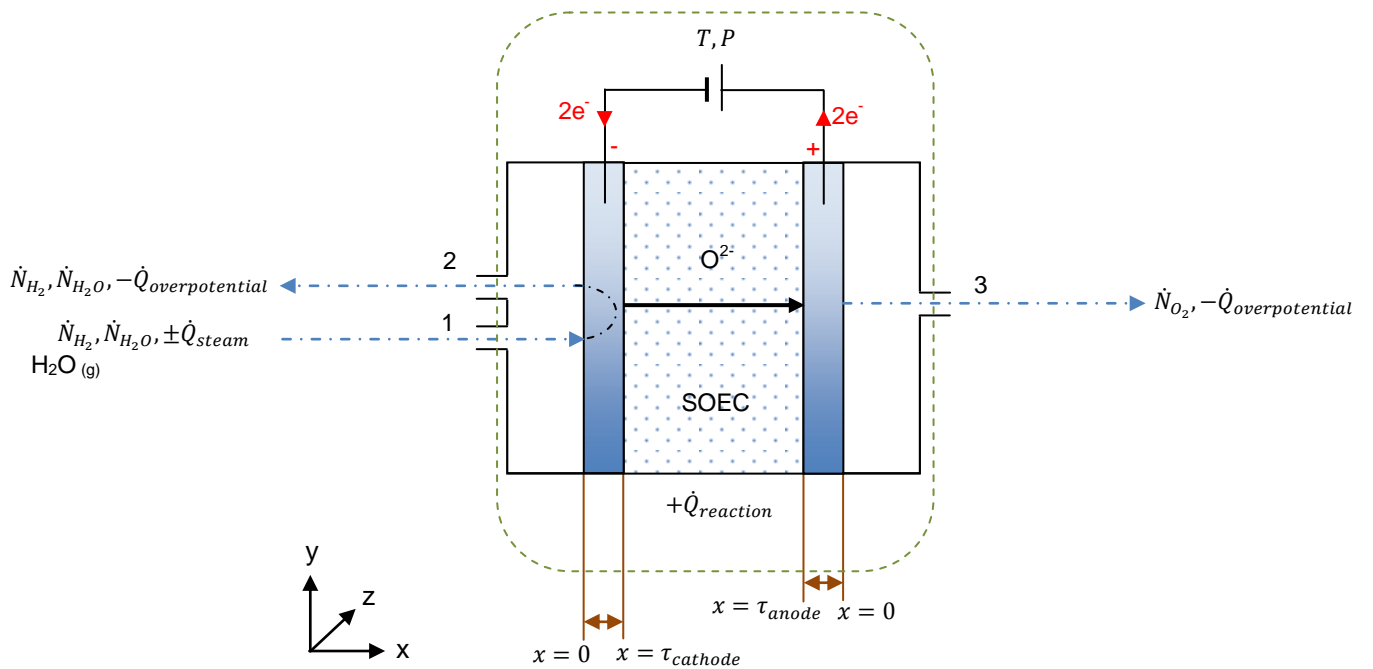


Figure 6-1: SOEC operation and a representation of the basis of the energy model.

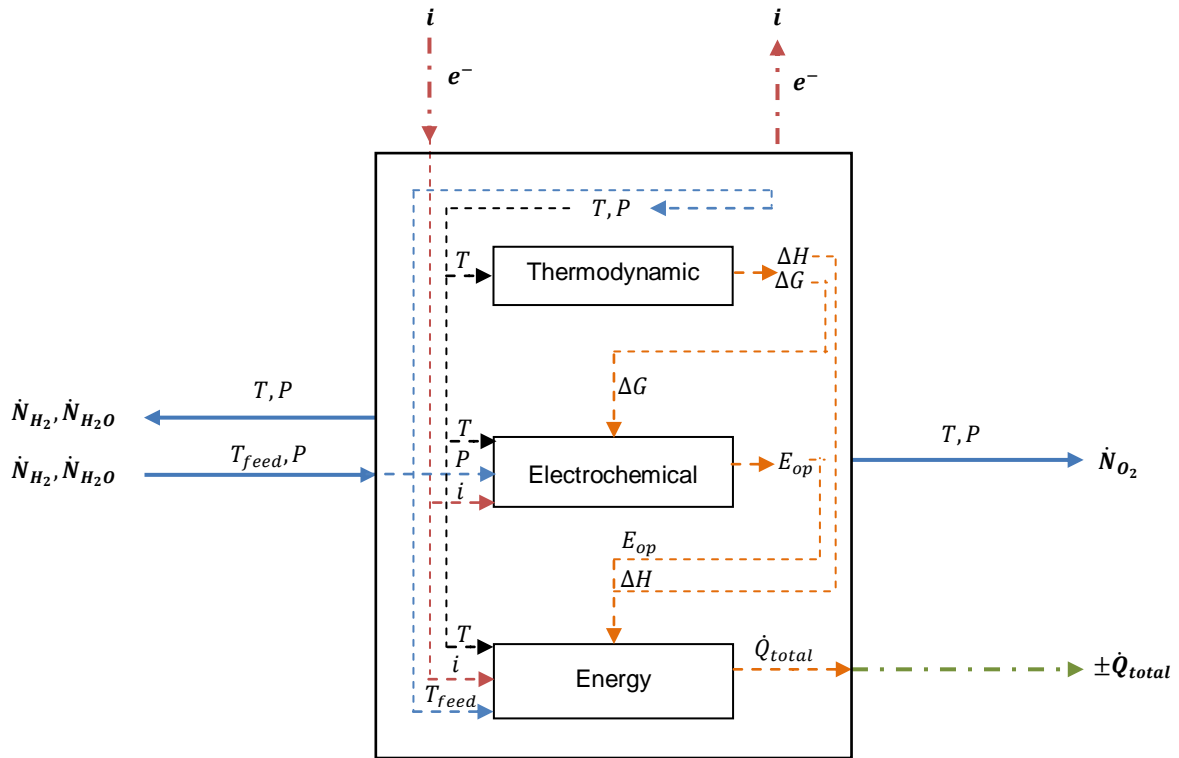


Figure 6-2: An overview of the inputs and outputs to the SOEC.
 The links between each section of the model in relation to physical inputs are shown.

Furthermore, a basis for optimisation can be found at the thermoneutral voltage (E_{tn}), the point at which the heat for the reaction (endothermic) is equal to the heat produced by Joule heating and electrode overpotentials. The SOEC efficiency combines the equations based on the amount of energy from the H_2 produced compared with the energy required to meet the operating conditions of the cell. A summary of the electrochemical equations is shown in Appendix A5.

6.2.1 Conservation of mass

The mass transport of components to and from the electrolyte is complex due to the porosity of the electrode material and the diffusion at the cathode and permeation at the anode through the three phase boundaries, which refers to the regions in the porous material of the electrode where the ceramic, metal and reactants meet.

6.2.1.1 Cathode

At steady state, the mass transport of a component can be represented by [190;202]:

$$\nabla \dot{N}_c = \frac{\delta \dot{N}_c}{\delta x} + \frac{\delta \dot{N}_c}{\delta y} + \frac{\delta \dot{N}_c}{\delta z} = 0 \quad (19)$$

which represents the change in the flow of component in directions x , y and z .

Steam is supplied to the cathode via convection; however, once at the electrode surface, diffusion occurs to the active sites for reaction. Due to the complex nature of porous materials, an average effective diffusivity term is used, which takes into account Knudsen and molecular diffusion. Knudsen diffusion takes into account gases passing through the smaller pores of the cathode and molecular diffusion accounts for mass transport through larger pores.

The concentrations at the three phase boundaries are based on Fick's law of diffusion [202]:

$$J_{H_2O}^* = -D_{Aeffave} \frac{\delta C_{H_2O}}{\delta x} \quad (20)$$

where $J_{H_2O}^*$ is the diffusion flux of H_2O flowing through the electrode in the x -direction and $D_{Aeffave}$ is the average diffusivity, which varies with temperature. Generally, a small amount of hydrogen is included in the inlet to maintain reducing conditions in the cathode.

The molar flux, \dot{N}_{H_2O} , describes the diffusion and flow of components in a system based on the diffusion flux and the convective flux, which is the product of concentration, C_{H_2O} and molar average velocity, v^* , [202]:

$$\dot{N}_{H_2O} = J_{H_2O}^* + v^* C_{H_2O} \quad (21)$$

For a system such as electrolysis, where steam in the gaseous phase reacts to produce another gas, hydrogen, at constant pressure and at steady state, molecular diffusion of steam occurs. Assuming that the reaction at the boundary is fast, which results in a small mole fraction and hence a small concentration of steam; the convective flux can be deemed negligible [202].

Equation (21) can therefore be simplified to:

$$\dot{N}_{H_2O} = J_{H_2O}^* = -D_{Aeffave} \frac{\delta C_{H_2O}}{\delta x} \quad (22)$$

By substituting Equation (22) into (19) and considering the diffusion through the electrode only occurring in the x -direction through the thickness of the electrode i.e., $x = \tau_{cathode}$ [190]:

$$\nabla \dot{N}_{H_2O} = \frac{\delta \dot{N}_{H_2O}}{\delta x} = \frac{\delta}{\delta x} \left(-D_{Aeffave} \frac{\delta C_{H_2O}}{\delta x} \right) = 0 \quad (23)$$

The flow of components to the cell (Figure 6-1) can be expressed by the current density, i :

$$\dot{N}_{H_2O} = \frac{i}{nF} \quad (24)$$

Substituting Equation (24) into (22) gives:

$$\frac{i}{nF} = -D_{Aeffave} \frac{\delta C_{H_2O}}{\delta x} \quad (25)$$

Across the electrode there are variations in the concentration of components. The fixed boundary is the thickness of the electrode and therefore concentration profiles can only occur within this layer, i.e. the boundary condition for Equation (23) is given by:

$$\left. \frac{\delta C_{H_2O}}{\delta x} \right|_{x=\tau_{cathode}} = -\frac{i}{nFD_{Aeffave}} \quad (26)$$

The amount of steam at the surface of the cathode can be denoted as the concentration of steam at the point where the thickness in the x -direction is zero and is as follows:

$$C_{H_2O}|_{x=0} = C_{H_2O}^0 \quad (27)$$

Solving Equation (23) with the boundary conditions in Equations (26) and (27) gives the concentration of steam at the three phase boundaries (TPBs) [24]:

$$C_{H_2O}^{TPB} = C_{H_2O}^0 - \frac{i\tau_{cathode}}{nFD_{Aeffave}} \quad (28)$$

The rate of the production of hydrogen is equal to the rate of consumption of steam, which means that the pressure remains constant; and a similar equation can therefore be written for the hydrogen produced at the cathode [24]:

$$C_{H_2}^{TPB} = C_{H_2}^0 + \frac{i\tau_{cathode}}{nFD_{Aeffave}} \quad (29)$$

The average effective diffusivity, $D_{Aeffave}$ takes into account both the Knudsen diffusion for the gases through the smaller pores of the cathode as well as the molecular diffusion, which takes place when the pores are larger.

$$\frac{1}{D_{AeffH_2O}} = \frac{\xi}{\varepsilon} \left(\frac{1}{D_{H_2O-H_2}} + \frac{1}{D_{kH_2O}} \right) \quad (30)$$

$$\frac{1}{D_{AeffH_2}} = \frac{\xi}{\varepsilon} \left(\frac{1}{D_{H_2O-H_2}} + \frac{1}{D_{kH_2}} \right)$$

where $D_{H_2O-H_2}$ represents the molecular diffusion and, D_{kH_2} and D_{kH_2O} are the Knudsen diffusion for hydrogen and steam, respectively and ξ and ε represent the tortuosity and porosity, respectively.

The Knudsen diffusion for each component, D_{kc} is given by [190]:

$$D_{kc} = \frac{4}{3} r_p \sqrt{\left(\frac{8RT}{\pi MW_c} \right)} \quad (31)$$

where MW_c is the molecular weight of each component and r_p is the pore radius.

The radius of the pore, r_p , is given by [203]:

$$r_p = \frac{2\varepsilon}{S_A \rho_B} \quad (32)$$

where S_A represents the surface area of the pore and ρ_B is the bulk density.

The molecular diffusion of the gases through large pores in the electrodes is given by [204]:

$$D_{H_2O-H_2} = 0.0018583 \sqrt{T^3 \left(\frac{1}{MW_{H_2O}} + \frac{1}{MW_{H_2}} \right) \times \frac{1}{P \delta_{H_2O-H_2}^2 \Omega_{DH_2O-H_2}}} \quad (33)$$

where P represents the total pressure (atm), δ_c is the collision diameter and $\Omega_{DH_2O-H_2}$ is the collision integral.

The collision integral, $\Omega_{DH_2O-H_2}$, can be interpolated from known T^* values as shown by Geankoplis [202], and is a function of the Lennard Jones Potential, which includes the operating temperature and the characteristic energy for each component, ε_{kc} :

$$T^* = \frac{k_B T}{\varepsilon_{kH_2O-H_2}} \quad (34)$$

where T^* refers to the Lennard-Jones Potential and k_B is the Boltzmann constant.

$$\varepsilon_{kH_2O-H_2} = (\varepsilon_{kH_2O}\varepsilon_{kH_2})^{0.5} \quad (35)$$

The collision diameter δ_c , is given as:

$$\delta_{H_2O-H_2} = \frac{\delta_{H_2O} + \delta_{H_2}}{2} \quad (36)$$

where the average diffusivity $D_{Aeffave}$, of the gas mixture at the three phase boundary is:

$$D_{Aeffave} = \frac{p_{H_2O}^0}{P} D_{AeffH_2O} + \frac{p_{H_2}^0}{P} D_{AeffH_2} \quad (37)$$

where p_c^0 is the partial pressure of components, H_2 and H_2O .

6.2.1.2 Anode

The flow of the components leaving at the anode side is assumed to be only oxygen and therefore only permeation occurs. The gas viscous flow is usually characterised through Darcy's equation [205]:

$$\dot{N}_{O_2} = \frac{-B_g}{RT\mu} \frac{p_{O_2}}{\tau_{anode}} \nabla p_{O_2} \quad (38)$$

where B_g is the flow permeability and μ is the dynamic viscosity given in Equations (39) and (40), respectively.

$$B_g = \frac{\varepsilon^3}{72\xi(1-\varepsilon)^2} (2r_p)^2 \quad (39)$$

$$\mu = \sum_{d=0}^6 b_d (T^{**})^d \quad (40)$$

where,

$$T^{**} = \frac{T(K)}{1000} \quad (41)$$

Recall Equation (19) applied to oxygen:

$$\nabla \dot{N}_{O_2} = \frac{\delta \dot{N}_{O_2}}{\delta x} + \frac{\delta \dot{N}_{O_2}}{\delta y} + \frac{\delta \dot{N}_{O_2}}{\delta z} = 0 \quad (19)$$

Combining Equations (19) and (38), we can describe the oxygen transport in the anode as [190]:

$$\frac{\delta}{\delta x} \left(-\frac{B_g p_{O_2}}{RT \mu \tau_{anode}} \frac{\delta p_{O_2}}{\delta x} \right) = 0 \quad (42)$$

At the electrolyte-electrode interface shown in Figure 6-1, where the oxidation reaction occurs, the rate of oxygen production is given in terms of the current density [190]:

$$N_{O_2} = -\frac{i}{4F} \quad (43)$$

where the number of electrons n , needed to form one mole of an oxygen molecule is 4.

The boundary conditions at the thickness of the electrode can then be represented by:

$$p_{O_2} \frac{\delta p_{O_2}}{\delta x} \Big|_{x=\tau_{cathode}} = \frac{iRT\mu}{4FB_g} \quad (44)$$

The amount of oxygen at the surface of the anode boundary can be denoted by:

$$p_{O_2} \Big|_{x=0} = p_{O_2}^0 \quad (45)$$

Based on the boundary conditions in Equations (44) and (45), Equation (42) can be solved to find the partial pressure of oxygen at the three phase boundaries [190]:

$$p_{O_2}^{TPB} = \sqrt{(p_{O_2}^0)^2 + \frac{RTi\mu\tau_{anode}}{2FB_g}} \quad (46)$$

where $p_{O_2}^{TPB}$ is the partial pressure of oxygen at the three phase boundaries (TPBs) and $p_{O_2}^0$ is the partial pressure of oxygen at the inlet.

6.2.2 Cell potential

The potential of the cell dictates the performance of the electrolyser and takes into account the theoretical potential as well as resistances created by electrolysis. As

discussed in Chapter 1, the electrochemical equations presented in this section aims to find the overpotentials and operating potentials, thus estimating the efficiency of the cell.

In reality, the system will have resistances, which produce overpotentials. The total overpotentials include that of ohmic (E_{ohm}), activation ($E_{act,tot}$) and concentration ($E_{conc,tot}$) losses. The overpotentials need to be overcome in order for the SOEC to function effectively; therefore, a larger voltage is required for the operation of an electrolyser above the Nernst potential, which is accounted for by the operating potential (E_{op}) [24]:

$$E_{op} = E_{rev} + E_{ohm} + E_{act,tot} + E_{conc,tot} = E_{rev} + E_{overpot} \quad (47)$$

For an electrolyser where there is a potential difference, E , between two electrodes and charge transfer through the circuit, electrical work (W_{elec}) is being done on the system [18]:

$$W_{elec} = qE = nFE = \Delta G \quad (4)$$

where $n = 2$ relates to the number of electrons per mole.

For the reaction in Equation (1), the change in the Gibbs free energy can be written as [15]:

$$\Delta G = \Delta G_0^\circ + RT \ln \left[\frac{\alpha_{H_2} \alpha_{O_2}^{0.5}}{\alpha_{H_2O}} \right] \quad (48)$$

where ΔG_0° is the Gibbs free energy at standard temperature and pressure of 25 °C and 1 atm, respectively and α_i is the activity of each component involved in the reaction. The activity of an ideal gas is the relationship between the partial pressure of the gas relative to standard conditions (i.e. p_c/p^0).

The Nernst potential or reversible potential, E_{rev} , can be obtained by combining Equations (4) and (48) and written in terms of partial pressure [15]:

$$E_{rev} = E_0 + \frac{RT}{nF} \ln \left[\frac{p_{H_2} p_{O_2}^{0.5}}{p_{H_2O}} \right] \quad (49)$$

where E_0 represents the potential between the electrodes at a constant pressure and temperature at zero current, and p_c is the partial pressure of components. The

reversible potential represents the open circuit voltage (OCV) (when there is no flow of current between electrodes), at the SOEC operating temperature.

At standard conditions, the equilibrium voltage for electrolysis of the reactant is represented by E_0° :

$$E_0^\circ = -\frac{\Delta G_0^\circ}{nF} \quad E_0 = -\frac{\Delta G}{nF} \quad (50)$$

For each one mole of steam, two electrons are required and the associated charge (q) transfer between the electrodes is shown in Equation (3) [18]:

$$q = 2N_A(-e) = 2F \quad (51)$$

where N_A is Avogadro's number, F is Faraday's constant and e is the charge on an electron.

6.2.2.1 Ohmic overpotential

The ohmic overpotentials, E_{ohm} , are produced as a result of the resistance to the current through the electrodes and ions through the electrolyte [24]:

$$E_{ohm} = i \left(\frac{\tau_{cathode}}{\sigma_{cathode}} + \frac{\tau_{electrolyte}}{\sigma_{electrolyte}} + \frac{\tau_{anode}}{\sigma_{anode}} \right) \quad (52)$$

where σ_{anode} , $\sigma_{cathode}$ and $\sigma_{electrolyte}$ is the conductivity, τ_{anode} , $\tau_{cathode}$ and $\tau_{electrolyte}$ are the thickness of the anode, cathode and electrolyte, respectively, and i is the current density. The model considers the resistances from the electrical connections and contacts to be negligible, based on assumption 6.

6.2.2.2 Activation overpotential

Activation overpotential, $E_{act,tot}$ is derived from the Butler-Volmer equation, assuming the charge transfer coefficients of the anode and cathode are equal (Appendix A6) [24;191;193]:

$$E_{act,tot} = \left[\frac{RT}{F} \operatorname{arcsinh} \left(\frac{i}{2i_{0,anode}} \right) \right] + \left[\frac{RT}{F} \operatorname{arcsinh} \left(\frac{i}{2i_{0,cathode}} \right) \right] \quad (53)$$

The overpotential is related to the charge transfer process and kinetics of the reaction at each electrode-electrolyte interface and accounts for the energy required to overcome the activation energy constraint of the electrolyser reaction (Equation (1)) [191;206]. The activation energy needs to be overcome both thermally and electrically [207]. The activation overpotential is also a function of the exchange

current densities, $i_{0,cathode}$ and $i_{0,anode}$ which represents the catalytic behaviour of the electrode to determine the rate of oxidation or reduction of the reaction.

6.2.2.3 Concentration overpotential

Concentration (mass transport) overpotentials are formed at times when there is resistance to the flow of reactant to, and product away from, the three phase boundaries, which are the regions in the porous material where the ceramic, metal and reactants meet and which is where the steam reduction reaction occurs. The total concentration overpotential takes into account the concentration overpotentials occurring on both electrodes of the SOEC and is given by:

$$E_{conc,tot} = E_{conc,anode} + E_{conc,cathode} \quad (54)$$

The concentration overpotential, $E_{conc,cathode}$ at the cathode is given by [187]:

$$E_{conc,cathode} = \frac{RT}{2F} \ln \left[\left(\frac{C_{H_2}^{TPB} C_{H_2O}^0}{C_{H_2O}^{TPB} C_{H_2}^0} \right) \right] \quad (55)$$

where $C_{H_2O}^0$, $C_{H_2}^0$, $C_{H_2O}^{TPB}$ and $C_{H_2}^{TPB}$ are the concentrations of steam and hydrogen at the surface of the electrode and at the three phase boundaries, respectively. The concentration overpotential at the anode side assumes that only O_2 is present and thus permeation takes place through the electrode [190]:

$$E_{conc,anode} = \frac{RT}{4F} \ln \left(\frac{p_{O_2}^{TPB}}{p_{O_2}^0} \right) \quad (56)$$

where $p_{O_2}^0$ and $p_{O_2}^{TPB}$ are the partial pressures of oxygen at the surface of the electrode and at the TPBs, respectively.

6.2.3 Energy requirement

6.2.3.1 Thermodynamic

The thermodynamic equations represents the total minimum energy requirements for the electrolysis reaction (Equation (1)), which is comprised of the sum of the electrical (ΔG) and thermal (Q) energies needed for the reaction to occur. $T\Delta S$ is equivalent to the heat energy of the system and at a certain temperature and pressure, with no changes in the system the available heat in the system is constant. At a stable temperature and pressure, the enthalpy remains constant and so does the available

heat, which thereby identifies the amount of electrical energy required to meet the minimum energy needed for the reaction.

The total minimum energy required for the reaction is governed by the enthalpy, ΔH [18]:

$$\Delta H = \Delta G + T\Delta S = \Delta G + Q \quad (57)$$

where T is the operating temperature and ΔS is the entropy change of the system.

The Gibbs free energy, ΔG , represents the amount of energy available within the system at constant temperature and pressure and governs whether or not the reaction will take place [18]:

$$\Delta G = \Delta H_0^\circ - \frac{T}{T_0}(\Delta H_0^\circ - \Delta G_0^\circ) + R \int_{T_0}^T \frac{\Delta C_p^\circ}{R} dT - RT \int_{T_0}^T \frac{\Delta C_p^\circ}{R} \frac{dT}{T} \quad (58)$$

Enthalpy can also be written in the following form:

$$\Delta H = \Delta H_0^\circ + R \int_{T_0}^T \frac{\Delta C_p^\circ}{R} dT \quad (59)$$

where ΔH_0° is the enthalpy at T_0 the standard temperature and R is the universal gas constant.

For each component in the reaction, ν_c is the stoichiometric coefficient and A_c , B_c , C_c and D_c are heat capacity constants.

$$\Delta A = \sum_c \nu_c A_c \quad \Delta B = \sum_c \nu_c B_c \quad \Delta C = \sum_c \nu_c C_c \quad \Delta D = \sum_c \nu_c D_c \quad (60)$$

The reduced temperature t , is defined as:

$$t \equiv \frac{T}{T_0} \quad (61)$$

The enthalpy is dependent on temperature and the components involved, which can be related to the specific heat capacity of the system, ΔC_p° by [18]:

$$\int_{T_0}^T \frac{\Delta C_p^\circ}{R} dT = (\Delta A)T_0(t-1) + \frac{\Delta B}{2}T_0^2(t^2-1) + \frac{\Delta C}{3}T_0^3(t^3-1) + \frac{\Delta D}{T_0} \left(\frac{t-1}{t} \right) \quad (62)$$

Equation (63) is the second integral of Equation (62) and is based on the second law of thermodynamics.

$$\int_{T_0}^T \frac{\Delta C_p^\circ}{R} \frac{dT}{T} = \Delta A \ln t + \left[\Delta B T_0 + \left(\Delta C T_0^2 + \frac{\Delta D}{t^2 T_0^2} \right) \left(\frac{t+1}{2} \right) \right] (t-1) \quad (63)$$

6.2.3.2 Additional energy requirement

In addition to the thermodynamic requirements, energy is also necessary to overcome overpotentials and for heating and cooling the cell in order to maintain its operating conditions. It is important to identify the thermoneutral point at which the heat produced by the overpotentials is equal to the heat required for the reaction. Current densities above this point would require cooling of the system as the overpotentials dominate, and current densities below this point would require heating to service the endothermic reaction (Equation (1)). The extent of heating or cooling required must therefore be considered.

Figure 6-1 illustrates the power needed for providing the heat associated with the process. \dot{Q}_{steam} is the power needed to raise the feed to the operating temperature and pressure of the system:

$$\dot{Q}_{steam} = \dot{m}_{H_2O} C_p (T - T_{feed}) \quad (64)$$

where \dot{m}_{H_2O} is the mass flow rate of steam and T_{feed} is the temperature of the feed inlet. If the feed is water rather than steam, then the total power requirement needed for heating water to the operating conditions is the sum of Equations (64) to (66). The power required to heat the water to 100 °C is:

$$\dot{Q}_1 = \dot{m}_{H_2O} C_p (T_{100\text{ °C}} - T_{feed}) \quad (65)$$

where $T_{100\text{ °C}}$ is the temperature of water, which is at 100 °C.

The power required to heat the water from 100 °C to steam at 100 °C:

$$\dot{Q}_2 = \dot{m}_{H_2O} H_v \quad (66)$$

The total power required for electrolysis, $\dot{Q}_{electrolysis}$, is the sum of the power generated by the overpotentials, $\dot{Q}_{overpotential}$, and the power needed for the endothermic steam electrolysis reaction, $\dot{Q}_{reaction}$:

$$\dot{Q}_{electrolysis} = i \left(-E_{op} + \frac{\Delta H}{nF} \right) \quad (67)$$

$$\dot{Q}_{overpotential} = -iE_{op} \quad (68)$$

$$\dot{Q}_{reaction} = i \frac{\Delta H}{nF} \quad (69)$$

Finding a balance between driving the reaction and maintaining the operating conditions is essential to avoid overheating or reducing efficiencies. A balance can be found through creating a control system and applying it to the process. The total amount of thermal power available for electrolysis based on the power from the steam inlet and the heat from the overpotentials is given by:

$$\dot{Q}_{total} = \dot{Q}_{electrolysis} + \dot{Q}_{steam} \quad (70)$$

6.2.4 Efficiency

The energy efficiency of the SOEC is given by [208]:

$$Efficiency = \frac{2F(E_{op} - E_{overpot})\dot{N}_{H_2}}{(iE_{op}) + \dot{Q}_{steam}} \times 100 \quad (71)$$

The efficiency takes into consideration the theoretical voltage required for electrolysis, $(E_{op} - E_{overpot})$, compared with the total power input to the system $(iE_{op} + \dot{Q}_{steam})$, which is related to the amount of hydrogen produced. The theoretical power required is calculated from the operating potential used to operate the SOEC and the overpotentials (resistances produced by the movement of species and reaction). The total power required to operate the cells is accounted for by considering the power input for electrolysis as well as the additional power consumed for conditioning the inlet steam.

The model takes into account the operation of solid oxide electrolyser cells and the effect of temperature and pressure on the efficiency. In addition, the power requirement of producing steam at the appropriate conditions and the power for SOEC operation can be studied. The model is similar to those published in literature; however, a simplistic approach has been taken as a basis for assessing an integrated system. The effect on the overall efficiency of the SOEC, based on the amount of power required for producing suitable steam, is the main objective of the computational study.

6.3 Solid oxide electrolyser modelling results

6.3.1 Model validation

6.3.1.1 Validating through experimentation

The results from the experimentation discussed in Chapter 4 were compared with predictions using the SOEC model to assess the suitability and limitations of the model. In order to compare the model and experimentation, exchange current density and conductivity variables for the ScSZ electrolyte and LSM anode, which have been widely researched, were used from literature [162;209]. Although ceria has been studied in fuel cell mode [210-212], data available for the characteristics of CGO and Ni-CGO as electrolyser material is limited [122;213;214]. The parameters that have the most significant impact on the results of the model are the conductivity and exchange current densities, with the latter varying in orders of magnitude with changing temperatures. The majority of experimental studies have investigated electrolysis using YSZ electrolytes and more recently, detailed studies on the properties of the material have been tested [215-218]. With little information on the conductivity and exchange current density of Ni-CGO and in order to provide a realistic representation of the changes in material performance with temperature, it has been assumed that Ni-CGO, the chosen material for this study, has a similar operating behaviour with changes in operating conditions such as temperature and pressure to Ni-YSZ as Ni-CGO is also a ceramic metal mixture (cermet) like Ni-YSZ, which has been widely researched [219-222].

In particular, it has been assumed that the conductivity for Ni-CGO (this work) follows the same trend in terms of temperature dependency as Ni-YSZ [223;224]. From the data on conductivity in literature for Ni-YSZ by Aruna *et al.* [215], a polynomial fit was made (Figure 6-3). A known value of $6 \times 10^4 \Omega^{-1} \text{ m}^{-1}$ at 650 °C

for Ni-CGO [122] was used as a basis from which to extrapolate based on the polynomial fit for Ni-YSZ. A 10 % sensitivity analysis on the parameters obtained from the literature was carried out. It was seen that the change to the graph is in fact negligible as the trend line remains unchanged. Therefore, the uncertainties in the conductivity for Ni-CGO can be viewed as negligible.

A similar analysis for estimating the changes in exchange current density is with varying temperature was also carried out. It has been assumed that the exchange current density for Ni-CGO follows the same trend as that for Ni-YSZ. A correlation in literature, based on an experimental study for Ni-YSZ by Leonide *et al.* [225], was fitted to an exponential equation, which is in the format of the Arrhenius Equation used for the activation overpotentials. The data used to estimate the exchange current density of Ni-CGO was then fitted to a similar function. The fit (Figure 6-4) was used to extrapolate from a known value of $1,580 \text{ A m}^{-2}$ at $650 \text{ }^\circ\text{C}$ for Ni-CGO [226]. A 10 % sensitivity analysis was studied on the effect on the efficiency of the SOEC. The results showed that the effect on changing the exchange current density was also negligible. All parameters and variables used in the model are shown in Table 6-2.

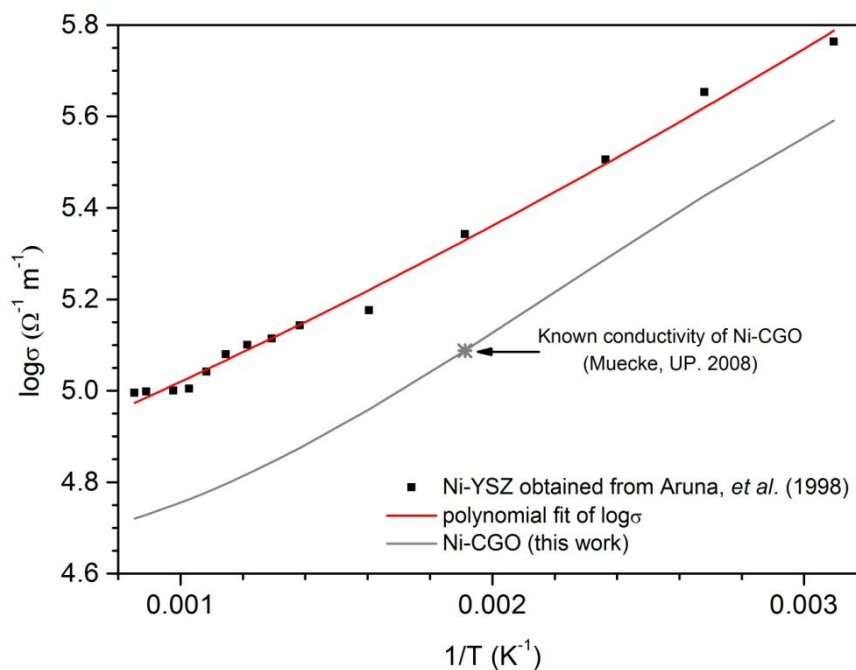


Figure 6-3: The conductivity (σ) of Ni-YSZ and the estimated values for Ni-CGO extrapolated from $60000 \text{ } \Omega^{-1} \text{ m}^{-1}$ at $650 \text{ }^\circ\text{C}$ [122;215].

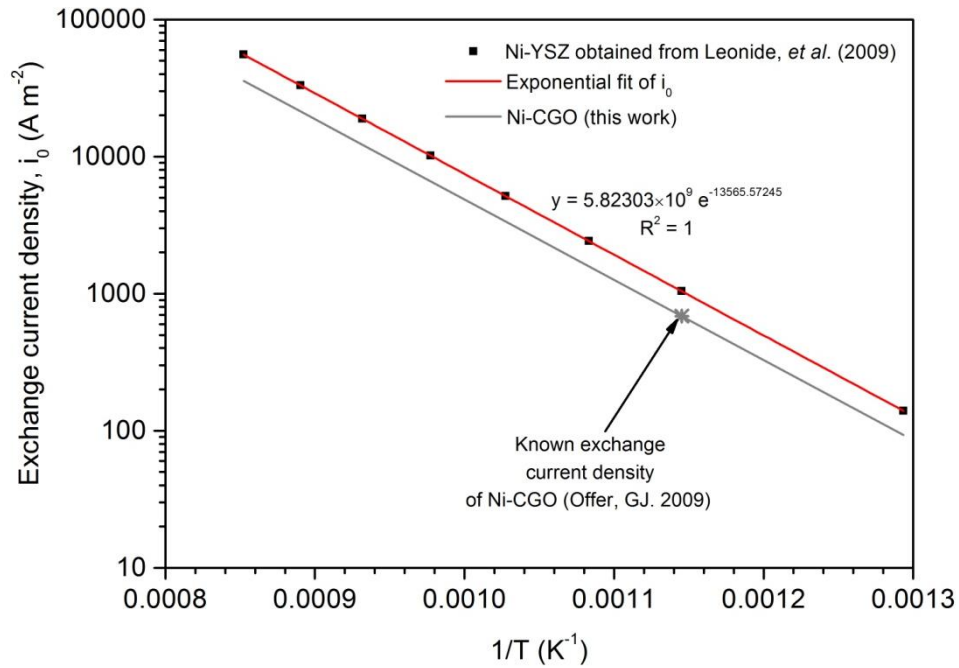


Figure 6-4: The exchange current density of Ni-YSZ and the estimated values for Ni-CGO extrapolated from 1580 A m⁻² [225;226].

The estimated parameters, along with those shown in Table 6-2 were used in the model shown in Section 6.2 and solved in gPROMS Modelbuilder 3.5.3. The model was used to produce polarization curves based on mass transfer (Equations (19) to (46)), cell potential (Equations (47) to (56)) and thermodynamic (Equations (57) to (63)) equations. The conditions used in the experimentation and the parameters estimated for conductivity and exchange current density were used as inputs to the model to generate the model results.

Figure 6-5 shows the results of validating the model with the experimental data discussed in Chapter 4. It can be seen from Figure 6-5 that the model does not represent the experimentation completely. According to theory, represented by the model, the concentration losses are minimal and the activation losses dominate with increasing temperature. This is clearly shown in Figure 6-13 to Figure 6-15 in the results section of this Chapter. The experimental data showed large ohmic resistances due to the electrical connections and activation overpotentials due to poor gas flow to and from the cell with increasing current density. However, it can be seen from Figure 6-5 that the open circuit voltage (OCV) of the model and the experimentation are close in value. The difference lies in the resistances being larger

in the experimentation due to the electrical connections, which have not been taken into account in the model.

As discussed in Chapter 4, many challenges that cannot be accounted for in the model were experienced such as cracking of the seals and cells at elevated temperatures and problems with delamination due to poor mass transfer, which resulted in poor model validation. Future developments in both the experimental and modelling studies may enable a more accurate computational representation of SOEC performance.

Due to the variations in the system and unforeseen complications, the performance of the SOEC did not conform to theory. Making changes to the experimental setup in order to carry out focused experiments would provide more accurate data for model validation. Due to time and resource restrictions, changes to the experimental setup and additional testing were not carried out. Therefore, the model developed in Section 6.2 has been validated against studies from literature.

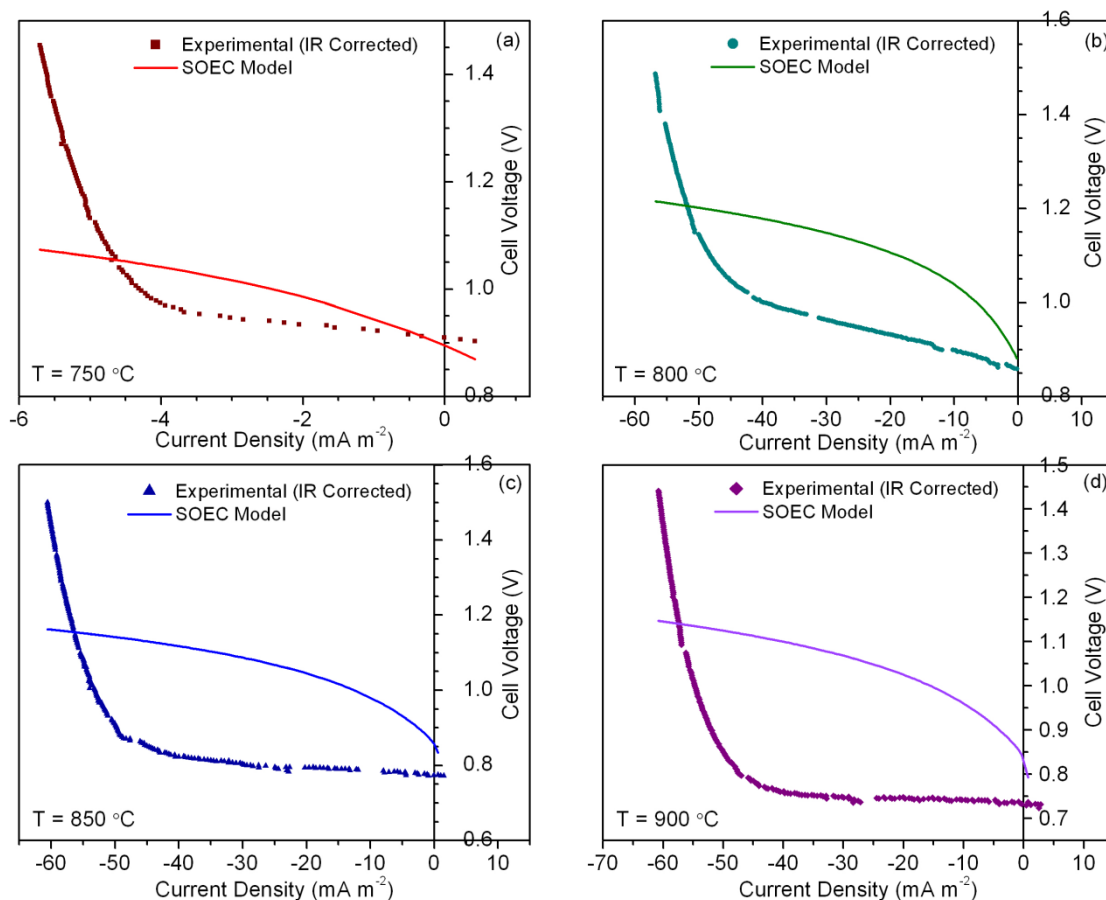


Figure 6-5: Comparison of model and experimental results at (a) 750 °C, (b) 800 °C, (c) 850 °C and (d) 900 °C at 90% N₂: 10% H₂ and RH 75%.

6.3.1.2 Validating against literature

The SOEC model was validated against results from literature and the values are shown in Table 6-1. The ohmic overpotential validation is shown in Figure 6-6 and are generated based on using both the parameters and Equation (52) shown in the study by Udagawa *et al.* [24]. The study focused on the modelling of SOECs and the effect on individual overpotentials across the thickness of the cell, thereby providing a benchmark for validation of the model in this study. The study presented a SOEC operating at 750 °C and 1 atm, and comprised of Ni-YSZ cathode, YSZ electrolyte and LSGM anode with thicknesses of 5×10^{-4} , 2×10^{-5} , and 5×10^{-5} m, respectively. The conductivity values used by Udagawa *et al.* [24] were also used in the validation of the model in this study; the values were 80,000, 1.416 and $8,400 \Omega^{-1} \text{ m}^{-1}$ for the cathode, electrolyte and anode, respectively. By using the parameters outlined in the paper in Equation (52) and solving in gPROMS, the result in Figure 6-6 was obtained and shows good agreement.

Table 6-1: Values taken from literature to validate the model.

| Overpotential | Values from literature | |
|-----------------------------|---|------------------------|
| Ohmic [24] | $\tau_{cathode}$ (m) | 500×10^{-6} |
| | τ_{anode} (m) | 50×10^{-6} |
| | $\tau_{electrolyte}$ (m) | 20×10^{-6} |
| | $\sigma_{cathode}$ ($\Omega^{-1} \text{ m}^{-1}$) | 8×10^4 |
| | σ_{anode} ($\Omega^{-1} \text{ m}^{-1}$) | 8.4×10^3 |
| | $\sigma_{electrolyte}$ ($\Omega^{-1} \text{ m}^{-1}$) | 1.416 |
| | T (°C) | 750 |
| Activation [191] | $i_{0,cathode}$ (A m^{-2}) | 5300 |
| | $i_{0,anode}$ (A m^{-2}) | 2000 |
| | T (°C) | 800 |
| Concentration: Cathode [24] | $\tau_{cathode}$ (m) | 500×10^{-6} |
| | C_{H_2O} (mol m^{-3}) | 10.58 |
| | C_{H_2} (mol m^{-3}) | 1.17 |
| | D_{eff} ($\text{m}^2 \text{ s}^{-1}$) | 1.416 |
| | T (°C) | 750 |
| | P (atm) | 1 |
| Concentration: Anode [190] | τ_{anode} (m) | 500×10^{-6} |
| | B_g (m^2) | 1.28×10^{-16} |
| | r_p (m) | 5×10^{-7} |
| | μ (Pa s) | 5.13×10^{-5} |
| | ξ | 6 |
| | ε | 0.3 |
| | T (°C) | 800 |
| | p_{O_2} | 0.2 |

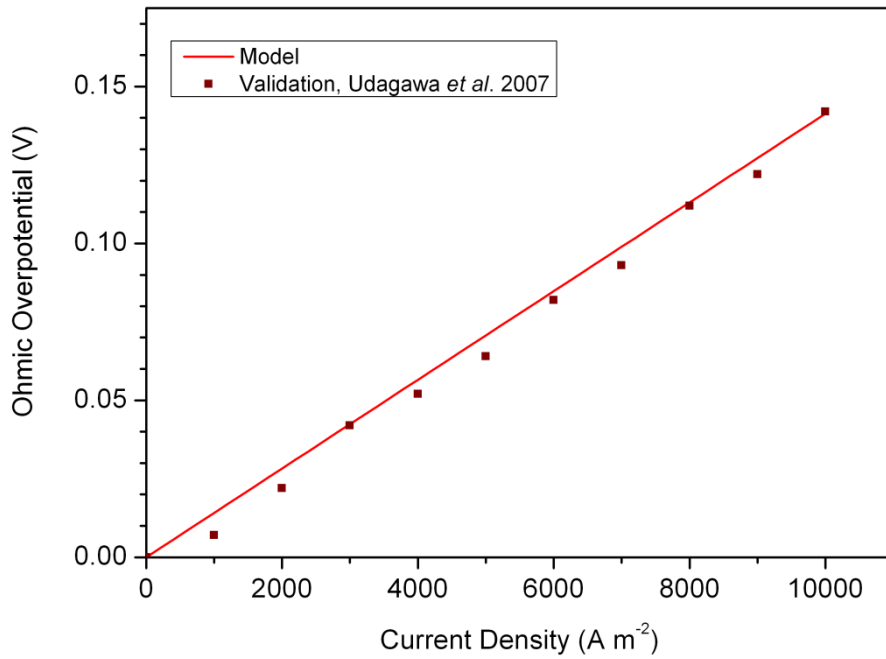


Figure 6-6: Validation of ohmic overpotential with values from Udagawa et al. 2007 [24].

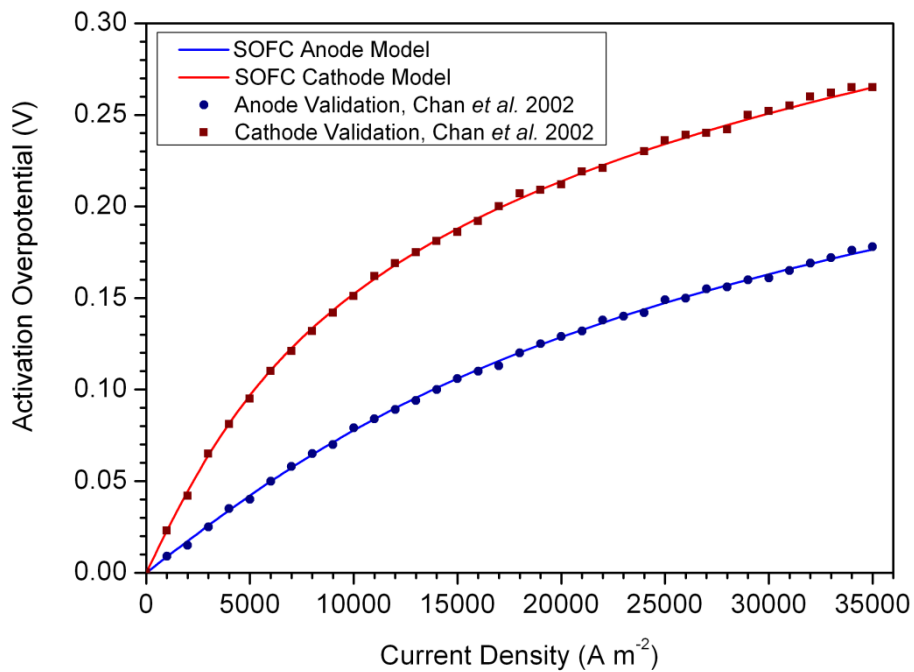


Figure 6-7: Validation of Activation overpotentials with values from Chan et al. 2002 [191].

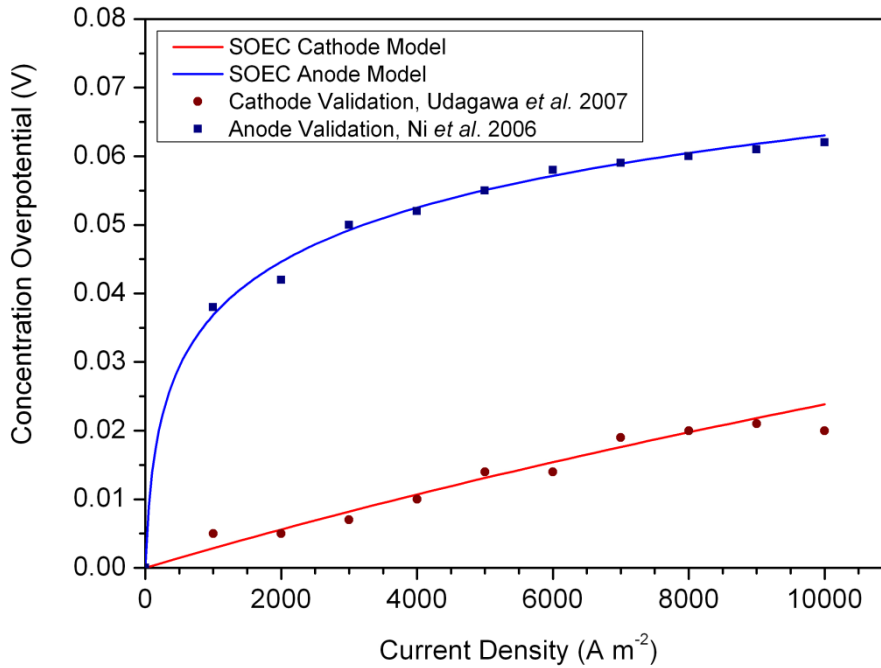


Figure 6-8: Validation of concentration overpotentials with values from Udagawa *et al.* 2007 [24] and Ni *et al.* 2006 [190].

The activation overpotentials for an SOFC operating at 800 °C with an LSGM electrolyte was studied by Chan *et al.* [191;203]. The modelling study carried out by Chan *et al.* was one of the first of its kind and has been used in several studies in literature. As the study focuses on particular overpotentials, the study was used for validation of overpotentials. The parameters for the validation of the activation overpotentials assigned in the study as well as Equation (53) was used for validation of the model in this work [191]. The result of the validation is shown in Figure 6-7. It has been assumed by Chan *et al.* [203], that the exchange current density is 5,300 and 2,300 A m⁻² for an LSM cathode and Ni-SDC anode, based on experimental results presented by Maric *et al.* [227], and Huang *et al.* [228]. The uncertainties in the experimental data of the exchange current densities were not noted in the literature. Through solving Equation (53) in gPROMs using parameters from Chan *et al.* [191], a good fit can be seen in Figure 6-7 for the validation of the activation overpotentials.

The validation of the concentration overpotentials of the anode assumed permeation of O₂ through the anode. It has already been stated that the collision integral and dynamic viscosity do not have a significant impact on the results of the SOEC model, as the model considers a small electrolyser area and therefore lateral temperature gradients will not be formed. For an anode thickness of 5×10⁻⁴ m, mole

fraction of O₂ of 0.2, flow permeability of 1.28×10^{-16} cm² (calculated from Equation (39)), and dynamic viscosity of 5.13×10^{-5} Pa s (calculated from Equation (40)), Equation (53) was used to validate the concentration overpotential. By solving the above equations in gPROMS, it can be seen from Figure 6-8 that there is a good fit and therefore, the concentration overpotential part of the SOEC model is validated.

6.4 Solid oxide electrolyser results

One of the greatest challenges related to SOECs is improving the efficiency in order for the cost and quantity of producing H₂ to become competitive with steam methane reforming (SMR). The largest operating cost has been shown in Chapter 3 to be the electricity required for electrolysis, and improving SOEC efficiency would therefore enable the cost of producing H₂ to decrease [218]. In addition, some studies have highlighted that pressurised systems improve efficiency, especially as pressurising water prior to use requires less energy than pressuring hydrogen after the electrolysis process [99;229;230]. However, raising the pressure of water initially requires more energy than at atmospheric pressure and therefore a trade-off is required [231].

One of the greatest impacts on the efficiency of H₂ production from SOECs is the energy required to raise the steam to the required operating temperature, and potentially to pressurise the system as well. Making use of high-grade steam such as from a coal fired power plant is one possibility for improving the overall efficiency of the system.

In order to move SOEC technology towards commercialisation, the efficiencies seen in lab scale systems need to be maintained through scale-up. Steam for electrolysis is commonly produced from a reservoir of water and heated to the temperatures required for the SOECs [75;232]. Efficiency and cost have been noted as barriers to commercialisation, and therefore to improve efficiency, heating water to operating conditions using hot streams from nuclear plants and solar energy has been studied [197;216;233;234]. The extent of the improvement in SOEC efficiency by using hot streams rather than raising steam from water will be assessed in the following.

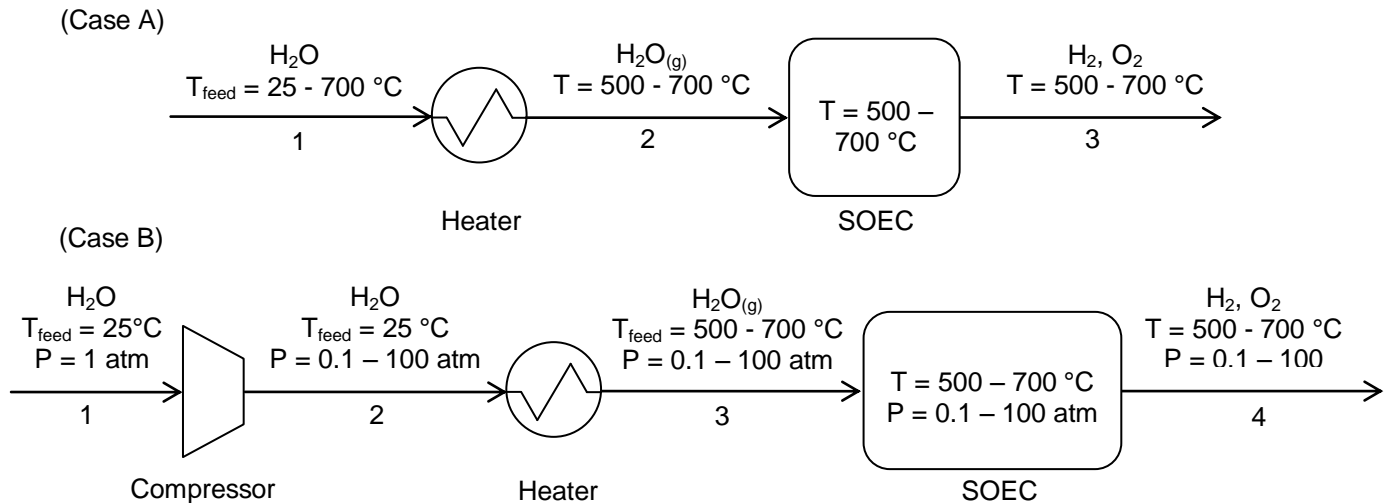


Figure 6-9: Process flow diagrams showing modelled systems: (Case A) The entering feed is heated and then used to operate the SOEC. (Case B) The entering feed is pressurised, heated and then used to operate the SOEC.

In the following, integrating an existing power plant with an SOEC system has been considered. Case A assumes that inlet water or steam (stream 1 in Figure 6-1 and Figure 6-9) for the SOEC could be sourced from a number of locations in the power plant at temperatures ranging between 25 and 700 °C at 1 atm, as shown in Figure 6-9 (Case A). In order for the feed stream to be suitable for use in the SOECs at an assigned operating temperature, the inlet stream would have to be either heated or cooled. It has been assumed that the heater is operated at 100 % efficiency.

Though there are advantages to using pressurised steam for electrolyser operation, such as a reduction in area specific resistance and the ability to carry a larger flow rate, the energy consumption for both pressurising and heating the steam prior to the SOEC may outweigh the benefits [99]. Case B considers the energy consumption of producing hot and pressurised steam from water sourced at 5°C and 1 atm. The power requirements for both these two Cases are calculated in gPROMS using Equations (64) to (66) to investigate the power requirements of the SOEC and Equation (71) effect on the efficiency of the cell.

This study is focused on intermediate temperature SOEC operation, which generally refers to temperatures of between 500 and 700 °C [116;235]. Intermediate temperature operation offers advantages as discussed in Section 4.1; conventionally used intermediate temperature materials have been chosen: gadolinium doped cerium oxide (CGO) electrolyte, lanthanum strontium cobalt ferrite (LSCF) anode and Ni-CGO cermet cathodes in a planar configuration. Ni-CGO and CGO have shown

good conductivities in SOFCs [117;236]. The parameters that have the most significant impact on the model are the conductivity and exchange current densities and were estimated through a fit based on Ni-YSZ in Section 5.2.1. Values from literature have been used in the model for the exchange current densities and conductivities of LSCF at varying temperatures [237], and all the parameters used in the model are shown in Table 6-2.

6.4.1 Case A: Producing hot steam at 1 atm

The results presented are based on a general Case A whereby water / steam is fed to the system at varying temperatures between 25 and 700 °C at 1 atm, as shown in Figure 6-11 (Case A). The first stage is heating the water or steam to the operating conditions. Figure 6-10 shows the energy required to raise steam to 500, 600 and 700 °C, respectively, which represents the possible range of operation for CGO electrolytes [119].

The graph (Figure 6-10) shows that there is a decrease in power requirement as the temperature of the inlet increases to the SOEC operating temperature. The sudden drop in the power requirement is due to the change of phase from water to steam. Using a feed steam close to the operating temperature of the SOEC, and particularly above the phase transition to steam, is clearly energetically beneficial. The benefit of increasing temperature is shown by the decrease in power requirement (Figure 6-10) and the increase in efficiency (moving toward the red zone) of Figure 6-11.

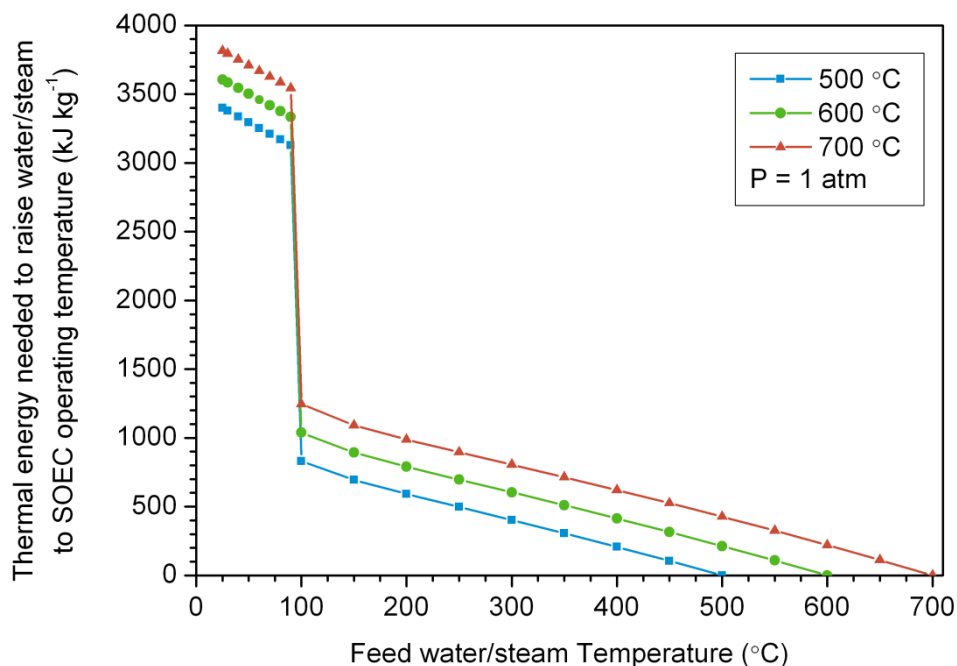


Figure 6-10: Energy required to heat water or steam to the SOEC operating temperature (500, 600 or 700 °C) at SOEC operating pressure of 1 atm.

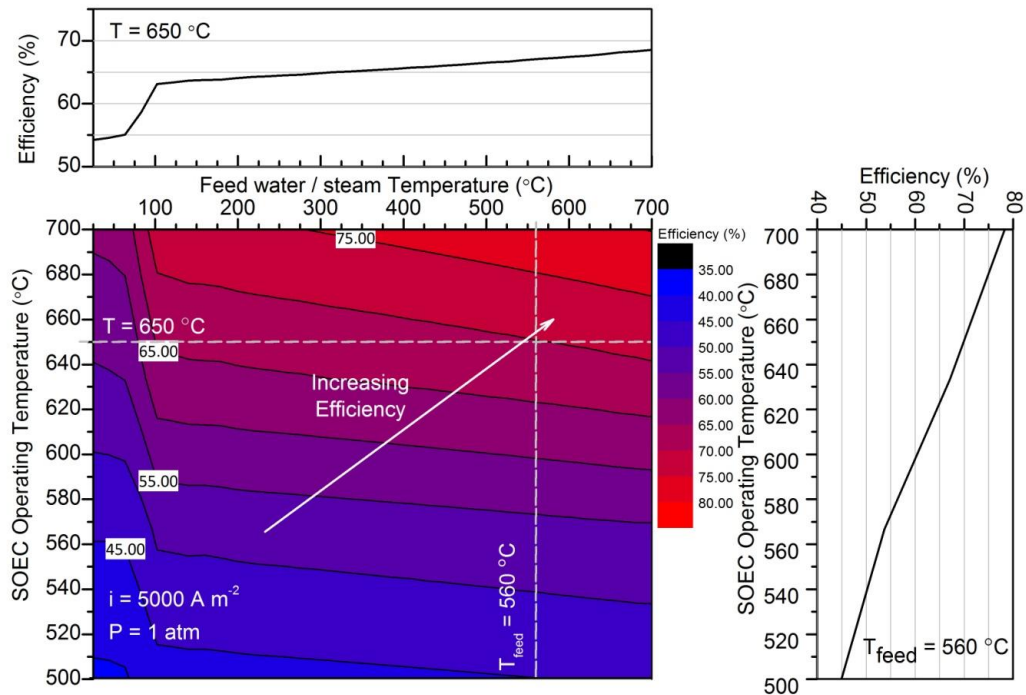


Figure 6-11: The SOEC efficiency across a range of operating temperatures and inlet feed water / steam temperatures for an SOEC operating at $5,000 \text{ A m}^{-2}$. The inserts show a cross section of the contour plot: (above) SOEC efficiency at SOEC operating temperature of $650 \text{ }^\circ\text{C}$ and (right) SOEC efficiency with feed temperature of $560 \text{ }^\circ\text{C}$.

Figure 6-10 to Figure 6-12 represents the energy requirement and efficiency related to varying the temperature of the inlet. It can be seen from Figure 6-10 that the power requirement decreases as the temperature of inlet increases. Furthermore, it shows that there is a significant drop in the power requirement of SOECs by using steam rather than water. Figure 6-11 shows the change in efficiency at SOEC operating condition of $5,000 \text{ A m}^{-2}$ with varying inlet temperatures and SOEC operating temperatures. The efficiency increase is represented by moving from the blue to red zone on the graph.

Figure 6-12 shows the change in efficiency at $650 \text{ }^\circ\text{C}$ and changing current density and inlet temperature. The current density of the SOEC defines the electrical input. Figure 6-12 shows the efficiency increases as the current density decreases; however, the temperature of the inlet still needs to be close to SOEC operating temperature for maximum efficiency. The efficiency increase is represented by moving from the blue to red zone.

The energy required to raise the temperature of the feed steam, combined with the energy necessary to operate the electrolyser, determines the overall efficiency of the

system. Figure 6-11 represents the change in the efficiency of the electrolyser with varying inlet feed steam temperature at a constant current density of $5,000 \text{ A m}^{-2}$. It can be seen that as the feed temperature tends toward the SOEC operating temperature (at a range of between 500 and $700 \text{ }^\circ\text{C}$), the efficiency increases. A maximum efficiency of 71.5% was seen when the temperature of steam was raised to the operating temperature of $650 \text{ }^\circ\text{C}$.

Figure 6-12 represents the performance of the SOEC as the current density and feed temperatures vary. The efficiency is seen to increase with decreasing current density, as the electrical input is reduced. For example, raising the steam from $25 \text{ }^\circ\text{C}$ to SOEC operating conditions of $650 \text{ }^\circ\text{C}$ and $5,000 \text{ A m}^{-2}$, results in system efficiency of 57% ; however, raising steam from $500 \text{ }^\circ\text{C}$ for the same SOEC operating conditions shows an efficiency of 70% . This percentage efficiency is significant and further indicates the need to source steam at suitable temperatures, if at all possible. Improvements in efficiency and reduction in energy requirement suggest a more cost effective process.

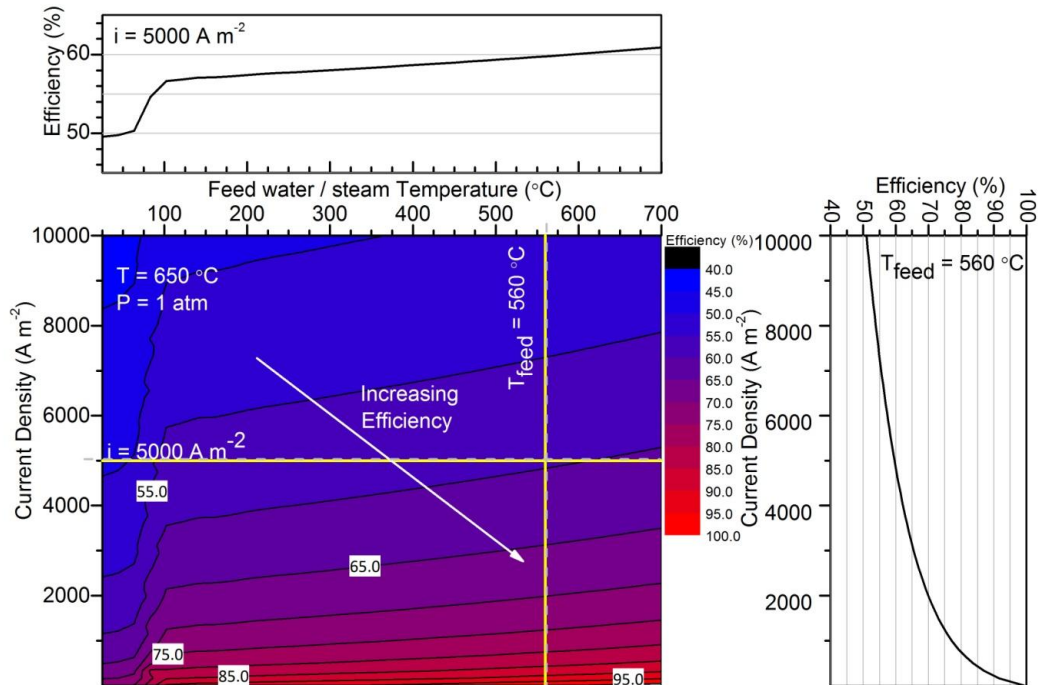


Figure 6-12: The efficiency across a range of current density and inlet feed water / steam for an SOEC operating at $650 \text{ }^\circ\text{C}$ and 1 atm . The inserts show a cross section of the contour plot: (above) SOEC efficiency at SOEC operating at 5000 A m^{-2} and (right) SOEC efficiency with feed temperature of $560 \text{ }^\circ\text{C}$.

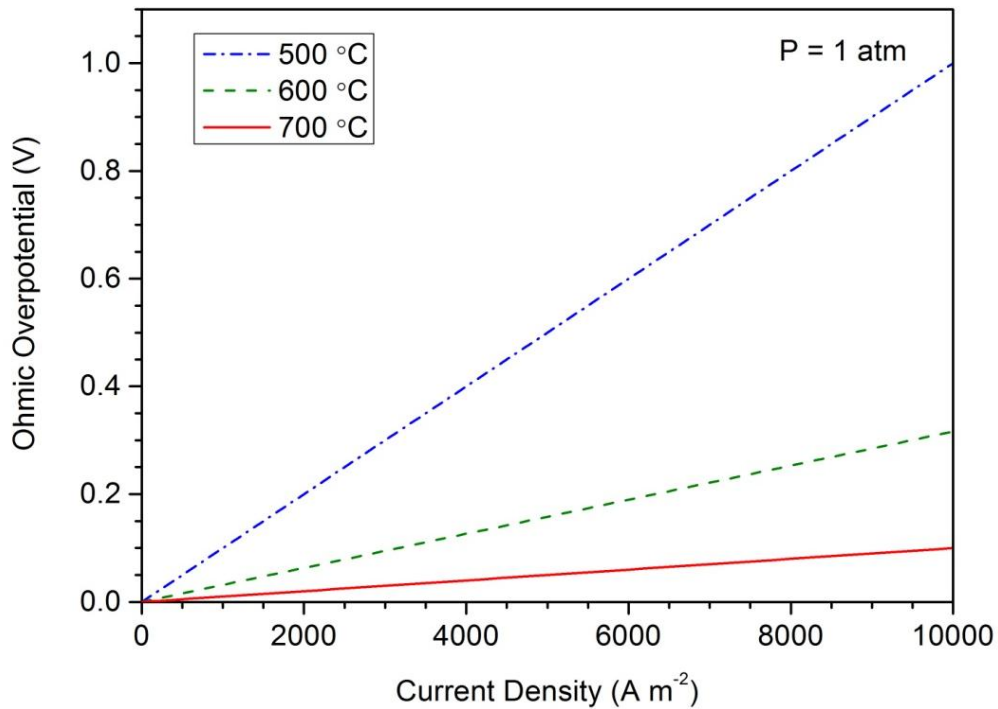


Figure 6-13: Ohmic overpotentials at SOEC operating temperature of 500, 600 and 700 °C, and SOEC operating pressure of 1 atm.

In addition to energy for producing steam, the efficiency is related to the overpotentials, which are created by the resistance to electronic and ionic transfers and need to be overcome in order for the electrolysis reaction to occur; the change in overpotentials with varying operating temperatures is shown in Figure 6-13 to Figure 6-15.

The ohmic, activation and concentration overpotentials were produced from modelling Equations (52), (53) and (54), respectively in gPROMS. Figure 6-13 shows the ohmic overpotential, which relates to the electrolyte and electrical connection resistance. It can be seen that as the temperature increases, the gradient and therefore the ohmic overpotential also decreases. The ohmic overpotential is a function of temperature and the materials used. In the case of this study, using a CGO electrolyte requires temperatures above 500 °C to obtain minimum ohmic overpotentials.

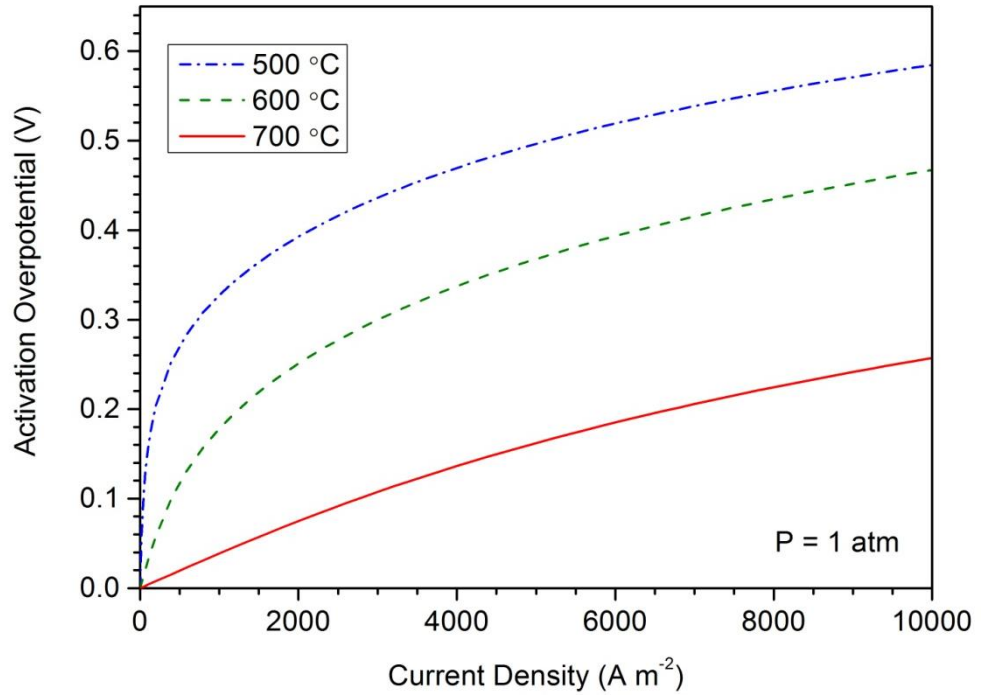


Figure 6-14: Activation overpotentials at SOEC operating temperature of 500, 600 and 700 °C, and SOEC operating pressure of 1 atm.

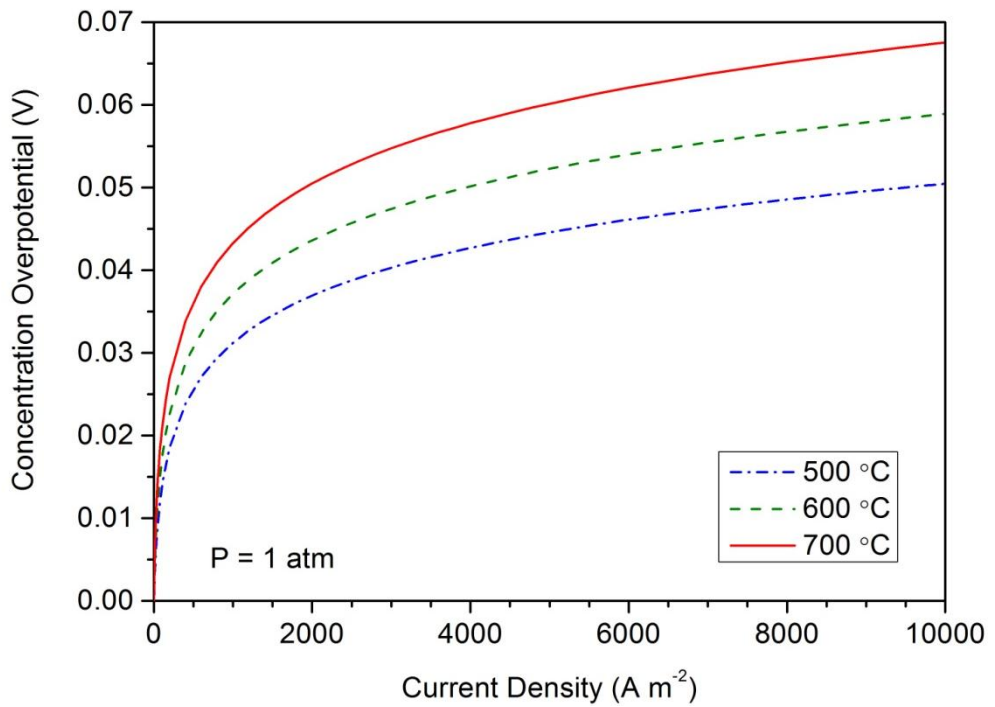


Figure 6-15: Concentration overpotentials at SOEC operating temperature of 500, 600 and 700 °C, and SOEC operating pressure of 1 atm.

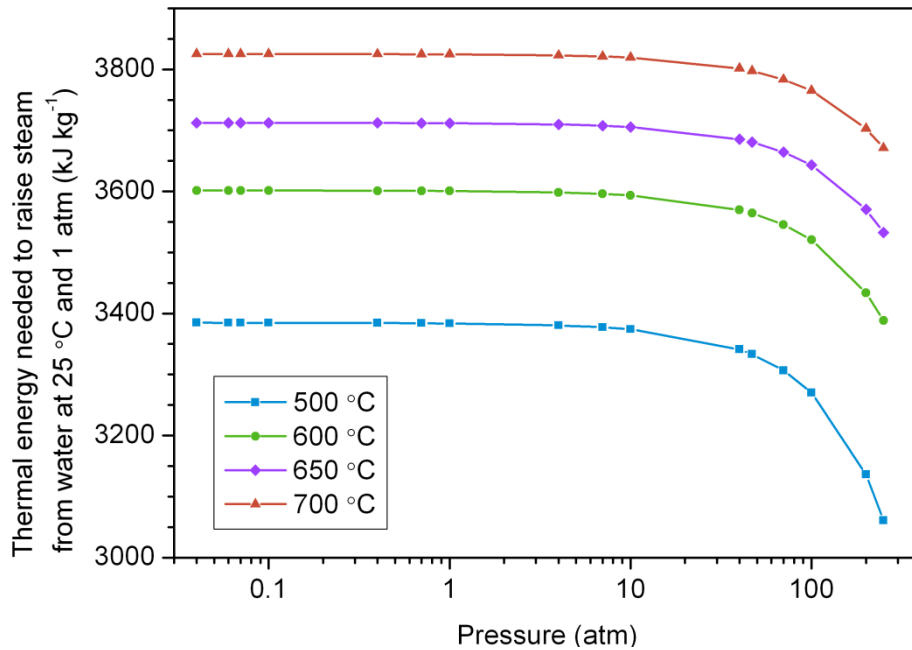


Figure 6-16: Thermal energy required for raising steam to various operating pressures at 500, 600, 650 and 700 °C from water at 25 °C and 1 atm.

Figure 6-14 shows that the activation overpotential also reduces with increasing temperature; the shape of the curves change, which relates to improved reaction kinetics as the temperature increases. The concentration overpotentials shown in Figure 6-15 are the least dominant and are significantly smaller than the ohmic or activation overpotentials. The concentration overpotentials show minimal change with temperature and therefore, it can be said that there is good mass transfer in the system.

Overall, it can be seen that the SOEC operating temperature is significant to the overpotentials. As the overpotentials contribute to efficiency losses, minimising the overpotentials or SOEC energy requirements will improve SOEC efficiency. Minimising overpotentials through suitable operating conditions for SOECs will contribute to improving SOEC efficiency. Based on these results, and in order to increase efficiency through reducing the electrical energy put into the system, a source for steam at elevated temperatures close to the SOEC operating temperature is required.

6.4.2 Case B: Producing hot and pressurised steam

Figure 6-16 shows the power requirement for producing steam at a set temperature and pressure. As the pressure increases, the power requirement to raise the steam

decreases. Considering both Figure 6-10 and Figure 6-16, it can be seen that less energy is required to raise the temperature of water as the pressure of the water increases. However, the improvement to SOEC performance and efficiency of a pressurised system is very small. Due to this, the efficiency of the SOEC operation is very similar to that shown in Figure 6-11 and Figure 6-12.

Furthermore, it has been shown by Jensen *et al.* [192] that an increase in pressure can reduce the overpotentials. Therefore, sourcing steam that has both elevated temperatures and pressures can provide improvement in the efficiency of the cell. The results from Figure 6-11, Figure 6-12 and Figure 6-16 have shown that efficiencies on average of around 60 % can be achieved based on heating and pressurising the inlet to the SOEC; however, if steam can be sourced that are already at suitable conditions, both the performance and cost efficiency may be improved.

6.5 Conclusions

A solid oxide electrolyser model was developed to show the extent of efficiency loss due to both the energy required to produce steam and the electrolysis process. An equation set discussed in the Chapter was solved in gPROMS to provide solid oxide electrolyser efficiency information on a steady-state and planar cell composed of Ni-CGO (cathode) / CGO (electrolyte) / LSCF (anode). The exchange current density and conductivity of the materials used in this study were based on correlations, and showed that there was little difference in overall cell efficiency with a sensitivity analysis. However, experimental studies are needed to be carried out in future work in order to provide a more accurate representation for modelling.

The results of the solid oxide electrolyser model have shown that temperature rather than pressure was a significant variable to system efficiency, which agrees with experimental results. The relationship between temperature and pressure on efficiency correlates with conclusions in literature [99;229;230]. It was also shown that the closer the temperature of the feed steam is to the SOEC operating potential, the greater the efficiency. For a SOEC operating at $5,000 \text{ A m}^{-2}$ and $650 \text{ }^\circ\text{C}$, the efficiency of the SOEC improves from 57 % to 70 % when using feed water at temperatures of $25 \text{ }^\circ\text{C}$ and $500 \text{ }^\circ\text{C}$, respectively. This is a significant improvement and represents the need for sourcing steam at suitable conditions as well as combining suitable electrolytes for the process.

From the results of Chapter 5, showing intermediate temperature steam extraction is possible from a power plant, and Chapter 6, it can be seen that combining intermediate-temperature SOEC with a coal fired power plant is an option for an integrated system. The temperatures of steam from the plant are close to that of the operating conditions for the intermediate-temperature CGO electrolyte. The extent of SOEC performance improvement and the impact on the plant of an integrated system is discussed in Chapter 7.

Table 6-2: List of parameters used in the SOEC model.

| Parameters | Parameter value | Ref |
|---|---|--|
| $A(H_2O, H_2, O_2)$ | 3.470, 3.249, 3.639 | [18] |
| $B(H_2O, H_2, O_2)$ | 0.001450, 0.000422, 0.000506 | [18] |
| $C(H_2O, H_2, O_2)$ | 0,0,0 | [18] |
| $D(H_2O, H_2, O_2)$ | 12100, 8300, -22700 | [18] |
| $\nu(H_2O, H_2, O_2)$ | -1, 1, 0.5 | |
| ΔH_0° | -241.818 (kJ mol ⁻¹) | [18] |
| H_v | 2256.9 (kJ kg ⁻¹) | |
| ΔG_0° | -228.572 (kJ mol ⁻¹) | [18] |
| T_0 | 273 (K) | [18] |
| n | 2 | |
| F | 96487 (C mol ⁻¹) | |
| R | 8.314 (J mol ⁻¹ K ⁻¹) | |
| $\alpha_{cathode}, \alpha_{anode}$ | 0.5 | |
| $b_d(b_0, b_1, b_2, b_3, b_4, b_5, b_6)$ | -1.6918, 889.75, -892.79, 905.98, -598.36, 221.64, -34.754 | [238] |
| τ_{anode} | 30×10^{-6} (m) | [239] |
| $\tau_{cathode}$ | 30×10^{-6} (m) | [239] |
| $\tau_{electrolyte}$ | 100×10^{-6} (m) | [239] |
| $x_{H_2O}, x_{H_2}, x_{O_2}$ | 0.9, 0.1, 1 | |
| MW_{H_2O}, MW_{H_2} | 18 (g mol ⁻¹), 2 (g mol ⁻¹) | |
| ε | 0.3 | [191] |
| S_A | 6×10^4 (cm ² g ⁻¹) | |
| ρ_B | 7.119 (g cm ⁻³) | |
| ξ | 6 | [191] |
| $\varepsilon_{ki}/k_{H_2O}$ | 809.1 (K) | [204] |
| ε_{ki}/k_{H_2} | 59.7 (K) | [204] |
| δ_{H_2O} | 2.641 (Å) | [204] |
| δ_{H_2} | 2.827 (Å) | [204] |
| $\Omega_{DH_2O-H_2}$ | 0.87 | [202] |
| $\sigma_{electrolyte(ScSZ)}(750, 800, 850, 900 \text{ }^\circ\text{C})$ | 6.31, 7.94, 12.59, 28.18 ($\Omega^{-1} \text{ m}^{-2}$) | [240] |
| $\sigma_{electrolyte(CGO)}(500, 600, 650, 700 \text{ }^\circ\text{C})$ | 1.00, 3.16, 3.98, 10.0 ($\Omega^{-1} \text{ m}^{-2}$) | [119] |
| $\sigma_{cathode(Ni-CGO)}(500, 600, 650, 700, 750, 800, 850, 900 \text{ }^\circ\text{C})$ | 69821, 62575, 60000 ^a , 57902, 56172, 54731, 53521, 52497 ($\Omega^{-1} \text{ m}^{-2}$) | ^a [122] |
| $\sigma_{anode(LSM)}(750, 800, 850, 900 \text{ }^\circ\text{C})$ | 19953, 22909, 23989, 25119 ($\Omega^{-1} \text{ m}^{-2}$) | [162] |
| $\sigma_{anode(LSCF)}(500, 600, 650, 700 \text{ }^\circ\text{C})$ | 25000, 28000, 30000, 31000 ($\Omega^{-1} \text{ m}^{-2}$) | [237] |
| $i_{0,cathode(Ni-CGO)}(500, 600, 650, 700, 750, 800, 850, 900 \text{ }^\circ\text{C})$ | 92.9, 685.7, 1580.0 ^b , 3356.5, 6610, 12220, 21389, 35695 (A m ⁻²) | ^b [226] |
| $i_{0,anode(LSM)}(750, 800, 850, 900 \text{ }^\circ\text{C})$ | 9.9, 25, 45, 50 (A m ⁻²) | [209] |
| $i_{0,anode(LSCF)}(500, 600, 650, 700 \text{ }^\circ\text{C})$ | 10.0 ^c , 130.0 ^c , 1800.0 ^d , 3328.8 ^d (A m ⁻²) | ^c [241] ^d [242] |
| Variable | Input values | |
| T | 773, 873, 923, 973 (K) | |
| P | 1 (atm) | |

7 Operation of an integrated power-solid oxide electrolyser plant

In this context, system integration refers to combining solid oxide electrolyser cells (SOECs) with a coal fired power plant to make the most of older technologies via retrofit, or for new systems, delivering electrical power and hydrogen fuel simultaneously. This chapter assesses the impact on both the plant and the electrolyser efficiency of an integrated system and aims to find the upper limit for steam and electricity extraction from the plant for SOEC operation. In addition, factors such as economics, infrastructure, storage and social aspects, which are important to the success of an integrated system, have also been evaluated.

7.1 Integrated systems in literature

Integrated systems refer to electrolysers coupled with other process plants such as nuclear, wind and fuel cell technologies in order to obtain either heat or power for large scale fuel manufacture. With proton electrolyte membrane (PEM) and alkaline cells being commercially available, most studies on integrated systems have concentrated on PEM and alkaline electrolysers with renewable sources of energy.

In addition to the economic analysis discussed in Chapter 3, studies have also been carried out on electrolysers with wind technology and have shown that wind technology can benefit from integration with electrolysers as one solution to reducing intermittency issues by producing, storing and using hydrogen on-site [243]. It has been shown that combining wind technology and alkaline cells at ambient conditions, rather than at the commonly used 80 °C, allows production of hydrogen more efficiently and dynamically due to a reduction in auxiliary equipment [61]. Such system-wide analysis provides an understanding of the interaction of electrolysers with other technologies and allows decisions on electrolyser operation to be made for an overall improvement in system performance.

Solar photo-voltaic (PV) cells being a renewable technology, has drawn a large interest for combining with electrolysers, commonly PEM cells, as a clean and renewable system for hydrogen production. The hydrogen production levels are shown to be dependent on intensity of solar radiation with 2.97 kg yr⁻¹ H₂ production with a 60 % efficient PEM electrolyser reported by one study [244]. The costs associated with PV cell technology have been shown to be 43.90 \$ kg⁻¹ by one study, which shows that the technology needs significant improvements in order to become competitive in the market. It has also been shown by Ghribi *et al.*, that a suitable

location for PV cells such as areas with good solar radiation can allow $29 \text{ m}^3 \text{ yr}^{-1}$ of H_2 to be produced from PV cells combined with PEM electrolyser stacks [245].

A test system based on a 10 cell (100 cm^2) PEM stack operating at 40 A and powered by a battery connected to both wind and solar cells was tested in Malaysia and produced an average electrolyser efficiency of 60 % over a day, with 134 ml min^{-1} H_2 produced [246]. Studies like this show that there is promise in electrolysers for hydrogen production as well as in improving the integration of renewable technologies to the grid.

The limited data on system-wide analysis and integrated processes have focused on low temperature cells as large amounts of heat and steam are not required. The most researched area for SOEC integration is that with nuclear power (Section 3.1) as both heat and electricity can be sourced from one place [75;247;248]. Taljan *et al.* have shown that an integrated SOEC and nuclear plant can produce steady profits with SOEC efficiencies between 60 and 90 % [248].

SOECs have also been studied as a way of mitigating CO_2 by using flue gas from power plants. It was seen that system energy and exergy efficiencies of 50 and 60 %, respectively were achievable at an optimum operating potential of 1.37 V [196]. It was shown by Davidson *et al.*, that supplying electricity to electrolysers from sources such as wind or coal gasification plants in times of low demand is not economically viable at the moment, especially with the additional costs of carbon capture and storage technologies [249]. It has been shown that electrolysers can obtain the necessary electricity from coal fired power plants [250]; however, the impact on efficiency of extracting both steam and electricity from the plant has not been considered. Therefore, this study seeks to address the possible option of combining electrolysers with power plants with the aim of reducing the costs and enabling hydrogen production to be an economically attractive option.

As alkaline and PEM cells are commercially available, most studies have focused on combining low temperature electrolysers with wind and solar PV technology; and there is limited research on SOECs for large scale applications. This study aims to assess the feasibility of large scale hydrogen production through combining SOECs with a coal fired power plant. The effect on the efficiencies of SOECs and the power plant by the integration of the two has been investigated. In addition, the energy requirement of the SOEC by using steam from the plant has been compared with

Cases A and B in Chapter 6. Furthermore, the costs associated with producing hydrogen from the integration has also been considered, and compared with the steam methane reforming process.

7.2 Results of system integration

In the following, the steam from the power plant (Figure 5-3) is considered to be integrated with the SOEC. Steam extracted before the high pressure (Case 1), intermediate pressure (Case 2) and low pressure (Case 3) turbines have been assessed for their suitability for integrating with SOECs. It can be seen that the outlet temperatures of the power station are in the range of intermediate temperature operation, with a nominal SOEC temperature of 650 °C chosen for the analysis to match CGO electrolyte operating conditions [119;226]. The operating pressure of the SOEC system is taken to be equal to that of the feed steam extracted from the power plant. Case 4, which considers using flue gas for co-electrolysis, has not been considered in this study due to the low temperatures of the stream after particulate removal.

This chapter focuses on the change in efficiency of an integrated system at different operating conditions and is based on Equation (72), which represents the overall efficiency of the integrated system ($Efficiency_{integrated}$):

$$Efficiency_{integrated} = \frac{P_{H_2}(i, A_{tot}) + P_{PP}(i, A_{tot})}{P_{input}} \times 100 \quad (72)$$

The efficiency takes into account the power produced by hydrogen (P_{H_2}) and the power which is produced from the plant once a fraction has been extracted for electrolysis (P_{PP}) as a function of current density and total area (A_{tot}) of the SOEC. P_{input} represents the chemical energy input to the system, in this case by the coal feed. Both the electrical power and heat required are taken into account in P_{PP} . The results of an integrated system on a per metre square SOEC basis (unsized SOEC) and sized SOEC systems are discussed.

Figure 7-1 illustrates the variations in efficiency of using steam from Cases 1 to 3 in SOECs and is based on Equation (71):

$$Efficiency = \frac{2F(E_{op} - E_{overpot})\dot{N}_{H_2}}{(iE_{op}) + \dot{Q}_{steam}} \times 100 \quad (71)$$

Figure 7-1 shows the change in SOEC efficiency with operating current density for Cases 1 to 3. It can be seen that the efficiency of the SOEC decreases with increasing current density and reduced inlet steam temperatures, i.e. Case 3 requires the most energy to meet SOEC requirements. The general operating methods discussed in Chapter 6 and represented by Case A in Figure 6-12 showed the same trend - SOEC efficiency is dependent on the inlet temperature and current density. Case A considered the power requirements and efficiency related to producing suitable steam from water at 25 °C. A comparison of the results of the integrated system in Figure 7-1 with the results of general Case A in Figure 6-12 has been shown in Table 7-1. As an example, Case A showed an SOEC efficiency of 60.0 % when water at 25 °C was raised to 560 °C; however, an improvement to 75.3 % and 75.1 % SOEC efficiency at 5,000 A m⁻² was seen with the integrated system of Case 1 and 2, respectively (results shown in Table 7-1). The elevated temperatures provided by the power plant can be utilised in SOECs, as the infrastructure is already available to produce steam. The capital costs may be reduced when comparing an integrated system with solely a SOEC system. The effect of pressure was seen in Chapter 6 and shown by Jensen et al. to have very little effect on the performance of the electrolyser [192].

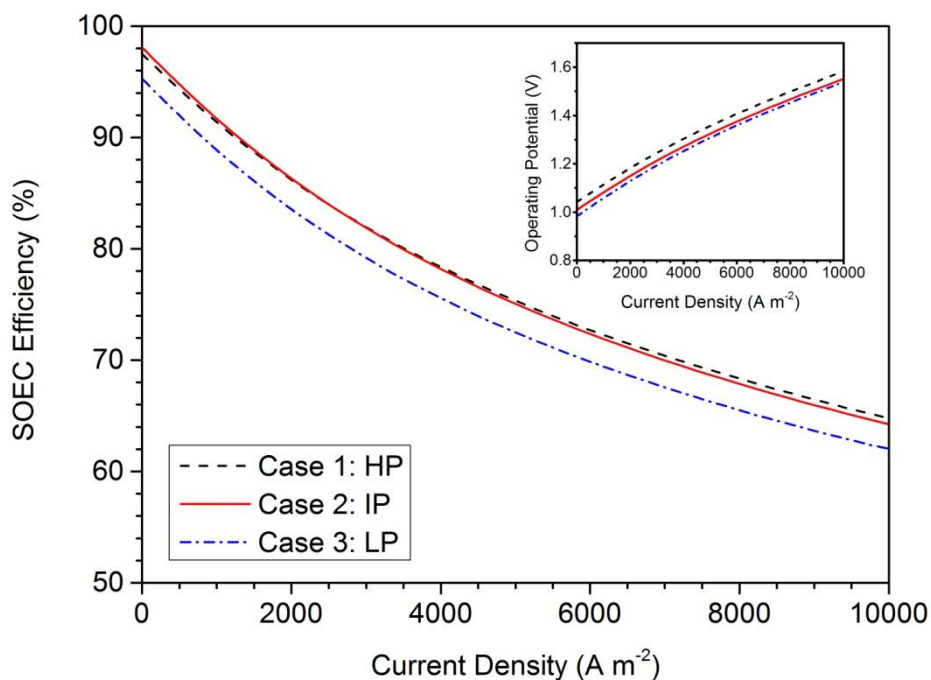
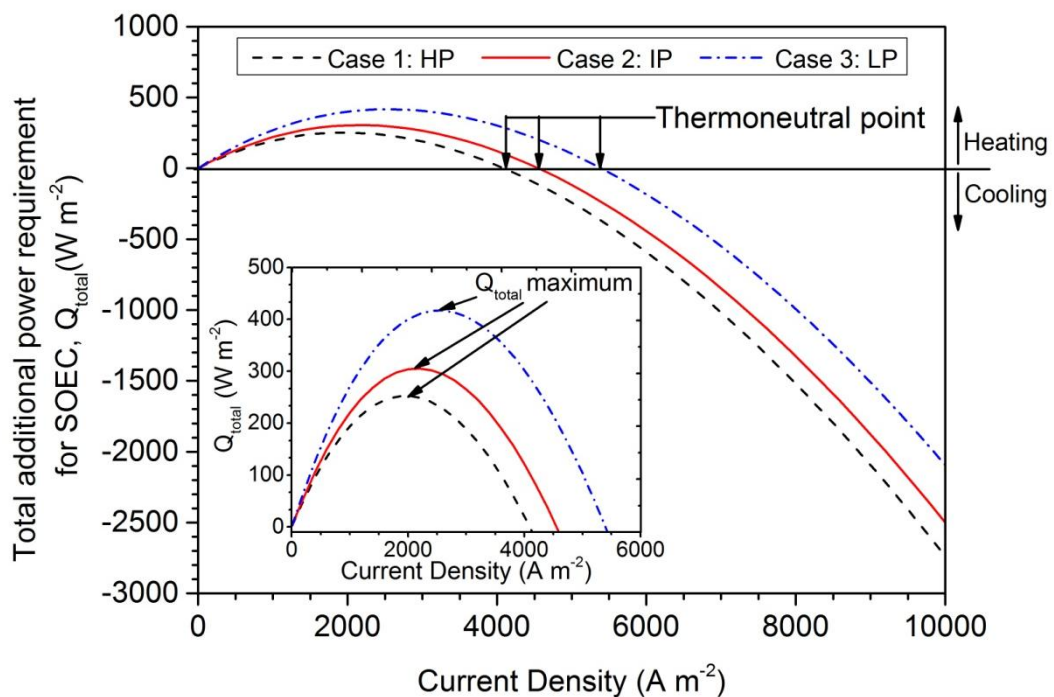


Figure 7-1: SOEC efficiency with changing current density at an operating temperature of 650 °C for Cases 1, 2 and 3. The insert shows the operating potential with current density for the three Cases.

Table 7-1: A comparison of SOEC efficiency based on the general (Chapter 6) and integrated cases at current densities of 5000 A m^{-2} .

| General Case | | Integrated Case | | Overall improvement in SOEC efficiency (%) |
|--|--|--|--|--|
| Steam condition from raising water at $25 \text{ }^\circ\text{C}$ and 1 atm (Case A) | SOEC Efficiency (%) (5000 A m^{-2} , $650 \text{ }^\circ\text{C}$) | Steam condition from power plant | SOEC Efficiency (%) (5000 A m^{-2} , $650 \text{ }^\circ\text{C}$) | |
| 560°C , 1 atm | 60.0 | $560 \text{ }^\circ\text{C}$, 250 atm (Case 1) | 75.3 | 25.5 |
| | | $560 \text{ }^\circ\text{C}$, 46 atm (Case 2) | 75.1 | 25.2 |
| 409°C , 1 atm | 58.0 | $409 \text{ }^\circ\text{C}$, 12.9 atm (Case 3) | 64.5 | 11.2 |

**Figure 7-2: Total additional power requirement for SOEC operating at $650 \text{ }^\circ\text{C}$ with steam from cases 1, 2 and 3. Insert: a close up of the peaks of the curves to show the maximum amount of additional heating power needed.**

As the steam from the power plant under certain conditions is insufficient to meet SOEC operating conditions, additional power (taken as being in the form of electricity from the plant) to heat the steam is needed, as shown in Figure 7-2. Below the zero power line, cooling is required; and the point at which the system has reached thermal equilibrium is called the thermoneutral point (at the zero power line). This is when the heat consumed by the endothermic reaction and heating steam to SOEC operating conditions is equal to that produced by the overpotentials. Based

7. Operation of an integrated power-solid oxide electrolyser plant

on the results in Figure 7-2, the thermoneutral point lies at current densities of 4,093, 4,553 and 5,432 A m⁻² for Cases 1, 2 and 3, respectively.

It should be noted that operating above the thermoneutral point may be beneficial when considering the system as a whole, as operating at current densities higher than the thermoneutral point will allow options for thermal integration with exiting gases. This may alleviate some of the resources extracted from the power plant, thus ensuring the overall efficiency loss is kept to a minimum. The maximum amount of power required is 252.6 W m⁻² (at 2,000 A m⁻²), 305.3 W m⁻² (at 2,200 A m⁻²) and 421.9 W m⁻² (at 2,600 A m⁻²) for Cases 1, 2 and 3, respectively. This provides the upper limit of electricity that the SOEC needs from the plant on a per metre square cell basis, as well as accounting for the further loss in power plant efficiency after steam extraction.

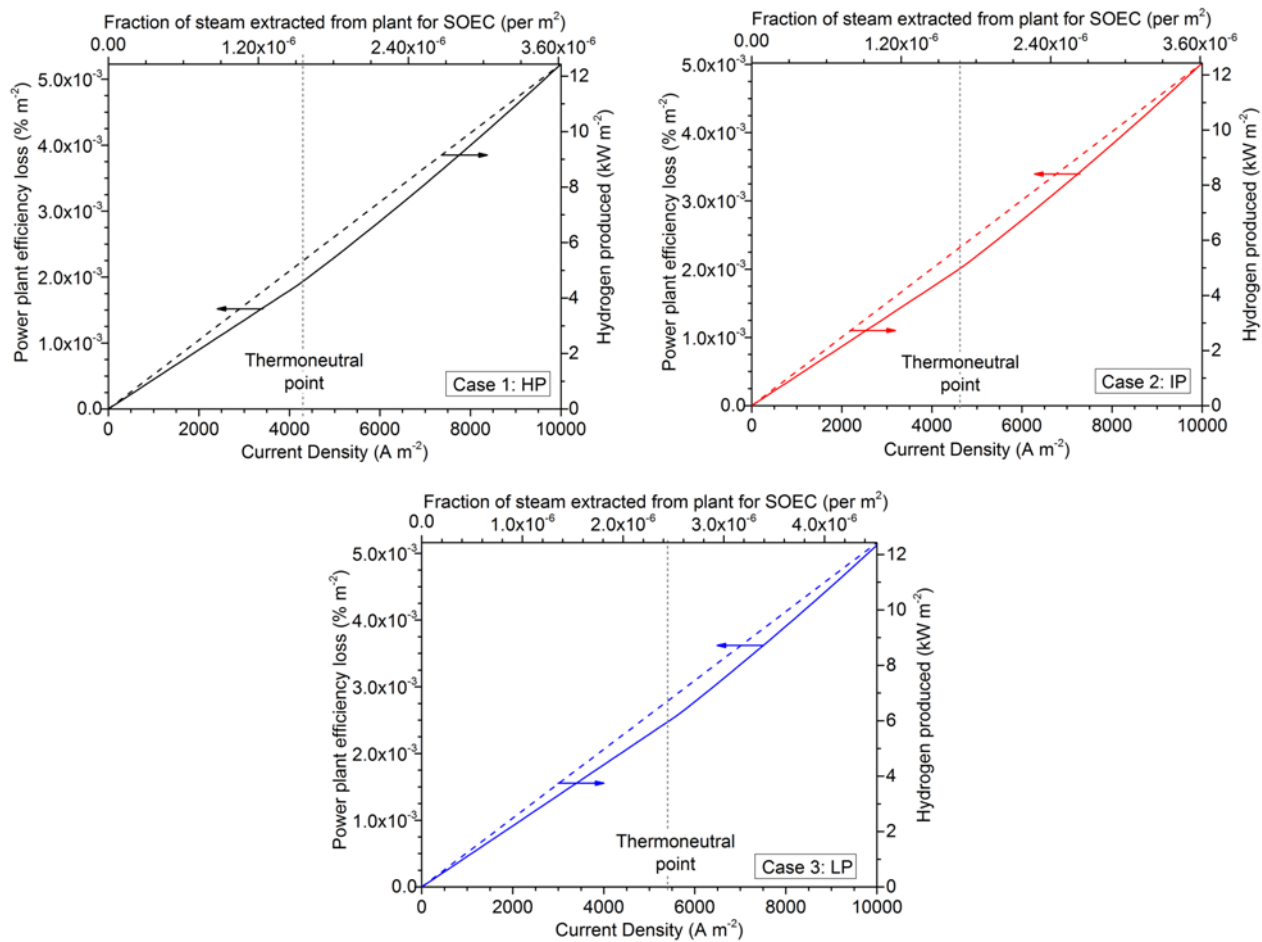


Figure 7-3: The loss of power plant efficiency (left axis) and associated hydrogen production (right axis) vs. current density and associated fraction of steam extracted from the plant; for an integrated system based on cases 1 to 3.

7. Operation of an integrated power-solid oxide electrolyser plant

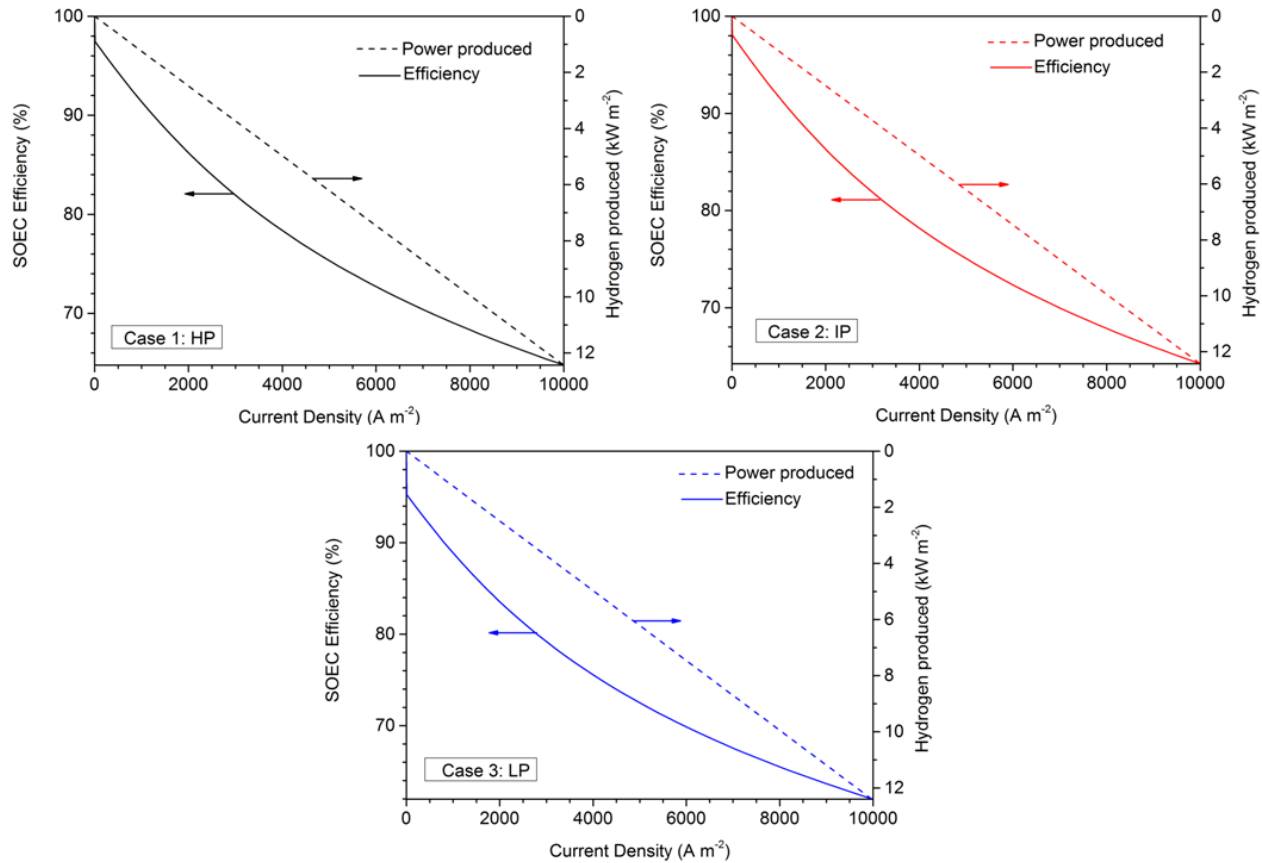


Figure 7-4: SOEC efficiency and power generation via hydrogen based on steam from Cases 1, 2 and 3.

The extent of loss of power plant efficiency from extracting the necessary steam and electricity to operate an SOEC is shown in Figure 7-3. Based on operating conditions of 80 % utilisation and $5,000 \text{ A m}^{-2}$, it is seen that SOEC efficiencies of 75.3 %, 75.1 % and 64.5 % for Cases 1, 2 and 3, respectively, can be produced; which correlate with hydrogen output per metre square of 0.19 kg hr^{-1} (6.21 kW m^{-2}) based on the lower heating value of hydrogen. The results align well with experimental data in literature, where Herring *et al.* [239] produced 0.12 kg hr^{-1} (3.38 kW m^{-2}) hydrogen at 2710 A m^{-2} . (Note that the effect of both steam and electricity extraction are affected by the size of the electrolyser and the study therefore represents efficiencies based on a per metre square active area of the SOEC.)

The loss in the power plant efficiency increases non-linearly as the current density increases, due to variations in the demand of energy for heating the steam before the thermoneutral point (Figure 7-3). However, after the thermoneutral point, heat is being produced, which reduces the additional energy requirements. Once the energy requirement for electrolysis and heating the steam to SOEC operating conditions

have been met, additional energy is not required; only electricity to operate the SOEC. Therefore, the efficiency losses of the power plant increase at a slower rate. There are still losses in efficiency as the heat produced at larger current densities are not being utilised in this study. Through adequate heat management, the losses in power plant efficiency may be smaller than those shown in Figure 7-3. Possible options for heat management include using exit streams from the SOEC to heat input streams to the SOEC and utilising hot oxygen in the boiler of the power plant to enhance coal combustion.

Figure 7-4 shows the decrease in efficiency with increasing operating current densities, as well as the associated hydrogen power production per metre square. It can be seen from Figure 7-4 that operating at lower current densities gives larger SOEC efficiencies due to the decrease of the curves; however, the amount of hydrogen produced is also lower. Operating the SOEC higher than the thermoneutral point, such as 6,000 A m⁻², enables larger amounts of hydrogen to be produced as shown in Table 7-2. However, it also has larger plant efficiency losses, with the greatest impact being Cases 1 and 3 (Figure 7-3).

Overall, it can be seen from Table 7-1 that using the high quality heat and steam from a power plant can improve the efficiency of the electrolyser significantly, by 25 % for Cases 1 and 2 and 11 % for Case 3, compared with conventional methods where water is heated from 25 °C. The change in efficiency of the SOEC is almost solely dependent on the temperature of the feed rather than the pressure. However, in order to achieve SOEC efficiency improvements, the power plant efficiency drops; it was seen for Cases 1, 2 and 3 with SOEC operation at 5,000 A m⁻², power plant efficiency losses of 2.30×10⁻³, 2.20×10⁻³ and 2.29×10⁻³ % m⁻², respectively.

Table 7-2: The change in SOEC and power plant efficiency, and H₂ production with SOEC operation at and above the thermoneutral point.

| Case | Thermoneutral point (TNP) (A m ⁻²) | SOEC Efficiency (%) | | Hydrogen produced (kW m ⁻²) | | Power plant efficiency loss (% m ⁻²) | |
|------|--|--------------------------|---------------------------|---|---------------------------|--|--|
| | | TNP (A m ⁻²) | 6000 (A m ⁻²) | TNP (A m ⁻²) | 6000 (A m ⁻²) | TNP (A m ⁻²) × 10 ⁻³ | 6000 (A m ⁻²) × 10 ⁻³ |
| 1 | 4,093 | 78.06 | 72.7 | 5.09 | 7.45 | 1.84 | 2.85 |
| 2 | 4,553 | 76.4 | 70.9 | 5.66 | 7.45 | 1.98 | 2.72 |
| 3 | 5,432 | 71.3 | 69.9 | 6.75 | 7.45 | 2.49 | 2.78 |

Depending on the operating point, a number of benefits and disadvantages can be noted. Generally, the thermoneutral point can allow a stable current density to meet the criteria needed for electrolysis and ensuring overpotentials are kept to a minimum. However, operating at higher current densities than the thermoneutral point may allow the heat produced from the overpotential in the SOEC to be integrated with entering gas streams to the SOEC; and as a result, reducing the electricity requirement of the plant for heating the steam. For a system operating at larger current densities, a suitable control strategy is needed to ensure that the material constraints of the SOEC are met.

The constraints of the materials and SOEC designs currently available are important factors when deciding on an optimum point for steam extraction from the plant. The steam extracted for Cases 1, 2 and 3 are at pressures of 250, 46 and 12.9 atm, respectively; pressurised SOEC systems have to date, been tested in the regions of 46 atm; therefore, IP conditions (Case 2) are expected to be a suitable practical option [99]. Further benefits of Case 2 include the extent of efficiency loss from the plant not being as high as Case 1 for an equivalent H_2 output (at $5,000 \text{ A m}^{-2}$, 6.21 kW m^{-2} of H_2 can be produced with power plant efficiency losses of 2.30×10^{-3} and $2.20 \times 10^{-3} \% \text{ m}^{-2}$ from Cases 1 and 2, respectively) and can be seen in Table 7-2 and Figure 7-4. Case 3 shows poor efficiencies and hydrogen output compared with Cases 1 and 2 (Figure 7-4) and is therefore not considered the best option (for an SOEC operating at $5,000 \text{ A m}^{-2}$, efficiencies of 75.3, 75.1 and 72.4 % were seen for Cases 1, 2 and 3, respectively). Based on the current state of SOEC technologies, the results suggest that using steam extracted from just before the IP turbine can provide suitable heat, steam and pressure for an efficient and productive system.

These results suggest that integration of SOECs with power plants requires further consideration to be able to enhance overall system efficiency. The results indicate that steam and electricity utilisation from the power plant is a feasible concept; however, the economic viability, future demand for hydrogen, SOEC size and location need to be further assessed. The key to assessing the efficacy of the approach will be to consider the economics of operation over a time-varying power demand profile of a power station and the value of the hydrogen produced from an energy storage and raw commodity perspective, as well as the capital cost of the SOEC, which is not known with any certainty at present. This is beyond the scope of this study; however, future work should consider an optimised system taking into

consideration heat integration of the system as well as the factors influencing the economics of hydrogen production in such a system.

To ensure that the most can be made from both the power plant and the SOEC without restricting the day-to-day operation of the power plant, the time of day that the SOECs are operational is key. In general, the plant's energy output drops significantly at night due to low energy demand and therefore turndown of up to 50 % occurs [172]. Extracting the steam at night and producing hydrogen during this period allows a way of producing alternative fuels or using hydrogen as a storage vector. Furthermore, the pure oxygen produced at the anode enables the possibility of improving boiler performance and reducing harmful gas by-products through oxy-fuel operation [251-254].

An example of a sized integrated system for a 350 MW_e power station is shown in Figure 7-5. The sizing of the SOEC was carried out at each operating condition in isolation assuming 80 % utilisation of steam for Case 2. The thermoneutral condition is again based on the operating condition where the heat from the overpotentials and Joule heating is equal to the energy required for heating steam and for the reaction.

Figure 7-5(a) shows that for a constant amount of steam extraction of 7 % from the steam cycle, the SOEC area required decreases in an exponential manner. To establish a standard fraction of steam extraction for the scenario in Figure 7-5(a) the amount of steam needed for the largest current density (10,000 A m⁻²) in this study was used. Current density of 10,000 A m⁻² would require the largest fraction of steam extraction from the power plant to maintain the 80 % utilisation outlined in this study. Therefore, a steam extraction of 7 % was chosen as this is the maximum extraction possible for the largest current density considered (10,000 A m⁻²). The system efficiency remains constant at 34.2 % before the thermoneutral point as all of the heat produced by the overpotentials is being used to raise the temperature of the extracted steam.

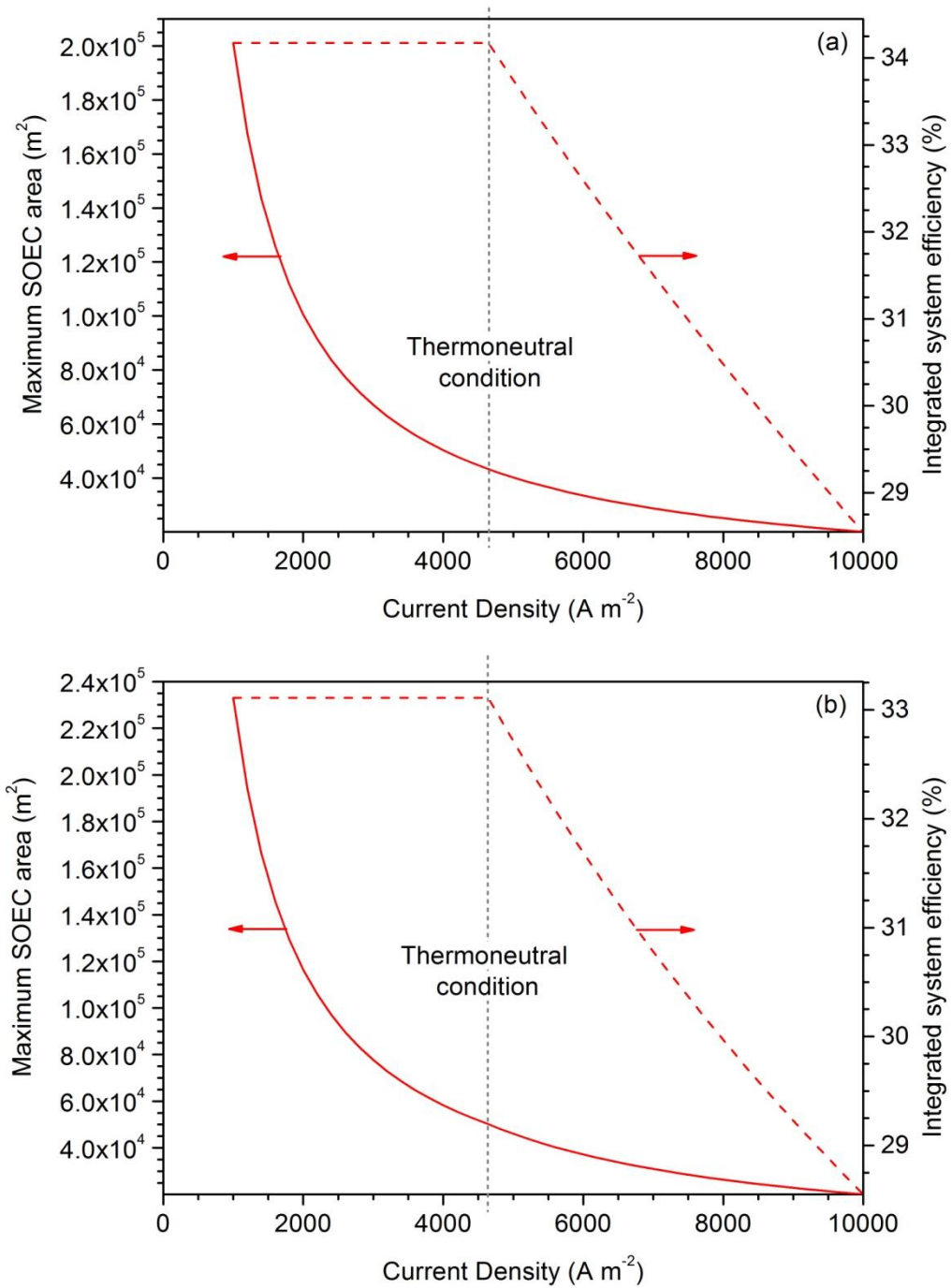


Figure 7-5: The maximum SOEC area and associated integrated system efficiency with varying current densities from case 2: IP at (a) with a constant steam extraction of 7% and (b) a case where the plant is producing hydrogen only i.e. zero electrical output to the grid.

Another option is to use the whole plant for making hydrogen (Figure 7-5(b)), such that there is no electrical energy sent to the grid (i.e. all of the electricity generated by the power plant is consumed in generating hydrogen). Once again, the analysis considered an individual design for each operating condition. However, this results in an overall system efficiency of 33.1 % before the thermoneutral condition. After the thermoneutral condition, further reduction in the system efficiency is due to changes in the steam and electrical energy requirements.

In both cases shown in Figure 7-5, the constant efficiency before the thermoneutral point is due to the area of the SOEC being sized using solver for each current density and therefore is considered in isolation at each current density on the graphs. The amount of steam extracted from the plant has been calculated and remains the same by changing the SOEC area. Varying the SOEC area at a particular current density results in a change in the steam required to meet the assumed 80 % utilisation.

As the amount of steam extracted remains the same, the energy required to heat the steam to the SOEC operating temperature is also constant and therefore, the power extracted from the plant to heat the steam is constant. The power to meet SOEC operating conditions varies at each current density; as the current density increases, the power needed to operate the SOEC also increases. The heat energy needed for the electrolysis process decreases as overpotentials increase with current density.

The overall power extracted from the plant before the thermoneutral point is used for producing hydrogen. After this point, power (above the required amount) is extracted from the plant to meet the current density requirements and any excess heat produced by the SOEC has not been used and therefore accounts for the loss of integrated system efficiency.

After the thermoneutral condition, the heat produced is in excess and not being used effectively to contribute to the efficiency of the system, as defined by Equation (72). To minimise efficiency fade after the thermoneutral point, the heat available from the hydrogen product stream needs to be utilised. Options are available for the heat to be used, such as to reduce electrical demands from the SOEC through heating steam or in other parts of the plant such as preheating air to the combustor or as part of heat exchangers.

Without considering heat integration options, the thermoneutral condition represents a sensible operating point for the electrolyser, allowing a trade-off between

electrolyser size and overall system efficiency. Therefore, at $4,644 \text{ A m}^{-2}$, 250 MW (7500 kg hr^{-1}) and 290 MW (8700 kg hr^{-1}) of H_2 (lower heating value (LHV)) can be produced with SOECs sized at 43,300 and 50,100 m^2 for scenarios of 7 % steam extraction and a purely H_2 production plant, respectively. Studies in literature for integrated systems with nuclear plants have also indicated that SOECs of this scale are necessary; for example, around $9 \times 10^4 \text{ m}^2$ [255]. Introducing heat integration options, such as heating the steam entering the SOEC with gases exiting the SOEC may reduce the electricity taken from the power plant.

In this study, two main scenarios have been presented; the first, considering only 7 % steam extraction and the second, a hydrogen plant. However, these are representative of extreme scenarios, which take the power plant to extreme operating conditions. It is possible to extract steam and electricity at ranges up to 7 % from the power plant depending on the available space for SOEC stacks on the plant as well as the demand for hydrogen. Although it can also be seen that there is a loss in overall power plant efficiency with an integrated system, benefits such as the ease of retrofitting SOEC stacks, which can be sized accordingly to power plant needs, the option of enhancing boiler efficiency for O_2 -enriched combustion of coal and utilising the plant during low energy demand may counteract the efficiency losses. The changing energy market and need for alternative fuels and technologies such as fuel cells may create need for large scale hydrogen production, thereby requiring the power plant to be used solely for hydrogen production. However, if the demand for hydrogen is low then a fraction of steam less than 7 % is possible, while still producing electricity to meet peak demand. In such cases, it may even be possible to utilise steam in the day, rather than at night. Therefore, further studies based on future energy demands, and the effect of changes to the current energy technologies is necessary to assess the actual demands placed on the power plant.

7.3 Other considerations

Though the efficiency and hydrogen output seem promising from using SOECs combined with power plants, there are a number of other factors that are imperative for large scale hydrogen production and deployment. These include economic factors, social, storage, available infrastructure and demand, all of which need to be addressed in order for the rapid move toward cleaner technologies and meeting CO_2 emission mitigation targets outlined by the government.

7.3.1 Economic

One of the main challenges of implementing SOECs commercially is producing hydrogen at a competitive rate with existing technologies, as well as selling hydrogen competitively with fuels such as petrol, especially as the UK focuses on the use of hydrogen fuel cells for transport rather than homes [165]. The economics of an integrated SOEC-power plant system is vital to the success of the concept in order for hydrogen to be produced at a competitive rate to steam methane reforming (SMR). It was seen in Chapter 3 that the most significant operating cost in producing hydrogen is the cost of electricity which can contribute up to 80 % of costs [256]. Generally, the costs are also affected by the electricity needed for the ancillary units, such as heaters to produce steam to the SOEC operating temperature; however, it was seen in Section 7.2 that some of the costs of heating the steam can be alleviated through extracting hot steam from the power plant itself via an integrated system.

In order to produce hydrogen through the integrated system, the power plant is turned down through extracting steam and some of the electricity produced by the plant is used by the SOEC, which reduces the income of the plant from electricity sales. Therefore, the minimum cost of producing hydrogen through an integrated system is directly related to the electricity loss from the plant. Figure 7-6 shows the minimum price for selling hydrogen to maintain the income generated currently by a coal fired plant selling electricity at 9 US¢ kWh⁻¹. It has been noted that the price of electricity can vary with demand based on the time of day and season within the year; however, an average cost has been used for this analysis. The cost accounts purely for operating costs. The capital and maintenance costs have not been included in this study, as SOECs are not yet commercially available. The capital cost has been shown to be the second largest cost for electrolysers and therefore this expense and the assigned payback period will have a significant effect on the selling price of hydrogen [256].

It can be seen from Figure 7-6(a) and (b) that as the current density increases, thereby demanding more energy for the SOECs, the efficiency of the integrated system decreases. As a result, of increased energy demand and efficiency losses, the cost of producing hydrogen increases. As discussed earlier, the efficiency of the system is related to the size of the SOEC and operating conditions. For both a system which extracts 7 % of steam from the plant, and a hydrogen generation plant, it can be seen that hydrogen costs around 0.11 US\$ kWh⁻¹ (3.76 \$ kg⁻¹) to produce before

7. Operation of an integrated power-solid oxide electrolyser plant

the thermoneutral point and varies with current density thereafter to around 0.13 US\$ kWh⁻¹ (4.35 \$ kg⁻¹) at 10,000 A m⁻². The increase in the production cost of hydrogen is due to unutilised heat that is produced after the thermoneutral condition.

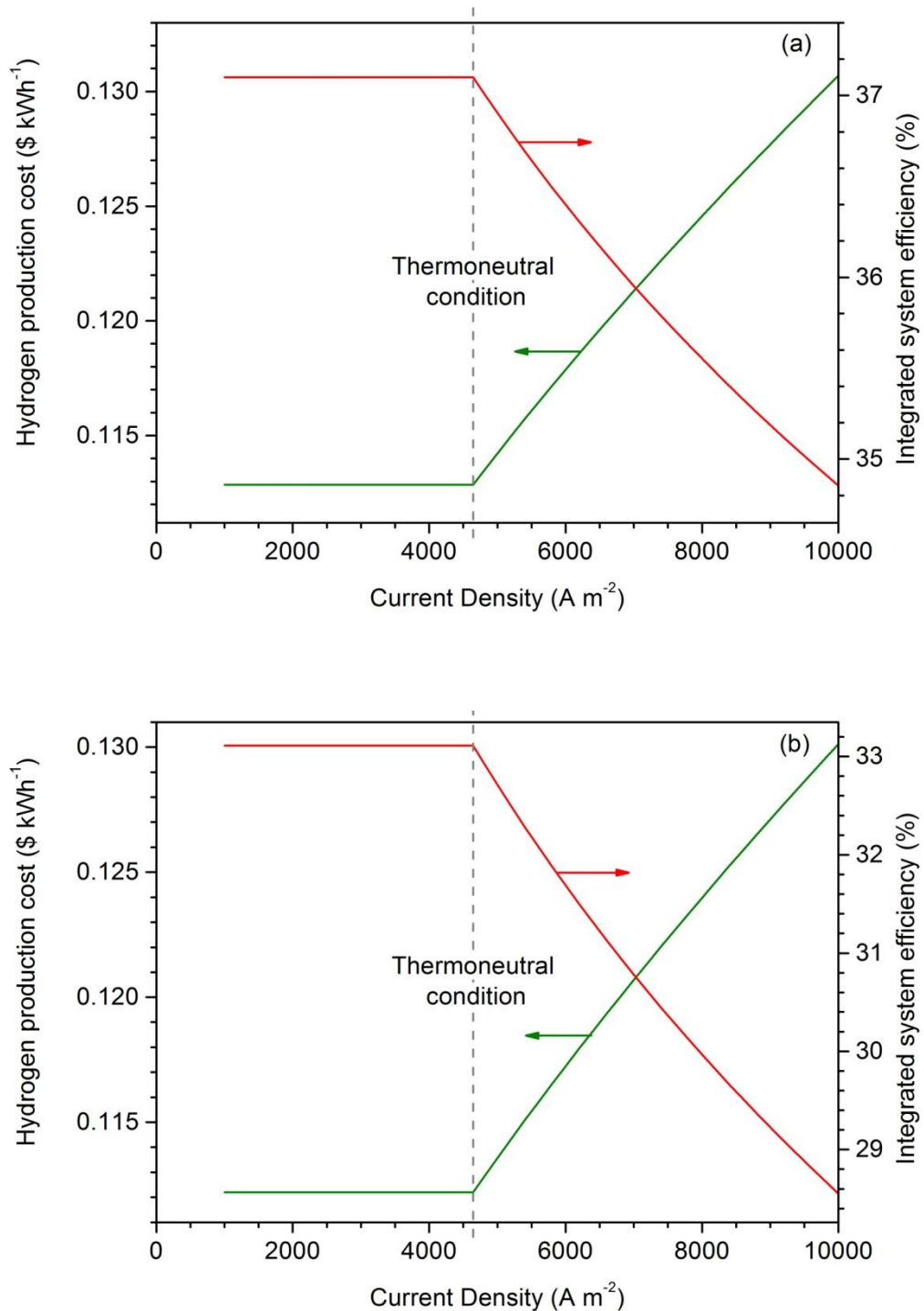


Figure 7-6: Minimum cost of producing hydrogen to maintain average power plant income compared with integrated system efficiencies for Case 2: IP at (a) with a constant steam extraction of 7%. (b) a case where the plant is producing hydrogen only i.e. zero electrical output to the grid.

According to an economic model by the US Energy Information Administration, which considers future energy consumption and fuel production globally [257], the cost of hydrogen production through steam methane reforming up until the point of distribution is 4.49 \$ kg⁻¹ with production costs of 2.03 \$ kg⁻¹ [258]. The cost of producing this hydrogen is dependent on the price of methane, which is predicted to increase in the future [257]. Such an increase in the price of methane, combined with improvements in electrolyser technology, can allow the cost of hydrogen production via SOECs to reduce. Improvements in SOEC technology has already seen an improvement in costs, where in 2009 the production cost of hydrogen from SOEC technology was improved to 3.32 \$ kg⁻¹ from 4.23 \$ kg⁻¹ in 2005 [257]. The two main reasons for a drop in production costs were improved capital costs and energy use with PEM electrolyzers. Therefore, the results obtained from the integrated system analysis is in line with studies carried out and represents improved production costs with increasing energy efficiency [256].

7.3.2 Infrastructure

With plans in place for hydrogen to be used for fuel cell vehicles and mass production of such vehicles, infrastructure needs to be created and implemented to provide ease of use [259]. Introducing an integrated SOEC and power plant system has the benefit of producing both syngas and hydrogen. For the near future where syngas is required for synthetic fuel production, flue gas may be used from the power plant and electrolyser for syngas production [37], which will also reduce carbon taxes imposed on the plant. This enables the current infrastructure to be used while new ones are put in place, as it has been suggested that suitable infrastructure will take several decades to be constructed across Europe [260]. In addition, new materials may need to be sourced for infrastructure rather than using cement due to the large amounts of CO₂ emitted from making cement [261]. Sourcing materials may be time consuming and creates uncertainty. Therefore, a large amount of work is required in order to construct infrastructure suitable for a hydrogen economy.

7.3.3 Storage

As infrastructure for using hydrogen in fuel cells is part of a long term plan, storage is key in the short term. Hydrogen storage is important for large-scale hydrogen production and is one of the greatest limitation towards the hydrogen economy [262]. The most popular and widely used are gas cylinders, which compress

hydrogen to a maximum of 200 atm at 25 °C, although new cylinders have been shown to handle 800 atm, which reduces the volume of the gas significantly [263]. The concern with this type of storage is the safety implications. Furthermore, for on-board hydrogen systems, compressed cylinders may not meet the US Department of Energy regulations as the gravimetric density decreases with increase of pressure [264]. An alternative to this is liquefying hydrogen and storing it at -252 °C, however, large amounts of energy are needed for this, which will increase the cost of hydrogen. Therefore, the most promising option is to use metal hydrides as they can store large amounts of hydrogen safely. Currently, Mg_2FeH_6 and $\text{Al}(\text{BH}_4)_3$ have shown large volumetric hydrogen density of 150 kg m^{-3} . The metal hydrides are able to store hydrogen by undergoing a strong chemisorption process, which traps hydrogen atoms to the metal hydride. To regenerate the hydrogen, a kinetic or thermodynamic change such as changing temperature or pressure is required. This is still an area that requires optimisation in order to provide suitable storage on-site and on-board [263;264].

7.3.4 Social

One of the greatest concerns is whether hydrogen will be accepted by the public, especially with the uncertainty of development of new technologies made by the government. Studies were carried out based on public knowledge, awareness and acceptance, which represented the views of the population on hydrogen fuel [265].

It has been shown by a number of studies that in general, there is a positive attitude toward the use of hydrogen, though little knowledge of the technologies [265;266]. Furthermore, the risks posed by the explosive and flammable nature of hydrogen were the focus of some studies carried out in places where the AcceptH2 bus trial took place. It was noted that there was not a substantial perception of the risks involved unless specifically asked to think. It was noted that risk and safety should be a priority in the development of technologies, however, not a focus of public engagement [265;267].

Overall, there is public acceptance, though knowledge of the technologies being developed for mass production and use in the future is currently not well known. This is something that requires future training and education.

7.4 Conclusions

Integrating SOECs with power plants have shown a significant improvement in SOEC efficiency compared with stand-alone SOECs, with improvements of around 25 % possible at practical current densities. This shows that a large proportion of efficiency loss is due to conditioning steam to have the required thermal energy content. For SOECs as stand-alone units or as part of an integrated system, the thermoneutral point is shown to be a fundamental factor influencing both the design and operation, and hence the SOEC efficiency.

In the absence of a full trade-off analysis that considers capital cost and operational expense, the system thermoneutral point represents a first-order approximation as a suitable design point. It was seen that utilising heat before the thermoneutral point gives hydrogen production costs of around 11.2 US¢ kWh⁻¹ (3.76 \$ kg⁻¹) and 13.0 US¢ kWh⁻¹ (4.35 \$ kg⁻¹) at 10,000 A m⁻². Improvements to SOEC technology can reduce the production costs. Although an integrated system shows a loss in overall system efficiency compared with the power plant alone, if used during times of low electricity demand, the economics may nevertheless still be favourable.

8 Conclusions and Future work

8.1 Conclusions

The growing concern of carbon emissions and the drive to improve energy technologies to become more environmentally friendly is currently of great interest. It has been seen that carbon dioxide emissions were around 32,600 Mt globally in 2011 and are set to increase with the growth of the energy sector in Asia [1]. As an alternative to fuel production via hydrocarbon-based fuels, electrolysis of steam has been considered in this study.

Solid oxide electrolyser cells (SOECs) rather than using commercially available proton exchange membrane (PEM) and alkaline electrolyzers, have recently been researched in literature as a more efficient electrolyser. The thermodynamic analysis of steam electrolysis in this study has shown that the total minimum energy requirement for electrolysis, which remained fairly uniform with increasing temperature. However, it was seen that the Gibbs free energy that is related to the electrical energy requirement was heavily dependent on the temperature. It was seen that an increase in temperature would increase the heat available to meet the enthalpy of the electrolysis reaction, resulting in a decrease of the electrical requirement for electrolysis. The reason for this is due to the heat energy of the steam contributing to the total energy requirement. Therefore, this analysis carried out in this study has highlighted that elevated temperatures provide increased electrolyser efficiency. SOECs were chosen as a suitable alternative to conventional steam methane reforming for hydrogen production.

The experimental evaluation verified the thermodynamic analysis and showed that increasing temperature results in improved SOEC performance. Challenges with materials, rig design and sealing showed that more research is required in order to enable SOECs to become suitable for commercialisation. The issues of delamination that arose with LSM, the SOEC anode, have been researched in literature; however, remains a favourite material for high temperature electrolysis. Furthermore, it was seen that using YSZ and ScSZ electrolytes requires temperatures of between 850 and 900 °C for improved SOEC performance.

Both the thermodynamic and techno-economic analysis suggested that the greatest variable of electrolyser operation is the electrical requirement, which is dependent on the operating temperature of the SOEC and the overpotentials. Therefore, combining

an SOEC with a coal fired power plant was considered to allow both hot steam and electricity required to run the SOEC to be sourced from the plant. The simulation of the coal fired power plant showed that extracting steam from before the high pressure (Case 1), intermediate pressure (Case 2) and low pressure (Case 3) turbines was possible, with steam temperatures of 560 °C for Cases 1 and 2, and 409 °C for Case 3. The steam temperatures from the plant were significantly lower than those suitable for ScSZ and YSZ electrolytes and therefore CGO electrolyte, which is known for intermediate-temperature operation, was used.

In addition, an analysis for the extent of the change in efficiency to energy use was carried out on a Ni-CGO (cathode) / CGO (electrolyte) / LSCF (anode) SOEC through modelling. The steady-state model developed in this study was solved in gPROMS and assumed that there was not a drop in pressure and negligible temperature profiles. Due to limitations in the experimental facility and data in the literature, the conductivity and exchange current densities of the SOEC materials were estimated through data fitted from literature. As a result, this creates uncertainties in the SOEC model. Through experimental studies, suitable data for the variables can be measured and used in future models. Sensitivity analysis on the variables has shown little variation in SOEC efficiency. Values taken from literature such as CGO density, tortuosity, conductivity and exchange current density were assumed to be suitable for the conditions of this study; however, those based on experimental data may vary with material, electrode thickness, concentration of gases, temperature and pressure, which can introduce uncertainties to the model. Further experimental testing can reduce the uncertainties in the model. This study has provided a representation of the trend expected from SOECs in an integrated system, which is dependent on the variation of the conductivity and exchange current density to temperature and material set.

The results showed that the closer the steam temperature entering the system is to the solid oxide electrolyser cell (SOEC) operating conditions, the lower the electricity demand. For example, for a SOEC operating at 650 °C and 5,000 A m⁻², an efficiency of 57 % is possible by raising steam from 25 °C, and 70 % from 500 °C. The increase in efficiency is significant and highlights the need for sourcing elevated temperature steam according to the electrolyte of the SOEC. Furthermore, it was also shown that the pressure did not have a significant impact on SOEC performance.

Therefore, for an improved performance of SOECs, steam needs to be sourced suitably.

Introducing electrolyzers into power stations allows the hot steam and electricity to be utilised by the SOECs. Although high temperature electrolysis using YSZ electrolytes have been favoured in research, they were not seen to be suitable for an integrated system and therefore, CGO was used in the study. Through an integrated system, SOEC efficiency could be improved by around 25 % at practical current densities compared with a general case. The most suitable point for steam extraction from the plant was Case 2, steam extraction from before the intermediate pressure turbine, as the pressure (46 atm) and temperature (560 °C) were in line with current SOEC limitations. With more research into the effects of pressure on the degradation of materials, Case 1 (steam extraction before the high pressure turbine) may be a possibility in the future.

The thermoneutral point showed a distinct difference in the integrated system efficiency for the utilisation of heat and a factor for sizing the SOECs. Before the thermoneutral point, the heat from the steam and that generated by the overpotentials were used to meet the energy demands of the system. However, after the thermoneutral point, the produced heat was wasted, which resulted in decreasing efficiencies with increasing current density. Using the heat produced through a heat exchanger system would reduce the overall losses from the plant. The thermoneutral point itself was seen to be a suitable operating condition, allowing a trade-off between SOEC size and system efficiency. It was seen at 4,644 A m⁻² (1.31 V), 250 MW (7500 kg hr⁻¹) and 290 MW (8700 kg hr⁻¹) of H₂ (lower heating value (LHV)) can be produced with SOECs sized at 43,300 and 50,100 m² for scenarios of 7 % steam extraction and a purely H₂ production plant, respectively and is comparable with around 90,000 m² in literature [255].

A successful integrated system requires competitive economics, reliable infrastructure and social acceptance. It was seen that the cost of producing hydrogen at the thermoneutral point was 11.2 US¢ kWh⁻¹ (3.76 \$ kg⁻¹), which is a direct factor of the loss of income of the plant and the cost of electricity. Further costing that includes capital, maintenance, storage and transportation expenses will provide the total cost of hydrogen production via an integrated system but was not considered here. Though the costs of hydrogen production was higher than that of steam

methane reforming (SMR), improvements in electrolytes suitable for temperatures of 500 °C may provide further SOEC efficiency improvements.

Overall, the study aimed to assess the feasibility of integrating SOECs into a power plant for large scale hydrogen production. A significant improvement in SOEC technology may be needed to integrate SOECs into coal fired power plants. However, with a prediction of increasing use of coal globally, traditional technologies cannot be disregarded. Though there are plans to decommission many coal fired power plants in the UK, the reliance on hydrocarbon based fuels is high at the moment. Therefore, it is suggested that hydrocarbon combusting technologies be utilised while being ‘phased out’ and allow a path toward a semi-hydrogen economy to be created. Though in the near future, this may be cost inefficient, the concept allows a transition toward the ultimate goal of using cleaner technologies and reducing carbon emissions.

8.2 Future work

The overall long term outcome of the project is to develop a way of integrating SOECs into chemical plants in order to provide a path to SOEC commercialisation. In addition, to create a part-solution to achieving the hydrogen economy through large scale hydrogen production for use as alternative fuel in vehicles. The first step has been to assess the feasibility of integrating SOECs into power plants and has revealed that if the limitations of current materials and technology are improved, then an integrated system is a possible option in the future.

In the short term, experimental studies on a number of electrolytes for intermediate-temperature operation such as CGO and LSGM ($\text{La}_{0.9}\text{Sr}_{0.1}\text{Ga}_{0.8}\text{Mg}_{0.2}\text{O}_{3-\delta}$), and complimentary electrodes such as LSCF could be tested [268;269]. The tests should aim to identify the conductivities and exchange current densities of each material at various temperatures and steam conditions to enable a more accurate model for the integrated system. Furthermore, using different materials to YSZ and LSM would reduce such problems as delamination. Testing to assess the rate of long-term degradation and possible methodologies to limiting the rapid oxidation of the cathode is necessary such as a batch operation to allow the cathode to be reduced from NiO to Ni.

As sealing of the SOEC to prevent leaks and crossover of gases from the cathode and anode sides was a major contributing factor to poor SOEC performance in this

investigation, it is necessary to obtain a suitable non-conductive seal, either a high temperature gasket or ceramic/glass sealant. Redesigning the cell holder to allow the cell to be held in place, sealed and supported in a different way, while allowing a good flow of gas to both the anode and cathode sides may reduce the large ohmic losses experienced in this study and reduce the risk of cracks and leaks forming while operating the SOEC.

Through improvements in the experimental facility as well as further testing of the materials, a more accurate model can be developed by using parameters obtained from testing the SOEC. The current model provided a trend to an integrated system; however, for complete validity of the SOEC model and to develop a thorough understanding of the effects on the energy requirement of the SOEC, more accurate data is needed to be gathered from experimental testing. Furthermore, studies on the effects through the thickness of the electrodes and electrolyte, e.g. temperature profiles and hotspots, can be assessed in the future to provide information for heat integration and system cooling strategies.

It was seen that utilising heat produced by the overpotentials enabled the integrated system to create a steady efficiency regardless of operating conditions. Further modelling on the heat integration to take advantage of excess heat produced after the thermoneutral point can show the improvements achievable in system efficiency. In addition, taking into account other possible areas for steam extraction from the plant such as from ancillary units may show options that do not interfere directly with the steam cycle.

Analysis of utilising the flue gas for syngas production, which provides a way to 'phase out' technologies and 'phase in' new electrolyser technologies was deemed unsuitable for the integrated system assessed in this study due to the low temperatures after the cleaning. However, with improvements in SOEC materials and development of other low-temperature electrolysers, utilising flue gas may be an option. Modelling and experimentation on more suitable electrolyser technologies than SOECs can provide a solution to carbon emissions from power plants and enable a pathway toward the hydrogen economy.

The above outlines short-term goals for improving experimental investigations, which should lead to the medium-term aim of testing SOEC stacks. The development and redesign of the experimental setup can be easily achieved through a

simple redesign of the cell holder, using suitable sealants and changes to SOEC preparation methodology, and may be achieved in a short time frame. The development of the experimental facility is crucial to the validity of the SOEC model, as well as providing detailed data on the underused CGO materials. Furthermore, developing the SOEC model to generate results of the whole electrolyser as well as the phenomenon occurring across the thickness of the electrodes and electrolytes may also be achieved in a relatively straight-forward way. Developing the SOEC model will enable the accuracy of the integrated system to be improved, which provides a more accurate representation of the energy extraction needed from the power plant.

Using stacks under pressure and at temperature enables the true characteristics that would evolve in an integrated system to be examined. In general, for large scale hydrogen production, many smaller stacks would be combined to create a large hydrogen production unit [239]. Therefore, understanding the requirements of manufacturing, materials and operation is important to a high performance SOEC stack. Based on the stack design, an outline of capital costs can be identified and can be included in a cost model.

As discussed earlier, for the integrated system to be successful the economics of the integrated system must be competitive with steam methane reforming. Therefore, assessing the capital costs of stack manufacture and future electricity costs provides a basis for improvements to the SOEC design. The costs are also affected by the choice of storage for hydrogen. As storage facilities are a new point of research, it is currently ineffective for large scale storage and therefore an integrated system is limited by storage and infrastructure. In the long-term, storage may not be necessary as hydrogen may be required to be delivered directly to the point of use, therefore investment into piping needs to be considered. Therefore, producing an economic model that can account for current and future hydrogen demands and changes to infrastructure may be required to allow the financial implications on power plants and SOECs to be fully analysed.

Long term goals for an integrated system include trialling a pilot plant by building SOEC stacks into a coal fired power plant to ultimately create a path towards the hydrogen economy. In the future, an integrated system may not be limited to electricity producers, but other chemical plants as well; though a similar analysis is required to assess the suitability of hydrogen production.

9 Nomenclature

| Parameters and variables | Description |
|---------------------------|---|
| A_c, B_c, C_c, D_c | Thermodynamic constants |
| A_{tot} | Total area of SOEC (m ²) |
| b_d | Constants for calculating dynamic viscosity |
| B_g | Flow permeability (m ²) |
| C | Capacitance (F) |
| C_c | Concentration of component c (mol m ⁻³) |
| C_p | heat capacity (J kg ⁻¹ K ⁻¹) |
| CPE | Constant phase element (F) |
| ΔC_p° | Change in specific heat capacity (J mol ⁻¹ K ⁻¹) |
| $D_{Aeffave}$ | Average effective diffusivity (m ² s ⁻¹) |
| D_{Aeffc} | Effective diffusivity of a component c (m ² s ⁻¹) |
| D_{c1-c2} | Molecular diffusion of a binary mixture (m ² s ⁻¹) |
| D_{kc} | Knudsen diffusivity of component c (m ² s ⁻¹) |
| e | Electron charge |
| E | Potential difference (V) |
| E_0 | Open circuit potential (V) |
| $E_{act,tot}$ | Total activation overpotential (V) |
| $E_{conc,anode}$ | Concentration overpotential at anode (V) |
| $E_{conc,cathode}$ | Concentration overpotential at cathode (V) |
| $E_{conc,tot}$ | Total concentration overpotentials (V) |
| E_m | Maximum amplitude (V) |
| E_{ohm} | Ohmic overpotential (V) |
| E_{op} | Operating potential (V) |
| $E_{overpot}$ | Total overpotentials (V) |
| E_{tn} | Thermoneutral voltage (V) |
| E_{rev} | Reversible potential (V) |
| $Efficiency$ | Efficiency of the electrolyser or system (%) |
| $Efficiency_{Integrated}$ | Efficiency of an integrated system (%) |
| $Efficiency_{Thermal}$ | Thermal efficiency of a heat engine or system (%) |
| F | Faraday's Constant (C mol ⁻¹) |

9. Nomenclature

| | |
|---------------------------|--|
| ΔG | Gibbs Free Energy change (J mol^{-1}) |
| ΔG_0° | Gibbs Free Energy at standard conditions (J mol^{-1}) |
| ΔH | Enthalpy change (J mol^{-1}) |
| ΔH_0° | Enthalpy at standard conditions (J mol^{-1}) |
| i | Current density (A m^{-2}) |
| I_m | Maximum value of sinusoidal current wave (A) |
| $i_{0,x}$ | Exchange current density of cathode and anode (A m^{-2}) |
| j | Imaginary operator |
| J^* | Diffusion flux ($\text{mol s}^{-1} \text{m}^{-2}$) |
| k_B | Boltzmann constant |
| L | Inductance (Ωs) |
| \dot{m}_c | Mass flowrate of component c ($\text{kg s}^{-1} \text{m}^{-1}$) |
| MW_c | Molecular weight for component c (g mol^{-1}) |
| n | Number of electrons |
| \dot{N}_c | Molar flowrate of component c ($\text{mol s}^{-1} \text{m}^{-1}$) |
| N_A | Avagadro's number |
| P | Operating pressure (atm) |
| p_c | Partial pressure of component c (atm) |
| P_{input} | Chemical energy input to the system (W) |
| P_{H_2} | Energy produced by hydrogen (W) |
| P_{PP} | Energy of the plant after extraction for SOEC use (W) |
| Q | Heat energy (J mol^{-1}) |
| \dot{Q}_H | Heat energy supplied to system ($\text{J mol}^{-1} \text{s}^{-1}$) |
| $\dot{Q}_{electrolysis}$ | Heat required for electrolysis (W m^{-2}) |
| $\dot{Q}_{overpotential}$ | Heat produced by overpotentials (W m^{-2}) |
| $\dot{Q}_{reaction}$ | Heat required by reaction (W m^{-2}) |
| \dot{Q}_{steam} | Heat required for steam production (W m^{-2}) |
| \dot{Q}_{total} | Total heat requirement (W m^{-2}) |
| q | Charge |
| R | Universal gas constant ($\text{J mol}^{-1} \text{K}^{-1}$) |
| R_{ct} | Charge transfer resistance (Ω) |
| R_o | Ohmic resistance (Ω) |
| r_p | Pore radius (m) |

| | |
|------------|---|
| S_A | Surface area of electrode ($\text{cm}^2 \text{g}^{-1}$) |
| ΔS | Entropy change (J mol^{-1}) |
| T | Operating Temperature (K) |
| t | T/T_0 ($T_0 = 298.15 \text{ K}$) |
| T_{feed} | Steam/Water Feed Temperature (K) |
| W_{elec} | Electrical work (J mol^{-1}) |
| \dot{W} | Net work output ($\text{J mol}^{-1} \text{s}^{-1}$) |
| Z_C | Capacitor impedance (Ω) |
| Z_L | Inductor impedance (Ω) |
| Z_C | Capacitor impedance (Ω) |
| Z_R | Resistor impedance (Ω) |
| Z' | Real part of impedance (Ω) |
| Z'' | Imaginary part of impedance (Ω) |

Greek letters

| | |
|------------------------|---|
| α_c | Activity of each component c |
| α_x | Charge transfer coefficient of cathode and anode |
| δ_c | Collision diameter for component i (\AA) |
| δ_{c1-c2} | Collision diameter for binary mixture (\AA) |
| ε | Porosity of electrode |
| ε_{kc}/k_B | Characteristic energy (K) |
| μ | Dynamic viscosity (Pa s) |
| ν_c | Stoichiometry of components c |
| ν^* | Molar average velocity (m s^{-1}) |
| Ω_{Dc1-c2} | Collision integral for binary mixture |
| ρ_B | Bulk density (g cm^3) |
| σ_x | Conductivity of cathode, electrolyte, anode ($\Omega^{-1} \text{m}^{-1}$) |
| τ_x | Thickness of cathode, electrolyte, anode (m) |
| ξ | Tortuosity |
| ω | Angular frequency (rad s^{-1}) |
| θ | Phase angle ($^\circ$) |

Subscripts

| | |
|--------|---|
| H_2O | Water / Steam |
| H_2 | Hydrogen |
| O_2 | Oxygen |
| c | For a given component |
| x | Relates to cathode, anode and electrolyte |

Superscripts

| | |
|-------|-----------------------------|
| 0 | Initial condition |
| TPB | At the three phase boundary |

Abbreviation**Description**

| | |
|------|--|
| ASU | Air separation unit |
| BSE | Back-scattered electron |
| CCGT | Combined cycle gas turbine |
| CFB | Circulating fluidised bed |
| EDS | Energy-dispersive spectrometer |
| HP | High pressure |
| HTGR | High temperature gas-cooled reactor |
| IGCC | Integrated gasification combined cycle |
| IP | Intermediate pressure |
| LHV | Lower heating value |
| LP | Low pressure |
| O&M | Operating and maintenance |
| OCGT | Open cycle gas turbine |
| OCV | Open circuit voltage |
| PEM | Proton exchange membrane |
| PF | Pulverised fuel |
| POX | Partial oxidation |
| PV | Photo-voltaic |
| SEM | Scanning electron microscopy |
| SMR | Steam methane reforming |
| SOFC | Solid oxide fuel cell |

10 References

- [1] U.S. Energy Information Administration, "International Energy Statistics," [online]. Available: <http://www.eia.gov/cfapps/ipdbproject/iedindex3.cfm?tid=90&pid=44&aid=8&cid=regions,&syid=2007&eyid=2011&unit=MMTCD> [Accessed: Feb 2013].
- [2] V. G. R. Chandran Govindaraju and C. F. Tang, "The dynamic links between CO₂ emissions, economic growth and coal consumption in China and India," *Applied Energy*, vol. 104, pp. 310-318, 2013.
- [3] T. J. Hammons, "Power Market Restructuring in Asia: Russia, China, India and Japan," 2009, pp. 26-35.
- [4] EIA, "Country Analysis Briefs, China," [online]. Available: <http://www.eia.doe.gov/emeu/cabs/China/Background.html> [Accessed: Sept 2009].
- [5] Q. Hang, Z. Jun, Y. Xiao, and C. Junkui, "Prospect of concentrating solar power in China - the sustainable future," *Renewable and Sustainable Energy Reviews*, vol. 12, pp. 2505-2514, 2008.
- [6] X. Liang, D. Reiner, J. Gibbins, and J. Li, "Assessing the value of CO₂ capture ready in new-build pulverised coal-fired power plants in China," *International Journal of Greenhouse Gas Control*, vol. 3, pp. 787-792, 2009.
- [7] L. Du, C. Wei, and S. Cai, "Economic development and carbon dioxide emissions in China: Provincial panel data analysis," *China Economic Review*, vol. 23, pp. 371-384, 2012.
- [8] International Energy Agency, "Key World Energy Statistics 2012," [online]. Available: <http://www.iea.org/publications/freepublications/publication/kwes.pdf> [Accessed: Feb 2013].

- [9] BP, "BP Statistical Review of World Energy," [online]. Available: http://www.bp.com/content/dam/bp/pdf/Statistical-Review-2012/statistical_review_of_world_energy_2012.pdf [Accessed: June 2012].
- [10] I. MacLay, K. Harris, and A. Annut, "Digest of United Kingdom Energy Statistics 2012," [online]. Available: <https://www.gov.uk/government/publications/digest-of-united-kingdom-energy-statistics-dukes-2012-printed-version-excluding-cover-pages> [Accessed: Apr 2013].
- [11] United Nations Framework Convention on Climate Change, "Background on the UNFCCC: The international response to climate change," [online]. Available: <http://unfccc.int/2860.php> Accessed: [June 2013].
- [12] Y. Hu and C. R. Monroy, "Chinese energy and climate policies after Durban: Save the Kyoto Protocol," *Renewable and Sustainable Energy Reviews*, vol. 16, pp. 3243-3250, 2012.
- [13] L. L. Viguier, M. H. Babiker, and J. M. Reilly, "The costs of the Kyoto Protocol in the European Union," *Energy Policy*, vol. 31, pp. 459-481, 2003.
- [14] Bellona Environmental CCS Team, "CCS Projects," [online]. Available: <http://bellona.org/ccs/home.html> [Accessed: July 2013].
- [15] R. B. Gupta, *Hydrogen Fuel, Production, Transport and Storage* CRC Press, 2008.
- [16] "UKH2Mobility," [online]. Available: <http://news.bis.gov.uk/content/detail.aspx?NewsAreaId=2&ReleaseID=422877&SubjectId=2> [Accessed: Nov 2012].
- [17] "2050 Pathways Analysis: Response to the Call for Evidence," [online.] Available: <http://www.decc.gov.uk/assets/decc/Consultations/2050/1344-2050-pathways-analysis-response-pt2.pdf> [Accessed: Mar 2013].

- [18] J. M. Smith, H.C. Van Ness, and M.M. Abbott, *Introduction to Chemical Engineering Thermodynamics*, 7th Edition ed McGraw-Hill, 2005.
- [19] J. D. Holladay, J. Hu, D. L. King, and Y. Wang, "An overview of hydrogen production technologies," *Catalysis Today*, vol. 139, pp. 244-260, 2009.
- [20] R. Jones and G. Thomas, *Materials for the Hydrogen Economy* CRC Press, 2008.
- [21] F. Mueller-Langer, E. Tzimas, M. Kaltschmitt, and S. Peteves, "Techno-economic assessment of hydrogen production processes for the hydrogen economy for the short and medium term," *International Journal of Hydrogen Energy*, vol. 32, pp. 3797-3810, 2007.
- [22] A. F. G. Smith and M. Newborough, "Low-cost polymer electrolysers and electrolyser implementation scenarios for carbon abatement. Report to the Carbon Trust and ITM-Power plc," Heriot-Watt University, 2004.
- [23] P. A. Lessing, "Materials for hydrogen generation via water electrolysis," *Journal of Materials Science*, vol. 42, pp. 3477-3487, 2007.
- [24] J. Udagawa, P. Aguiar, and N. P. Brandon, "Hydrogen production through steam electrolysis: Model-based steady state performance of a cathode-supported intermediate temperature solid oxide electrolysis cell," *Journal of Power Sources*, vol. 166, pp. 127-136, 2007.
- [25] P. A. Stuart, T. Unno, J. A. Kilner, and S. J. Skinner, "Solid oxide proton conducting steam electrolysers," *Solid State Ionics*, vol. 179, pp. 1120-1124, 2008.
- [26] V. Karakoussis, N. P. Brandon, M. Leach, and R. van der Vorst, "The environmental impact of manufacturing planar and tubular solid oxide fuel cells," *Journal of Power Sources*, vol. 101, pp. 10-26, 2001.

- [27] L. Shao, S. Wang, J. Qian, X. Ye, and T. Wen, "Optimization of the electrode-supported tubular solid oxide cells for application on fuel cell and steam electrolysis," *International Journal of Hydrogen Energy*, vol. 38, pp. 4272-4280, 2013.
- [28] M. Ni, M. K. H. Leung, and D. Y. C. Leung, "Technological development of hydrogen production by solid oxide electrolyzer cell (SOEC)," *International Journal of Hydrogen Energy*, vol. 33, pp. 2337-2354, 2008.
- [29] M. A. Laguna-Bercero, S. J. Skinner, and J. A. Kilner, "Performance of solid oxide electrolysis cells based on scandia stabilised zirconia," *Journal of Power Sources*, vol. 192, pp. 126-131, 2009.
- [30] X. Yue and J. T. S. Irvine, "(La,Sr)(Cr,Mn)O₃/GDC cathode for high temperature steam electrolysis and steam-carbon dioxide co-electrolysis," *Solid State Ionics*, vol. 225, pp. 131-135, 2012.
- [31] S. D. Ebbesen and M. Mogensen, "Electrolysis of carbon dioxide in Solid Oxide Electrolysis Cells," *Journal of Power Sources*, vol. 193, pp. 349-358, 2009.
- [32] "Solid oxide electrolysis," [online]. Available: <http://www.energy.columbia.edu/solid-oxide-electrolysis> [Accessed: Nov 2009].
- [33] K. R. Sridhar and B. T. Vaniman, "Oxygen production on Mars using solid oxide electrolysis," *Solid State Ionics*, vol. 93, pp. 321-328, 1997.
- [34] "Space Habitat Carbon Dioxide Electrolysis to Hydrogen," [online]. Available: <http://rtreport.ksc.nasa.gov/techreports/2002report/600%20Fluid%20Systems/609.html> [Accessed: Nov 2009].

- [35] W. L. Becker, R. J. Braun, M. Penev, and M. Melaina, "Production of Fischer-Tropsch liquid fuels from high temperature solid oxide co-electrolysis units," *Energy*, vol. 47, pp. 99-115, 2012.
- [36] P. Kim-Lohsoontorn, D. Brett, N. Laosiripojana, Y.M. Kim, and J.M. Bae, "Performance of solid oxide electrolysis cells based on composite $\text{La}_{0.8}\text{Sr}_{0.2}\text{MnO}_{3-\delta}$ -yttria stabilized zirconia and $\text{Ba}_{0.5}\text{Sr}_{0.5}\text{Co}_{0.8}\text{Fe}_{0.2}\text{O}_{3-\delta}$ oxygen electrodes," *International Journal of Hydrogen Energy*, vol. 35, no. 9, pp. 3958-3966, May 2010.
- [37] C. Stoots, J. O'Brien, and J. Hartvigsen, "Results of recent high temperature coelectrolysis studies at the Idaho National Laboratory," *International Journal of Hydrogen Energy*, vol. 34, pp. 4208-4215, 2009.
- [38] W. Li, H. Wang, Y. Shi, and N. Cai, "Performance and methane production characteristics of $\text{H}_2\text{O}-\text{CO}_2$ co-electrolysis in solid oxide electrolysis cells," *International Journal of Hydrogen Energy*, vol. 38, pp. 11104-11109, 2013.
- [39] G. Olah and G. K. S. Prakesh, "Electrolysis of carbon dioxide in aqueous media to carbon monoxide and hydrogen for production of methanol," KR20100036317, 2010.
- [40] G. L. Hawkes, J. E. O'Brien, C. M. Stoots, S. J. Herring, M. G. McKellar, R. A. Wood, R. A. Carrington, and R. D. Boardman, "Methods and system for producing syngas," US2009235587, 2009.
- [41] J.D. Mackaluso, "The use of syngas derived from biomass and waste products to produce ethanol and hydrogen," *MMG 445 Basic Biotechnology eJournal*, vol. 3, pp. 98-103, 2007.
- [42] J. H. Gary and G. E. Handwerk, "Supporting Processes," in *Petroleum Refining, Technology and Economics*, 4th Edition ed Marcel Dekker Inc, 2001.

- [43] D. H. Lee, K. T. Kim, M. S. Cha, and Y. H. Song, "Plasma-controlled chemistry in plasma reforming of methane," *International Journal of Hydrogen Energy*, vol. 35, pp. 10967-10976, 2010.
- [44] T. Paulmier and L. Fulcheri, "Use of non-thermal plasma for hydrocarbon reforming," *Chemical Engineering Journal*, vol. 106, pp. 59-71, 2005.
- [45] G. Petitpas, J. D. Rollier, A. Darmon, J. Gonzalez-Aguilar, R. Metkemeijer, and L. Fulcheri, "A comparative study of non-thermal plasma assisted reforming technologies," *International Journal of Hydrogen Energy*, vol. 32, pp. 2848-2867, 2007.
- [46] M. G. McKellar, G. L. Hawkes, and J. E. O'Brien, "The production of syngas via high temperature electrolysis and biomass gasification," 2008.
- [47] B. Hejazi, J. R. Grace, X. Bi, and A. Mahecha-Botero, "Steam gasification of biomass coupled with lime-based CO₂ capture in a dual fluidized bed reactor: A modeling study," *Fuel*, vol. 117, Part B, pp. 1256-1266, 2014.
- [48] "Hydrogen Energy," [online]. Available: www.hydrogen.energy.gov [Accessed: Nov 2009].
- [49] M. Cooney, N. Maynard, C. Cannizzaro, and J. Benemann, "Two-phase anaerobic digestion for production of hydrogen – methane mixtures," *Bioresource Technology*, vol. 98, pp. 2641-2651, 2007.
- [50] E. C. Koutrouli, H. Kalfas, H. N. Gavala, I. V. Skiadas, K. Stamatelatou, and G. Lyberatos, "Hydrogen and methane production through two-stage mesophilic anaerobic digestion of olive pulp," *Bioresource Technology*, vol. 100, pp. 3718-3723, 2009.
- [51] F. Monnet, "An introduction to anaerobic digestion of organic wastes," 2003.
- [52] "Anaerobic digestion," [online]. Available: <http://www.biogas-info.co.uk/> [Accessed: Feb 2014].

- [53] X. M. Guo, E. Trably, E. Latrille, H. Carrère, and J. P. Steyer, "Hydrogen production from agricultural waste by dark fermentation: A review," *International Journal of Hydrogen Energy*, vol. 35, pp. 10660-10673, 2010.
- [54] N. Dubey, N. K. Labhsetwar, S. Devotta, and S. S. Rayalu, "Hydrogen evolution by water splitting using novel composite zeolite-based photocatalyst," *Catalysis Today*, vol. 129, pp. 428-434, 2007.
- [55] D. Jing, M. Liu, Q. Chen, and L. Guo, "Efficient photocatalytic hydrogen production under visible light over a novel W-based ternary chalcogenide photocatalyst prepared by a hydrothermal process," *International Journal of Hydrogen Energy*, vol. 35, pp. 8521-8527, 2010.
- [56] G. S. Tasic, U. Lacnjevac, M. M. Tasic, M. M. Kaninski, V. M. Nikolic, D. L. Žugic, and V. D. Jovic, "Influence of electrodeposition parameters of Ni-W on Ni cathode for alkaline water electrolyser," *International Journal of Hydrogen Energy*, vol. 38, pp. 4291-4297, 2013.
- [57] A. Cruden, D. Infield, M. Kiaee, T. G. Douglas, and A. Roy, "Development of new materials for alkaline electrolyzers and investigation of the potential electrolysis impact on the electrical grid," *Renewable Energy*, vol. 49, pp. 53-57, 2013.
- [58] M. P. Marceta Kaninski, D. P. Saponjic, V. M. Nikolic, D. L. Zugic, and G. S. Tasic, "Energy consumption and stability of the Ni-Mo electrodes for the alkaline hydrogen production at industrial conditions," *International Journal of Hydrogen Energy*, vol. 36, pp. 8864-8868, 2011.
- [59] K. Zeng and D. Zhang, "Evaluating the effect of surface modifications on Ni based electrodes for alkaline water electrolysis," *Fuel*, vol. 116, pp. 692-698, 2014.
- [60] A. Ursúa, I. San Martin, E. L. Barrios, and P. Sanchis, "Stand-alone operation of an alkaline water electrolyser fed by wind and photovoltaic systems," *International Journal of Hydrogen Energy*, vol. 38, pp. 14952-14967, 2013.

- [61] T. G. Douglas, A. Cruden, and D. Infield, "Development of an ambient temperature alkaline electrolyser for dynamic operation with renewable energy sources," *International Journal of Hydrogen Energy*, vol. 38, pp. 723-739, 2013.
- [62] A. Djafour, M. Matoug, H. Bouras, B. Bouchekima, M. S. Aida, and B. Azoui, "Photovoltaic-assisted alkaline water electrolysis: Basic principles," *International Journal of Hydrogen Energy*, vol. 36, pp. 4117-4124, 2011.
- [63] M. S. Herdem, S. Farhad, I. Dincer, and F. Hamdullahpur, "Thermodynamic modeling and assessment of a combined coal gasification and alkaline water electrolysis system for hydrogen production," *International Journal of Hydrogen Energy*, vol. 39, pp. 3061-3071, 2014.
- [64] A. Khalilnejad and G. H. Riahy, "A hybrid wind-PV system performance investigation for the purpose of maximum hydrogen production and storage using advanced alkaline electrolyzer," *Energy Conversion and Management*, vol. 80, pp. 398-406, 2014.
- [65] M. Carmo, D. L. Fritz, J. Mergel, and D. Stolten, "A comprehensive review on PEM water electrolysis," *International Journal of Hydrogen Energy*, vol. 38, pp. 4901-4934, 2013.
- [66] R. García-Valverde, N. Espinosa, and A. Urbina, "Simple PEM water electrolyser model and experimental validation," *International Journal of Hydrogen Energy*, vol. 37, pp. 1927-1938, 2012.
- [67] F. Marangio, M. Pagani, and M. Santarelli, "Concept of a high pressure PEM electrolyser prototype," *International Journal of Hydrogen Energy*, vol. 36, pp. 7807-7815, 2011.
- [68] J. Nieminen, I. Dincer, and G. Naterer, "Comparative performance analysis of PEM and solid oxide steam electrolyzers," *International Journal of Hydrogen Energy*, vol. 35, pp. 10842-10850, 2010.

- [69] J. Polonsky, P. Mazur, M. Paidar, E. Christensen, and K. Bouzek, "Performance of a PEM water electrolyser using a TaC-supported iridium oxide electrocatalyst," *International Journal of Hydrogen Energy*, vol. 39, pp. 3072-3078, 2014.
- [70] C. P. De Pauli and S. Trasatti, "Composite materials for electrocatalysis of O₂ evolution: IrO₂+SnO₂ in acid solution," *Journal of Electroanalytical Chemistry*, vol. 538-539, pp. 145-151, 2002.
- [71] A. T. Marshall and R. G. Haverkamp, "Electrocatalytic activity of IrO₂-RuO₂ supported on Sb-doped SnO₂ nanoparticles," *Electrochimica Acta*, vol. 55, pp. 1978-1984, 2010.
- [72] K. B. Kokoh, E. Mayousse, T. W. Napporn, K. Servat, N. Guillet, E. Soyez, A. Grosjean, A. Rakotondrainibé, and J. Paul-Joseph, "Efficient multi-metallic anode catalysts in a PEM water electrolyzer," *International Journal of Hydrogen Energy*, vol. 39, pp. 1924-1931, 2014.
- [73] R. E. Clarke, S. Giddey, and S. P. S. Badwal, "Stand-alone PEM water electrolysis system for fail safe operation with a renewable energy source," *International Journal of Hydrogen Energy*, vol. 35, pp. 928-935, 2010.
- [74] N. Briguglio, G. Brunaccini, S. Siracusano, N. Randazzo, G. Dispenza, M. Ferraro, R. Ornelas, A. S. Arico, and V. Antonucci, "Design and testing of a compact PEM electrolyzer system," *International Journal of Hydrogen Energy*, vol. 38, pp. 11519-11529, 2013.
- [75] C. M. Stoots, J. E. O'Brien, K. G. Condie, and J. J. Hartvigsen, "High-temperature electrolysis for large-scale hydrogen production from nuclear energy - Experimental investigations," *International Journal of Hydrogen Energy*, vol. 35, pp. 4861-4870, 2010.
- [76] J. Udagawa, P. Aguiar, and N. P. Brandon, "Hydrogen production through steam electrolysis: Model-based dynamic behaviour of a cathode-supported

- intermediate temperature solid oxide electrolysis cell," *Journal of Power Sources*, vol. 180, pp. 46-55, 2008.
- [77] J. S. Herring, J. E. O'Brien, C. M. Stoots, G. L. Hawkes, J. J. Hartvigsen, and M. Shahnam, "Progress in high-temperature electrolysis for hydrogen production using planar SOFC technology," *International Journal of Hydrogen Energy*, vol. 32, pp. 440-450, 2007.
- [78] B. Yu, W. Zhang, J. Xu, J. Chen, X. Luo, and K. Stephan, "Preparation and electrochemical behavior of dense YSZ film for SOEC," *International Journal of Hydrogen Energy*, vol. 37, pp. 12074-12080, 2012.
- [79] S. J. Kim and G. M. Choi, "Stability of LSCF electrode with GDC interlayer in YSZ-based solid oxide electrolysis cell," *Solid State Ionics*, 2014.
- [80] F. Tietz, D. Sebold, A. Brisse, and J. Schefold, "Degradation phenomena in a solid oxide electrolysis cell after 9000 h of operation," *Journal of Power Sources*, vol. 223, pp. 129-135, 2013.
- [81] Z. Wang, M. Mori, and T. Araki, "Steam electrolysis performance of intermediate-temperature solid oxide electrolysis cell and efficiency of hydrogen production system at $300 \text{ Nm}^3 \text{ h}^{-1}$," *International Journal of Hydrogen Energy*, vol. 35, pp. 4451-4458, 2010.
- [82] Y. Zheng, Q. Li, W. Guan, C. Xu, W. Wu, and W. G. Wang, "Investigation of 30-cell solid oxide electrolyzer stack modules for hydrogen production," *Ceramics International*, vol. 40, pp. 5801-5809, 2014.
- [83] X. Zhang, J. E. O'Brien, R. C. O'Brien, J. J. Hartvigsen, G. Tao, and G. K. Housley, "Improved durability of SOEC stacks for high temperature electrolysis," *International Journal of Hydrogen Energy*, vol. 38, pp. 20-28, 2013.
- [84] C. Gaudillere, L. Navarrete, and J. M. Serra, "Syngas production at intermediate temperature through H_2O and CO_2 electrolysis with a Cu-based

- solid oxide electrolyzer cell," *International Journal of Hydrogen Energy*, vol. 39, pp. 3047-3054, 2014.
- [85] J. Yan, H. Chen, E. Dogdibegovic, J. W. Stevenson, M. Cheng, and X. D. Zhou, "High-efficiency intermediate temperature solid oxide electrolyzer cells for the conversion of carbon dioxide to fuels," *Journal of Power Sources*, vol. 252, pp. 79-84, 2014.
- [86] S. E. Yoon, S. H. Song, J. Choi, J. Y. Ahn, B. K. Kim, and J. S. Park, "Co-electrolysis of steam and CO₂ in a solid oxide electrolysis cell with ceramic composite electrodes," *International Journal of Hydrogen Energy*, vol. 39, pp. 5497-5504, 2014.
- [87] P. Kim-Lohsoontorn, N. Laosiripojana, and J. Bae, "Performance of solid oxide electrolysis cell having bi-layered electrolyte during steam electrolysis and carbon dioxide electrolysis," *Current Applied Physics*, vol. 1, p. S223-S228, 2011.
- [88] J. E. O'Brien, M. G. McKellar, C. M. Stoots, J. S. Herring, and G. L. Hawkes, "Parametric study of large-scale production of syngas via high-temperature co-electrolysis," *International Journal of Hydrogen Energy*, vol. 34, pp. 4216-4226, 2009.
- [89] J. D. Mackaluso, "The use of syngas derived from biomass and waste products to produce ethanol and hydrogen," *MMG 445 Basic Biotechnology eJournal*, vol. 3, pp. 98-103, 2007.
- [90] United States Environmental Protection Agency, "Clean Alternative Fuel: Fischer-Tropsch," United States Environmental Protection Agency, Mar. 2002.
- [91] "Global wind council," [online]. Available: <http://www.gwec.net> [Accessed: May 2010].

- [92] C. Jørgensen and S. Ropenus, "Production price of hydrogen from grid connected electrolysis in a power market with high wind penetration," *International Journal of Hydrogen Energy*, vol. 33, pp. 5335-5344, 2008.
- [93] R. Wiser and M. Bolinger, "2012 Wind Technologies Market Report," [online]. Available: <http://energy.gov/wind-report> [Accessed: Feb 2014].
- [94] J. O. Bockris and T. N. Veziroglu, "Estimates of the price of hydrogen as a medium for wind and solar sources," *International Journal of Hydrogen Energy*, vol. 32, pp. 1605-1610, 2007.
- [95] K. Karlsson and P. Meibom, "Optimal investment paths for future renewable based energy systems-Using the optimisation model Balmorel," *International Journal of Hydrogen Energy*, vol. 33, pp. 1777-1787, 2008.
- [96] D. Graf, N. Monnerie, M. Roeb, M. Schmitz, and C. Sattler, "Economic comparison of solar hydrogen generation by means of thermochemical cycles and electrolysis," *International Journal of Hydrogen Energy*, vol. 33, no. 17, pp. 4511-4519, Sept.2008.
- [97] F. Hedenus, S. Karlsson, C. Azar, and F. Sprei, "Cost-effective energy carriers for transport - The role of the energy supply system in a carbon-constrained world," *International Journal of Hydrogen Energy*, vol. 35, pp. 4638-4651, 2010.
- [98] T. L. Gibson and N. A. Kelly, "Predicting efficiency of solar powered hydrogen generation using photovoltaic-electrolysis devices," *International Journal of Hydrogen Energy*, vol. 35, pp. 900-911, 2010.
- [99] J. E. O'Brien, M. G. McKellar, E. A. Harvego, and C. M. Stoots, "High-temperature electrolysis for large-scale hydrogen and syngas production from nuclear energy - summary of system simulation and economic analyses," *International Journal of Hydrogen Energy*, vol. 35, pp. 4808-4819, 2010.

- [100] D. Petti, "Very High Temperature Gas Reactor (VHTR) Technology, VHTR Development Office, Idaho National Laboratory," 2010.
- [101] E. A. Harvego, M. G. McKellar, M. S. Sohal, and J. E. O'Brien, "Economic analysis of a nuclear reactor powered high temperature electrolysis hydrogen production plant," 2008.
- [102] S. Herring, "High Temperature Electrolysis, Unlocking Hydrogen's Potential with Nuclear Energy, Fact Sheet," 2007.
- [103] "The Cost of Generating Electricity, Report," The Royal Academy of Engineering, [online]. Available: <https://www.raeng.org.uk> [Accessed: Feb 2010].
- [104] "The Cost of New Generating Capacity in Perspective, White Paper," Nuclear Energy Institute, [online]. Available: www.nei.org [Accessed: Feb 2010].
- [105] "Quarterly Energy Prices, A National Statistics Publication," Department of Energy and Climate Change, [online]. Available: <https://www.gov.uk/government/collections/quarterly-energy-prices> [Accessed: Mar 2010].
- [106] B. Sørensen, P. A. Hauge, C. Juhl, H. Ravn, C. Søndergren, P. Simonsen, K. Jørgensen, NL. Henrik, V. Larsen, MP. Erik, L. Schleisner, F. Sørensen, and PT. Engberg, "Hydrogen as an energy carrier: scenarios for future use of hydrogen in the Danish energy system," *International Journal of Hydrogen Energy*, vol. 29, pp. 23-32, 2004.
- [107] S. H. Jensen, P. H. Larsen, and M. Mogensen, "Hydrogen and synthetic fuel production from renewable energy sources," *International Journal of Hydrogen Energy*, vol. 32, pp. 3253-3257, 2007.
- [108] M. B. Choi, B. Singh, E. D. Wachsman, and S. J. Song, "Performance of $\text{La}_{0.1}\text{Sr}_{0.9}\text{Co}_{0.8}\text{Fe}_{0.2}\text{O}_{3-\delta}$ and $\text{La}_{0.1}\text{Sr}_{0.9}\text{Co}_{0.8}\text{Fe}_{0.2}\text{O}_{3-\delta}\text{-Ce}_{0.9}\text{Gd}_{0.1}\text{O}_2$ oxygen

- electrodes with $\text{Ce}_{0.9}\text{Gd}_{0.1}\text{O}_2$ barrier layer in reversible solid oxide fuel cells," *Journal of Power Sources*, vol. 239, pp. 361-373, 2013.
- [109] C. Jin, C. Yang, F. Zhao, D. Cui, and F. Chen, " $\text{La}_{0.75}\text{Sr}_{0.25}\text{Cr}_{0.5}\text{Mn}_{0.5}\text{O}_3$ as hydrogen electrode for solid oxide electrolysis cells," *International Journal of Hydrogen Energy*, vol. 36, pp. 3340-3346, 2011.
- [110] M. Liang, B. Yu, M. Wen, J. Chen, J. Xu, and Y. Zhai, "Preparation of NiO-YSZ composite powder by a combustion method and its application for cathode of SOEC," *International Journal of Hydrogen Energy*, vol. 35, pp. 2852-2857, 2010.
- [111] H. S. Hong, U. S. Chae, and S. T. Choo, "The effect of ball milling parameters and Ni concentration on a YSZ-coated Ni composite for a high temperature electrolysis cathode," *Journal of Alloys and Compounds*, vol. 449, pp. 331-334, 2008.
- [112] S. Lee, K. H. Kang, J. M. Kim, H. S. Hong, Y. Yun, and S. K. Woo, "Fabrication and characterization of Cu/YSZ cermet high-temperature electrolysis cathode material prepared by high-energy ball-milling method: I. 900 °C-sintered," *Journal of Alloys and Compounds*, vol. 448, pp. 363-367, 2008.
- [113] M. Liang, B. Yu, M. Wen, J. Chen, J. Xu, and Y. Zhai, "Preparation of LSM-YSZ composite powder for anode of solid oxide electrolysis cell and its activation mechanism," *Journal of Power Sources*, vol. 190, pp. 341-345, 2009.
- [114] S. Boulfrad, M. Cassidy, E. Djurado, J. T. S. Irvine, and G. Jabbour, "Pre-coating of LSCM perovskite with metal catalyst for scalable high performance anodes," *International Journal of Hydrogen Energy*, vol. 38, pp. 9519-9524, 2013.

- [115] E. Lay, G. Gauthier, and L. Dessemond, "Preliminary studies of the new Ce-doped La/Sr chromo-manganite series as potential SOFC anode or SOEC cathode materials," *Solid State Ionics*, vol. 189, pp. 91-99, 2011.
- [116] J. Huang, F. Xie, C. Wang, and Z. Mao, "Development of solid oxide fuel cell materials for intermediate-to-low temperature operation," *International Journal of Hydrogen Energy*, vol. 37, pp. 877-883, 2012.
- [117] Y. D. Zhen, A. I. Y. Tok, S. P. Jiang, and F. Y. C. Boey, "Fabrication and performance of gadolinia-doped ceria-based intermediate-temperature solid oxide fuel cells," *Journal of Power Sources*, vol. 178, pp. 69-74, 2008.
- [118] B. Zhu, I. Albinsson, C. Andersson, K. Borsand, M. Nilsson, and B. E. Mellander, "Electrolysis studies based on ceria-based composites," *Electrochemistry Communications*, vol. 8, pp. 495-498, 2006.
- [119] D. J. L. Brett, A. Atkinson, N. P. Brandon, and S. J. Skinner, "Intermediate temperature solid oxide fuel cells," *Chem. Soc. Rev.*, vol. 37, pp. 1568-1578, 2008.
- [120] P. K. Patro, T. Delahaye, E. Bouyer, and P. K. Sinha, "Microstructural development of Ni-1Ce10ScSZ cermet electrode for Solid Oxide Electrolysis Cell (SOEC) application," *International Journal of Hydrogen Energy*, vol. 37, pp. 3865-3873, 2012.
- [121] W. Zhang, B. Yu, and J. Xu, "Investigation of single SOEC with BSCF anode and SDC barrier layer," *International Journal of Hydrogen Energy*, vol. 37, pp. 837-842, 2012.
- [122] U. P. Muecke, S. Graf, U. Rhyner, and L. J. Gauckler, "Microstructure and electrical conductivity of nanocrystalline nickel- and nickel oxide/gadolinia-doped ceria thin films," *Acta Materialia*, vol. 56, pp. 677-687, 2008.

- [123] H. Duncan and A. Lasia, "Influence of the electrode nature on conductivity measurements of gadolinia-doped ceria," *Solid State Ionics*, vol. 176, pp. 1429-1437, 2005.
- [124] Y. Zhang, Q. Zhou, and T. He, " $\text{La}_{0.7}\text{Ca}_{0.3}\text{CrO}_3\text{-Ce}_{0.8}\text{Gd}_{0.2}\text{O}_{1.9}$ composites as symmetrical electrodes for solid-oxide fuel cells," *Journal of Power Sources*, vol. 196, pp. 76-83, 2011.
- [125] J. Canales-Vázquez, J. C. Ruiz-Morales, D. Marrero-López, J. Peña-Martínez, P. Núñez, and P. Gómez-Romero, "Fe-substituted $(\text{La,Sr})\text{TiO}_3$ as potential electrodes for symmetrical fuel cells (SFCs)," *Journal of Power Sources*, vol. 171, pp. 552-557, 2007.
- [126] J. C. Ruiz-Morales, J. Canales-Vázquez, B. Ballesteros-Pérez, J. Peña-Martínez, D. Marrero-López, J. T. S. Irvine, and P. Núñez, "LSCM-(YSZ-CGO) composites as improved symmetrical electrodes for solid oxide fuel cells," *Journal of the European Ceramic Society*, vol. 27, pp. 4223-4227, 2007.
- [127] Y. Zhang, Y. Shen, X. Du, J. Li, X. Cao, and T. He, "Nanostructured GDC-impregnated $\text{La}_{0.7}\text{Ca}_{0.3}\text{CrO}_{3-\delta}$ symmetrical electrodes for solid oxide fuel cells operating on hydrogen and city gas," *International Journal of Hydrogen Energy*, vol. 36, pp. 3673-3680, 2011.
- [128] S. D. Ebbesen, J. Høgh, K. A. Nielsen, J. U. Nielsen, and M. Mogensen, "Durable SOC stacks for production of hydrogen and synthesis gas by high temperature electrolysis," *International Journal of Hydrogen Energy*, vol. 36, pp. 7363-7373, 2011.
- [129] S. D. Kim, D. W. Seo, A. K. Dorai, and S. K. Woo, "The effect of gas compositions on the performance and durability of solid oxide electrolysis cells," *International Journal of Hydrogen Energy*, vol. 38, pp. 6569-6576, 2013.

- [130] D. Ferrero, A. Lanzini, M. Santarelli, and P. Leone, "A comparative assessment on hydrogen production from low- and high-temperature electrolysis," *International Journal of Hydrogen Energy*, vol. 38, pp. 3523-3536, 2013.
- [131] Q. Liu, C. Yang, X. Dong, and F. Chen, "Perovskite $\text{Sr}_2\text{Fe}_{1.5}\text{Mo}_{0.5}\text{O}_{6-\delta}$ as electrode materials for symmetrical solid oxide electrolysis cells," *International Journal of Hydrogen Energy*, vol. 35, pp. 10039-10044, 2010.
- [132] E. Ivers-Tiffée, A. Weber, and D. Herbstritt, "Materials and technologies for SOFC-components," *Journal of the European Ceramic Society*, vol. 21, pp. 1805-1811, 2001.
- [133] R. D. Green, "Gadolinia-Doped Ceria Cathodes for Electrolysis of CO_2 , Tech Briefs," NASA, [online]. Available: <http://www.techbriefs.com/component/content/article/5-ntb/tech-briefs/materials/3495> [Accessed: Nov 2009].
- [134] K. L. Duncan, H. E. Hagelin-Weaver, S. R. Bishop, H. L. Paul, and E. D. Wachsman, "Concurrent CO_2 control and O_2 generation for advanced life support," NASA, 2007.
- [135] O. Yamamoto, Y. Takeda, R. Kanno, and M. Noda, "Perovskite-type oxides as oxygen electrodes for high temperature oxide fuel cells," *Solid State Ionics*, vol. 22, pp. 241-246, 1987.
- [136] K. C. Eccleston, "Solid oxide steam electrolysis for high temperature hydrogen production," University of St. Andrews, 2006.
- [137] E. Brightman, D. G. Ivey, D. J. L. Brett, and N. P. Brandon, "The effect of current density on H_2S -poisoning of nickel-based solid oxide fuel cell anodes," *Journal of Power Sources*, vol. 196, pp. 7182-7187, 2011.

- [138] F. Chauveau, J. Mougin, J. M. Bassat, F. Mauvy, and J. C. Grenier, "A new anode material for solid oxide electrolyser: The neodymium nickelate $\text{Nd}_2\text{NiO}_{4+\delta}$," *Journal of Power Sources*, vol. 195, pp. 744-749, 2010.
- [139] A. Hauch, S. D. Ebbesen, S. H. Jensen, and M. Mogensen, "Highly efficient high temperature electrolysis," *J. Mater. Chem.*, vol. 18, pp. 2331-2340, 2008.
- [140] X. Z. Yuan, C. Song, H. Wang, and J. Zhang, *Electrochemical Impedance Spectroscopy in PEM Fuel Cells, Fundamentals and Applications* Springer-Verlag London Limited, 2010.
- [141] J. R. Macdonald, "Impedance spectroscopy," *Ann Biomed Eng*, vol. 20, pp. 289-305, 1992.
- [142] R. F. Egerton, *Physical Principles of Electron Microscopy, An Introduction to TEM, SEM, and AEM*. New York: Springer Science+Business Media, LLC, 2005.
- [143] J. Goldstein, D. E. Newbury, D. C. Joy, C. E. Lyman, P. Echlin, E. Lifshin, L. Sawyer, and J. Michael, *Scanning Electron Microscopy and X-ray Microanalysis*, 3rd ed. New York: Kluwer Academic/Plenum Publishers, 2003.
- [144] Earth Science and Montana State Univeristy, "Scanning Electron Microscopy (SEM)," [online]. Available: http://serc.carleton.edu/research_education/geochemsheets/techniques/SEM.html [Accessed: Oct 2013].
- [145] D. Vladikova, J. A. Kilner, S. J. Skinner, G. Raikova, and Z. Stoyanov, "Differential impedance analysis of single crystal and polycrystalline yttria stabilized zirconia," *Electrochimica Acta*, vol. 51, pp. 1611-1621, 2006.
- [146] D. Sarantaridis and A. Atkinson, "Redox Cycling of Ni-Based Solid Oxide Fuel Cell Anodes: A Review," *Fuel Cells*, vol. 7, pp. 246-258, 2007.

- [147] P. Lohsoontorn, D. J. L. Brett, and N. P. Brandon, "The effect of fuel composition and temperature on the interaction of H₂S with nickel-ceria anodes for Solid Oxide Fuel Cells," *Journal of Power Sources*, vol. 183, pp. 232-239, 2008.
- [148] I. M. Hung, C. Y. Liang, C. J. Ciou, and Y. C. Lee, "Conductivity and electrochemical performance of (Ba_{0.5}Sr_{0.5})_{0.8}La_{0.2}CoO_{3-δ} cathode for intermediate-temperature solid oxide fuel cell," *Ceramics International*, vol. 36, pp. 1937-1943, 2010.
- [149] O. H. Kwon and G. M. Choi, "Electrical conductivity of thick film YSZ," *Solid State Ionics*, vol. 177, pp. 3057-3062, 2006.
- [150] C. Zhang, C. J. Li, G. Zhang, X. J. Ning, C. X. Li, H. Liao, and C. Coddet, "Ionic conductivity and its temperature dependence of atmospheric plasma-sprayed yttria stabilized zirconia electrolyte," *Materials Science and Engineering: B*, vol. 137, pp. 24-30, 2007.
- [151] Y. Z. Xing, C. J. Li, Q. Zhang, C. X. Li, and G. J. Yang, "Influence of Microstructure on the Ionic Conductivity of Plasma-Sprayed Yttria-Stabilized Zirconia Deposits," *Journal of the American Ceramic Society*, vol. 91, pp. 3931-3936, 2008.
- [152] J. H. Joo and G. M. Choi, "Electrical conductivity of YSZ film grown by pulsed laser deposition," *Solid State Ionics*, vol. 177, pp. 1053-1057, 2006.
- [153] P. A. Lessing, "A review of sealing technologies applicable to solid oxide electrolysis cells," *J Mater Sci*, vol. 42, pp. 3465-3476, 2007.
- [154] M. Keane, M. K. Mahapatra, A. Verma, and P. Singh, "LSM-YSZ interactions and anode delamination in solid oxide electrolysis cells," *International Journal of Hydrogen Energy*, vol. 37, pp. 16776-16785, 2012.
- [155] T. I. Politova and J. T. S. Irvine, "Investigation of scandia-yttria-zirconia system as an electrolyte material for intermediate temperature fuel cells-

- influence of yttria content in system $(Y_2O_3)_x(Sc_2O_3)_{(11-x)}(ZrO_2)_{89}$," *Solid State Ionics*, vol. 168, pp. 153-165, 2004.
- [156] D. Meyer, U. Eisele, R. Satet, and J. Rödel, "Codoping of zirconia with yttria and scandia," *Scripta Materialia*, vol. 58, pp. 215-218, 2008.
- [157] C. Yang, A. Coffin, and F. Chen, "High temperature solid oxide electrolysis cell employing porous structured $(La_{0.75}Sr_{0.25})_{0.95}MnO_3$ with enhanced oxygen electrode performance," *International Journal of Hydrogen Energy*, vol. 35, pp. 3221-3226, 2010.
- [158] Y. Li, Y. Gan, Y. Wang, K. Xie, and Y. Wu, "Composite cathode based on Ni-loaded $La_{0.75}Sr_{0.25}Cr_{0.5}Mn_{0.5}O_{3-\delta}$ for direct steam electrolysis in an oxide-ion-conducting solid oxide electrolyzer," *International Journal of Hydrogen Energy*, vol. 38, pp. 10196-10207, 2013.
- [159] A. Brisse, J. Schefold, and M. Zahid, "High temperature water electrolysis in solid oxide cells," *International Journal of Hydrogen Energy*, vol. 33, pp. 5375-5382, 2008.
- [160] S. Xu, S. Li, W. Yao, D. Dong, and K. Xie, "Direct electrolysis of CO_2 using an oxygen-ion conducting solid oxide electrolyzer based on $La_{0.75}Sr_{0.25}Cr_{0.5}Mn_{0.5}O_{3-\delta}$ electrode," *Journal of Power Sources*, vol. 230, pp. 115-121, 2013.
- [161] Flexitallic UK Ltd., "Fuel Cell Sealing Materials for Automotive and Auxiliary Power Units," [online]. Available: <http://www.flexitallicsofc.com/> [Accessed: Nov 2013].
- [162] Y. Ji, J. A. Kilner, and M. F. Carolan, "Electrical properties and oxygen diffusion in yttria-stabilised zirconia (YSZ)- $La_{0.8}Sr_{0.2}MnO_{3\pm\delta}$ (LSM) composites," *Solid State Ionics*, vol. 176, pp. 937-943, 2005.
- [163] BM reports, "BM reports," [online]. Available: http://www.bmreports.com/bsp/bsp_home.htm [Accessed: Mar 2013].

- [164] Institution of Civil Engineers, "Post-2020 Energy Scenarios and Pathways to 2030," Institution of Civil Engineers, [online]. Available: <http://www.ice.org.uk/Information-resources/Document-Library/energy-2030> [Accessed: Mar 2013].
- [165] HM Government, "The Carbon Plan: Delivering our low carbon future," [online]. Available: <https://www.gov.uk/government/publications/the-carbon-plan-reducing-greenhouse-gas-emissions--2> [Accessed: May 2013].
- [166] Department of Energy, "International Energy Outlook 2011," U.S. Energy Information Administration, [online]. Available: <http://www.eia.gov/forecasts/ieo/index.cfm> [Accessed: Aug 2012].
- [167] T. Sanpasertparnich, R. Idem, I. Bolea, D. deMontigny, and P. Tontiwachwuthikul, "Integration of post-combustion capture and storage into a pulverized coal-fired power plant," *International Journal of Greenhouse Gas Control*, vol. 4, pp. 499-510, 2010.
- [168] World Coal Association, "World Coal Association," [online]. Available: www.worldcoal.org [Accessed: Feb 2014].
- [169] M. Finkenath, J. Smith, and D. Volk, "CCS Retrofit, Analysis of the Globally Installed Coal-Fired Power Plant Fleet," International Energy Agency, 2012.
- [170] J. M. Beér, "High efficiency electric power generation: The environmental role," *Progress in Energy and Combustion Science*, vol. 33, pp. 107-134, 2007.
- [171] S. Yeh and E. S. Rubin, "A centurial history of technological change and learning curves for pulverized coal-fired utility boilers," *Energy*, vol. 32, pp. 1996-2005, 2007.
- [172] L. F. Drbal, P. G. Boston, K. L. Westra, and R. B. Erickson, *Power Plant Engineering* CBS Publishers, 2005.

- [173] E. B. Woodruff, H. B. Lammers, and T. F. Lammers, *Steam Plant Operation*, 8th Edition ed McGraw-Hill, 2005.
- [174] K. Stepczynska-Drygas, H. Lukowicz, and S. Dykas, "Calculation of an advanced ultra-supercritical power unit with CO₂ capture installation," *Energy Conversion and Management*, vol. 74, pp. 201-208, 2013.
- [175] T. Sanpasertparnich and A. Aroonwilas, "Simulation and optimization of coal-fired power plants," *Energy Procedia*, vol. 1, pp. 3851-3858, 2009.
- [176] H. Chalmers, M. Lucquiaud, J. Gibbins, and M. Leach, "Flexible Operation of Coal Fired Power Plants with Postcombustion Capture of Carbon Dioxide," *J. Environ. Eng.*, vol. 135, pp. 449-458, 2009.
- [177] T. Harkin, A. Hoadley, and B. Hooper, "Reducing the energy penalty of CO₂ capture and compression using pinch analysis," *Journal of Cleaner Production*, vol. 18, pp. 857-866, 2010.
- [178] J. C. Eslick and D. C. Miller, "A multi-objective analysis for the retrofit of a pulverized coal power plant with a CO₂ capture and compression process," *Computers & Chemical Engineering*, vol. 35, pp. 1488-1500, 2011.
- [179] Y. Huang, M. Wang, P. Stephenson, S. Rezvani, D. Ilveen-Wright, A. Minchener, N. Hewitt, A. Dave, and A. Fleche, "Hybrid coal-fired power plants with CO₂ capture: A technical and economic evaluation based on computational simulations," *Fuel*, vol. 101, pp. 244-253, 2012.
- [180] C. C. Cormos, F. Starr, E. Tzimas, and S. Peteves, "Innovative concepts for hydrogen production processes based on coal gasification with capture," *International Journal of Hydrogen Energy*, vol. 33, pp. 1286-1294, 2008.
- [181] J. Huang and I. Dincer, "Parametric analysis and assessment of a coal gasification plant for hydrogen production," *International Journal of Hydrogen Energy*, vol. 39, pp. 3294-3303, 2014.

- [182] J. Wang, G. Cheng, Y. You, B. Xiao, S. Liu, P. He, D. Guo, X. Guo, and G. Zhang, "Hydrogen-rich gas production by steam gasification of municipal solid waste (MSW) using NiO supported on modified dolomite," *International Journal of Hydrogen Energy*, vol. 37, pp. 6503-6510, 2012.
- [183] L. Guo and H. Jin, "Boiling coal in water: Hydrogen production and power generation system with zero net CO₂ emission based on coal and supercritical water gasification," *International Journal of Hydrogen Energy*, vol. 38, pp. 12953-12967, 2013.
- [184] "CHEMCAD 6.0, Chemstations™," 2008. [online]. Available: www.chemstations.com
- [185] US Department of Energy, "Market-Based advanced coal power systems," Washington DC, 1999.
- [186] "Paiton III Power Station, Subcritical versus supercritical boiler study," International Power plc., 2003.
- [187] Q. Cai, E. Luna-Ortiz, C. S. Adjiman, and N. P. Brandon, "The Effects of Operating Conditions on the Performance of a Solid Oxide Steam Electrolyser: A Model-Based Study," *Fuel Cells*, vol. 10, pp. 1114-1128, 2010.
- [188] N. Perdikaris, K. D. Panopoulos, P. Hofmann, S. Spyrikis, and E. Kakaras, "Design and exergetic analysis of a novel carbon free tri-generation system for hydrogen, power and heat production from natural gas, based on combined solid oxide fuel and electrolyser cells," *International Journal of Hydrogen Energy*, vol. 35, pp. 2446-2456, 2010.
- [189] P. Aguiar, C. S. Adjiman, and N. P. Brandon, "Anode-supported intermediate temperature direct internal reforming solid oxide fuel cell. I: model-based steady-state performance," *Journal of Power Sources*, vol. 138, pp. 120-136, 2004.

- [190] M. Ni, M. K. H. Leung, and D. Y. C. Leung, "A modeling study on concentration overpotentials of a reversible solid oxide fuel cell," *Journal of Power Sources*, vol. 163, pp. 460-466, 2006.
- [191] S. H. Chan and Z. T. Xia, "Polarization effects in electrolyte/electrode-supported solid oxide fuel cells," *Journal of Applied Electrochemistry*, vol. 32, pp. 339-347, 2002.
- [192] S. H. Jensen, X. Sun, S. D. Ebbesen, R. Knibbe, and M. Mogensen, "Hydrogen and synthetic fuel production using pressurized solid oxide electrolysis cells," *International Journal of Hydrogen Energy*, vol. 35, pp. 9544-9549, 2010.
- [193] J. Laurencin, D. Kane, G. Delette, J. Deseure, and F. Lefebvre-Joud, "Modelling of solid oxide steam electrolyser: Impact of the operating conditions on hydrogen production," *Journal of Power Sources*, vol. 196, pp. 2080-2093, 2011.
- [194] P. Kim-Lohsoontorn, Y. M. Kim, N. Laosiripojana, and J. Bae, "Gadolinium doped ceria-impregnated nickel–yttria stabilised zirconia cathode for solid oxide electrolysis cell," *International Journal of Hydrogen Energy*, vol. 36, pp. 9420-9427, 2011.
- [195] M. Ni, M. K. H. Leung, and D. Y. C. Leung, "Energy and exergy analysis of hydrogen production by solid oxide steam electrolyzer plant," *International Journal of Hydrogen Energy*, vol. 32, pp. 4648-4660, 2007.
- [196] J. P. Stempien, O. L. Ding, Q. Sun, and S. H. Chan, "Energy and exergy analysis of Solid Oxide Electrolyser Cell (SOEC) working as a CO₂ mitigation device," *International Journal of Hydrogen Energy*, vol. 37, pp. 14518-14527, 2012.
- [197] S. Fujiwara, S. Kasai, H. Yamauchi, K. Yamada, S. Makino, K. Matsunaga, M. Yoshino, T. Kameda, T. Ogawa, S. Momma, and E. Hoashi, "Hydrogen

- production by high temperature electrolysis with nuclear reactor," *Progress in Nuclear Energy*, vol. 50, pp. 422-426, 2008.
- [198] T. Zhou and B. Francois, "Modeling and control design of hydrogen production process for an active hydrogen/wind hybrid power system," *International Journal of Hydrogen Energy*, vol. 34, pp. 21-30, 2009.
- [199] E. Bilgen, "Solar hydrogen from photovoltaic-electrolyzer systems," *Energy Conversion and Management*, vol. 42, pp. 1047-1057, 2001.
- [200] R. E. Clarke, S. Giddey, F. T. Ciacchi, S. P. S. Badwal, B. Paul, and J. Andrews, "Direct coupling of an electrolyser to a solar PV system for generating hydrogen," *International Journal of Hydrogen Energy*, vol. 34, pp. 2531-2542, 2009.
- [201] E. Hernández-Pacheco, D. Singh, P. N. Hutton, N. Patel, and M. D. Mann, "A macro-level model for determining the performance characteristics of solid oxide fuel cells," *Journal of Power Sources*, vol. 138, pp. 174-186, 2004.
- [202] C. J. Geankoplis, *Mass Transport Phenomena* Holt, Rinehart and Winston, Inc, 1972.
- [203] S. H. Chan, K. A. Khor, and Z. T. Xia, "A complete polarization model of a solid oxide fuel cell and its sensitivity to the change of cell component thickness," *Journal of Power Sources*, vol. 93, pp. 130-140, 2001.
- [204] E. N. Lightfoot, W. Stewart, and R. B. Bird, *Transport Phenomena*, 2nd ed John Wiley & Sons Inc, 2002, pp. 527-528, 866.
- [205] D. H. Jeon, J. H. Nam, and C. J. Kim, "Microstructural Optimization of Anode-Supported Solid Oxide Fuel Cells by a Comprehensive Microscale Model," *Journal of The Electrochemical Society*, vol. 153, p. A406-A417, 2006.

- [206] M. M. Mench, *Fuel Cell Engines* John Wiley & Sons, Inc, 2008.
- [207] H. Zhu and R. J. Kee, "A general mathematical model for analyzing the performance of fuel-cell membrane-electrode assemblies," *Journal of Power Sources*, vol. 117, pp. 61-74, 2003.
- [208] F. Walsh, *A First Course in Electrochemical Engineering* The Electrochemical Consultancy, 1993.
- [209] B. C. H. Steele, "Oxygen transport and exchange in oxide ceramics," *Journal of Power Sources*, vol. 49, pp. 1-14, 1994.
- [210] S. J. A. Livermore, J. W. Cotton, and R. M. Ormerod, "Fuel reforming and electrical performance studies in intermediate temperature ceria-gadolinia-based SOFCs," *Journal of Power Sources*, vol. 86, pp. 411-416, 2000.
- [211] C. Veranitisagul, A. Kaewvilai, W. Wattanathana, N. Koonsaeng, E. Traversa, and A. Laobuthee, "Electrolyte materials for solid oxide fuel cells derived from metal complexes: Gadolinia-doped ceria," *Ceramics International*, vol. 38, pp. 2403-2409, 2012.
- [212] Z. Liu, D. Ding, M. Liu, X. Ding, D. Chen, X. Li, C. Xia, and M. Liu, "High-performance, ceria-based solid oxide fuel cells fabricated at low temperatures," *Journal of Power Sources*, vol. 241, pp. 454-459, 2013.
- [213] D. Pérez-Coll, P. Núñez, J. R. Frade, and J. C. C. Abrantes, "Conductivity of CGO and CSO ceramics obtained from freeze-dried precursors," *Electrochimica Acta*, vol. 48, pp. 1551-1557, 2003.
- [214] M. H. D. Othman, Z. Wu, N. Droushiotis, G. Kelsall, and K. Li, "Morphological studies of macrostructure of Ni-CGO anode hollow fibres for intermediate temperature solid oxide fuel cells," *Journal of Membrane Science*, vol. 360, pp. 410-417, 2010.

- [215] S. T. Aruna, M. Muthuraman, and K. C. Patil, "Synthesis and properties of Ni-YSZ cermet: anode material for solid oxide fuel cells," *Solid State Ionics*, vol. 111, pp. 45-51, 1998.
- [216] Y. Shin, W. Park, J. Chang, and J. Park, "Evaluation of the high temperature electrolysis of steam to produce hydrogen," *International Journal of Hydrogen Energy*, vol. 32, pp. 1486-1491, 2007.
- [217] P. Kim-Lohsoontorn and J. Bae, "Electrochemical performance of solid oxide electrolysis cell electrodes under high-temperature coelectrolysis of steam and carbon dioxide," *Journal of Power Sources*, vol. 196, pp. 7161-7168, 2011.
- [218] M. N. Manage, D. Hodgson, N. Milligan, S. J. R. Simons, and D. J. L. Brett, "A techno-economic appraisal of hydrogen generation and the case for solid oxide electrolyser cells," *International Journal of Hydrogen Energy*, vol. 36, pp. 5782-5796, 2011.
- [219] T. Matsushima, H. Ohruai, and T. Hirai, "Effects of sinterability of YSZ powder and NiO content on characteristics of Ni-YSZ cermets," *Solid State Ionics*, vol. 111, pp. 315-321, 1998.
- [220] M. Marinsek, S. Pejovnik, and J. Macek, "Modelling of electrical properties of Ni-YSZ composites," *Journal of the European Ceramic Society*, vol. 27, pp. 959-964, 2007.
- [221] M. B. Kakade, S. Ramanathan, and D. Das, "Gel-combustion, characterization and processing of porous Ni-YSZ cermet for anodes of solid oxide fuel cells (SOFCs)," *Ceramics International*, vol. 37, pp. 195-200, 2011.
- [222] M. H. Pihlatie, A. Kaiser, and M. B. Mogensen, "Electrical conductivity of Ni-YSZ composites: Variants and redox cycling," *Solid State Ionics*, pp. 38-46, 2012.

- [223] B. C. H. Steele and A. Heinzl, "Materials for fuel-cell technologies," *Nature*, vol. 414, pp. 345-352, 2001.
- [224] P. Jasinski, T. Suzuki, F. Dogan, and H. U. Anderson, "Impedance spectroscopy of single chamber SOFC," *Solid State Ionics*, vol. 175, pp. 35-38, 2004.
- [225] A. Leonide, Y. Apel, and E. Ivers-Tiffée, "SOFC Modeling and Parameter Identification by Means of Impedance Spectroscopy," *ECS Transactions*, vol. 19, pp. 81-109, 2009.
- [226] G. J. Offer and N. P. Brandon, "The effect of current density and temperature on the degradation of nickel cermet electrodes by carbon monoxide in solid oxide fuel cells," *Chemical Engineering Science*, vol. 64, pp. 2291-2300, 2009.
- [227] R. Maric, S. Ohara, T. Fukui, H. Yoshida, M. Nishimura, T. Inagaki, and K. Miura, "Solid Oxide Fuel Cells with Doped Lanthanum Gallate Electrolyte and LaSrCoO₃ Cathode, and Ni - Samaria - Doped Ceria Cermet Anode," *Journal of The Electrochemical Society*, vol. 146, pp. 2006-2010, 1999.
- [228] K. Huang, M. Feng, J. B. Goodenough, and C. Milliken, "Electrode Performance Test on Single Ceramic Fuel Cells Using as Electrolyte Sr and Mg Doped LaGaO₃," *Journal of The Electrochemical Society*, vol. 144, pp. 3620-3624, 1997.
- [229] A. Roy, S. Watson, and D. Infield, "Comparison of electrical energy efficiency of atmospheric and high-pressure electrolyzers," *International Journal of Hydrogen Energy*, vol. 31, pp. 1964-1979, 2006.
- [230] M. Santarelli, P. Medina, and M. Cali, "Fitting regression model and experimental validation for a high-pressure PEM electrolyzer," *International Journal of Hydrogen Energy*, vol. 34, pp. 2519-2530, 2009.

- [231] K. Onda, T. Kyakuno, K. Hattori, and K. Ito, "Prediction of production power for high-pressure hydrogen by high-pressure water electrolysis," *Journal of Power Sources*, vol. 132, pp. 64-70, 2004.
- [232] J. Mougin, A. Chatroux, K. Couturier, M. Petitjean, M. Reytier, G. Gousseau, and F. Lefebvre-Joud, "High Temperature Steam Electrolysis Stack with Enhanced Performance and Durability," *Energy Procedia*, vol. 29, pp. 445-454, 2012.
- [233] Y. Bo, Z. Wenqiang, X. Jingming, and C. Jing, "Status and research of highly efficient hydrogen production through high temperature steam electrolysis at INET," *International Journal of Hydrogen Energy*, vol. 35, pp. 2829-2835, 2010.
- [234] H. Zhang, S. Su, X. Chen, G. Lin, and J. Chen, "Configuration design and performance optimum analysis of a solar-driven high temperature steam electrolysis system for hydrogen production," *International Journal of Hydrogen Energy*, vol. 38, pp. 4298-4307, 2013.
- [235] S. S. Baek, N. Lee, B. K. Kim, H. Chang, S. J. Song, and J. Y. Park, "Addition effects of erbia-stabilized bismuth oxide on ceria-based carbonate composite electrolytes for intermediate temperature-solid oxide fuel cells," *International Journal of Hydrogen Energy*, vol. 37, pp. 16823-16834, 2012.
- [236] Y. G. Choi, J. Y. Park, J. W. Son, J. H. Lee, H. J. Je, B. K. Kim, H. W. Lee, and K. J. Yoon, "Ceria-based electrolyte reinforced by sol-gel technique for intermediate-temperature solid oxide fuel cells," *International Journal of Hydrogen Energy*, vol. 38, pp. 9867-9872, 2013.
- [237] A. Petric, P. Huang, and F. Tietz, "Evaluation of La-Sr-Co-Fe-O perovskites for solid oxide fuel cells and gas separation membranes," *Solid State Ionics*, vol. 135, pp. 719-725, 2000.

- [238] B. Todd and J. B. Young, "Thermodynamic and transport properties of gases for use in solid oxide fuel cell modelling," *Journal of Power Sources*, vol. 110, pp. 186-200, 2002.
- [239] S. Herring, "Laboratory-Scale High Temperature Electrolysis System," 2006. [online]. Available: http://www.hydrogen.energy.gov/pdfs/review06/pd_17_herring.pdf [Accessed: Aug 2010]
- [240] O. Yamamoto, Y. Arati, Y. Takeda, N. Imanishi, Y. Mizutani, M. Kawai, and Y. Nakamura, "Electrical conductivity of stabilized zirconia with ytterbia and scandia," *Solid State Ionics*, vol. 79, pp. 137-142, 1995.
- [241] J. Liu, A. C. Co, S. Paulson, and V. I. Birss, "Oxygen reduction at sol-gel derived $\text{La}_{0.8}\text{Sr}_{0.2}\text{Co}_{0.8}\text{Fe}_{0.2}\text{O}_3$ cathodes," *Solid State Ionics*, vol. 177, pp. 377-387, 2006.
- [242] X. D. Zhou, L. R. Pederson, J. W. Templeton, and J. W. Stevenson, "Electrochemical performance and stability of the cathode for Solid Oxide Fuel Cells. I. Cross validation of polarization measurements by impedance spectroscopy and current-potential sweep," *Journal of The Electrochemical Society*, p. B220-B227, 2010.
- [243] C. Brunetto and G. Tina, "Optimal hydrogen storage sizing for wind power plants in day ahead electricity market.," *IET Renewable Power Generation*, vol. 1, pp. 220-226, 2007.
- [244] E. Akyuz, C. Coskun, Z. Oktay, and I. Dincer, "Hydrogen production probability distributions for a PV-electrolyser system," *International Journal of Hydrogen Energy*, vol. 36, pp. 11292-11299, 2011.
- [245] D. Ghribi, A. Khelifa, S. Diaf, and M. Belhamel, "Study of hydrogen production system by using PV solar energy and PEM electrolyser in Algeria," *International Journal of Hydrogen Energy*, vol. 38, pp. 8480-8490, 2013.

- [246] K. Sopian, M. Z. Ibrahim, W. R. Wan Daud, M. Y. Othman, B. Yatim, and N. Amin, "Performance of a PV-wind hybrid system for hydrogen production," *Renewable Energy*, vol. 34, pp. 1973-1978, 2009.
- [247] C. W. Forsberg, "Hydrogen, nuclear energy, and the advanced high-temperature reactor," *International Journal of Hydrogen Energy*, vol. 28, pp. 1073-1081, 2003.
- [248] G. Taljan, M. Fowler, C. Cañizares, and G. Verbic, "Hydrogen storage for mixed wind–nuclear power plants in the context of a Hydrogen Economy," *International Journal of Hydrogen Energy*, vol. 33, pp. 4463-4475, 2008.
- [249] J. Davison, "Electricity systems with near-zero emissions of CO₂ based on wind energy and coal gasification with CCS and hydrogen storage," *International Journal of Greenhouse Gas Control*, vol. 3, pp. 683-692, 2009.
- [250] D. Mignard, M. Sahibzada, J. M. Duthie, and H. W. Whittington, "Methanol synthesis from flue-gas CO₂ and renewable electricity: a feasibility study," *International Journal of Hydrogen Energy*, vol. 28, pp. 455-464, 2003.
- [251] V. White, L. Torrente-Murciano, D. Sturgeon, and D. Chadwick, "Purification of oxyfuel-derived CO₂," *Energy Procedia*, vol. 1, pp. 399-406, 2009.
- [252] A. Kather and S. Kownatzki, "Assessment of the different parameters affecting the CO₂ purity from coal fired oxyfuel process," *International Journal of Greenhouse Gas Control*, vol. 5, Supplement 1, p. S204-S209, 2011.
- [253] S. Rehfeldt, C. Kuhr, F. P. Schiffer, P. Weckes, and C. Bergins, "First test results of Oxyfuel combustion with Hitachi's DST-burner at Vattenfall's 30 MWth Pilot Plant at Schwarze Pumpe," *Energy Procedia*, vol. 4, pp. 1002-1009, 2011.

- [254] C. Wang, X. Zhang, Y. Liu, and D. Che, "Pyrolysis and combustion characteristics of coals in oxyfuel combustion," *Applied Energy*, vol. 97, pp. 264-273, 2012.
- [255] M. S. Sohal, J. E. O'Brien, C. M. Stoots, M. G. McKellar, E. A. Harvego, and J. S. Herring, "Challenges in generating hydrogen by high temperature electrolysis using solid oxide cells," Idaho National Laboratory, U.S. Department of Energy, 2008.
- [256] National Renewable Energy Laboratory, "Current (2009) state-of-the-art hydrogen production cost estimate using water electrolysis," [online]. Available: www.hydrogen.energy.gov/pdfs/46676.pdf [Accessed: Nov 2013].
- [257] EIA, "Annual Energy Outlook 2013, Market Trends - Natural Gas," [online]. Available: http://www.eia.gov/forecasts/aeo/MT_naturalgas.cfm [Accessed: Nov 2013].
- [258] Department of Energy, "Hydrogen production cost using low-cost natural gas," [online]. Available: [hydrogen.energy.gov/pdfs/12024_h2_production_cost_natural_gas.pdf](http://www.hydrogen.energy.gov/pdfs/12024_h2_production_cost_natural_gas.pdf) [Accessed: Nov 2013].
- [259] L. Barreto, A. Makihira, and K. Riahi, "The hydrogen economy in the 21st century: a sustainable development scenario," *International Journal of Hydrogen Energy*, vol. 28, pp. 267-284, 2003.
- [260] G. Mulder, J. Hetland, and G. Lenaers, "Towards a sustainable hydrogen economy: Hydrogen pathways and infrastructure," *International Journal of Hydrogen Energy*, vol. 32, pp. 1324-1331, 2007.
- [261] N. Z. Muradov and T. N. Veziroglu, "From hydrocarbon to hydrogen-carbon to hydrogen economy," *International Journal of Hydrogen Energy*, vol. 30, pp. 225-237, 2005.

- [262] L. Zhou, "Progress and problems in hydrogen storage methods," *Renewable and Sustainable Energy Reviews*, vol. 9, pp. 395-408, 2005.
- [263] A. Züttel, "Hydrogen storage methods," *Naturwissenschaften*, vol. 91, pp. 157-172, 2004.
- [264] J. Graetz, "New approaches to hydrogen storage," *Chem. Soc. Rev.*, vol. 38, pp. 73-82, 2009.
- [265] F. Sherry-Brennan, H. Devine-Wright, and P. Devine-Wright, "Public understanding of hydrogen energy: A theoretical approach," *Energy Policy*, vol. 38, pp. 5311-5319, 2010.
- [266] M. Ricci, "Exploring public attitudes towards hydrogen energy: Conceptual and methodological challenges," University of Salford, UKSHEC Social Science Working Paper No. 13, 2006.
- [267] M. Altmann, P. Schmidt, S. Mourato, and T. O'Garra, "Public acceptance of hydrogen transport technologies.," The European Commission, 2003.
- [268] S. Lü, G. Long, X. Meng, Y. Ji, B. Lü, and H. Zhao, "PrBa_{0.5}Sr_{0.5}Co₂O_{5+x} as cathode material based on LSGM and GDC electrolyte for intermediate-temperature solid oxide fuel cells," *International Journal of Hydrogen Energy*, vol. 37, pp. 5914-5919, 2012.
- [269] H. A. Taroco, J. A. F. R. Z. Domingues, and T. Matencio, "Ceramic Materials for Solid Oxide Fuel Cells," in *Advances in Ceramics - Synthesis and Characterization, Processing and Specific Applications*. C. Sikalidis, Ed. 2011, pp. 423-446.
- [270] J. Kong, Y. Zhang, C. Deng, and J. Xu, "Synthesis and electrochemical properties of LSM and LSF perovskites as anode materials for high temperature steam electrolysis," *Journal of Power Sources*, vol. 186, pp. 485-489, 2009.

- [271] W. Wang, R. J. Gorte, and J. M. Vohs, "Analysis of the performance of the electrodes in a natural gas assisted steam electrolysis cell," *Chemical Engineering Science*, vol. 63, pp. 765-769, 2008.
- [272] J. C. Ganley, "High temperature and pressure alkaline electrolysis," *International Journal of Hydrogen Energy*, vol. 34, pp. 3604-3611, 2009.
- [273] S. Giddey, F. T. Ciacchi, and S. P. S. Badwal, "High purity oxygen production with a polymer electrolyte membrane electrolyser," *Journal of Membrane Science*, vol. 346, pp. 227-232, 2010.
- [274] S. Sawada, T. Yamaki, T. Maeno, M. Asano, A. Suzuki, T. Terai, and Y. Maekawa, "Solid polymer electrolyte water electrolysis systems for hydrogen production based on our newly developed membranes, Part I: Analysis of voltage-current characteristics," *Progress in Nuclear Energy*, vol. 50, pp. 443-448, 2003.
- [275] X. Yang and J. T. S. Irvine, " $(\text{La}_{0.75}\text{Sr}_{0.25})_{0.95}\text{Mn}_{0.5}\text{Cr}_{0.5}\text{O}_3$ as the cathode of solid oxide electrolysis cells for high temperature hydrogen production from steam," *J. Mater. Chem.*, vol. 18, pp. 2349-2354, 2008.

11 Appendix

A1: Summary of experimental results of area specific resistance for a range of electrolyser technologies.

| Ref | Cathode | Electrolyte | Anode | Voltage (V) | Current density (A cm^{-2}) | ASR ($\Omega \text{ cm}^2$) | Temperature ($^{\circ}\text{C}$) | Comments | |
|--------------------|--------------------------|-------------|--|-------------|--|---|------------------------------------|---|--|
| [270] | | YSZ | $\text{La}_{0.8}\text{Sr}_{0.2}\text{MnO}_3$ (LSM)-YSZ | 0.1 | 0.1776 | 0.88 | 800 | Half cell with Pt work, reference and counter electrode Overpotentials are shown YSZ (yttria stabilised zirconia) ASR from impedance experiments [SOEC] | |
| | | YSZ | $\text{La}_{0.8}\text{Sr}_{0.2}\text{FeO}_2$ (LSF)-YSZ | 0.1 | 0.336 | 0.82 | | | |
| [271] | Co-CeO ₂ -YSZ | YSZ | Pd-ceria-YSZ | | | 0.69 for H ₂ +3%H ₂ O 0.66 for 80% CH ₄ conversion 1.1 for humidified CH ₄ 0.35 for electrodes at 10, 50, 80% CH ₄ conversion | 700 | Where the system is a natural gas assisted steam electrolysis process at a pressure of 0.57 atm and H ₂ O/H ₂ =13 [SOEC] | |
| [272] | Monel® Alloy | KOH (19M) | Monel® Alloy (Ni 400) | | | 2.44 | 200 | Open atmosphere | |
| | | | | | | 1.88 | | | |
| | | | | | | 1.56 | | | |
| | | | Monel® Alloy (Ni 400) | | | 1.94 | 200 | | Under pressure of self generated steam |
| | | | | | | 2.34 | 300 | | |
| | | | | | | 2.73 | 400 | | |
| | | | Ni | | | 1.71 | 400 | | Under pressure with varying anode material |
| | | | Monel® Alloy (Ni 400) | | | 1.71 | | | |
| | | | Lithiated Ni | | | 1.76 | | | |
| Cobalt – plated Ni | 1.59 | | | | | | | | |

11. Appendix

| | | | | | | | | |
|-------|--|-----------------------------|--|------------------------------|---|--|--|--|
| | | | | | | | | All values interpreted from graphs [Alkaline Electrolyser] |
| [273] | 20wt% Pt/C and 5wt% Nafion on carbon paper | Nafion N115 | 20wt% Pt/C on titanium | | | 0.23 | 75 – 80 | Based on a single cell with an active area of 50 cm ² Efficiency is 83% operating at 1 A cm ⁻² Values interpreted from graph [PEM Electrolyser] |
| [233] | Ni-YSZ Ni-YSZ Ni-YSZ | YSZ YSZ YSZ | LSM Ba _{0.5} Sr _{0.5} Co _{0.8} Fe _{0.2} O _{3-δ} (BSCF) LSMBSCF | 1.0 | 0.012 | 3.7 0.93 0.33 2.58 0.56 0.66 0.27 0.077 | 950 850 850 750 800 850 | Based on the whole cell Low current density High current density Low current density High current density Based on the anode [SOEC] |
| [75] | Ni-cermet | Scandia-stabilised zirconia | Strontium-doped manganite | 10 10 10 0 – 15 | 0.09 (6 A) 0.04 (2.5 A) 0.09 (6 A) 0 – 0.34 (0 – 110 A) | 1.36 3.84 1.38 2 (per cell) | 800 800 | Steam electrolysis Carbon dioxide electrolysis Co-electrolysis of CO ₂ and H ₂ O These values based on a 10 cell stack with an active area of 64cm ² per cell. Based on a 10 cell stack with active area of 324 cm ² per cell. |

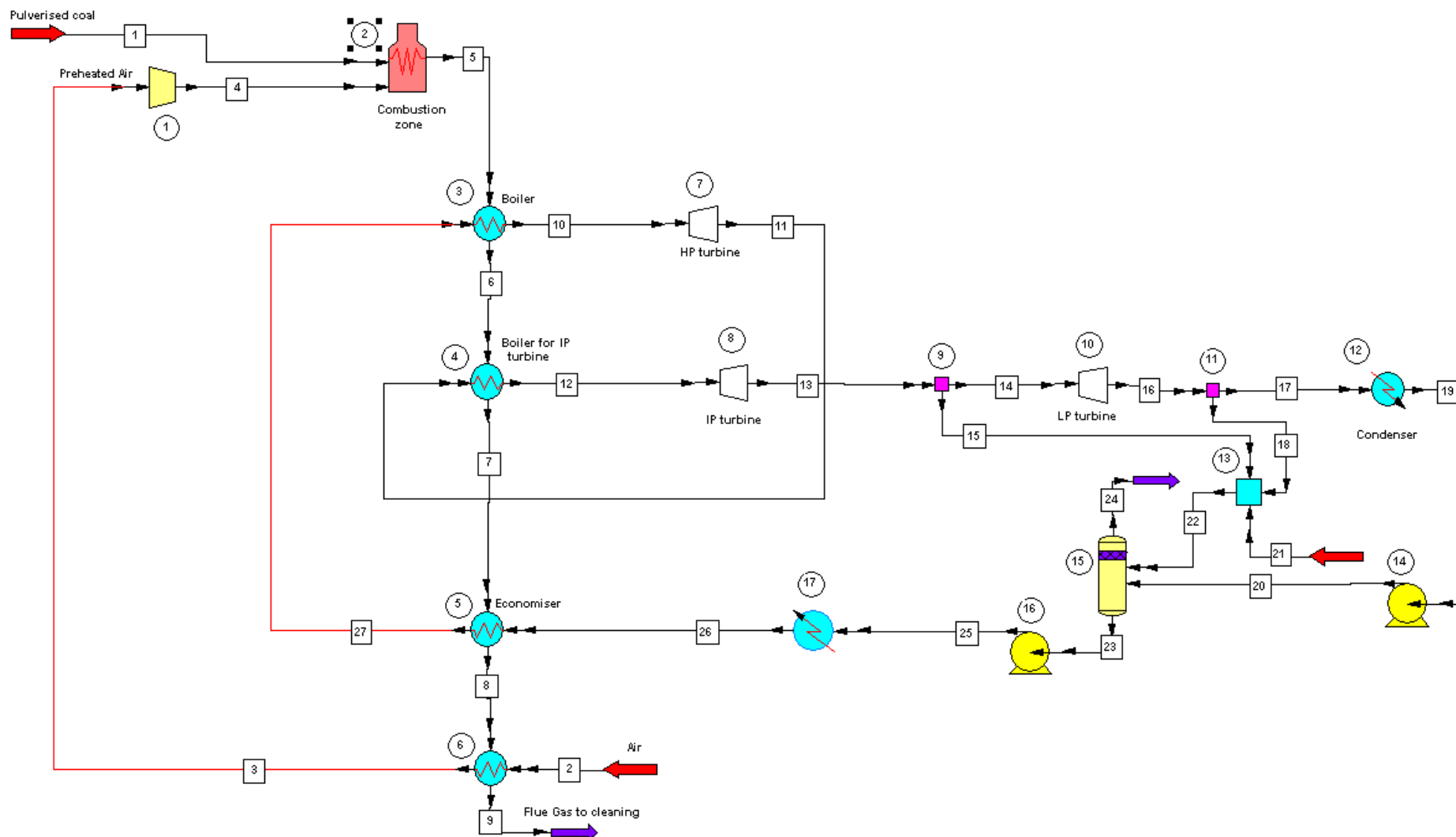
11. Appendix

| | | | | | | | | |
|-------|------------------|--|---|------|---|--|--|---|
| | | | | | | | | [SOEC] |
| [159] | Ni-YSZ | YSZ | Strontium-doped LSM | 1.25 | 1 | 0.69 0.42 | 800 | 30vol% absolute humidity 82vol% absolute humidity |
| | | | | 1 | 1 | 0.32 0.2 | 900 | 30vol% absolute humidity 82vol% absolute humidity Active surface area of 45cm ² . [SOEC] |
| [274] | Pt loaded Carbon | Crosslinked-polytetraflouroethylene (PTFE) – PEM | Pt loaded Carbon | | | 34 25 18 13 | 50 60 70 80 | Resistances based on PEM and interface between PEM and electrodes. Active surface area of 5 cm ² . [PEM Electrolyser] |
| [192] | Ni-YSZ | YSZ | SrO doped LaMnO ₃ (LSM)/YSZ | | | 0.59 0.52 0.47 0.42 0.62 0.55 0.49 0.40 | 750 | H ₂ :H ₂ O inlet is 0.5:0.5 Pressure:0.04 MPa 0.1 MPa 0.3 MPa 1.0 MPa H ₂ :H ₂ O inlet is 0.8:0.2 Pressure:0.04 MPa 0.1 MPa 0.3 MPa 1.0 MPaActive surface area of 16 cm ² . [SOEC] |
| [36] | Ni-YSZ | YSZ | Ba _{0.5} Sr _{0.5} Co _{0.8} Fe _{0.2} O _{3-δ} (BASF) | | | 0.73 2.15 1.60 0.75 0.65 0.8 0.83 0.82 | 800 700 750 800 850 800 | Steam: Hydrogen is 50:50 Steam: Hydrogen is 70:30 Steam: Hydrogen is 50:50 Steam: Hydrogen is 70:30 Steam: Hydrogen is 90:10 |

11. Appendix

| | | | | | | | | |
|-------|---|-----|---|------------|--|--|---------------------------------|---|
| | | | La _{0.8} Sr _{0.2} MnO _{3-δ} – YSZ (LSM-YSZ) | | | 2.65 1.6 1.35 0.85 0.9 0.85 0.87 | 700 750 800 850 850 | Steam: Hydrogen is 70:30 Steam: Hydrogen is 50:50 Steam: Hydrogen is 70:30 Steam: Hydrogen is 90:10 Values interpreted from graphs [SOEC] |
| [275] | Ni-YSZ (La _{0.75} Sr _{0.25}) _{0.95} Mn _{0.5} Cr _{0.5} O ₃ /CGO LSCM/CGO LSCM/YSZ | YSZ | LSM | 1.5 1.0 | | 12 2700 6.2 4.2 | 920 | 3% steam/Ar – 4% H ₂ 3% steam/Ar 3% steam/Ar – 4% H ₂ 3% steam/Ar – 4% H ₂ Surface area 3.14 cm ² Values interpreted from graphs [SOEC] |

A2: Flowsheet of power plant produced in CHEMCAD 6.0™.



A3: Table of data to show flowrates and conditions of the streams in of the power plant in A2.

11. Appendix

| Stream No. | 1 | 2 | 3 | 4 | 5 | 6 | 7 | 8 | 9 | 10 |
|---------------------------------------|-----------------------|---------|----------------------|----------------------|-----------------------|-----------------------|-----------------------|-----------------------|-----------------------|-----------------------|
| Stream Name | Pulverised coal | Air | Preheated Air | Compressed Air | Flue Gas | Flue Gas | Flue Gas | Flue Gas | Flue Gas to cleaning | Main Steam |
| Temperature (°C) | 25 | 25 | 265 | 302 | 1292 | 931 | 502 | 449 | 276 | 560 |
| Pressure (atm) | 1 | 1 | 1 | 1.2 | 1.5 | 1.5 | 1.5 | 1.5 | 1.5 | 250 |
| Enthalpy (MJ hr ⁻¹) | -4.13×10 ⁵ | -205.57 | 2.22×10 ⁵ | 2.57×10 ⁵ | -1.57×10 ⁵ | -7.03×10 ⁵ | -1.30×10 ⁶ | -1.37×10 ⁶ | -1.60×10 ⁶ | -1.46×10 ⁷ |
| Total flowrate (kg hr ⁻¹) | 209,000 | 900,000 | 900,000 | 900,000 | 1,109,000 | 1,109,000 | 1,109,000 | 1,109,000 | 1,109,000 | 1,160,000 |
| Mass fraction | | | | | | | | | | |
| O ₂ | 0 | 0.21 | 0.21 | 0.21 | 0 | 0 | 0 | 0 | 0 | 0 |
| N ₂ | 0.16 | 0.79 | 0.79 | 0.79 | 0.67 | 0.67 | 0.67 | 0.67 | 0.67 | 0 |
| CO ₂ | 0 | 0 | 0 | 0 | 0.0008 | 0.0008 | 0.0008 | 0.0008 | 0.0008 | 0 |
| CO | 0 | 0 | 0 | 0 | 0.25 | 0.25 | 0.25 | 0.25 | 0.25 | 0 |
| H ₂ O | 0 | 0 | 0 | 0 | 0.04 | 0.04 | 0.04 | 0.04 | 0.04 | 1 |
| H ₂ S | 0 | 0 | 0 | 0 | 0 | 0 | 0 | 0 | 0 | 0 |
| SiO ₂ | 0 | 0 | 0 | 0 | 0.017 | 0.017 | 0.017 | 0.017 | 0.017 | 0 |
| CH ₄ | 0 | 0 | 0 | 0 | 0.013 | 0.013 | 0.013 | 0.013 | 0.013 | 0 |
| Coal | 0.84 | 0 | 0 | 0 | 0 | 0 | 0 | 0 | 0 | 0 |
| SO ₂ | 0 | 0 | 0 | 0 | 0.003 | 0.003 | 0.003 | 0.003 | 0.003 | 0 |

| Stream No. | 11 | 12 | 13 | 14 | 15 | 16 | 17 | 18 | 19 | 20 |
|---------------------------------------|-----------------------|-----------------------|-----------------------|-----------------------|-----------------------|-----------------------|-----------------------|-----------------------|-----------------------|-----------------------|
| Stream Name | Reheat Steam | Reheated Steam | Steam exiting IP | Steam to LP turbine | Steam to Flash | Steam exiting LP | Steam to condenser | Steam to Flash | Condensed Water | Pumped Water |
| Temperature (°C) | 342 | 560 | 409 | 409 | 409 | 39 | 39 | 39 | 30 | 30 |
| Pressure (atm) | 46 | 46 | 12.9 | 12.9 | 12.9 | 0.05 | 0.05 | 0.05 | 0.05 | 12 |
| Enthalpy (MJ hr ⁻¹) | -1.50×10 ⁷ | -1.44×10 ⁷ | -1.47×10 ⁷ | -1.18×10 ⁷ | -2.95×10 ⁶ | -1.24×10 ⁷ | -9.96×10 ⁶ | -2.49×10 ⁶ | -1.18×10 ⁷ | -1.18×10 ⁷ |
| Total flowrate (kg hr ⁻¹) | 1,160,000 | 1,160,000 | 1,160,000 | 928,000 | 232,000 | 928,000 | 743,000 | 186,000 | 743,000 | 743,000 |
| Flowrate (kg hr ⁻¹) | | | | | | | | | | |
| O ₂ | 0 | 0 | 0 | 0 | 0 | 0 | 0 | 0 | 0 | 0 |
| N ₂ | 0 | 0 | 0 | 0 | 0 | 0 | 0 | 0 | 0 | 0 |
| CO ₂ | 0 | 0 | 0 | 0 | 0 | 0 | 0 | 0 | 0 | 0 |

11. Appendix

| | | | | | | | | | | |
|------------------|---|---|---|---|---|---|---|---|---|---|
| CO | 0 | 0 | 0 | 0 | 0 | 0 | 0 | 0 | 0 | 0 |
| H ₂ O | 1 | 1 | 1 | 1 | 1 | 1 | 1 | 1 | 1 | 1 |
| H ₂ S | 0 | 0 | 0 | 0 | 0 | 0 | 0 | 0 | 0 | 0 |
| SiO ₂ | 0 | 0 | 0 | 0 | 0 | 0 | 0 | 0 | 0 | 0 |
| CH ₄ | 0 | 0 | 0 | 0 | 0 | 0 | 0 | 0 | 0 | 0 |
| Coal | 0 | 0 | 0 | 0 | 0 | 0 | 0 | 0 | 0 | 0 |
| SO ₂ | 0 | 0 | 0 | 0 | 0 | 0 | 0 | 0 | 0 | 0 |

| | | | | | | | |
|--|-----------------------|-----------------------|-----------------------|-----------------------|-----------------------|-----------------------|-----------------------|
| Stream No. | 21 | 22 | 23 | 24 | 25 | 26 | 27 |
| Stream Name | Make-up Water | Steam to Flash | Water | Exiting Water | Pumped Water | Heated Water | Heated Steam |
| Temperature (°C) | 25 | 36 | 36 | 36 | 42 | 430 | 440 |
| Pressure (atm) | 2 | 0.05 | 0.05 | 0.05 | 250 | 250 | 250 |
| Enthalpy (MJ hr⁻¹) | -7.46×10 ⁶ | -1.29×10 ⁷ | -1.84×10 ⁷ | -6.30×10 ⁶ | -1.83×10 ⁷ | -1.52×10 ⁷ | -1.52×10 ⁷ |
| Total flowrate (kg hr⁻¹) | 470,000 | 888,800 | 1,160,000 | 470,000 | 1,160,000 | 1,160,000 | 1,160,000 |
| Flowrate (kg hr⁻¹) | | | | | | | |
| O ₂ | 0 | 0 | 0 | 0 | 0 | 0 | 0 |
| N ₂ | 0 | 0 | 0 | 0 | 0 | 0 | 0 |
| CO ₂ | 0 | 0 | 0 | 0 | 0 | 0 | 0 |
| CO | 0 | 0 | 0 | 0 | 0 | 0 | 0 |
| H ₂ O | 1 | 1 | 1 | 1 | 1 | 1 | 1 |
| H ₂ S | 0 | 0 | 0 | 0 | 0 | 0 | 0 |
| SiO ₂ | 0 | 0 | 0 | 0 | 0 | 0 | 0 |
| CH ₄ | 0 | 0 | 0 | 0 | 0 | 0 | 0 |
| Coal | 0 | 0 | 0 | 0 | 0 | 0 | 0 |
| SO ₂ | 0 | 0 | 0 | 0 | 0 | 0 | 0 |

11. Appendix

A4: Table of data to show operating conditions of the units of the power plant in A2.

| | |
|--|------------|
| Unit No. | 1 |
| Unit | Compressor |
| Pressure out (atm) [186] | 1.2 |
| Efficiency (%) [172] | 75 |
| Actual power (MJ hr⁻¹) | 34900 |
| Cp/Cv | 1.3823 |

| | |
|--|-------------------------|
| Unit No. | 2 |
| Unit | Combustor |
| Temperature (°C) | 1292 |
| Pressure (atm) [186] | 1.5 |
| Overall Heat (MJ hr⁻¹) | -1.49 × 10 ⁶ |
| Cp/Cv | 1.3823 |

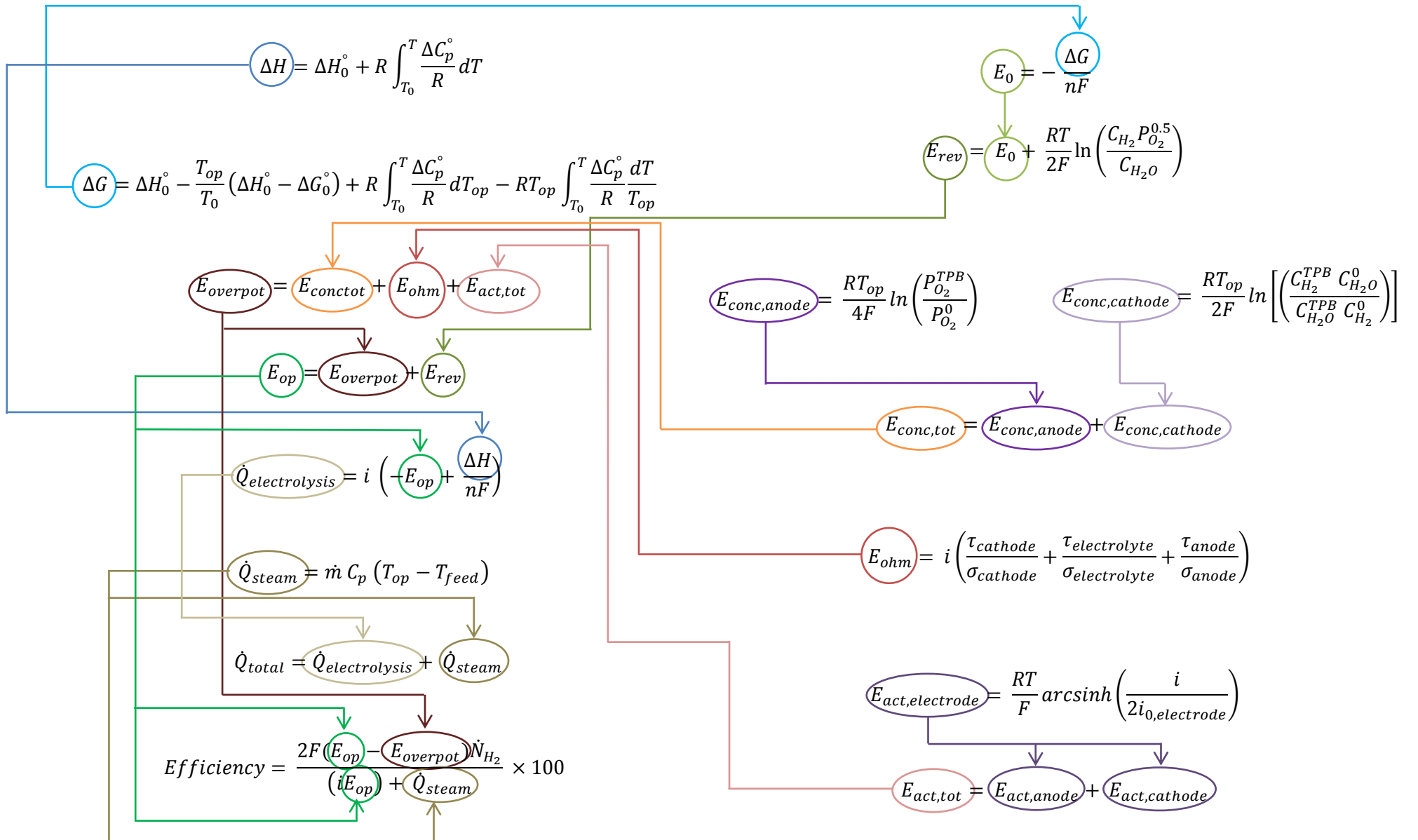
| | | |
|------------------------|---------|-----|
| Unit No. | 9 | 11 |
| Unit | Divider | |
| Output stream 1 | 0.2 | 0.2 |
| Output stream 2 | 0.8 | 0.8 |

| | | | | | | |
|---|-----------------|--------|-------|--------|-------------------------|------------------------|
| Unit No. | 3 | 4 | 5 | 6 | 12 | 17 |
| Unit | Heat exchangers | | | | | |
| Temperature of first stream out (°C) [186] | | | | | 30 | 430 |
| Temperature of second stream out (°C) | 560 | 560 | 440 | 265 | | |
| Pressure of first stream out (atm) | 1.5 | 1.5 | 1.5 | 1.5 | 0.05 | 250 |
| Pressure of second stream out (atm) [186] | 250 | 47 | 250 | 1 | | |
| Heat duty (MJ hr⁻¹) | 546500 | 600700 | 69200 | 221900 | -1.82 × 10 ⁶ | 3.09 × 10 ⁶ |

| | | | |
|--|------------|------------|------------|
| Unit No. | 7 | 8 | 10 |
| Unit | HP turbine | IP turbine | LP turbine |
| Pressure out (atm) [186] | 46 | 12.9 | 0.05 |
| Efficiency [172] | 0.7 | 0.7 | 0.7 |
| Actual power (MJ hr⁻¹) | -368700 | -342000 | -654900 |
| Cp/Cv | 1.6267 | 1.317 | 1.3107 |

| | | |
|------------------------------------|------|-------|
| Unit No. | 14 | 16 |
| Unit | Pump | |
| Output pressure (atm) [186] | 12 | 250 |
| Efficiency (%) [172] | 100 | 100 |
| Power (MJ hr⁻¹) | 890 | 29200 |

A5: A summary of the main electrochemical equations of the SOEC model



A6: Derivation of the Butler-Volmer and activation overpotential.

The Butler-Volmer equation is derived through the following equations. As the electrolyte and electrode conduct ions and electrons respectively, there is not a direct route for charge transfer. Therefore, one or more electrochemical steps are needed for charge transfer between the two layers [207].

At the interface between the electrolyte and electrode an electric double layer is formed, where excess charge builds up. There is a potential difference across the electric double layer, which drives the ionic species charge transfer [206;207]. Before a suitable current, which favours the overall electrolysis reaction is placed on the system, the charge transfer reaction undergoes both oxidation and reduction at each electrode as shown in Equation (73).



Where v_1 and v_2 are the stoichiometry of each species in the reaction, k_{red} and k_{ox} are the reaction rate constants for the reduction and oxidation reactions respectively.

Considering the reducing reaction, at a state where the reduction charge transfer reaction is not favoured, the electrode potential at this point can be represented by φ_1 . The electrode potential at a state where the reduction reaction charge transfer is favoured is φ_2 . In order to achieve a spontaneous reduction reaction at the electrode, additional energy is required and is represented by $nF(\varphi_2 - \varphi_1)$. The energy that is introduced to the system can be used either for the oxidation or the reduction reactions occurring at the electrode; the fraction of which is represented by β , the symmetry factor. Therefore, the activation energy (potential) required to facilitate charge transfer across the electric double layer for the reduction reaction is shown in Equation (74) [206]. E_{a1red} is the activation energy at the state where reduction is not favoured, and E_{a2red} is the activation energy where the reduction reaction is favoured.

$$E_{a2red} = E_{a1red} + \beta nF(\varphi_2 - \varphi_1) \quad (74)$$

For the oxidation reaction, the activation energy needed to allow charge transfer across the electric double layer is shown in (75) [206]. Where E_{a1ox} is the activation energy at the state where oxidation is not favoured, and E_{a2ox} is the activation energy where the oxidation reaction is favoured.

$$E_{a2ox} = E_{a1ox} - (1 - \beta)nF(\varphi_2 - \varphi_1) \quad (75)$$

The reaction needs to overcome the activation energy of the charge transfer reaction. The rate of reaction can be expressed using the Arrhenius equation in Equation (76) [206]. k is the reaction rate constant, k_{ref} is the reference rate constant and E_a is the activation energy.

$$k = k_{ref} \exp\left(\frac{-E_a}{RT}\right) \quad (76)$$

For the electrochemical reaction, the rate of reaction can be represented through a combination of the Faraday's law and the Arrhenius equation as shown in Equation (77) [206]. Where γ is the order of the charge transfer reaction, r is the rate of reaction, C is the concentration of species and i is the current density.

$$r = \frac{i}{nF} = k'[C]^\gamma \exp\left[\frac{-E_a}{RT}\right] \quad (77)$$

Based on the ideal gas law, the concentration can be written as Equation (78), where P is pressure.

$$C = \frac{P}{RT} \quad (78)$$

Considering the oxidation reaction (the backwards reaction) only of Equation (73), the rate of reaction for the oxidation charge transfer r_{ox} , can be expressed as in Equation (79) [206] and is based on Equations (74) and (76) to (78).

$$r_{ox} = \frac{i_{ox}}{n_{ox}F} = k'_{ox}[C_R]^{P_{ox}} \exp\left[-E_{a_{ox}} - \frac{(1 - \beta)nF(\varphi - \varphi_{ref})}{RT}\right] \quad (79)$$

Let the reference potential φ_{ref} be 0 V, based on the standard hydrogen electrode and we can form Equation (80) [206]. The expression has been simplified, where the oxidation reaction reference electrode $E_{a_{ox}}$ has been integrated with k'_{ox} to form one rate constant, k_{ox} .

$$r_{ox} = \frac{i_{ox}}{n_{ox}F} = k_{ox}[C_R]^{P_{ox}} \exp\left[\frac{(1 - \beta)nF\varphi}{RT}\right] \quad (80)$$

A similar equation can be derived for the rate of reaction for reduction (Equation (81)).

$$r_{red} = \frac{i_{red}}{n_{red}F} = k_{red}[C_O]^{P_{red}} \exp\left[\frac{\beta nF\varphi}{RT}\right] \quad (81)$$

Introducing the charge transfer coefficient, α_{ox} and α_{red} can simplify the equations further and is shown in Equation (82). The charge transfer coefficients are the fraction of additional energy that is put into the system that aids the reduction reaction or the oxidation reaction of the electrode and can be found through experimentation.

$$\alpha_{ox} = n(1 - \beta) \quad \alpha_{red} = n\beta \quad (82)$$

Combining the oxidation and reduction rate equations, the charge transfer reaction can be characterised through Equation (83).

$$r_{electrode} = r_{ox} - r_{red} = \frac{i_{ox}}{n_{ox}F} - \frac{i_{red}}{n_{red}F} = \frac{i}{nF} \quad (83)$$

At open circuit, the net current density is 0, therefore there is no external current driving the reaction. The rates of reaction for oxidation and reduction are equal as the system is in equilibrium. The exchange current density can show how effective an electrode is at equilibrium to facilitating the charge transfer reaction. The rate of reaction at equilibrium is shown in Equation (84).

$$\begin{aligned} r_{ox} = r_{red} &= \frac{i_0}{nF} = k_{ox}[C_R]^{P_{ox}} \exp\left[\frac{(1 - \beta)nF\varphi^\circ}{RT}\right] \\ &= k_{red}[C_O]^{P_{red}} \exp\left[\frac{\beta nF\varphi^\circ}{RT}\right] \end{aligned} \quad (84)$$

Where φ° is the equilibrium potential at open circuit.

Rearranging Equation (84) and taking the natural logarithms of the result, we can obtain Equation (85). This correlated with the Nernst potential, which characterises a system at open circuit.

$$\varphi^\circ = \frac{RT}{nF} \ln \frac{k_{red}}{k_{ox}} - \frac{RT}{nF} \ln \frac{C_R^{P_{ox}}}{C_O^{P_{red}}} \quad (85)$$

The overpotential at an electrode can be shown as Equation (86).

$$\eta = \varphi - \varphi^\circ \quad (86)$$

$$\therefore r_{total} = \frac{i}{nF} = k_{ox}[C_R]^{P_{ox}} \exp\left[\frac{\alpha_{ox}nF\phi}{RT}\right] - k_{red}[C_O]^{P_{red}} \exp\left[\frac{\alpha_{red}nF\phi}{RT}\right] \quad (87)$$

Rearranging and substituting Equation (85) into (87) gives the current density for one electrode in relation to the overpotential as shown in Equation.

$$i = nFk_{red}^{(1-\beta)}k_{ox}^{(\beta)}C_O^{(1-\beta)P_{red}}C_R^{(\beta)P_{ox}} \left[\exp\left(\frac{\alpha_{ox}F\eta}{RT}\right) - \exp\left(\frac{-\alpha_{red}F\eta}{RT}\right) \right] \quad (88)$$

As shown earlier, at open circuit, when the current density is 0, the exchange current density is present and can be substituted for part of Equation (88) as shown in Equation (89), which is the general form of the Butler-Volmer equation for one electrode.

$$i = i_0 \left[\exp\left(\frac{\alpha_{ox}F\eta}{RT}\right) - \exp\left(\frac{-\alpha_{red}F\eta}{RT}\right) \right] \quad (89)$$

$$i_0 = nFk_{red}^{(1-\beta)}k_{ox}^{(\beta)}C_O^{(1-\beta)P_{red}}C_R^{(\beta)P_{ox}}$$

For an electrolyser with both an anode and a cathode, Equation (90) can be used.

$$i = i_{0anode} \left[\exp\left(\frac{\alpha_{ox,anode}F\eta}{RT}\right) - \exp\left(\frac{-\alpha_{red,anode}F\eta}{RT}\right) \right] \quad (90)$$

$$i = i_{0cathode} \left[\exp\left(\frac{\alpha_{ox,cathode}F\eta}{RT}\right) - \exp\left(\frac{-\alpha_{red,cathode}F\eta}{RT}\right) \right]$$

However, this can be simplified through assuming that the charge transfer coefficients are equal, i.e., $\alpha_{ox} = \alpha_{red} = \alpha$, which is an assumption made in this study. Therefore, from Equation (89) the Butler-Volmer equation can now be expressed as Equation (91) [206].

$$i = i_0 \left[\exp\left(\frac{\alpha F\eta}{RT}\right) - \exp\left(\frac{-\alpha F\eta}{RT}\right) \right] \quad (91)$$

Let,
$$x = \frac{\alpha F\eta}{RT} \quad (92)$$

Which gives
$$i = i_0[\exp(x) - \exp(-x)] \quad (93)$$

From mathematics,
$$\sinh(x) = \frac{1}{2} [\exp(x) - \exp(-x)] \quad (94)$$

$$i = 2i_0 \frac{1}{2} \left[\exp\left(\frac{\alpha F \eta}{RT}\right) - \exp\left(\frac{-\alpha F \eta}{RT}\right) \right] \quad (95)$$
$$i = 2i_0 \sinh\left(\frac{\alpha F \eta}{RT}\right)$$

Taking the inverse, we can show the total activation overpotential for the electrolyser in Equation (53) [191;206].

12 Publications and presentations

12.1 Papers

M. N. Manage, D. Hodgson, N. Milligan, S. J. R. Simons, and D. J. L. Brett, "A techno-economic appraisal of hydrogen generation and the case for solid oxide electrolyser cells," *International Journal of Hydrogen Energy*, vol. 36, no. 10, pp. 5782-5796, May 2011

M. N. Manage, E. Sorensen, S. J. R. Simons and D. J. L. Brett, "A modelling approach to assessing the feasibility of the integration of power stations with steam electrolyzers," *Chemical Engineering Research and Design*, 2014 (Accepted)

12.2 Book chapters

D. J. L. Brett, M. Manage, E. Agante, N. P. Brandon, E. Brightman, R. J. C. Brown, and I. Staffell, "Fuels and fuel processing for low temperature fuel cells," in *Polymer electrolyte membrane and direct methanol fuel cell technology. Volume 1: Fundamentals and performance of low temperature fuel cells*. C. Hartnig and C. Roth, Eds. Cambridge: Woodhead Publishing Limited, 2012, pp. 3-26.

D. J. L. Brett, M. Manage, E. Agante, N. P. Brandon, E. Brightman, R. J. C. Brown, and I. Staffell, "The role of the fuel in the operation, performance and degradation of fuel cells," in *Functional materials for sustainable energy applications*. J. Kilber, S. Skinner, S. Irvine, P. Edwards, Eds. Cambridge: Woodhead Publishing Limited, 2012.

12.3 Presentations

[Poster] Capture and conversion of CO₂ into sustainable hydrocarbon fuels. Risø and HyFC research school and workshop. Copenhagen, Denmark, April 2011.

[Poster] London and South East Region Postgraduate Electrochemistry Symposium, Royal Society of Chemistry Electrochemistry group and International Society of Electrochemistry. Chemistry Department, University College London, UK, June 2011.

[Talk and Poster] Zing Conferences: Hydrogen and Fuel Cells Conference. Cancun, Mexico, December 2011.

[Talk] EPSRC CO₂ Chemistry Network, Electrochemical Approaches Research Cluster Meeting. Chemistry Department, University of Hull, UK, November 2012.

[Poster] CPSE Consortium. Imperial College London, UK, December 2012

[Talk] EPSRC CO₂ Chemistry Network, Advances in Carbon Dioxide Utilisation. Chemical Engineering Department, University College London, UK, December 2012.

[Poster] 9th European Congress of Chemical Engineering. The Hague, The Netherlands, April 2013.